THE
PHYSICAL REVIEW

A journal of experimental and theoretical physics established by E. L. Nichols in 1893

SECOND SERIES, VOL. 74, NO. 2 JULY 15, 1948

On the Application of Heisenberg's Theory of *S*-Matrix to the Problems of Resonance Scattering and Reactions in Nuclear Physics

NING HU
Universitetets Institut for Teoretisk Fysik, Copenhagen, Denmark
(Received April 15, 1948)

It is shown in the present paper that the Heisenberg *S*-matrix can have only simple poles and zeros in the complex plane of momentum and energy variables when the range of force is short. This fact is sufficient to determine the dispersion formulae in nuclear physics.

1. INTRODUCTION

THE nuclear dispersion formulae as derived by various authors[1] account quite satisfactorily for the resonance phenomena in nuclear physics. We may classify all the derivations into two groups. The first group follows the perturbation method and the treatment is closely analogous to Dirac's theory of dispersion of light by charged particles. The perturbation treatment can hardly be considered as justified, as the interaction is usually very strong in the nuclear reactions. The second group makes use of complex energy states introduced by Gamow. A simplified model is usually needed in this method, and as a consequence the results vary with the different assumptions about the model that have to be introduced. Furthermore these derivations give no account of the potential scattering.

It has been pointed out recently by Heisenberg[2] that the divergence difficulty of the present quantum-field theory is perhaps due to the fact that the phenomena at small distances between the particles have not been described correctly. He proposed that in the future the collision matrix,[3] or the *S*-matrix, which gives only the asymptotic behavior of the wave functions, should be considered as the only fundamental quantity. Heisenberg and Møller[4] have shown that the knowledge of the *S*-matrix is sufficient to predict all the observable quantities if the analytic and unitary properties of the *S*-matrix and the completeness condition are assumed. In the present paper we shall show that the nuclear dispersion formulae also follow from these general properties of *S*-matrix. This means that these formulae really rest on a much

[1] G. Breit and E. P. Wigner, Phys. Rev. **49**, 519, 642 (1936). N. Bohr, Nature **137**, 344 (1936). H. A. Bethe and Placzek, Phys. Rev. **51**, 450 (1937). F. Kalcker, J. R. Oppenheimer, and R. Serber, Phys. Rev. **52**, 273 (1937). H. A. Bethe, Rev. Mod. Phys. **9**, 71 (1937). P. L. Kapur and R. Peierls, Proc. Roy. Soc. **166**, 277 (1938). A. J. F. Siegert, Phys. Rev. **56**, 750 (1939). G. Breit, Phys. Rev. **58**, 606 (1940). E. P. Wigner, Phys. Rev. **70**, 15 (1946); Proc. Nat. Acad. Sci **32**, 302 (1946). H. Feshbach, D. C. Pearlee and V. F. Weisskoff, Phys. Rev. **71**, 145 (1947).

[2] W. Heisenberg, Zeits. f. Physik **120**, 513, 673 (1943); Zeits. f. Naturforsch., 11/12, 607 (1946), and several as yet unpublished papers, a complete account of which is given by C. Møller, Kgl. Danske Vid. Sels. Math-Fys. Medd. **23**, No. 1 (1945).

[3] This matrix was first introduced by Wheeler, see J. A. Wheeler, Phys. Rev. **52**, 1107 (1937).

[4] C. Møller, Kgl. Danske Vid. Sels. Math-Fys. Medd. **23**, No. 1 (1945); **22**, No. 19 (1946); Nature **158**, 403 (1946).

more solid basis than other theoretical derivations hitherto used.

2. GENERAL INVESTIGATION ON THE S-MATRIX

We shall first give a brief account of Heisenberg's theory. It is sufficient for this purpose to consider the simplest case of a non-relativistic particle in a central field of force. The Schrödinger equation is given by

$$[(1/r)(d^2/dr^2)](r\psi)+k^2\psi - [l(l+1)/r^2]\psi+V(r)\psi=0, \quad (1)$$

where l is the angular momentum. The asymptotic solution for ψ at large distance r in the continuous spectrum is given by

$$\psi\sim(1/r)\sin[kr+\eta_l(k)], \quad (2)$$

where $\eta(k)$ is the phase shift due to the interaction potential $V(r)$. Equation (2) can also be written in the following form, apart from an irrelevant factor depending on k:

$$\psi\sim(1/r)(e^{-ikr}-S_l(k)e^{ikr}), \quad (3)$$

where

$$S_l(k)=\exp[-2i\eta_l(k)] \quad (4)$$

is Heisenberg's S which is a matrix in the general case when the angular momentum and the number of particles is not fixed. Since $\eta_l(k)$ must be a real and odd function of k (this can be seen from the fact that if we reverse the sign of k in (2), no new solution of (1) should be obtained since (1) is even in k), it follows from (4) that

$$S^*(k)S(k)=1 \quad (5)$$

and

$$S(k)S(-k)=1. \quad (6)$$

It is expected that when $V(r)$ is a regular function of r, $S(k)$ should be an analytic function of k. According to the suggestion of Kramers and Heisenberg, the bounded states of the system is given by the negative imaginary values k_n of k, which satisfy $S(k_n)=0$ (or positive imaginary values k_n^* or $-k_n$ of k, which satisfy $S(k_n^*)=\infty$). Then ψ is given by

$$\psi_n\sim(1/r)e^{-ik_nr}=(1/r)e^{-|k_n|r}, \quad (7)$$

which falls off exponentially with r, and therefore represents a closed state. It has also been shown that the zeros of $S(k)$ for complex values of k represent quasi-stationary states of the system. For real values of k, $S(k)$ gives directly the scattering cross section of the particle by the central field of force. We see then that $S(k)$ determines all the observable quantities that can be obtained by solving (1). The above results hold also when the relativistic wave function is used.

In the following we shall show that with a possible exception at infinity the only singularities that $S(k)$ can have in the upper half of the complex k plane are poles of the first order. This follows directly from the general properties of $S(k)$. At least for the case when the range of force is very short, we can show that $S(k)$ can only have poles of the first order in the lower half of the complex k plane also. To show these we need a relation for $S(k)$ derived by Heisenberg from the completeness condition of the asymptotic wave functions. As probably most readers have not yet read Heisenberg's papers, we shall derive this relation once again as follows: The asymptotic wave functions for the continuous and discrete states are, respectively, given by

$$\psi_k(r)\sim A_k[\sin[kr+\eta(k)]/r] \quad (8)$$

and

$$\psi_n(r)\sim C_n[e^{ik_nr}/2\pi\sqrt{2}r], \quad (9)$$

where A_k and C_n are normalization constant and k_n is now given by $S(k_n)=\infty$. A_k is determined by the normalization condition for the continuous spectra:

$$\int 4\pi r^2\psi_k^*(r)\psi_{k'}(r)dr=\delta(k-k') \quad (10)$$

to be $A_k=1/\sqrt{2}\pi$. C_n can also be determined from the normalization condition by a method due to Kramers,[5] but it is determined more conveniently by the completeness condition

$$\int_0^\infty dk\psi_k(r)\psi_k^*(r') + \sum_n\psi_n(r)\psi_n^*(r')=(1/4\pi r^2)\delta(r-r'). \quad (11)$$

Inserting (8) and (9) into (11) and using the relation

$$\eta(k)=-\eta(-k), \quad (12)$$

[5] Kramers, Hand- und Jahrbuch d. Chem. Physik **1**, 312 (1938).

we easily obtain

$$\int_{-\infty}^{+\infty} dkS(k)e^{ik(r+r')} = \sum_n |C_n^2| e^{ik_n(r+r')}. \quad (13)$$

Now $S(k)$ has a pole at every point $k=k_n$ above the real axis in the complex k plane. By changing the path of integration towards increasing positive imaginary values of k, this path finally reduces to circles around the poles at k_n and an infinite semicircle above the real k axis. Therefore, one gets

$$\sum_n \oint_{k=k_n} dkS(k)e^{ik(r+r')} + \int_\Gamma dkS(k)e^{ik(r+r')} = \sum_n |C_n^2| e^{ik_n(r+r')}, \quad (14)$$

where $\int_\Gamma$ is the integration along the infinite semicircle. Since (14) holds for any value of $r+r'$, the coefficient of $\exp[ik_n(r+r')]$ of both sides must be equal. So we finally have

$$\oint_{k=k_n} dkS(k) = |C_n^2|, \quad (15)$$

$$\int_\Gamma dkS(k)e^{ik(r+r')} = 0. \quad (16)$$

Equation (15) is the relation for $S(k)$ obtained by Heisenberg in his papers in 1946. Equation (16) determines the nature of singularity, if it exists, at infinity. This point will be discussed later. From the above derivation we see immediately that if there is a quasi-stationary state determined by the poles of $S(k)$ above the real k axis, it should be included in the summation of (11) since other wise both sides of (14) cannot be equal. In fact, the wave function for this quasi-stationary state

$$\psi_n \sim \exp[iK_1 r - K_2 r] (K_2 > 0) \quad (17)$$

satisfies the same boundary conditions as the closed state. We have shown[6] that (17) represents a quasi-stationary state of the K-capturing type. It should be noted that this result is not contradictory to the conclusion from wave mechanics that the quasi-stationary states should not be included in the completeness condition (i.e., they cannot be considered as members of the orthonormal system determined by the wave equation), as the complex poles above the real k axis are only possible in the theories where particles can be created and annihilated; in that case the Hamiltonians are certainly not Hermitian so that complex eigenvalues cannot be excluded.

The complex poles of $S(k)$ below the real k axis give rise to the usual quasi-stationary radioactive states.[4] These states should not be included in the sum of the left-hand side of (11) since these poles make no contribution to the residue of the integral of (13).

For the case of relativistic particles, (15) and (16) are also obtained by the same procedure, except that, perhaps, some remarks should be added here. From the relation

$$E = (k^2+\mu^2)^{\frac{1}{2}}, \quad (18)$$

E being the energy and μ the rest mass of the particle, we see that E is a double-valued function of k. Consequently, the wave function ψ, which is a function of k and E, is also double valued. We may imagine the complex k plane as consisting of two Riemann sheets jointed along two cuts on the imaginary axis from $k=i\mu$ to $k=i\infty$ and from $k=-i\mu$ to $k=-i\infty$. The upper sheet represents only states with positive energy and the lower sheet only those with negative energy. The integral in (13) will then be along the real axes of both Riemann sheets and the summation in (13) contains the states determined by the poles in the upper half of the plane of both sheets. The same conditions (15) and (16) are obtained except that $\int_\Gamma$ is now taken along the two infinite semicircles in the upper half of the plane of both Riemann sheets.

We shall now extend Heisenberg's investigation to find the nature of the singularities of $S(k)$ in the upper half of the complex k plane. The general expression of $S(k)$ around the singular point k_n can be written

$$S(k) = f(k) + \sum_{s=1}^{\infty} [A_s/(k-k_n)^s], \quad (19)$$

where $f(k)$ is regular at the point $k=k_n$ and $A_s (s=1, 2, \cdots)$ are constants. Inserting this

[6] W. Heitler and N. Hu, Proc. Roy. Irish Acad. **51A**, No. 9 (1947), Nature **159**, 776 (1947).

into (14) and using (15), we have

$$\oint_{k=k_n} dkS(k)e^{ik(r+r')} = \oint_{k=k_n} \sum_{s=1}^{\infty} [A_s e^{ik(r+r')}/(k-k_n)^s] = \sum_{s=1}^{\infty} [2\pi i/(s-1)!] \times A_s[i(r+r')]^{s-1}e^{ik_n(r+r')}. \quad (20)$$

Since the above equation must hold for any value of $r+r'$, the coefficients of $(r+r')^s$ of both sides of (14) must be equal. Thus we have

$$A_1=(1/2\pi i)|C_n^2|, \quad A_2=A_3=\cdots=0 \quad (21)$$

and (19) becomes

$$S(k)=f(k)+(1/2\pi i)[|C_n^2|/(k-k_n)]. \quad (22)$$

Therefore, $S(k)$ has only poles of the first order in the upper half of the complex k plane. It should be noted that the same result can be obtained by Kramer's method of determining the normalization constant of the closed state.[5] The conclusion for the closed states was obtained also by Møller.

The relation (14) does not give any information about the nature of singularities in the lower half of the complex k-plane since these singularities are not included in the summation of (11). However, at least in the case of nuclear reaction where the range of force is much smaller than $1/K_1$, $k=-K=-K_1-iK_2(K_2>0)$ being the position of the pole, we can show that $S(k)$ has only poles of the first order also below the real k axis. From (6) we see that $k=K$ must be a zero of $S(k)$. The wave function becomes at this point

$$\psi_K=\varphi_K/r, \quad \varphi_K\sim e^{-iKr}=\exp[-iK_1r+K_2r], \quad (23)$$

which represents a radioactive decaying (capturing) state when K_1 is negative (positive). We have therefore at $k=K$ and, when r is very large,

$$\frac{d}{dk}\left[\varphi\left(\frac{d\varphi}{dr}+ik\varphi\right)\right]_{k=K} = \varphi_K\left(\frac{d^2\varphi}{dkdr}\right)_{k=K} + i\varphi_K^2 + iK\varphi_K\left(\frac{d\varphi}{dk}\right)_{k=K} = \varphi_K\left(\frac{d^2\varphi}{dkdr}\right)_{k=K} - \frac{d\varphi_K}{dr}\left(\frac{d\varphi}{dk}\right)_{k=K} + i\varphi_K^2. \quad (24)$$

For very large r, the left-hand side becomes simply $-2iK(dS/dk)_{k=K}$ if small terms of higher orders are neglected. Now inserting $\psi=\varphi/r$ into (1) we obtain

$$[(d^2/dr^2)+k^2-[l(l+1)/r^2]+V(r)]\varphi=0. \quad (25)$$

Differentiating with respect to k, we have

$$[(d^2/dr^2)+k^2-[l(l+1)/r^2]+V(r)](d\varphi/dk)+2k\varphi=0. \quad (26)$$

Multiplying (25) by $d\varphi/dk$ and (26) by φ and subtracting and integrating the result with respect to r, we obtain

$$\varphi(d^2\varphi/dkdr)-(d\varphi/dr)(d\varphi/dk) = -2k\int_0^r \varphi^2 dr. \quad (27)$$

Therefore, (24) becomes

$$-2iK(dS/dk)_{k=K}=-2K\int_0^r \varphi_K^2 dr+i\varphi_K^2. \quad (28)$$

We shall now introduce the assumption that the range of force is very small so that for $r>a$, where $a\ll 1/K_1$, φ_K represents a free wave:

$$\varphi_K(r)=(-i)^{l+1}(\pi Kr/2)^{\frac{1}{2}}H_{l+\frac{1}{2}}^{(2)}(Kr). \quad (29)$$

The integral in (28) may be broken into two parts

$$\int_0^r \varphi_K^2 dr=\int_0^a \varphi_K^2 dr+\int_a^r \varphi_K^2 dr. \quad (30)$$

The last integral can be evaluated easily and gives

$$\int_a^r \varphi_K^2 dr=(-1)^{l+1}(K\pi/2)\cdot(r^2/2) \times\{[H_{l+\frac{1}{2}}^{(2)}(Kr)]^2-[H_{l+\frac{1}{2}}^{(2)}(Kr)] \times[H_{l+\frac{1}{2}}^{(2)}(Kr)]\}|_a^r. \quad (31)$$

The upper limit cancels with the last term of (28) when r is very large. For the lower limit we use the following approximate expression for small r:

$$H_{l+\frac{1}{2}}^{(2)}(Kr)\approx(2/\pi Kr)^{\frac{1}{2}}[(2l)!i/(l!(2Kr)^l)]. \quad (32)$$

We have, for $l>0$,

$$\int_a^r \varphi_K^2 dr - i(1/2K)\varphi_K^2 \approx (-1)^l[1/(2K)^{2l}] \cdot (1/a^{2l-1})[(2l)!/l!]^2(1/2l-1). \quad (33)$$

To evaluate the first integral on the right-hand side of (30), we assume that the wave function for $r<a$ is nearly stationary so that the density of outgoing current is much smaller than the charge density. In other words, we assume that the wave function for $r<a$ is nearly real or nearly pure imaginary. From (29) and (33) we see that when l is even, φ_K is nearly real just outside $r=a$. Thus, by continuation, the wave function should also be nearly real inside $r=a$. When l is odd, φ_K is nearly pure imaginary just outside $r=a$ and, consequently, the wave function should be nearly pure imaginary also inside $r=a$. We have, therefore,

$$\int_0^a \varphi_K^2 dr \approx (-1)^l \int_0^a \varphi_K^* \varphi_K dr. \quad (34)$$

Adding (33) to (34), we have

$$i\left(\frac{dS}{dk}\right)_{k=K} = (-1)^l \left\{ \int_0^a \varphi_K^* \varphi_K dr + \frac{1}{(2K)^{2l}} \frac{1}{a^{2l-1}} \left[\frac{(2l)!}{l!}\right]^2 \frac{1}{2l-1} \right\}. \quad (35)$$

It is seen that for $l>0$, (35) cannot vanish since both terms in the bracket are positive. For the case $l=0$, we have

$$\int_0^a \varphi_K^* \varphi_K dr \approx (1/2K_2)\varphi^*(a)\varphi(a) = 1/2K_2, \quad (36)$$

and (28) becomes

$$i(dS/dk)_{k=K} = (1/2K_2) - (1/2K_1 + 2iK_2). \quad (37)$$

Equations (35) and (37) furnish the proof that $(dS/dk)_{k=K} \neq 0$ and, consequently, the zero of $S(k)$ at $k=K$ is of the first order. From (6) we see that the pole of $S(k)$ at $k=-K$ below the real axis must also be of the first order.

In the above investigation we have only considered the isolated singularities of $S(k)$. It can easily be seen that $S(k)$ cannot have unisolated singularities such as those along a cut connecting different Riemann sheets other than the original two sheets in the relativistic case introduced by the fact that energy is a double-valued function of momentum. For if there is a cut between any two points a and b introduced by the factor like $[(k-a)(k-b)]^{\frac{1}{2}}$ in the expression for $S(k)$, from the condition $S(k)=1/S(-k)$, there must be another cut between $-a$ and $-b$. None of these two cuts can pass across the real axis, because if they do, additional degeneracy would be introduced to the continuous spectrum. Therefore at least one of these two cuts must lie above the real axis. Thus when we change the path of integration towards increasing positive imaginary values of k, in passing from (13) to (14), we would get an additional closed integral around this cut. Following the same argument leading to (16) we see that this closed integral must vanish separately. This however means that the cut cannot be there at all. Similar argument shows that $S(k)$ cannot have other factors which are irrational functions of E and k such as $(E-a)^{\frac{1}{2}}$, $(k-c)^{\frac{1}{2}}$, etc., because they would inevitably introduce cuts in the complex k plane. Therefore $S(k)$ can only be a rational function of E and k.

There is, however, a possibility that $S(k)$ may have an isolated singularity on the real k axis of the form

$$e^{ic(k-k_0)} \quad (38)$$

with c and k real and c also negative. The unitary condition $S^*(k)S(k)=1$ for real k will not be violated by this singularity. In the Appendix we shall show that (38) is the only possible essential singularity that $S(k)$ can have. Physically, this singularity amounts to the phenomena that the scattering cross section given by

$$\sin^2\eta = \sin^2[c/(k-k_0)] \quad (39)$$

will oscillate very rapidly as k approaches k_0. We shall dismiss the possibility of this singularity for finite value of k_0, on the physical ground that the cross section should be a smooth function of k. When k_0 goes to infinity, (38) becomes

$$e^{ic_\infty k}, \quad (40)$$

where c_∞ is a real negative constant. It will be of interest to note that $S(k)$ with this factor has been found in some known examples already. The simplest example is the case of scattering by a potential well of constant depth discussed by Møller.[4]

The general form of $S(k)$ for the non-relativistic case when the range of force is very small,

is therefore given by

$$S_l(k)=\pm e^{ick}\pi_n[(k-k_n^*)/(k-k_n)], \quad (41)$$

where $k_n(n=1, 2, \cdots)$ are the positions of the poles and are all distinct since all the poles are of the first order. The form of the factor $(k-k_n^*)/(k-k_n)$ follows from the unitary condition for real k: $S(k)S^*(k)=1$. From the further condition that $S(k)S(-k)=1$, we see that for any pole k_n of $S(k)$ not on the imaginary axis, there must be another pole $k_s=-k_n^*$. On the imaginary axis the last condition gives no other poles and zeros than those already demanded by the unitary condition. Thus if we denote by k_λ all the poles of $S(k)$ on the imaginary axis and by k_s all the poles on the right side of the imaginary axis, the final expression for $S(k)$ for the non-relativistic case becomes

$$S(k)=\pm e^{ick}\prod_\lambda\frac{(k-k_\lambda^*)}{(k-k_\lambda)}\prod_s\frac{(k-k_s^*)(k+k_s)}{(k-k_s)(k+k_s^*)}. \quad (42)$$

For the relativistic case a singularity of $S(k)$ is not only specified by its position k_s in the complex k plane, but also by the sign of $E_s=\pm(k_s^2+1)^{\frac{1}{2}}$ (in the following we shall put $\mu=1$) which shows whether the singularity is in the upper or the lower Riemann sheet. If $S(k)$ has a pole at $k=k_s$, $E=E_s(E_s^2=k_s^2+1)$, then from (5) and (6) we see that S has also a singularity at $k=-k_s^*$, $E=E_s^*$ and two zeros at $k=k_s^*$, $E=E_s^*$ and at $k=-k_s$, $E=E_s$. Therefore S must have a factor of the following form

$$S_s=\frac{(k_s+k_s^*)(E-E_s^*)-(E_s^*-E_s)(k-k_s^*)}{(k_s+k_s^*)(E-E_s)-(E_s-E_s^*)(k-k_s)}. \quad (43)$$

We can easily verify that the poles and zeros of (43) are simple. If S has also a pole at $k=k_s$, $E=-E_s$, then, following the same argument as before, it will have another factor given by (43) with E_s replaced by $-E_s$. We can easily verify that these two factors multiplied together are equal to the same factor

$$\text{Const.}\frac{(k-k_s^*)(k+k_s)}{(k-k_s)(k+k_s^*)} \quad (44)$$

of (42) as we would have expected. Next, if S has a pole at $k=k_\lambda$, $E=E_\lambda$ on the imaginary k axis, then it has also a zero at $k=k_\lambda^*=-k_\lambda$, $E=E_\lambda^*$. The expression for S has then the following factor

$$S_\lambda=(E-1+ib_\lambda k)/(E-1-ib_\lambda k) \quad b_\lambda=\text{real}. \quad 45$$

It can easily be verified that the pole and zero are simple and the position of the pole is given by

$$k_\lambda=2ib_\lambda/(1+b_\lambda^2), \quad E_\lambda=(1-b_\lambda^2)/(1+b_\lambda^2). \quad (46)$$

We see from (46) that $|k_\lambda|\leqslant 1$ and $|E_\lambda|\leqslant 1$, as should be the case for any closed state. Lastly, if S has an essential singularity at infinity, then it must contain a factor of the form

$$e^{ick}, \quad c<0, \quad (47)$$

which means that the same singularities are present in both Riemann sheets as (47) does not depend on the sign of E. That this must be so follows from the fact that $E=\pm\infty$, and $k=\pm\infty$ should be counted as only one point in the complex k- or E-plane. The final expression for $S(k)$ for the relativistic case is therefore:

$$S(k)=\pm e^{ick}\prod_\lambda\frac{E-1-ib_\lambda k}{E-1+ib_\lambda k}\prod_s\frac{(k_s+k_s^*)(E-E_s^*)-(E_s^*-E_s)(k-k_s^*)}{(k_s+k_s^*)(E-E_s)-(E_s-E_s^*)(k-k_s)}. \quad (48)$$

The sign $\pm$ in (42) and (48) remains so far undetermined. It should be noted that for any pole k_n of $S(k)$ above the real axis, we have from (15) the following additional condition to be satisfied by $S(k)$:

$$\oint_{k=k_n} dkS(k)>0. \quad (15')$$

Similarly, for any zero k_s of $S(k)$ above the real axis, we have, from (35) and (37) when the imaginary part of k_s is very small,

$$Rl\{(-1)^l i(dS/dk)_{k=k_s}\}>0 \quad (35')$$

(15') and (35') will determine among other things the sign of $S(k)$. It is rather difficult to write down explicitly the general form of $S(k)$ which also satisfies (15') and (35'). Therefore we shall consider (42) and (48) as our final form of $S(k)$ and (15') and (35') as additional conditions.

3. THE SCATTERING FORMULA

The wave function (3) can also be written in the following form:

$$\psi(r)\sim(1/r)(e^{-ikr}+(-1)^{l+1}e^{ikr}+[(-1)^l-S_l]e^{ikr}).$$

The first two terms represent the incident wave when there is no scattering. The last term represents the scattered wave. The scattering cross section is given by

$$Q_l(k)=(\pi/k^2)\,|\,1-(-1)^lS_l(k)\,|^2. \qquad (49)$$

We shall first consider a special non-relativistic case where $S(k)$ has only two poles, k_s and $-k_s^*$, below the real axis. The sign can be fixed easily by (35′) to be $(-1)^l$. We put further $c=0$. This gives the so-called "one-level" formula:

$$Q(k)=\frac{\pi}{k^2}\left|1-\frac{(k-k_s^*)(k+k_s)}{(k-k_s)(k+k_s^*)}\right|^2=\frac{\pi}{k^2}\left|\frac{2k(k_s-k_s^*)}{k^2-k_s^2}\right|^2. \qquad (50)$$

Now, since $E=k^2/2\mu$, where μ is the rest mass of the particle, we have

$$Q(k)=(4\pi\mu^2/k^2)\,|[2k(k_s-k_s^*)/(E-E_s)]|^2, \qquad (51)$$

where $E_s=k_s^2/2\mu$. Since E_s is a complex quantity, we may write $E_s=W_s-\frac{1}{2}i\gamma_s$, thus

$$1/[\,|E-E_s|^2]=1/[(E-W_s)^2+\tfrac{1}{4}\gamma_s^2].$$

This gives the essential feature of the usual dispersion formulae. Using the relation

$$(1/4\mu)(k_s^{*2}-k_s^2)=\tfrac{1}{2}\gamma_s,$$

we have

$$Q(k)=[2\pi/(k_s^2+k_s^{*2})]\times\gamma_s^2/[(E-W_s)^2+\tfrac{1}{4}\gamma_s^2]. \qquad (52)$$

Equation (52) becomes the well-known one-level formula when $(k_s^2+k_s^{*2})$ in the denominator is replaced by $2k^2$. From the above derivation we see that (52) holds only when $c=0$ and is therefore not the most general form. In the general case, where we have

$$Q(k)=\frac{2\pi}{(k_s^2+k_s^{*2})}\,\frac{4(E-W_s)^2\sin^2\tfrac{1}{2}ck+2(E-W_s)\gamma_s\sin ck+\gamma_s^2\cos^2\tfrac{1}{2}ck}{(E-W_s)^2+\tfrac{1}{4}\gamma_s^2}, \qquad (53)$$

we shall have antiresonance scattering if $\cos^2\frac{1}{2}ck=0$. In that case $Q(k)$ vanishes when $E=W_s$. It seems, however, that c can only be a length of the order of the range of force a. We have, therefore, for nuclear scattering, $e^{ick}\approx 1$, and hence (52) will always be a good approximation except when $ka\approx 1$.

The corresponding one-level formula for the relativistic case when $c=0$ is given by

$$Q(k)=\frac{\pi}{k^2}\left|1-\frac{k_1(E-E_s^*)-\frac{1}{2}i\gamma_s(k-k_s^*)}{k_1(E-E_s)+\frac{1}{2}i\gamma_s(k-k_s)}\right|^2=\frac{\pi\gamma_s^2}{[k_1(E-W_s)-\frac{1}{2}\gamma_sk_2]^2+\frac{1}{4}\gamma_s^2(E^2-1)}, \qquad (54)$$

where $E_s=W_s-i\frac{1}{2}\gamma_s$, $k_s=k_1+ik_2$, $E_s^2=k_s^2+1$. If we consider $E-W_s$, k_2, and γ_s as small quantities of higher order in comparison with W_s and k_1 in the neighborhood of resonance scattering, and retain only terms of the lowest order in them, we shall see after some easy calculation that (54) reduces to the same formula (52).

The many-level formulae can be easily evaluated from (42) and (48), but we shall not write them down here. From the above derivation we see that the scattering cross section is entirely determined by the value of c and the positions of all the poles of $S(k)$. These values depend on the particular form of potential function $V(r)$. The resonance scattering takes place around those levels for which $W_s\gg\gamma_s$, i.e., when E_s lies very near to the positive real E axis. Those poles far from the positive real E axis shall only contribute to the potential scattering or the background scattering. In the former theories no account of the potential scattering can be given. According to the present theory, the potential scattering is really the resonance scattering due to quasi-stationary states determined by poles far away from the positive real k axis and closed states of the system. Our formula differs in detail from other derivations given before. For instance, (52) differs from the usual one-level formula by a factor. The discrepancy must be due to the simplified assumptions about the model introduced in those derivations.

Equation (43) gives only the scattering when the incident wave is a spherical wave of angular momentum l. When the incident wave is a plane wave, the total cross section is given by

$$Q=\sum_l(2l+1)Q_l. \tag{55}$$

4. THE RESONANCE REACTIONS

We can easily apply our foregoing result to the nuclear reactions of the type

$$A+B\rightleftarrows C+D. \tag{56}$$

When the incident plane wave contains only A and B, the wave function for the system are given by

$$\begin{aligned}\psi(\mathbf{k}_A\mathbf{k}_B)&=\delta(\mathbf{k}_A-\mathbf{k}_A{}^0)\delta(\mathbf{k}_B-\mathbf{k}_B{}^0)\\&\quad+p(E_A+E_B-E_A{}^0-E_B{}^0)\\&\quad\times(\mathbf{k}_A\mathbf{k}_B|\,U|\,\mathbf{k}_A{}^0\mathbf{k}_B{}^0),\\\psi(\mathbf{k}_C\mathbf{k}_D)&=p(E_C+E_D-E_A{}^0-E_B{}^0)\\&\quad\times(\mathbf{k}_C\mathbf{k}_D|\,U|\,\mathbf{k}_A{}^0\mathbf{k}_B{}^0),\end{aligned} \tag{57}$$

where

$$p(E)=(1/E)-\tfrac{1}{2}i\pi\delta(E). \tag{58}$$

In the other case when the incident wave contains only C and D, we have

$$\begin{aligned}\psi(\mathbf{k}_A\mathbf{k}_B)&=p(E_A+E_B-E_C{}^0-E_D{}^0)\\&\quad\times(\mathbf{k}_A\mathbf{k}_B|\,U|\,\mathbf{k}_C{}^0\mathbf{k}_D{}^0),\\\psi(\mathbf{k}_C\mathbf{k}_D)&=\delta(\mathbf{k}_C-\mathbf{k}_C{}^0)\delta(\mathbf{k}_D-\mathbf{k}_D{}^0)\\&\quad+p(E_C+E_D-E_C{}^0-E_D{}^0)\\&\quad\times(\mathbf{k}_C\mathbf{k}_D|\,U|\,\mathbf{k}_C{}^0\mathbf{k}_D{}^0).\end{aligned} \tag{59}$$

The S-matrix for the system is given by

$$S=1+2i\pi U, \tag{60}$$

where

$$U^0=\begin{pmatrix}(\mathbf{k}_A\mathbf{k}_B|\,U^0|\,\mathbf{k}_A{}^0\mathbf{k}_B{}^0) & (\mathbf{k}_A\mathbf{k}_B|\,U^0|\,\mathbf{k}_C{}^0\mathbf{k}_D{}^0)\\(\mathbf{k}_C\mathbf{k}_D|\,U^0|\,\mathbf{k}_A{}^0\mathbf{k}_B{}^0) & (\mathbf{k}_C\mathbf{k}_D|\,U^0|\,\mathbf{k}_C{}^0\mathbf{k}_D{}^0)\end{pmatrix}. \tag{61}$$

$\mathbf{k}_A$, $\mathbf{k}_B$, $\cdots$ are the momenta of the particles A, B, $\cdots$, respectively. U^0 is the submatrix of U with the initial and final states having the same total energy and momentum. Since the S-matrix is unitary, we may apply an unitary transformation to transform it into the following normal form

$$\bar{S}=u^+Su, \tag{62}$$

where

$$\bar{S}=\begin{pmatrix}(\mathbf{k}_A\mathbf{k}_B|\,\bar{S}_1|\,\mathbf{k}_A{}^0\mathbf{k}_B{}^0) & 0\\0 & (\mathbf{k}_C\mathbf{k}_D|\,\bar{S}_2|\,\mathbf{k}_C{}^0\mathbf{k}_D{}^0)\end{pmatrix}, \tag{63}$$

where $(\mathbf{k}_A,\mathbf{k}_B|\,\bar{S}_1|\,\mathbf{k}_A{}^0,\mathbf{k}_B{}^0)$ and $(\mathbf{k}_C,\mathbf{k}_D|\,\bar{S}_2|\,\mathbf{k}_C{}^0,\mathbf{k}_D{}^0)$ are two unitary matrices, and u is the unitary matrix given by

$$u=\begin{pmatrix}(\mathbf{k}_A\mathbf{k}_B|\,u_{11}|\,\mathbf{k}_A{}^0\mathbf{k}_B{}^0) & (\mathbf{k}_A\mathbf{k}_B|\,u_{12}|\,\mathbf{k}_C{}^0\mathbf{k}_D{}^0)\\(\mathbf{k}_C\mathbf{k}_D|\,u_{21}|\,\mathbf{k}_A{}^0\mathbf{k}_B{}^0) & (\mathbf{k}_C\mathbf{k}_D|\,u_{22}|\,\mathbf{k}_C{}^0\mathbf{k}_D{}^0)\end{pmatrix}, \tag{64}$$

u^+ is the adjoint of u. If we use the center of mass coordinate system, we have $-\mathbf{k}_A=\mathbf{k}_B$, $-\mathbf{k}_C=\mathbf{k}_D$. Therefore all the states can be labeled by a single variable $\mathbf{k}_A$ or $\mathbf{k}_C$. $\bar{S}_1$ and $\bar{S}_2$ can further be transformed into diagonal form by using the representation of spherical harmonics. Let u_l, S_l, and $\bar{S}_l$ be the submatrices of u, S, and $\bar{S}$ when the angular momentum has a definite value l. The general form of u and S can then be written

$$u_l=\begin{pmatrix}\cos\alpha_l e^{i\beta_l} & \sin\alpha_l e^{i\beta_l}\\-\sin\alpha_l e^{-i\beta_l} & \cos\alpha_l e^{-i\beta_l}\end{pmatrix}\quad \bar{S}_l=\begin{pmatrix}\bar{S}_{l1} & 0\\0 & \bar{S}_{l2}\end{pmatrix}, \tag{65}$$

where α_l and β_l are two arbitrary parameters and $\bar{S}_{l1}$ and $\bar{S}_{l2}$ are pure numbers. S_l is thus given by

$$S=\begin{pmatrix}\cos^2\alpha\bar{S}_1+\sin^2\alpha\bar{S}_2 & \sin\alpha\cos\alpha e^{2i\beta}(-\bar{S}_1+\bar{S}_2)\\\sin\alpha\cos\alpha e^{-2i\beta}(-\bar{S}_1+\bar{S}_2) & \sin^2\alpha\bar{S}_1+\cos^2\alpha\bar{S}_2\end{pmatrix}. \tag{66}$$

$\bar{S}_1$ and $\bar{S}_2$ may be considered as representing two normal modes of the system in analogy to the system of coupling oscillators. As is seen from (63), each normal mode represents a pure scattering system. We can, therefore, determine $\bar{S}_1$ and $\bar{S}_2$ by applying the theory developed in the last two sections. We obtain

$$\begin{aligned}\bar{S}_1&=e^{ic_1k_A}\prod_\lambda\frac{(k_A-k_{A\lambda}{}^*)}{(k_A-k_{A\lambda})}\\&\qquad\prod_s\frac{(k_A-k_{As}{}^*)(k_A+k_{As}{}^*)}{(k_A-k_{As})(k_A+k_{As})},\\\bar{S}_2&=e^{ic_2k_c}\prod_\lambda\frac{(k_c-k_{c\lambda}{}^*)}{(k_c-k_{c\lambda})}\prod_s\frac{(k_c-k_{cs}{}^*)(k_c-k_{cs}{}^*)}{(k_c-k_{c\lambda})(k_c+k_{cs})},\end{aligned} \tag{67}$$

with $-k_A=k_B$, and $-k_C=k_D$ in the center of mass system. The reaction cross section is given by

$$\begin{aligned}
Q_l^{AB\to AB}&=(\pi/k_A^2)\,|1-(k_A|S_l|k_A)|^2\\
&=(\pi/k_A^2)\,|1-\cos^2\alpha\bar{S}_1-\sin^2\alpha\bar{S}_2|^2,\\
Q_l^{AB\to CD}&=(\pi/k_A^2)\,|1-(k_c|S_l|k_A)|^2\\
&=(\pi/k_A^2)\,|1-\sin\alpha\cos\alpha e^{2i\beta}\\
&\qquad\times(-\bar{S}_1+\bar{S}_2)|^2,\\
Q_l^{CD\to CD}&=(\pi/k_c^2)\,|1-(k_c|S_l|k_c)|^2\\
&=(\pi/k_c^2)\,|1-\sin^2\alpha\bar{S}_1-\cos^2\alpha\bar{S}_2|^2,\\
Q_l^{CD\to AB}&=(\pi/k_c^2)\,|1-(k_A|S_l|k_c)|^2\\
&=(\pi/k_c^2)\,|1-\sin\alpha\cos\alpha e^{-2i\beta}\\
&\qquad\times(-\bar{S}_1+\bar{S}_2)|^2. \qquad (68)
\end{aligned}$$

The cross sections are completely determined by the constant parameters α and β, the energy levels, the line breadth, and the value of c_1 and c_2 of the two equivalent systems. The values of these constants cannot be given in a general theory of resonance without knowledge of the interaction potentials of the particular system. Their theoretical determination will be very tedious or even impossible for a complicated system. It is usually more practical to determine these constants empirically from experiments. Equation (68) gives only the cross sections when the incident wave has a definite total angular momentum l. The total cross section when the incident wave is a plane wave is given by

$$Q=\sum_l(2l+1)Q_l. \qquad (69)$$

Finally, the author wishes to express his thanks to Professor C. Møller for his kind interest.

APPENDIX

We shall now show that $S(k)$ can only have singularities of the form

$$e^{ic/(k-k_0)} \qquad (70)$$

on the real k axis, where c is a negative real constant. The general form of the function $F(k)$, which has a singularity at $k=k_0$, k_0 being real, and satisfies the unitary condition $F^*(k)F(k)=1$ for real k, is

$$F(k)=\exp\left\{i\sum_{n=1}^{\infty}[C_n/(k-k_0)^n]\right\}, \qquad (71)$$

where c_n are real constants. To identify $F(k)$ with $S(k)$ we have further to satisfy the condition (13) of Section 2, which requires that the integral

$$\oint_c dkS(k)e^{ik(r+r')}, \qquad (72)$$

which appears on the left-hand side of (14), obtained by deforming the path of integration towards increasing imaginary value of k in passing from (13) to (14), should vanish separately. $\oint_c$ means the integration along a closed path starting from $k=k_0-a$ (a being real and positive) to $k=k_0+a$ along the real k axis, and then returning to $k=k_0-a$ along a half-circle above the real axis of radius a with the center at $k=k_0$. For a given value of a we can find an integer N such that the value of the series

$$\sum_{n=1}^{\infty}C_n/(k-k_0)^n$$

on this circle may be replaced by

$$\sum_{n=1}^{N}C_n/(k-k_0)^n$$

with a negligible error. The integration along the real k axis gives a contribution of the order of a since $|S(k)|=1$ on the real axis. The condition for the vanishing of (72) becomes therefore, on neglecting terms of order a when a is very small,

$$\oint_{|k-k_0|=a}dk\exp\left\{i\sum_{n=1}^{N}[C_n/(k-k_0)^n]\right\}\cdot e^{ik(r+r')}\approx 0, \qquad (73)$$

where the integration is taken along the half-circle of radius a. We may deform this path to a new path starting from $k=k_0-a$ to k_0-b (b being positive and real and smaller than a), then along a half-circle above the real axis with center $k=k_0$ to the point $k=k_0+b$, and finally along the real axis from $k=k_0+b$ to $k=k_0+a$. The contribution to the integral from the path along the real axis is again negligible since it is of the order $a-b$. We may choose b so small that the summation

$$\sum_{n=1}^{N}[C_n/(k-k_0)^n]$$

can be replaced by a single term $c_N/(k-k_0)^N$ on the smaller half-circle. Equation (73) then

becomes

$$\int_{|k-k_0|=b} dk \exp\{i[C_N/(k-k_0)^N]\} \times e^{ik(r+r')} \approx 0. \quad (74)$$

The integral (74) for very small values of $|k-k_0|=b$ can be evaluated easily by the method of variational phase. We have

$$\int_{|k-k_0|=b} dk e^{ic_N/(k-k_0)N} e^{ik(r+r')} = e^{ik_0(r+r')} \times \int_0^{\pi} \exp[ic_N(1/b^N)(\cos N\theta - i \sin N\theta)] b e^{i\theta} d\theta$$
$$= 2\pi i e^{ik_0(r+r')} b \sum_l \exp[c_N(1/b^N)(-1)^l] \times \exp[i(2l+1/2N)\pi]. \quad (75)$$

Where the summation is over the range $0<(2l+1)\leqslant 2N$, i.e., from $l=0$ to $l\leqq(2N-1)/2$. Equation (75) will be of the order $\exp(1/b^N)$, which is a very large quantity when b is very small, except when $N=1$ and $c_N<0$. In the latter case (75) will be a very small quantity and thus only in this case can (74) be satisfied. This furnishes the proof that the singularity of $S(k)$ on the real k axis can at most be of the form

$$\exp[ic/(k-k_0)] \qquad (c<0). \quad (76)$$

When k_0 goes to infinity, (73) goes just to (16) of Section 2, and (76) becomes, on putting $c_\infty = c/k_0^2$,

$$e^{ic_\infty k}. \quad (77)$$

PHYSICAL REVIEW VOLUME 74, NUMBER 2 JULY 15, 1948

Scattering of Particles by the Gas in a Synchrotron*

NELSON M. BLACHMAN
Brookhaven National Laboratory, Upton, New York

AND

ERNEST D. COURANT
Cornell University, Ithaca, New York

(Received April 5, 1948)

Successive elastic encounters of a proton with atoms of air in a proton synchrotron may build up a betatron oscillation whose amplitude exceeds the aperture of the vacuum chamber; in this case the particle is lost. The Rutherford scattering formula, suitably cut off at large and small scattering angles, is used to determine the r.m.s. amplitude of this oscillation as a function of the increasing kinetic energy of the particle. It reaches a maximum, given by Eq. (11), when the latter is four times its value at injection. The differential equation is found, which the distribution of amplitudes as a function of path length must obey, and it is solved, by use of appropriate boundary conditions, for the case in which damping of the oscillations is ignored. The solution makes possible an estimate of the fraction of the original particles which is scattered to the wall (Fig. 1). These results are applied to two proposed synchrotrons to determine the air pressures which gives a ten percent loss of particles.

I. INTRODUCTION

THE protons in a proton synchrotron will move through a path of length nearly ct_0 if the acceleration takes place over a time t_0. For $t_0=1$ sec. this is 3×10^{10} cm. Even at a pressure of 10^{-6} mm Hg this is equivalent to about 40 cm of air at atmospheric pressure, and appreciable scattering and loss may occur. Since cross sections for inelastic scattering, which includes all nuclear disintegration processes, are generally smaller by factors of about 10^{-7} than those for elastic or Rutherford scattering, it is necessary only to be sure that the elastic scattering is not serious.

The elastic scattering gives rise to "betatron"

* Work done under the auspices of the Atomic Energy Commission.

oscillations.[1] These are rapid oscillations of the particles about the equilibrium orbit. The "horizontal" (radial) and "vertical" (axial) components of these oscillations have frequencies equal, respectively, to $(1-n)^{\frac{1}{2}}$ and $n^{\frac{1}{2}}$ times the frequency of revolution of the particles, where $n=-(r/H)(\partial H/\partial r)$ is the index of the fall off of magnetic field with radius. Thus, the wavelengths of the two betatron oscillations are constant.

Since the scattering is incoherent, its general effect is continually to increase the amplitudes of these vertical and horizontal betatron oscillations, with the possible result that the particles will hit the wall of the vacuum chamber and be lost. Because the vertical aperture is usually made smaller than the horizontal, any loss will usually be due to the vertical oscillations. We may notice here that if a particle which is executing such oscillations is deviated by angle θ upward or downward from its path, the amplitude of its vertical oscillations will change by

$$n^{-\frac{1}{2}}R\theta\cos\phi+R^2\theta^2\sin^2\phi/2nB, \qquad (1)$$

where ϕ is the phase and B the amplitude of the oscillation just before scattering and R is the orbit radius. The two terms are due to the components of the oscillation due to the scattering, respectively, in phase and in quadrature with the already present oscillation.

II. SCATTERING FORMULA

We may consider the probability and the effect of a single collision. We shall use the Rutherford scattering formula,[2,3]

$$d\sigma=(Z^2e^4d\omega)/(4M^2v^4\sin^4\tfrac{1}{2}\Theta), \qquad (2)$$

in c.g.s. electrostatic units, in which Ze is the charge on the stationary scattering nucleus and e is the charge on the scattered particle, which has *relativistic* mass M and velocity v; $d\sigma$ is the cross section for scattering into any solid angle $d\omega$ at angle Θ away from the direction of the incident particles. On account of the shielding effect of the electrons in the scattering atoms, the cross section falls off sharply for $\Theta<\lambda\!\!\!^{-}/a$, where $\lambda\!\!\!^{-}=h/Mv$ is the de Broglie wave-length of the particles and $a=5.3\times10^{-9}Z^{-\frac{1}{3}}$ cm is the "radius" of the atom. Because of the finite size of the nucleus there will also be an upper limit on Θ, given by $\lambda\!\!\!^{-}/b$, where $b=1.6\times10^{-13}Z^{\frac{1}{3}}$ cm is the "radius" of the nucleus. Thus, we shall use (2) between the limits $\Theta_{\min}$ and $\Theta_{\max}$, where

$$\Theta_{\min}=\lambda\!\!\!^{-}/a \quad \text{and} \quad \Theta_{\max}=\lambda\!\!\!^{-}/b. \qquad (3)$$

In the cases that will be of interest the angles within this range will be sufficiently small for the rewriting of (2) in the form

$$d\sigma=(4Z^2e^4d\omega)/(M^2v^4\Theta^4). \qquad (4)$$

Integrating (4) over the range of solid angle specified by (3), we obtain for the total cross section for elastic scattering

$$\sigma=(4\pi Z^2e^4)/(M^2v^4\Theta_{\min}^2), \qquad (5)$$

since $\Theta_{\min}\ll\Theta_{\max}$. Notice that σ is proportional to T^{-1}, with T the kinetic energy of the particles, since $\Theta_{\min}^2$ is proportional to T^{-1}. We need to consider only the non-relativistic range near the injection energy of the particle, where considerable scattering may occur.

We may divide the scattering into its vertical and horizontal components. The square of the total angle of scattering is the sum of the squares of the two components, which, on account of symmetry, must have the same mean-square values. Hence, the mean-square vertical component of the scattering angle for a single collision is $\langle\theta^2\rangle=\frac{1}{2}\langle\Theta^2\rangle$, which, from (4), is

$$\langle\theta^2\rangle=\Theta_{\min}^2\log(\Theta_{\max}/\Theta_{\min}). \qquad (6)$$

We are using angular brackets to indicate mean values. Notice that $\langle\theta^2\rangle$ also is proportional to T^{-1}.

III. BUILDING UP OF BETATRON OSCILLATIONS

The oscillation which a particle executes is the linear superposition of the small oscillations which are set up by each separate encounter with a scatterer. A new scattering will add a small contribution given by (1) to the already present oscillation. The phase angle ϕ between these two is completely random. It will be convenient to resolve the new small oscillations into two components, one in phase and one in quadrature with some reference oscillation. The amplitudes of these two components then add alge-

[1] D. W. Kerst and R. Serber, Phys. Rev. **60**, 53 (1941).
[2] Williams, Proc. Roy. Soc. **169**, 531 (1939).
[3] B. Rossi and K. Greisen, Rev. Mod. Phys. **13**, 262 (1941).

braically, and the total amplitude of betatron oscillation B is the square root of the sum of the squares of these two sums. The amplitude of the in-phase component of the oscillation set up by a scattering is given by the first term of (1). Its mean value is zero, since ϕ is a random angle, and its mean-square value is $(R^2/2n)\langle\theta^2\rangle$. The quadrature component of the oscillation set up by a scattering has the same mean and mean-square values and is statistically uncorrelated with the in-phase component.

We shall use b to denote the amplitude of either component of the vertical betatron oscillations. The mean-square value of b, which is half the mean-square value of B, is the sum of the mean-square contributions to b from all of the collisions a particle suffers, each of which contributes, on the average $(R^2/2n)\langle\theta^2\rangle$. Thus, if N is the number of scattering atoms per cc and x is distance in the scattering medium, we have

$$\langle b^2\rangle=(R^2/2n)\int_0^x\langle\theta^2\rangle N\sigma dx. \tag{7}$$

With T a linear function of x that increases by eV every revolution, i.e., increase of $2\pi R$ in x, (7) becomes

$$\begin{aligned}\langle b^2\rangle&=(\pi R^3/neV)N\int_{T_i}^{T}\langle\theta^2\rangle\sigma dT\\&=(\pi NR^3/neV)\int_{T_i}^{T}\langle\theta^2\rangle_i(T_i/T)\sigma_i(T_i/T)dT\\&=(R^2/2n)\langle\theta^2\rangle_iN\sigma_ix_2(1-T_i/T)\\&\rightarrow(R^2/2n)\langle\theta^2\rangle_iN\sigma_ix_2\quad\text{as}\quad T\rightarrow\infty,\end{aligned}\tag{8}$$

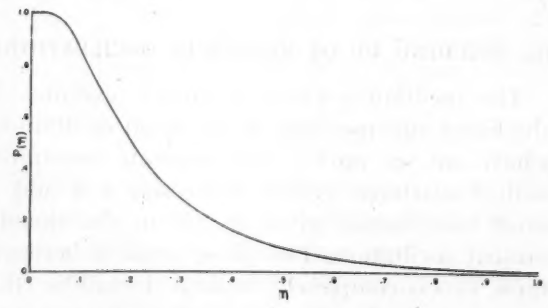

FIG. 1. Fraction—P—of original number of particles that are not scattered to the wall as a function of η.

$$P=\frac{4}{\pi}\sum_{s=0}^{s=\infty}\left(\frac{(-1)^s}{2s+1}\right)\exp[-(2s+1)^2\eta],$$

where

$$x_2=(2\pi R/eV)T_i \tag{9}$$

is the distance the particles must go to double their initial injection energy, T_i. $\langle\theta^2\rangle_i$ and σ_i are the values of these quantities at injection.

From (8), then, we see that the mean-square value of b approaches, as the particles are accelerated to energies much larger than the injection energy, the same value which one would compute by supposing that σ and $\langle\theta^2\rangle$ were constant from injection until the kinetic energy had been doubled, and then fell from the values at injection to zero.

IV. DAMPING

We have thus far neglected the damping of the betatron oscillations. These oscillations are damped[1] as $T^{-\frac{1}{2}}$. We shall consider the damping of the small oscillations set up by each encounter with a scatterer. The square of the amplitude of each small oscillation is damped as $T^{-\frac{1}{2}}$. When the kinetic energy of the particle has increased to T_f, the small oscillation which was initiated when the kinetic energy was T has been reduced in mean-square amplitude by the factor $(T/T_f)^{\frac{1}{2}}$. We may insert this factor into the integrand of (8) and integrate from T_i to T_f. We thus find for the mean-square b when the kinetic energy of the particle is T_f

$$\begin{aligned}\langle b^2\rangle=(R^2/2n)\langle\theta^2\rangle_iN\sigma_ix_2\\\times2[(T_i/T_f)^{\frac{1}{2}}-(T_i/T_f)].\end{aligned}\tag{10}$$

This quantity begins to increase just like (8). However, instead of monotonically approaching a certain asymptotic value for infinite T_f, it reaches a maximum when $T_f=4T_i$ and then falls asymptotically to zero.

It is the maximum that is of interest; if this maximum corresponds to oscillations that do not reach the wall of the vacuum chamber, the particles will not be lost. The value of twice the bracket in (10) at this maximum is $\frac{1}{2}$. Thus, we see by comparison with (8) that consideration of the damping of the betatron oscillations halves the maximum mean-square value of b, which becomes

$$\langle b^2\rangle=(R^2/4n)\langle\theta^2\rangle_ix_2/x_i, \tag{11}$$

where

$$x_i=1/(N\sigma_i)$$

is the mean free path of the particles at injection.

Because b is the sum of many small independent random contributions, it is distributed normally (according to the Gaussian law) with standard deviation $\langle b^2\rangle^{\frac{1}{2}}$. Therefore, the total amplitude of vertical betatron oscillation B, which is the positive square root of the sum of the squares of two components, each behaving like b, obeys a Rayleigh distribution, i.e., the probability that B lies between B and $B+dB$ is

$$\langle b^2\rangle^{-1}B\exp-(B^2/2\langle b^2\rangle)dB. \qquad (12)$$

This distribution will hold, of course, only if the aperture of the vacuum chamber does not restrict the amplitude of betatron oscillation.

V. DIFFUSION INTO WALL

If this r.m.s. maximum amplitude is comparable with the vertical semi-aperture of the vacuum chamber, the amplitudes of vertical oscillation of the particles will not be distributed according to (12) with the mere loss of the particles having amplitudes exceeding the semi-aperture, since it has been assumed above that no particles are lost, and so a particle which at one time has an excessive amplitude may be scattered back down to an amplitude less than the semi-aperture. We shall now determine the actual distribution of amplitudes, whence we can find the loss exactly; however, it will be necessary to ignore the damping of the betatron oscillations in order to obtain an integrable equation. Nevertheless, if the result given by (11) indicates that few particles or that most of the particles are lost, one can be sure that, respectively, few particles or practically all of the particles will be lost.

Let $p(x,B)dB$ be the probability that after a particle has traversed a distance x it is executing oscillations of amplitude between B and $B+dB$. We then have the relation

$$\partial p(x,B)/\partial x=-p(x,B)+\int_{-\infty}^{\infty}p(x,B-\Delta B)q(B-\Delta B,\Delta B)d(\Delta B). \qquad (13)$$

where $q(B,\Delta B)d(\Delta B)dx$ is the probability that the amplitude of oscillations of a proton with amplitude B is changed by an amount between ΔB and $\Delta B+d(\Delta B)$ in traversing a distance dx.

Expanding $p(x,B-\Delta B)$ and $q(B-\Delta B,\Delta B)$ in power series in the ΔB of $B-\Delta B$ and noting that

TABLE I. Pressures at which half the particles are lost.

Accelerator	R cm	A cm	T_i kev	V kev	Pressure 10^{-5} mm Hg
Birmingham 1.3-Bev proton synchrotron*	450	5	2000	0.2	0.7
Brookhaven 3-Bev proton synchrotron**	915	8	3000	1.15	1.1

* Oliphant, Gooden, and Hide, Proc. Phys. Soc. **59**, 666 (1947).
** Livingston, Bull. Am. Phys. Soc. **23**, 2, 28 (1948).

q is different from zero only for small Δb, we transform (13) into the differential equation

$$\partial p(x,B)/\partial x=(\partial/\partial B)\{(\partial/\partial B)[\tfrac{1}{2}\langle(\Delta B)^2\rangle p]-\langle\Delta B\rangle p\}, \qquad (14)$$

where $\langle(\Delta B)^2\rangle$ and $\langle\Delta B\rangle$ are the mean-square and mean change of amplitude per unit distance of travel. ΔB is given by (1), from which we see that

$$\langle\Delta B\rangle=\langle(\Delta B)^2\rangle/2B$$

and

$$\langle(\Delta B)^2\rangle=\langle(\Delta b)^2\rangle.$$

Thus, since $\langle(\Delta B)^2\rangle$ is independent of B, (14) becomes

$$\partial p(x,B)/\partial x=\tfrac{1}{2}\langle(\Delta B)^2\rangle(\partial/\partial B)[B(\partial/\partial B)(p/B)]. \qquad (14a)$$

From (7) we have

$$\langle(\Delta B)^2\rangle=\langle(\Delta b)^2\rangle=(R^2/2n)N\sigma\langle\theta^2\rangle. \qquad (15)$$

In an accelerator, where the energy is constantly changing, this is a function of x.

Using the new variable

$$\xi=\tfrac{1}{2}\int_0^x\langle(\Delta b)^2\rangle dx', \qquad (16)$$

we can write Eq. (14) in the form

$$\partial p/\partial\xi=(\partial/\partial B)[B(\partial/\partial B)(p/B)], \qquad (17)$$

which is the well-known heat conduction equation. The boundary conditions for (17) are

$$p=0 \quad \text{for} \quad B=A,$$

where A is the effective vertical semi-aperture, and

$$p(0,b)=\delta(b) \quad \text{for} \quad 0\leqslant B\leqslant A.$$

The solution of (17) with these boundary condi-

tions is

$$p=(2B/A^2)\sum_{s=1}^{\infty}[J_1(\lambda_s)]^{-2}J_0(\lambda_s B/A)\times\exp-(\lambda_s^2\xi/A^2),$$

where λ_s is the s-th positive root of $J_0(\lambda)=0$. The total probability that a particle remains at ξ is

$$P(\xi)=\int_{-A}^{A}pdB=2\sum_{s=1}^{\infty}[\lambda_s J_1(\lambda_s)]^{-1}\exp-(\lambda_s^2\xi/A^2). \tag{18}$$

Comparing (15) and (16) with (7) and (8) we see that $\xi=\frac{1}{2}\langle b^2\rangle$ and that it asymptotically approaches the value

$$(R^2/4n)\langle\theta^2\rangle_i N\sigma_i x_2,$$

still ignoring the effects of damping. The value of P depends on

$$\eta=\xi/A^2=\langle b^2\rangle/2A^2, \tag{19}$$

which is one fourth the ratio of the mean-square maximum amplitude to the square of the semi-aperture. P is plotted as a function of η in Fig. 1. We may take partial account of the effects of damping by using in (19) the value of $\langle b^2\rangle$ given by (11) rather than by (8), and thus halving η.

When proper account is taken of the damping of the betatron oscillations, a term $\frac{1}{4}(p+B\partial p/\partial B)/(x+2\pi RT_i/eV)$ is added to the right side of (14). The resulting differential equation is not separable, and no solution has been obtained for it.

VI. APPLICATION

We may apply the foregoing to the cases of the Birmingham and Brookhaven synchrotrons. From the graph (Fig. 1) of P as a function of η we see that if no more than a 10 percent loss through vertical scattering of particles is to be permitted, η must be no more than 0.089, and if no more than a 50 percent loss is permitted, η must be no more than 0.20. Evaluating (19) in terms of the given constants of the system, and including the damping factor of $\frac{1}{2}$, we have

$$\eta=[\pi^2NR^3Z^2e^4/2nA^2T_i eV]\log(183Z^{-\frac{1}{3}}), \tag{20}$$

where N is the number of scattering atoms per cm^3, R the radius of the orbit, Z the atomic number of the scatterer, n is the index of fall off with radius of the magnetic field, A is the vertical semi-aperture of the vacuum chamber, T_i the kinetic energy of the particles at injection and eV is the energy gained per revolution near injection.

Equation (20) may be written as a condition on the gas pressure. If we assume that the gas in the vacuum chamber is air at 300°K, we obtain for the allowable pressure in mm Hg

$$0.667n(A^2/R^3)T_i eV\eta, \tag{21}$$

where A and R are measured in cm, and T_i and eV in kev. Note that (21) is independent of the mass of the particles being accelerated; it is thus applicable to all heavy-particle circular accelerators. If the gas in the vacuum chamber is not air, the factor 0.667 in (21) must be replaced by

$$303/\sum n_i Z_i^2\log(183Z_i^{-\frac{1}{3}}),$$

where n_i is the number of atoms of atomic number Z_i present in one molecule of the gas. For a synchrotron with straight sections, one of the R's in (20) and (21) should be replaced by $\frac{1}{2}\pi$ of the circumference.

Table I shows the pressure at which $\eta=0.089$, i.e., 10 percent of the particles are lost, for the two synchrotrons. We have taken $n=0.72$ in each case.

For 50 percent loss of particles the above pressures should be multiplied by 2.25. For a machine whose effective horizontal semi-aperture is less than its vertical, one may use (21) provided n is replaced by $(1-n)$; A then becomes the horizontal semi-aperture.

VII. ACKNOWLEDGMENTS

We are indebted to Dr. John Blewett for suggestions concerning the writing of this paper, to Dr. Hartland Snyder for several very valuable discussions of the scattering problem, and to Drs. T. H. Berlin and J. M. Greenberg for pointing out two errors in our original draft.

The Radial Dependence of the Tensor Force in the Deuteron

WILLIAM G. GUINDON, S. J.*
Massachusetts Institute of Technology, Cambridge, Massachusetts

(Received March 15, 1948)

The properties of the deuteron are discussed by means of a neutron-proton potential consisting of but two terms: ordinary force and tensor force, with different radial dependences. Assuming the latter to be square wells of different ranges, the wave functions corresponding to selected pairs of radii for the ordinary and tensor wells are computed, and from these the quadrupole moment is calculated. In summary, the results indicate that (a) no special pair of ranges appears preferred in the light of scattering experiments and of the comparison between observed and calculated magnetic moments, (b) the binding energies of heavy nuclei apparently limit the ordinary force range to about $(2.6\pm0.1)\times10^{-13}$ cm, and (c) all empirical data may be fitted, within experimental error, by a very simple potential with equal ranges: $-[1+S_{12}]J(r)$, with $J(r)$ a square well of depth 13.25 Mev, and of radius 2.663×10^{-13} cm.

I. INTRODUCTION

A PHENOMENOLOGICAL description of the neutron-proton system has been given by Rarita and Schwinger[1] which satisfactorily accounts for the empirical masses and magnetic moments of the neutron, proton, and deuteron, the measured quadrupole moment of the deuteron, and the experimental cross section for low energy neutron-proton scattering. Their essential contribution was the introduction into the neutron-proton potential,

$$V=-[1-g/2+(g/2)\boldsymbol{\sigma}_1\cdot\boldsymbol{\sigma}_2+\gamma S_{12}]J(r), \quad (1)$$

of the spin-dependent tensor operator

$$S_{12}=(3\boldsymbol{\sigma}_1\cdot\mathbf{r}\boldsymbol{\sigma}_2\cdot\mathbf{r})/r^2-\boldsymbol{\sigma}_1\cdot\boldsymbol{\sigma}_2. \quad (2)$$

As a result of this introduction, only the total angular momentum will, in general, be conserved, and the deuteron ground state must be described as a combination of states with all values of orbital angular momentum consistent with the total momentum and with parity: ${}^3S_1+{}^3D_1$. Simplifying the radial dependence of (1) to a square well of depth V_0 and radius r_0, they solved the Schroedinger equation for the deuteron subject to the assumption of the then current values for binding energy, quadrupole moment, and scattering cross section.[2] This calculation gave, for the choice: $r_0=2.8\times10^{-13}$ cm, the values

$$\begin{aligned} V_0&=13.89 \text{ Mev},\\ \gamma&=0.775,\\ g&=0.0715. \end{aligned} \quad (3)$$

In the process of obtaining these results the D-state probability (the fraction of the ground state with orbital angular momentum of two units) was found to be 0.039, in remarkable agreement with recent precise measurements of magnetic moments.[3]

II. NEUTRON-PROTON INTERACTION POTENTIAL

The smallness of the factor g of the spin-exchange interaction term as obtained by Rarita and Schwinger on the one hand, and the meson theories of nuclear forces on the other, suggest the potential

$$V=-[J_1(r)+\gamma S_{12}J_2(r)], \quad (4)$$

in which only ordinary and tensor force terms occur. It is expected, however, that J_1 and J_2 have different dependence upon the internucleonic separation, r. Substituting this potential and the ground state wave function,

$$\psi=(4\pi)^{-\frac{1}{2}}[u(r)/r+2^{-\frac{1}{2}}S_{12}w(r)/r]\chi_1{}^m, \quad (5)$$

into the Schroedinger equation, the following differential equations result:

$$\begin{aligned} &[d^2/dr^2+(M/\hbar^2)(E+J_1(r))]u(r)\\ &\qquad=-2^{\frac{1}{2}}\gamma[(M/\hbar^2)J_2(r)]w(r),\\ &[d^2/dr^2-6/r^2+(M/\hbar^2)(E+J_1(r)\\ &\quad-2\gamma J_2(r))]w(r)=-2^{\frac{1}{2}}\gamma[(M/\hbar^2)J_2(r)]u(r). \end{aligned} \quad (6)$$

* Now at Weston College, Weston, Massachusetts.

[1] W. Rarita and J. Schwinger, Phys. Rev. **59**, 436 (1941).

[2] Binding energy: 2.17 Mev, quadrupole moment: $+(2.73\pm0.05)\times10^{-27}$ cm², and scattering cross section: 20×10^{-24} cm².

[3] W. R. Arnold and A. Roberts, Phys. Rev. **71**, 878 (1947).

TABLE I. Interaction strengths and virtual singlet energies, for deuteron binding energy, E_0, equal to 2.184_1 Mev, and total scattering cross section equal to 21×10^{-24} cm².

r_0 (10^{-13} cm)	V_0 (Mev)	E_1 (kev)
2.40	16.415	65.28
2.50	15.079	65.21
2.60	13.896	65.13
2.70	12.844	65.06
2.80	11.904$_5$	64.99
2.90	11.061	64.92
3.00	10.302	64.86
3.10	9.617	64.79
3.20	8.996	64.73

Here $u(r)$ and $w(r)$ are the radial wave functions for S and D states, multiplied by r. For simplicity the radial dependences $J_1(r)$ and $J_2(r)$ are assumed to be square wells of common depth V_0 and of radii r_0 and ϵr_0, respectively. Consequently, in view of (4), the positive number ϵ is the ratio of the range of the tensor force to that of the ordinary interaction, while γ may be considered as the ratio of the strengths of these interactions.

Since in singlet states the potential (4) reduces to

$$V_s=-J_1(r), \tag{4'}$$

the value of the singlet state scattering cross section determines the value of V_0, the strength of the interaction. Experiment provides only the total scattering cross section; however, the theoretical triplet cross section is largely independent of the neutron-proton potential, and hence a semi-empirical singlet cross section can be deduced. Combining the experimental total cross section,[4]

$$\sigma(0)=(21\pm1)\times10^{-24}\text{ cm}^2, \tag{7}$$

with the triplet cross section, derived by Schwinger by a variational calculation,[5]

$$\sigma_t(0)=(4\pi/\alpha^2)[1+\alpha r_0+(\tfrac{3}{4}-4/\pi^2)(\alpha r_0)^2], \tag{8}$$

where r_0 and α have their usual meaning,[6] the singlet cross section is obtained as a function of the force range r_0. By equating this value of the singlet cross section to the zero-energy limit of the cross section calculated from the square well of depth V_0 and range r_0, we obtain finally the value of V_0 as a function of r_0. Values of V_0, and of the corresponding energy of the singlet virtual level, E_1, are given in Table I. The arbitrary selection of a pair of values for r_0 and ϵ is all that is required to make the solution of (6) unique, for by such a selection γ is implicitly determined: only one (non-vanishing) value will make the two equations (6) consistent.

III. THE RADIAL EQUATIONS IN DETAIL

We now find the solutions of (6) with methods very much akin to the ones used by Rarita and Schwinger. We will use the following abbreviations:

$$\begin{aligned}\alpha&=+[ME_0]^{\frac{1}{2}}/\hbar,\\ \alpha'&=+[M(E_0+2\gamma V_0)]^{\frac{1}{2}}/\hbar,\\ \kappa&=+[M(V_0-E_0)]^{\frac{1}{2}}/\hbar,\\ \kappa'&=+[M([1-2\gamma]V_0-E_0)]^{\frac{1}{2}}/\hbar,\\ \lambda&=+[2^{\frac{1}{2}}\gamma MV_0]^{\frac{1}{2}}/\hbar,\end{aligned} \tag{9}$$

$$\begin{aligned}x&=r/r_0,\\ y&=r/\epsilon r_0.\end{aligned} \tag{10}$$

The assumption of a square-well shape for both J_1 and J_2 leads to three cases, differing in the value of ϵ.

A. Range of Tensor Force Equal to Range of Ordinary Force: $\epsilon=1$

Region I: $r_0\geq r\geq0$.

Equations:

$$\begin{aligned}[d^2/dr^2+\kappa^2]u&=-\lambda^2w,\\ [d^2/dr^2-6/r^2+\kappa'^2]w&=-\lambda^2u.\end{aligned} \tag{11}$$

Solutions:[7]

$$\begin{aligned}u&=\Sigma(A_n+C_n\ln x)x^n,\\ w&=\Sigma(B_n+D_n\ln x)x^n.\end{aligned} \tag{12}$$

Region II: $\infty\geq r\geq r_0$.

Equations:

$$\begin{aligned}[d^2/dr^2-\alpha^2]u&=0,\\ [d^2/dr^2-6/r^2-\alpha^2]w&=0.\end{aligned} \tag{13}$$

[4] H. B. Hanstein, Phys. Rev. **59**, 489 (1941); D. Bohm and C. Richman, Phys. Rev. **71**, 567 (1947).

[5] Private communication.

[6] That is, r_0 is the radius of the single square well used in the variational calculation, and α is as defined in (9) of the present paper. All values of masses have been taken from the July 1946 Segrè chart; consistent with these values the binding energy of the deuteron is $E_0=2.184_1$ Mev.

[7] In all series solutions the summation is to be extended over all integers, $-\infty$ to $+\infty$.

Solutions:

$$u=Ae^{-\alpha(r-r_0)}+Ce^{+\alpha(r-r_0)},$$
$$w=Be^{-\alpha(r-r_0)}[1+3/\alpha r+3/(\alpha r)^2]+De^{+\alpha(r-r_0)}[1-3/\alpha r+3/(\alpha r)^2]. \quad (14)$$

B. Range of Tensor Force Less than Range of Ordinary Force: $\epsilon<1$

Region I: $\epsilon r_0\geq r\geq 0$.

Equations:

$$[d^2/dr^2+\kappa^2]u=-\lambda^2 w,$$
$$[d^2/dr^2-6/r^2+\kappa'^2]w=-\lambda^2 u. \quad (15)$$

Solutions:

$$u=\Sigma(A_n+C_n\ln y)y^n,$$
$$w=\Sigma(B_n+D_n\ln y)y^n. \quad (16)$$

Region II: $r_0\geq r\geq \epsilon r_0$.

Equations:

$$[d^2/dr^2+\kappa^2]u=0,$$
$$[d^2/dr^2-6/r^2+\kappa^2]w=0. \quad (17)$$

Solutions:

$$u=A'\sin\kappa r+C'\cos\kappa r,$$
$$w=B'[\sin\kappa r+(3/\kappa r)\cos\kappa r-(3/[\kappa r]^2)\sin\kappa r]+D'[\cos\kappa r-(3/\kappa r)\sin\kappa r-(3/[\kappa r]^2)\cos\kappa r]. \quad (18)$$

Region III: $\infty\geq r\geq r_0$.

Equations:

$$[d^2/dr^2-\alpha^2]u=0,$$
$$[d^2/dr^2-6/r^2-\alpha^2]w=0. \quad (19)$$

Solutions:

$$u=Ae^{-\alpha(r-r_0)}+Ce^{+\alpha(r-r_0)},$$
$$w=Be^{-\alpha(r-r_0)}[1+3/\alpha r+3/(\alpha r)^2]+De^{+\alpha(r-r_0)}[1-3/\alpha r+3/(\alpha r)^2]. \quad (20)$$

C. Range of Tensor Force Greater than Range of Ordinary Force: $\epsilon>1$

Region I: $r_0\geq r\geq 0$.

Equations:

$$[d^2/dr^2+\kappa^2]u=-\lambda^2 w,$$
$$[d^2/dr^2-6/r^2+\kappa'^2]w=-\lambda^2 u. \quad (21)$$

Solutions:

$$u=\Sigma(A_n+C_n\ln x)x^n,$$
$$w=\Sigma(B_n+D_n\ln x)x^n. \quad (22)$$

Region II: $\epsilon r_0\geq r\geq r_0$.

Equations:

$$[d^2/dr^2-\alpha^2]u=-\lambda^2 w,$$
$$[d^2/dr^2-6/r^2-\alpha'^2]w=-\lambda^2 u. \quad (23)$$

Solutions:

$$u=\Sigma(A'_n+C'_n\ln y)y^n,$$
$$w=\Sigma(B'_n+D'_n\ln y)y^n. \quad (24)$$

Region III: $\infty\geq r\geq \epsilon r_0$.

Equations:

$$[d^2/dr^2-\alpha^2]u=0,$$
$$[d^2/dr^2-6/r^2-\alpha^2]w=0. \quad (25)$$

Solutions:

$$u=Ae^{-\alpha(r-\epsilon r_0)}+Ce^{+\alpha(r-\epsilon r_0)},$$
$$w=Be^{-\alpha(r-\epsilon r_0)}[1+3/\alpha r+3/(\alpha r)^2]+De^{+\alpha(r-\epsilon r_0)}[1-3/\alpha r+3/(\alpha r)^2]. \quad (26)$$

The series coefficients, when the variable is x, satisfy the recurrence relations:

$$(n+1)(n+2)A_{n+2}+(2n+3)C_{n+2}+aA_n+cB_n=0,$$
$$(n+1)(n+2)C_{n+2}+aC_n+cD_n=0,$$
$$(n-1)(n+4)B_{n+2}+(2n+3)D_{n+2}+bB_n+cA_n=0,$$
$$(n-1)(n+4)D_{n+2}+bD_n+cC_n=0, \quad (27)$$

according to the definitions:

$$a=(\kappa r_0)^2,$$
$$a'=(\alpha r_0)^2,$$
$$b=(\kappa' r_0)^2,$$
$$b'=(\alpha' r_0)^2,$$
$$c=(\lambda r_0)^2. \quad (28)$$

When the variable is y, the coefficients satisfy the same relations with ϵr_0 in place of r_0 in the definitions (28), except that for C, Region II $-a'$ and $-b'$ must be put for a and b, respectively. Two types of series solutions occur, one in odd powers, one in even powers, differing in

TABLE II. Ratio of ranges, quadrupole moment, and D-state probability. Values enclosed in parentheses have not been computed directly, but derived from extrapolation on the other values, which have been calculated directly.

ϵ	r_0 (10^{-13} cm)	γ	Q (10^{-27} cm^2)	$^3D_1$
0.900	2.70	(1.2180)	(2.325)	(0.0396)
0.900	2.80	1.25103	2.505	0.0418
0.900	2.90	1.2843	2.692	0.0440
0.900	3.00	(1.3176)	(2.884)	(0.0462)
1.000	2.50	(0.9540)	(2.355)	(0.0400)
1.000	2.60	0.98218	2.555	0.0424
1.000	2.70	1.0107	2.760	0.0448
1.000	2.80	1.0392	2.971	0.0472
1.000	2.90	1.0680	3.189	0.0496
1.000	3.00	(1.0968)	(3.415)	(0.0520)
1.100	2.60	0.8405	2.871	0.0444

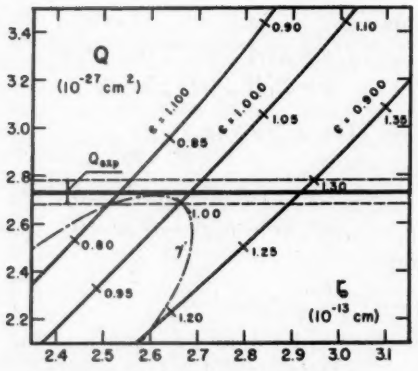

FIG. 1. Quadrupole moment of the deuteron plotted against ordinary force range. The three horizontal lines represent the experimental value of the quadrupole moment (full line) and its probable error (dashed lines): $Q=(2.73\pm0.05)\times10^{-27}$ cm². The three parallel curves connect points of equal range-ratio. Numbers given at intervals along these curves are values of γ interpolated from the computed values given in Table II. The dashed curve, marked γ', is intended to indicate roughly the limiting values of γ, required by the binding energy of heavy nuclei.

behavior at the origin. Coefficients of the odd-powers solution begin with A_1 and B_3 and can be expressed as linear combinations of these two; the A_0 and B_{-2} terms are the first non-vanishing ones in the even-powers solution and all subsequent coefficients can be reduced to combinations of these two.

The independent coefficients in these general solutions are determined by three types of conditions: regularity conditions at zero and at infinity, continuity conditions at internal boundaries, and the condition of normalization.

Depending on whether there are two or three regions in the case considered, the general solution contains eight or twelve independent coefficients. Correspondingly, eight or twelve equations in these coefficients are given by the vanishing of both u and w at infinity, by the vanishing of both functions at least as fast as r at the origin, and by the continuity of the functions and their first derivatives at r_0 and ϵr_0. These equations are linear and homogeneous in the unknown coefficients; the factors multiplying the coefficients are functions of γ, which is as yet undetermined. The only possible set of solutions for the coefficients, not all zero, is had when the determinant of the factors multiplying the coefficients vanishes. This determines γ: the correct value is found by trial and error, using as the criterion the vanishing of the determinant. All but one of the coefficients may now be expressed in terms of that one, and this determined by the normalization condition:

$$^3S_1+{}^3D_1=\int_0^\infty u^2dr+\int_0^\infty w^2dr=1. \qquad (29)$$

TABLE III. Ratios of ranges and of strengths of tensor and ordinary forces, and D-state probability, interpolated to give the experimental quadrupole moment: $Q=2.73\times10^{-27}$ cm². Values enclosed in parentheses are the results of interpolation on values similarly enclosed in Table II.

r_0 $(10^{-13}\,cm)$	$\epsilon_{2.73}$	$\gamma_{2.73}$	$(^3D_1)_{2.73}$
2.60	1.055	0.9037	0.0435
2.70	(0.993)	(1.0250)	(0.0444)
2.80	0.948	1.1489	0.0444
2.90	0.908	1.2677	0.0444
3.00	(0.871)	(1.3816)	(0.0445)

IV. COMPUTATIONS BASED ON THE WAVE FUNCTIONS

By the determination of the value of γ and of all the amplitude coefficients the wave function (5) is completely specified, and hence the means are at hand for calculating the quadrupole moment, here given by[8]

$$Q=(2^{\frac{1}{2}}/10)\int_0^\infty (uw-2^{-\frac{1}{2}}w^2)r^2dr. \qquad (30)$$

The value of Q has been computed for a selection of values for r_0 and ϵ, and the results are given in Table II, graphically in Fig. 1.

In the normalization process the value of a quantity important for comparison with experiment has been determined: the D-state probability, $^3D_1$. According to the hypothesis that the neutron and the proton retain their intrinsic magnetic moments in the deuteron and that the effect of relativity can be entirely neglected,[9] the deuteron magnetic moment is given by[10]

$$\mu_d=\mu_n+\mu_p-(3/2)(\mu_n+\mu_p-\tfrac{1}{2})(^3D_1). \qquad (31)$$

The best experimental values for the three

[8] Reference 1, p. 439.

[9] On this point several recent articles, containing fuller references, have appeared: Phys. Rev. **72**, 91, 118, 135 (1947).

[10] Reference 1, p. 440.

magnetic moments are taken to be[11]

$$\mu_n = -1.9103 \pm 0.0012 \text{ n. m.},$$
$$\mu_p = +2.7896 \pm 0.0008 \text{ n. m.}, \quad (32)$$
$$\mu_d = +0.85647 \pm 0.0003 \text{ n. m.},$$

which give a D-state probability of 0.040 ± 0.004.

Now the results given in Table II may be interpolated on to yield, for each value of the range r_0, that value of ϵ for which the quadrupole moment has the experimental value of 2.73×10^{-27} cm^2. Similar interpolations give the corresponding γ-values and D-state probabilities. These "correct" values, denoted as such by the subscript 2.73, are given in Table III.

V. DISCUSSION OF THE RESULTS

Consideration of the results as exhibited in Table III shows that the quadrupole moment is relatively sensitive to the ratio of the ranges of the two force components, and that the parameter γ varies strongly with r_0. The D-state probability corresponding to the correct value of the quadrupole moment is practically independent of the range of the ordinary force.

The results may be examined in the light of the criterion for acceptable values of γ, derived by Schwinger,[12]

$$\langle J_1(r)^2 \rangle_{Av} \geq \gamma \langle J_2(r)^2 \rangle_{Av} \quad (33)$$

where the averages are over the radius r. This rule expresses, in the form of a necessary condition on γ, the limitations on the potential (4) arising from the empirical constancy of the binding energy per nuclear particle in heavy nuclei. In the derivation of this rule the potential (4) is generalized, in the exchange force formalism, as the potential between the ith and the jth particles of the nucleus:

$$V_{ij} = (1/3)\tau_i \cdot \tau_j [\sigma_i \cdot \sigma_j J_1(r_{ij}) + \gamma S_{ij} J_2(r_{ij})]. \quad (34)$$

Assuming for the sake of definiteness that the wave functions in the relative coordinates of the ith and jth particles are all identical with the wave functions of the deuteron, estimated maximum values of γ are obtained for various values of the ratio of the force ranges. These values, designated γ', are tabulated in Table IV, and plotted in Fig. 1. In this figure all points, each of which corresponds to a pair of choices ϵ and r_0, which lie to the left of the curve γ' are allowed by this rough criterion, all to the right are forbidden. A glance at Fig. 1 shows that if this test has any validity, the correct range of the forces is about 2.6×10^{-13} cm. But this conclusion is open to obvious objections: (a) condition (33) is a necessary, not a sufficient, one, (b) the deuteron wave functions are surely not exactly applicable to heavier nuclei, (c) the curve of γ' is determined at but three estimated points, and (d) considerable indefiniteness is introduced by the experimental uncertainty in the quadrupole moment. And, even assuming the validity of the criterion, the square well form of the potential may certainly be questioned. Further study of high energy scattering may lead to the removal of some of this obscurity.

TABLE IV. Estimated limiting values of γ, required by constant binding energy per nuclear particle in heavy nuclei.

ϵ	γ'
0.900	1.184
1.000	1.000
1.100	0.817

One may conjecture, from the fact that when r_0 has the value 2.7×10^{-13} cm both ϵ and γ are practically unity, that nuclear data may be fitted by a very simple potential. All the experimental requirements considered in this research may be met by using

$$V = -[1 + S_{12}]J(r), \quad (35)$$

where $J(r)$ is a square well of depth 13.25 Mev, and of radius 2.663×10^{-13} cm, as determined by interpolation on Tables I and II.

It is a pleasure to acknowledge the stimulating helpfulness of Professor V. F. Weisskopf, under whose direction this work was carried out, and of Professor H. Feshbach. Special gratitude is due Dr. J. M. Blatt, and also Professor J. S. Schwinger of Harvard University, for helpful discussions of the problem.

[11] Reference 3, p. 885.
[12] Private communication.

Fission Excitation Functions

J. JUNGERMAN AND S. C. WRIGHT
Department of Physics and Radiation Laboratory, University of California, Berkeley, California
(Received March 19, 1948)

Excitation functions of the reactions U(α, fission), Th(α, fission), U(d, fission), Th(d, fission) were measured by use of alpha-particles and deuterons of maximum energies of 37.6 and 18.8 Mev, respectively. This was done using a stacked-foil technique. Recoil fission fragments were collected on aluminum "catchers" and their beta-activities formed a relative measure of the number of fissions occurring during a bombardment. An absolute calibration is described. If no competing processes are assumed, comparison with theory results in effective nuclear radii of 11.0×10^{-13} cm for the interaction of alpha-particles with uranium and 9.9×10^{-13} cm for the interaction of deuterons with uranium.

I. INTRODUCTION

FISSION induced in thorium and uranium of ordinary isotopic composition under alpha-particle, deuteron, and proton bombardment has been reported.[1] Measurements of the excitation functions of these reactions, using the higher energies available at the Berkeley sixty-inch cyclotron, have been attempted.

II. METHOD

Thorium or uranium coated aluminum foils placed alternately with aluminum "catchers" in a stack were bombarded with alpha-particles, deuterons, or protons. Later the beta-activities of the recoil fission fragments collected in these "catchers" foils were counted. If it is assumed for a particular reaction that the distribution of fission products is independent of the energy of the bombarding particle, then the measurement of these beta-activities at a given time after bombardment gives a relative excitation function. Evidence that this assumption is reasonable is presented under results. Absolute calibration of the cross sections was made possible by the measurements of E. Segrè. He used the Chicago pile to produce a known number of fissions in one of the foil stacks. The decay curve obtained from the beta-activity of one of these "catchers" provides an absolute cross-section scale assuming that counters of identical construction used in Berkeley and Chicago had the same efficiency for fragment activities when they had the same counting rates for a uranium glass standard. It must also be assumed that the complex of the fission products formed in the slow neutron and charged particle reactions have the same decay curves for a given number of fissions. It is fully realized that this last assumption is open to serious objections because of the probability of different composition of the product complexes in the various cases.

III. EXPERIMENTAL DETAILS

The thorium or uranium coated foils were prepared by being alternately painted with a solution of the nitrate on 0.001-in. aluminum and then baked at 550°C until the oxide was formed.[2] About 130 coats produced a 1 mg/cm^2 layer. Alpha-counting determined the amount of material per foil. Counting one foil with a mask in several positions showed the fissionable material on it to be uniform within 1.5 percent.

The collimating, energy, and current measuring equipment were similar to the apparatus used by Clark and Irvine[3] and will be described elsewhere.

The beta-activities of the fragments collected on the "catchers" were measured with cylindrical Geiger counters with 0.005-in. aluminum walls. Two bombardments were made for each of the following reactions: U(α, fission), U(d, fission), Th(α, fission), Th(d, fission), and one each with alpha-particles and deuterons on "catcher" aluminum.[4] The aluminum bombardments were

[1] G. Dessauer and E. M. Hafner, Phys. Rev. **59**, 840 (1941); E. Fermi and E. Segrè, Phys. Rev. **59**, 680 (1941); D. H. T. Gant, Nature **144**, 707 (1939); I. C. Jacobsen and N. O. Lassen, Phys. Rev. **58**, 867 (1940).

[2] T. Jorgenson, M.D.D.C. No. 467.

[3] E. T. Clark and J. W. Irvine, Phys. Rev. **66**, 213 (1944).

[4] We wish to thank Professor E. Segrè for the use of an unpublished Al(d; α, p) excitation function.

used to determine the "catcher" background activity. Bombardments were of 40 minutes to 90 minutes duration.

The beta-activity of the "catcher" foils was counted at standard times after bombardment, corrected for the aluminum background, and for counter coincidence when necessary. Then all counts were reduced to one microampere hour of particles incident upon a fixed number of uranium or thorium atoms. The initial beam energy was measured before and after each bombardment. Conversion to Mev from mg/cm^2 of aluminum was made using the range ratio of air to aluminum obtained by R. R. Wilson[5] and the range in air obtained by M. S. Livingston and H. A. Bethe.[6]

IV. RESULTS

Activities of the fission products in the various "catchers" of a foil stack remain in a constant ratio during the course of time within the limits of experimental error. This constant ratio indicates that the distribution of the fission products in the complex, for a given reaction, is independent of the energy of the particle causing the fission. This circumstance supports the use of the fragment activity as an indicator of the relative number of fissions occurring at different energies in a given reaction and also makes it possible to obtain a more accurate decay curve of the fragment complex of each reaction by averaging the activities of several of the associated "catchers."

Figure 1 shows the decay curves of the fission product complexes formed in the various reactions. To obtain these curves the activity of each of twenty or more "catchers" associated with a particular reaction was measured at a given time after bombardment. The average of these activities gives a point on the corresponding decay curve. All these curves are normalized to 100 c/m at 66 hours after the end of a bombardment.

Figure 2 shows the fission excitation functions measured. The absolute cross sections for the alpha-fission reactions were obtained by matching the recoil fragment decay curves directly to the slow neutron fission fragment decay curve at 2.75, 3.0, and 5.0 days and averaging. As a slow neutron fission fragment decay curve was not available beyond 5 days, the deuteron decay curves were matched to the thorium alpha-curve of Fig. 1 at 12, 28, and 42 days and averaged. The experimental probable error due to beta-counting, uniformity of foils, integrated current measurement, etc., is estimated to be about twenty percent.

This method was found inapplicable to proton-induced fission because the maximum proton energy (9.4 Mev) available was just above the fission threshold and therefore the aluminum background was prohibitive. This background activity was instead less than five percent of the fragment activity seven days after a short alpha-particle bombardment and twelve days after a short deuteron bombardment.

V. DISCUSSION

If no competing processes are assumed, a calculation of the cross section may be made by a method given by Bethe[7] and Bethe and

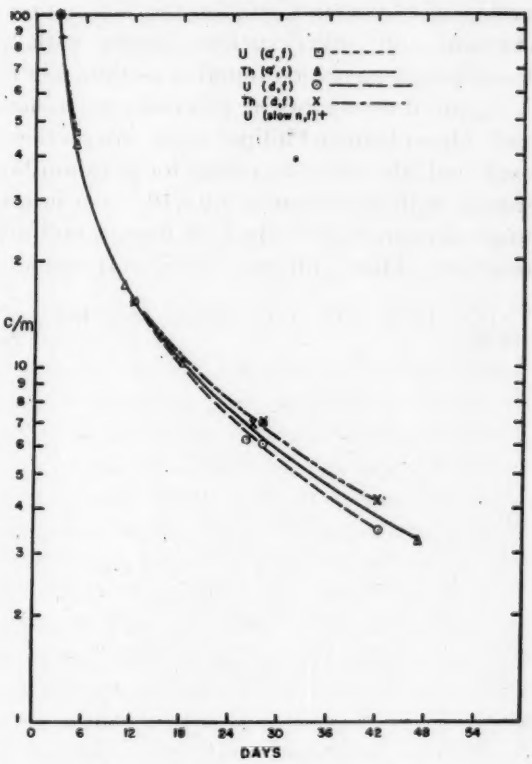

FIG. 1. Fission product decay curves.

[5] R. R. Wilson, Phys. Rev. 60, 749 (1941).
[6] M. S. Livingston and H. A. Bethe, Rev. Mod. Phys. 9, 261 (1937).
[7] H. A. Bethe, Rev. Mod. Phys. 9, 177 (1937).

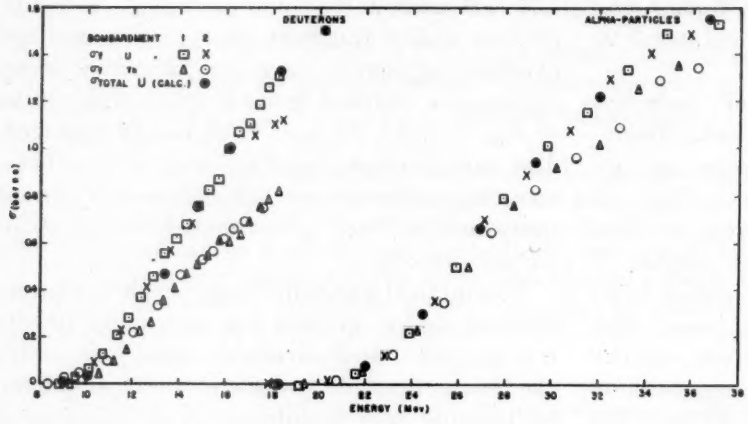

FIG. 2. Fission excitation functions.

Konopinski.[8] According to this treatment

$$\sigma_{\text{total}} = \pi\lambda^2 \sum_l (2l+1)P_l. \qquad (1)$$

σ_{total} is the total cross section for formation of the compound nucleus. λ is the wave-length of the incident particle divided by 2π. P_l is the probability of penetration of the incoming wave having an angular momentum $l\hbar$ with respect to the nucleus. Using (1), an effective nuclear radius of 11.0×10^{-13} cm for the interaction of uranium and alpha-particles agrees with the U(α, fission) excitation function as shown in Fig. 2. Again, if no competing processes are assumed and Oppenheimer-Philips type interaction is neglected, the effective radius for uranium bombarded with deuterons is 9.9×10^{-13} cm in order to get agreement with the U(d, fission) excitation function. These nuclear radii correspond to $1.78\times10^{-13}A^{\frac{1}{3}}$ cm and $1.60\times10^{-13}A^{\frac{1}{3}}$ cm for the interaction of alpha-particles and deuterons, respectively. In each case, the theory predicts that bombardments on thorium should give higher total cross sections at a given energy than the same particle bombarding uranium. Since the opposite is observed, it appears that there is more competition with the fission process for bombardments on thorium than on uranium.

[8] H. A. Bethe and E. J. Konopinski, Phys. Rev. **54**, 130 (1938).

VI. ACKNOWLEDGMENT

We wish to thank Professor R. Serber for some theoretical discussions and Mr. M. C. Walske for some calculations. Thanks are also due the crew of the 60-in. cyclotron for their valuable cooperation. We are indebted to Professor E. Segrè for his stimulating guidance and for suggesting this problem, which is part of a general program of determination of excitation functions.

High Energy States of N_2^+ and N_2*

R. B. SETLOW
Sloane Physics Laboratory, Yale University, New Haven, Connecticut
(Received April 7, 1948)

The rotational structure of the $C-X$ bands of N_2^+ has been analyzed. A rotational perturbation appears in the $v=0$ level of the C state. Evidence is presented against postulating a vibrational perturbation in the $v=0$, $v=1$ levels of this state. Construction of potential curves using the new rotational data shows that previous assignments of vibrational levels are incorrect. A new vibrational numbering is proposed, which is in conformity with the Franck-Condon principle. The use of the Franck-Condon principle in predicting intensities in collisions of the second kind has been verified. Measurement of the rotational structure of the $c-X$ bands of N_2 shows that the c state is the $v=1$ level of the b' state. The vibrational analysis confirms this identification, as does the intensity distribution. Perturbations between states p' and b' are discussed. Evidence is cited to show that the c state of Worley is identical with the p' state of Gaydon.

A. THE $C-X$ SYSTEM OF N_2^+

1. Introduction

THE more intense bands of the N_2^+ spectrum around 1860A were discovered by Birge and Hopfield.[1] They were first identified by Watson and Koontz,[2] using a ten-foot normal incidence spectrograph having a dispersion of about 5.5A/mm. The bands represent transitions from an upper electronic state $C\,^2\Sigma_u^+$ to the ground state of N_2^+, $X\,^2\Sigma_g^+$. In addition, Watson and Koontz found many weaker bands, using a condensed discharge in pure nitrogen. The strong bands, on the other hand, are brought out by a condensed discharge in helium containing nitrogen as an impurity. Additional weak bands were discovered by Takamine and co-workers.[3] No bands were found with upper vibrational quantum number v', less than 5 (using the assignments given by Watson and Koontz). Moreover, the intensity distribution was by no means normal. Levels with $v'=8$ or more were strongly enhanced. The explanation for this intensity anomaly was given by Watson and Koontz in pointing out that collisions of the second kind between ionized helium atoms and N_2 in the ground state would raise unexcited N_2 to the $v=8$ level of $C\,^2\Sigma_u^+$ of N_2^+. An additional point of interest was an observed discontinuity of about 6 cm^{-1} in vibrational levels at $v'=8$.

In an effort to understand this discontinuity more fully, the rotational structure of this system of bands has been measured. Moreover, a rotational analysis of these bands supplies evidence concerning the validity of the Franck-Condon principle as applied to collisions of the second kind.[4]

2. Data

The plates used were those obtained by Watson and Koontz. The vibrational analysis and intensity distribution are given in their paper. The bands measured, together with accompanying information, are given in the following tables.

All bands except 5–6 show only the P branch resolved. The 5–6 band shows one line of the R branch. All bands show the expected alternation of intensities, even though the P branch is blended with lines of the returning R branch. This is simply due to the fact that the returning R lines have higher K values than the P lines with which they blend, and hence are of lower intensity. The intensity alternation then has the same character as the P branch; lines with even K are strong. Since none of the bands shows evidence of a Q branch, it is reasonable to suppose that the transition involved is $^2\Sigma_u^+ \rightarrow {}^2\Sigma_g^+$. The lower state of this transition,

* Part of a dissertation presented to the faculty of the Graduate School of Yale University in candidacy for the degree of Doctor of Philosophy.

[1] R. T. Birge and J. J. Hopfield, Astrophys. J. **68**, 257 (1928).

[2] W. W. Watson and P. G. Koontz, Phys. Rev. **46**, 32 (1934).

[3] T. Takamine, T. Suga, and Y. Tanaka, Sci. Pap. I.P.C.R. **36**, 437 (1939).

[4] R. E. Meyerott, Phys. Rev. **71**, 553 (1947).

TABLE I. Observed rotational lines of the $C-X$ bands of N_2^+ (in cm^{-1}).

Band 5–6	K_P		K_P
51,983.0	$R(0)$	51,939.6	8
973.2	2	926.8	10
962.6	4	913.5	12
951.9	6	906.8	13
Band 8–9	K_P		K_P
52,240.3	2	52,084.3	20
231.0	4	070.8	21
225.9	5	057.5	22
219.6	6	042.8	23
213.7	7	028.1	24
206.2	8	012.0	25
198.7	9	51,997.2	26
190.9	10	981.0	27
181.9	11	964.1	28
173.6	12	946.8	29
165.3	13	929.6	30
154.4	14	910.8	31
142.9	15	893.0	32
132.7	16	872.0	33
121.8	17	854.9	34
109.4	18	834.8	35
097.3	19	813.8	36
		772.3	38

TABLE II. Summary of values of B' and ν_0 for the $C^2\Sigma_u^+$ state of N_2^+ (in cm^{-1}).

v'	B'	Estimated error	Measured from band	ν_0
5	1.62	0.02	5–6	51,979.1
	1.62	0.03	5–5	53,995.0
7	1.513	0.002	7–5	
8	1.492		8–6	58,070.2
	1.493		8–8	54,155.5
	1.492		8–9	52,248.2
	1.493		8–10	50,376.2
	1.494		8–11	48,540.1
	av. 1.493	0.001		
9	1.480	0.003	9–11	50,516.3
10	1.476	0.002	10–12	50,660.7
11	1.472	0.003	11–12	52,573.7
	1.469	0.002	11–13	50,809.1
	av. 1.470	0.002		

$D' = 2.0 \times 10^{-6} \pm 20$ percent
(determined from bands 8–8, 8–9, and 8–10)

the ground state of N_2^+, has been measured by Coster and Brons.[5] Since B'' is known, we may find B' from $B'-B''$ as found from measurements on one branch. Since all the bands show essentially the same structure, the complete data for only two typical ones are presented (see Tables I and II).

The accuracy of these measurements depends, of course, upon those of the ground state.

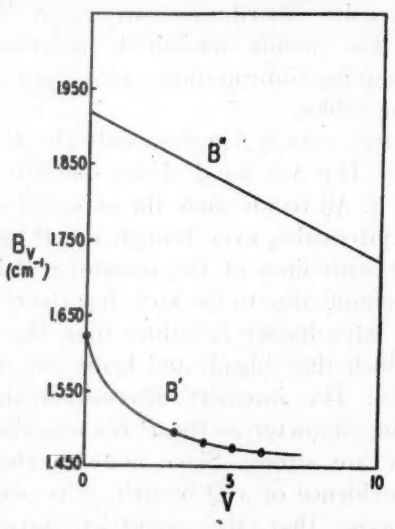

FIG. 1. B_v *versus* v for the C and X states of N_2^+.

[5] D. Coster and H. H. Brons, Zeits. f. Physik **73**, 747 (1932).

Judging from the internal consistency of the results, the ground state B values are certainly good to within the errors of these measurements.

A plot of B_v *versus* v is shown in Fig. 1. The vibrational numbering is in accord with the reassignment given below. For $v'>8$ this is the usual straight line. Below this there is a marked deviation from the usual course. The explanation for this is not clear. Perhaps it is due to a perturbation by one of the many repulsive states of N_2^+ in this region. It is interesting to note that the discontinuity in the B_v-v curve occurs where there is a suspected discontinuity in the vibrational structure.

3. Discussion of Results

From a knowledge of the B values one can compute approximate potential curves using a Morse function. For the ground state of N_2^+ the data of Coster and Brons were used. The potential curves are shown in Fig. 2a. The equilibrium separation for the ground state of N_2, about 1.1A, is indicated by the vertical line.

If the Franck-Condon principle is to be obeyed, transitions should take place straight up and down for the more intense bands, or, quantum mechanically, the larger the overlap integral, the more intense the transition. A cursory glance at these potential curves will show that if they are correct the Franck-Condon principle does not hold. For instance, a transition from $v'=5$ would have a maximum somewhere in the neighborhood of $v''=12$, not $v''=5$ as

observed. Likewise transitions from other levels are also at variance with observed intensities. Another anomaly exists in the method of excitation of the $v=8$ level. The mechanism of this excitation is as follows. The ionization potential of N_2 is 15.53 volts (see Worley[6]). This represents a transition from the ground state of N_2 to the ground state of N_2^+. The energy of the $v'=8$ level above the ground state of N_2^+ is 8.72 volts. Thus this excited level is 24.30 volts above the ground state of N_2. Transitions from this level are strongly enhanced in a discharge in helium, which has an ionization potential of 24.46 volts. Thus a collision of the second kind between ionized helium atoms and N_2 in the ground state can excite the $v'=8$ level and a few higher ones, while the helium takes the extra electron and goes to its ground state without radiation. Because of the rather close energy resonance, one would expect that the cross section for this process would be large. Thus the distance of closest approach of ion and molecule is large. We might expect the Franck-Condon principle to hold for a collision of this sort. The potential curves in Fig. 2a indicate that an upward transition from the N_2 ground state to the $v'=8$ level is not too probable. It is even less so for the levels $v'=9$, 10, 11, which are also enhanced, although not as much as $v'=8$.

If we wish to bring the observed emission intensities into agreement with those predicted by the Franck-Condon principle, it is necessary to change the vibrational numbering of the upper state. The proper change to make is from $v'=5$ to $v'=0$, and so on. This reassignment does not conflict with observed data, since, using the previous vibrational assignment, no transitions from $v'<5$ are observed. While this renumbering will change the vibrational constants slightly, it will not alter the general shape of the potential curve for the upper $C^2\Sigma_u^+$ state. Thus the new potential curve is derived from the old one simply by a shift of five vibrational levels, as shown in Fig. 2b.

The transition from $v'=3$ to the ground state of N_2^+ is indicated by the right-hand solid line. This transition should have maximum intensity for $v''=9$, 10. Such is indeed the case. A subsidiary maximum representing a transition from the left side of $v'=3$ to the ground state should appear around $v''=0$, 1. These bands are not observed, perhaps because of the masking effect of the prominent $a-X$ system of N_2. According to the new numbering, transitions from $v'=1$ will have maximum intensity for $v''=6$ and $v''=1$. Again this agrees with observation. Similar analyses for other transitions yield results in accordance with observation. The one striking anomaly seems to be the intensity of the 3–6 band. One would expect this band to have a rather low intensity. It does not. This band has been given the triple assignment 2–5, 3–6, 4–7. Of the three possibilities, the 2–5 transition seems to have the greatest transition probability, especially if one recalls that the deviation toward higher B values (smaller r) seems to set in at this point (see Fig. 1). If this band is assigned to the transition $v'=2\rightarrow v''=5$, we then find B_2 (the previous B_7) $=1.513$ cm^{-1}. This point falls on the B_v *versus* v curve of Fig. 1.

To obtain agreement between the Franck-Condon principle and the observed intensities,

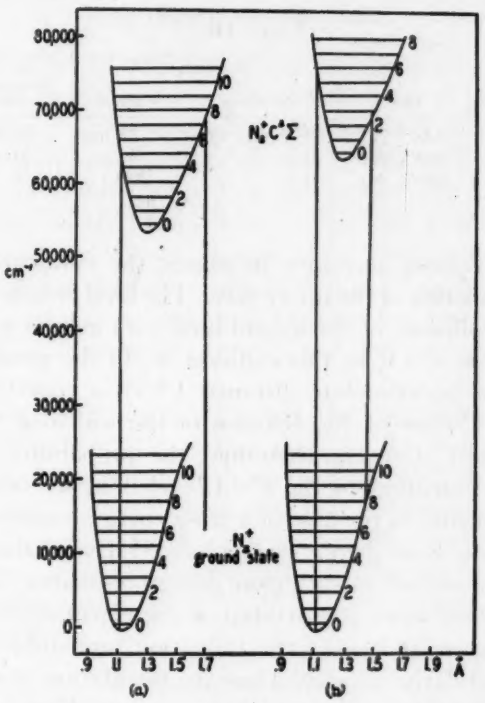

FIG. 2. Potential energy curves for the C and X states of N_2^+: (a) Previous vibrational assignments; (b) corrected assignments.

[6] R. E. Worley, Phys. Rev. 64, 207 (1943).

TABLE III.

Spectrogram	Gas	Pressure	Current	Exposure time
1	100% N_2	0.05 mm Hg	25 ma	24 hr.
2	100% N_2	0.3	35	20
3	100% N_2	0.5	200	8

it has been necessary to change the vibrational numbering of the upper state. The level enhanced by collisions of the second kind with helium ions is now $v'=3$. In this collision N_2 in the ground state (internuclear distance 1.1A) is raised to the C state of N_2. Because of the width of the ground state eigenfunction, the probability of the transition to the $v'=3$ level is appreciable, especially in the case of a close energy resonance as we have here. The enhanced levels above $v'=3$ are not in such close energy resonance, but in these cases the overlap of the eigenfunctions is larger and hence the transition probability is still relatively large. Thus the population of the C state by collisions of the second kind also seems to obey the Franck-Condon principle. The vibrational states $v'=0$, 1, 2 are probably populated by collisions of the second kind between N_2 in the ground state and the metastable $a\,^1\Pi_g$ state of N_2. Again these transitions obey the Franck-Condon principle.

The discontinuity in the rotational structure is probably due to a perturbing state. The perturbation manifests itself in an increase in B'. This means that the perturbation increases with the value of K, and since the rotational level spacing is increased above normal, the perturbing state lies below the $v'=3$ level. The perturbing state must be a Π-state.

For perturbations between Π- and Σ-states, as is the case in this work, no vibrational perturbation should appear. This implies, however, that band origins are used in computing vibrational constants. Such is not the case for the majority of bands in the $C-X$ system. Band heads have been measured. A comparison of the band origins calculated from the heads with the measured origins shows differences as high as 3 cm^{-1}. Because of inaccuracies in the data and the presence of a rotational perturbation, one is justified in concluding that the vibrational perturbation does not exist.

B. THE b' AND c STATES OF N_2

1. Introduction

A system of bands in the far ultraviolet, found by Birge and Hopfield,[1] was tentatively identified by them as a transition from an upper electronic state b' to the ground state of N_2, designated $X\,^1\Sigma_g^+$. Watson and Koontz[2] were able to confirm this identification by rotational structure analysis. They obtained $B'=1.147$ cm^{-1} and identified the upper state as $^1\Pi$. Subsequently Tschulanowsky,[7] working with high members of the ground state progression, showed that the upper state was not $^1\Pi$ but $^1\Sigma_u^+$. He obtained $B'=1.144$ cm^{-1}. The latter worker also found the $v=1$ ($B=1.142$ cm^{-1}) level of the b' state, and was thus able to identify Watson and Koontz's d and e states as vibrational levels 2 and 3, respectively, of b'.

The results of the above investigators thus indicate four vibrational levels of the b' state. The ground state progression from $v'=0$ extends from $v''=4$ through 21. The progression from $v'=1$, on the other hand, only goes from $v''=18$ through 21. The short length of this progression is surprising, especially since the progression from $v'=2$ is about three times as long. In general one would expect the $v'=1$ progression to be somewhat similar to that from $v'=0$.

If the positions of these missing bands are calculated, they fall in the approximate position of another ground state progression observed by Birge and Hopfield, the progression from the state designated as c. The $0-0$ band of this progression has been tentatively identified in absorption by Worley,[6] who obtained $B'=1.92$ cm^{-1} for the upper state. Thus this state cannot possibly be the $v'=1$ level of b'.

There is one additional factor to note. The c state, as observed in emission by Birge and Hopfield, extends from lower state vibrational numbers 5 through 13. The length of this progression is very difficult to account for on the assumption that Worley's c state is the same as Birge and Hopfield's c state. In an effort to straighten out these difficulties, spectrograms in the vacuum ultraviolet were taken of a discharge in pure nitrogen.

[7] W. M. Tschulanowsky, Bull. Acad. Sci. U.R.S.S. 1, 1313 (1935).

2. Experimental Procedure

The instrument used for the present investigation was a grazing incidence spectrograph using a 15,000 line per inch grating of twenty-one foot radius of curvature. The dispersion was about 1A per mm. A description of this spectrograph will be given elsewhere. The light source was a condensed discharge in a π-shaped water-cooled discharge tube 30 cm long and of internal diameter 1.0 cm. Three spectrograms were obtained. The pertinent information for each spectrogram is given in Table III. The nitrogen flowing continuously through the discharge tube and then into the spectrograph (maintained at a pressure of less than 10^{-4} mm Hg) was tank nitrogen passed over hot CuO. Hydrogen and oxygen showed up as atomic lines on all plates. The slit width was about 0.025 mm. The plates used were Eastman 103–0 U.V. sensitized, developed in D-19.

Spectrograms 1 and 2 were essentially the same. They showed little rotational structure. Spectrogram 3 showed a well developed rotational structure. Portions of the spectrograms are shown in Fig. 3.

3. Method of Analysis

The plates were reduced by assuming that the wave-length was a quadratic function of plate distance. The unknown constants were found using the standard lines given by Boyce.[8] Wave-lengths found from this expression were then corrected by use of a correction curve. If the wave-length range is about 150A, the maximum correction is of the order of 0.010A. The limitations of this method lie in the scarcity of readily available standard lines in the vacuum ultraviolet.

Let us tentatively identify the progression in the neighborhood of that due to the c state as caused by transitions from the $v=1$ level of the b' state. The rotational structure of these bands was measured on all three plates. The measurements agreed to within a few tenths of a wave number. Averages of the three spectrograms are reported.

4. Rotational Structure

Since the rotational structure of none of the bands measured was completely resolved, it was only possible to measure $B'-B''$. Thus to find B' we must know B''. To evaluate B'' the data

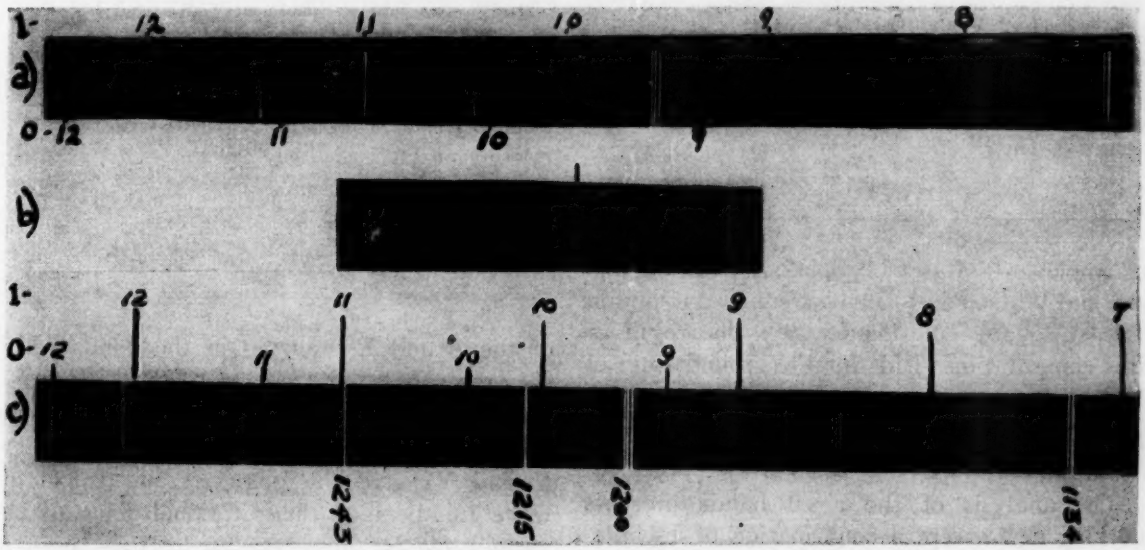

FIG. 3. Spectrograms of the $b'-X$ system of N_2; (a) Spectrograms 1 and 2 (actual size)—note the intensity alternation in the b_0' progression and the peculiar intensity distribution of the b_1' progression; (b) enlargement (3.4×) of the 1–9 band to show rotational structure; (c) Spectrogram 3—focus not as good as in spectrograms 1 and 2, but much higher intensity. Note the many rotational lines as compared with a.

[8] J. C. Boyce, Rev. Mod. Phys. 13, 1 (1947).

TABLE IV. Observed and calculated rotational lines of the $b'-X$ system of N_2 (in cm^{-1}).

Observed	Obs.-calc.	J_P	Calculated	J_R	Calculated	Remarks
Band 1–7						
88,714.4						head, all lines
666.5	−1.2	6	88,667.1	9	88,669.0	ss diffuse
654.3	−1.8	7	654.7	10	656.8	s
641.0	−0.6	8	640.8	11	643.1	
625.8	−1.4	9	625.5	12	628.0	
612.3	0.9			13	611.4	
609.2	0.6	10	608.6			
593.0	0.6	11	590.4	14	593.4	s
580.2	5.3			15	574.9	? ss
568.2	−2.5	12	570.7			s
552.1	0.2	13	549.6	16	553.0	
530.5	2.3	14	527.0	17	530.7	
504.1	−1.5	15	503.0	18	506.9	
479.5	0.6	16	477.5	19	481.6	
453.1	−0.4	17	450.6	20	454.9	
425.9	2.3	18	422.1	21	426.7	
394.7	−0.8	19	392.3	22	397.1	
224.4	6.1	24	215.3	27	227.3	?
Band 1–8						
86,586.1						head
542.6	2.2	6	86,539.5	9	86,542.3	s
529.1	−0.3	7	527.3	10	530.5	ss
516.0	1.1	8	513.7	11	517.2	
502.2	1.0	9	498.7	12	502.5	
484.5	0.8	10	482.3	13	486.4	
468.1	0.6	11	464.5	14	469.0	s
455.0	−4.9			15	450.1	ss
444.1	−1.1	12	445.2			ss
429.3	1.4	13	424.2	16	429.8	diffuse from
405.3	0.9	14	402.6	17	408.1	here on
382.5	−0.5	15	379.2	18	384.9	
357.5	1.2	16	354.3	19	360.4	
302.7	0.1	18	300.3	21	307.1	
275.6	−0.3	19	271.1	22	278.3	
Band 1–9						
84,485.9						head
455.5	1.8	5	84,452.1	8	84,455.3	
443.3	0.9	6	441.6	9	445.3	s
430.6	−1.1	7	429.7	10	433.8	ss
418.2	0.8	8	416.4	11	421.0	
404.8	−1.5			12	406.8	
397.7	−4.1	9	401.8			?
385.7	−1.1	10	385.7	13	391.2	
372.6	1.3	11	368.3	14	374.3	s
358.5	2.5			15	356.0	? ss
346.7	−2.8	12	349.5			ss
339.5	3.2			16	336.3	?
327.6	−1.8	13	329.4			
307.4	−2.0	14	307.9	17	315.2	
288.5	−0.4	15	285.0	18	292.8	
260.5	−0.2	16	260.7			
242.7	−1.0	17		20	243.7	
211.9	−2.1	18	208.1	21	217.2	
190.5	−1.3			22	189.2	
152.8	0.9	20	149.9		159.9	

TABLE IV.—*Continued.*

Observed	Obs.-calc.	J_P	Calculated	J_R	Calculated	Remarks
Band 1–10						
82,415.0						head
391.7	0.4	4	82,390.2	7	82,393.6	
374.5	2.2	6	370.8	9	374.9	s
361.7	−0.5	7	358.7	10	363.9	ss
347.7	0.1	8	345.7	11	351.6	
338.2	0.6			12	337.6	
318.6	0.6	10	315.7	13	322.5	
303.0	−0.6	11	306.1	14	298.7	s
290.8	3.0			15	287.8	ss
279.0	−1.3	12	280.3			
240.1	0.6	14	239.5			
194.4	1.4	16	193.0			
Band 1–11						
80,377.5						head
349.7	0.3	4	80,352.0	8	80,348.1	
341.0	0.0	5	343.3	9	338.6	s
335.4	2.2	6	333.2			
324.4	−1.5	7	321.8	10	327.9	ss
309.6	0.5	8	309.1			
299.0	−1.1	9	295.1	12	302.6	
280.7	0.9	10	279.8			
264.6	1.3	11	263.3			s
254.7	−0.1			15	254.8	ss
243.6	−2.4	12	245.3			ss
225.2	−1.0	13	226.2			
205.0	−0.6	14	205.6			
195.6	0.1			18	195.5	
182.1	−1.8	15	183.9			ss
176.4	3.4			19	173.0	
161.9	1.1	16	160.8			
148.0	−1.3			20	149.3	
136.2	−0.2	17	136.4			
109.3	−1.4	18	110.7			
095.5	−1.3			22	096.8	
081.4	−2.3	19	083.7			
054.5	0.1	20	054.4			
042.5	−0.2			24	042.7	
023.7	−2.2	21	025.9			
79,994.3	−0.6	22	79,994.9			
977.7	−0.7			26	79,978.4	
963.5	1.9	23	961.6			
925.4	−3.8	24	929.2			
893.9	−1.9	25	895.8			
872.5	−4.9			30	877.4	?
857.7	−0.7	26	858.4			
777.6	−4.7	30	782.3			?
Band 1–12						
78,364.8						head
352.6	−1.2	2	78,354.5	6	78,352.4	
339.6	−0.5	4	341.1	8	338.1	
330.3	−1.0	5	332.5	9	329.0	s
323.4	0.7	6	322.7			
315.2	−3.7			10	318.7	s
299.0	−0.1	8	299.1			
294.7	0.5			12	294.2	
271.2	0.6	10	270.6			
256.2	1.8	11	254.4			s
245.6	−2.5			15	248.1	ss
233.6	−3.4	12	237.0			ss
217.4	−0.9	13	218.3			
197.0	−1.3	14	198.3			

of Appleyard,[9] Rasetti,[10] Spinks,[11] Tschulanowsky and Watson and Koontz were used to obtain a least squares solution for B''. The result of this computation yields for the ground state of N_2:

$$B_0 = 2.0007 \pm 0.0027 \text{ cm}^{-1},$$
$$\alpha = 0.01869 \pm 0.00017 \text{ cm}^{-1}.$$

The analysis of the $v'=0$ bands presents nothing new except a confirmation of Tschulanowsky's designation of this state as a Σ-state. The previous designation of Π by Watson and Koontz was due to an almost exact superposition of the P and R branches in the bands which they measured.

Since the data for the $v'=1$ level are of some interest, they are presented in detail. Tables IV, V and VI give the observed and calculated wave numbers of the rotational lines of the various bands. The calculated values used in finding the observed-calculated values are taken as the center of the P and R branch lines. Strong lines are weighted twice.

The lines with even J are observed to be strong, except in the blending of weak and

[9] E. T. S. Appleyard, Phys. Rev. **41**, 254 (1932).
[10] F. Rasetti, Phys. Rev. **34**, 367 (1929).
[11] J. W. T. Spinks, Can. J. Research **20**, 1 (1942).

strong lines in the P and R branches. Unusually strong lines are indicated by s or ss. Blends of the two branches are, in general, diffuse.

Tschulanowsky gives for the b' state

$$B_0' = 1.144 \text{ cm}^{-1}, \quad B_1' = 1.142 \text{ cm}^{-1}.$$

The close agreement with our values is good reason for assigning the bands observed in this work to the b' state.

5. Vibrational Structure

As a further check on the assignment of these bands to the $b'-X$ system, let us consider the vibrational structure. The present data plus those of Tschulanowsky and Watson and Koontz are shown in Table VI. All wave numbers refer to band origins. For the bands of $v'=2$, 3, the origins have been calculated from band head measurements. This undoubtedly introduces an error.

The bands measured in this work fit so well in the Deslandres table that there can be no doubt that they are the vibrational level $v=1$ of the b' state.

To find the vibrational constants of this state, the following procedure was adopted. The energy levels of the ground state of N_2 are rather well known. Knowing these values, the energy of each vibrational level of state b' measured from $v=0$ of the ground state may be found. We thus obtain the following vibrational energies with their probable errors (see Table VII). Solution gives:

$$E_0 = 103{,}678.9 \pm 0{,}3 \text{ cm}^{-1},$$
$$\omega_0 = 746.9 \pm 0.6 \text{ cm}^{-1},$$
$$\omega_0 x_0 = 4.82 \pm 0.23 \text{ cm}^{-1}.$$

These values are in good agreement with those of Tschulanowsky except for E_0 (he gives 103,767.1 cm^{-1}). However, Tschulanowsky's value for E_0 is obtained by an extrapolation from his data, and since the N_2 ground state ΔG *versus* v is no longer a straight line in the region of these data, the extrapolated value of E_0 is bound to be wrong.

If terms in v^3 are included, the vibrational constants change quite radically.

6. Discussion of Results

We may now use the accumulated spectroscopic data to construct potential energy curves for the b' and ground state of N_2. These potential energy curves are shown in Fig. 4. The potential energy curve for b' has been found using a Morse function, which is a rather good approximation near the potential minimum. In the ground state, however, we are interested in the shape of the potential curve up to $v=21$. Over this range a Morse curve is badly in error. The broken line curve is a Morse function for the ground state of N_2, while the solid line gives a corrected potential curve as given by Hulbert

TABLE V. Summary of data on $b'\,{}^1\Sigma_u^+$ state of N_2 (in cm^{-1}).

Band	B'	Probable error	ν_0	Remarks
0–10			81,672.0	
0–11	1.149	0.020	79,632.2	
0–12	1.158	0.015	77,618.6	
0–13	1.151	0.010	75,634.7	
0–14	1.143	0.003	73,679.0	
0–15	1.140	0.003	71,744.4	beyond accurate
av.	1.143	0.002		plate calibration
1–7	1.146	0.008	88,711.7	
1–8	1.143	0.003	86,583.4	
1–9	1.145	0.010	84,484.2	
1–10	1.141	0.008	82,412.7	
1–11	1.144	0.003	80,374.2	
1–12	1.137	0.008	78,362.9	
1–13			76,380.0	
av.	1.143	0.001		

TABLE VI. Deslandres table for the system $b'-X$ of N_2.

$v''\backslash v'$	0		1		2		3
4					95,996.3		
5					93,778.8		
6					91,594.8		
7			88,711.7	734.5	89,446.2		
8			86,583.4	735.6	87,319.0		
9			84,484.2	731.4	85,215.6		
10	81,672.0	740.7	82,412.7	734.8	83,147.5	723.8	83,871.3
11	79,632.2	742.0	80,374.2	738.1	81,112.3	715.9	81,828.2
12	77,618.6	744.3	78,362.9				79,811.1
13	75,634.0	746.0	76,380.0				77,832.6
14	73,679.2						
15	71,755.9						
16	69,863.4						
17	67,992.9						
18	66,163.5	741.6	66,905.1				
19	64,358.4	740.6	65,099.0				
20	62,583.2	741.6	63,324.8				
21	60,839.3	739.8	61,579.1				

TABLE VII. Vibrational energies of the b' state (in cm^{-1}).

Energy	First difference	Second difference
$E_0 = 103{,}678.8 \pm 0.4$		
	742.5 ± 0.6	
$E_1 = 104{,}421.1 \quad 0.5$		11.4 ± 1.5
	731.1 1.4	
$E_2 = 105{,}152.4 \quad 1.3$		7.0 2.1
	724.1 1.6	
$E_3 = 105{,}876.5 \quad 1.0$		

and Hirschfelder.[12] The difference is appreciable for high vibrational states.

An important point to note in the upper state is the large spread in the eigenfunction (about 1.2–1.7A). Because of this width, we obtain a very long $v'=0$ ground state progression, extending from $v''=4$ through 21. The ground state progression from the $v'=1$ level should be of about the same length, although in this case there should be some bands missing at the center of the progression. If we assume that the Birge and Hopfield c state is $v=1$ of b', then the observed bands are 1–5 through 1–14, and 1–18 through 1–21. Thus again we get good qualitative agreement. The observed intensity maximum is around $v''=9$. This also agrees qualitatively with the Franck-Condon principle.

If we apply the Franck-Condon principle to $v=2$, 3, we would predict additional bands, especially in the neighborhood of 2–20 and 3–5, 3–20. It is planned to look for these bands at a later date.

We conclude that qualitatively the intensity distribution is given by the Franck-Condon principle, thus offering another check on the identification of the vibrational levels of the b' state.

One additional point should be noted. To obtain the emission spectrum $b'-X$ it is necessary to populate state b from the ground state of N_2. Since the vibrational levels in the ground state are about one quarter of a volt apart, by far the great majority of the N_2 molecules are in the zero vibrational state. The probability of an upward transition $v''=0 \rightarrow b$ is rather small, because of the very low value of the overlap integral. Also any absorption of light representing a downward transition from b' to a high vibrational level of the ground state will be vanishingly small because of the small population of these high lying levels. Thus the observed intensity will depend primarily on transitions from $v''=0$ to the b' state. Since the probability of these transitions is small, we would expect the over-all intensity of these bands to be small compared with other electronic transitions. This point is verified by noting that in emission the intensity of the $b'-X$ system is not too far from the intensity of the $a-X$ system of bands. But, as shown by Herzberg,[13] the $a-X$ transition is a forbidden transition in that it is $g-g$, and it thus has a smaller intensity than an electric dipole transition by a factor of 10^4.

It now remains to correlate the $v=1$ level of the b' state with other observed states. There are three other known states of N_2 of about the same energy. They are:

(a) p' (Gaydon[14])
$E=104{,}327.9\ cm^{-1}$ $B=1.93\ cm^{-1}$

(b) c (Worley)
$E_R=104{,}365.6$ $B=1.92$
$E_Q=104{,}316.1$

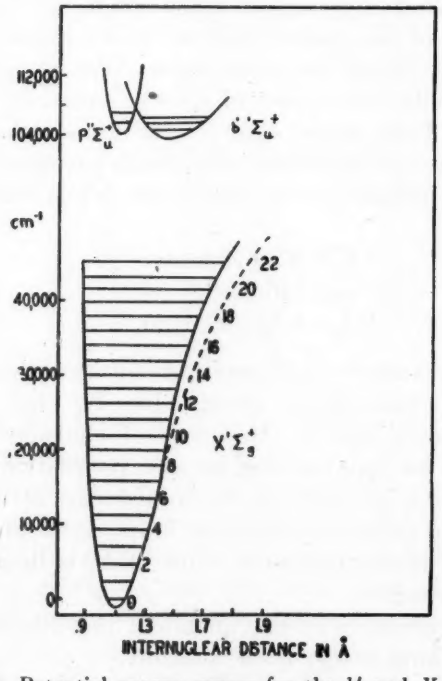

FIG. 4. Potential energy curves for the b' and X states of N_2.

[12] H. M. Hulbert and J. O. Hirschfelder, J. Chem. Phys. 9, 61 (1941).

[13] G. Herzberg, Phys. Rev. 69, 362 (1946).

[14] A. G. Gaydon, Proc. Roy. Soc. A182, 286 (1944).

(c) c (Birge and Hopfield)
$E_R = 104{,}394.6$
$E_Q = 104{,}318.7$

As far as states p' and c (Worley) are concerned, the B values preclude any possibility of their being $v=1$ of b'. Furthermore, it seems highly probable that these states are identical, now that Worley's c state cannot be identified with the rather long ground state progression of $v'=1$. If Gaydon's data, verified by Janin,[15] are used to calculate the position of the head of the $0-0$ band of $p'-X$ and also the position of the first strong lines of the P branch, one obtains:

$$\nu_{\text{head}} = 104{,}377 \text{ cm}^{-1}, \quad \nu_P = 104{,}320 \text{ cm}^{-1}.$$

The agreement between these values and Worley's c state is good, especially since the head is formed by lines somewhere around $J=30$, where the intensity has begun to fall off. It should be noted that the observation of the transition $c-X$ in emission is almost impossible, because of the large self-absorption.

The difficulty in correlating Birge and Hopfield's c state with the first vibrational level of b' lies in their observation of the $c-X$ system as double-headed bands. These measurements

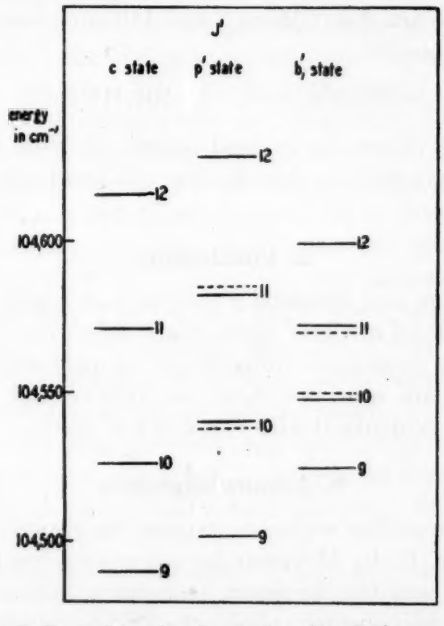

FIG. 5. Perturbing levels of the p' and b' states. For comparison, the rotational levels of the c state are shown. If this state is distinct from p', then a different set of perturbations in b' would be found.

[15] J. Janin, Ann. d. Physik 1, 538 (1946).

TABLE VIII. Rotational levels of the p' and b' states (in cm^{-1}).

J	(p' state)	(b' state)	Diff.
9	104,501.7	104,524.0	22.3
10	104,540.2	104,546.8	6.6
11	104,582.7	104,572.0	−10.7
12	104,629.0	104,599.4	−29.6

were taken at low dispersion (15A per mm) and thus would be expected only to reproduce the gross features of these bands. In our higher dispersion spectrograms, the $v'=1$ progression appears as two unusually strong lines surrounded by many weak ones, the intensity falling off away from these lines. Qualitatively one would expect that under low dispersion these bands would appear as symmetrical doublets, as observed by Birge and Hopfield.

7. Perturbations between p' and b'

The explanation of this intensity anomaly follows. Gaydon's p' state (or Worley's c state) is a $^1\Sigma_u^+$ state and thus has the proper symmetry to perturb the $v=1$ level of b', which is also $^1\Sigma_u^+$. Perturbation will only occur for equal J values in the two states. Moreover, to be noticeable, the energy difference between the two states must be small. The rotational levels of the p' state are given by:

$$\nu = 104{,}327.9 + 1.93J'(J'+1),$$

while the rotational levels of $b'(v=1)$ are given by:

$$\nu = 104{,}421.1 + 1.143J'(J'+1).$$

Table VIII gives the calculated values for rotational levels 9, 10, 11, and 12.

According to Table VIII, we would expect maximum perturbation for $J'=10$, 11, with rapidly decreasing effects on either side of these values. Moreover, since the perturbation depends on the overlap of the eigenfunctions involved, we would expect a rather small effect, since the overlap integral is small, as in the case of the ground state and b'. Figure 5 shows the perturbed (broken-line) and unperturbed positions of these levels.

The probability of a transition from the ground state ($B=2.007$ cm^{-1}) to the p' state ($B=1.93$ cm^{-1}) is high, since the internuclear separation

is about the same for the two states. Because of the perturbation between p' and b', we expect the perturbed levels of b' to have a population above normal. Thus transitions from these levels will not only be displaced, but will show up as unusually strong lines. Note that lines originating from these levels in the R branch are $J_R=9$, 10, while those in the P branch are $J_P=11$, 12.

Because of the blending of the two branches near the head, it is not possible to detect any perturbation in this region. However, the strong intensity lines agree well with those for $J_R=9$, 10. The line with $J_R=10$ is by far the most prominent. This, however, may be due to better line separation.

An examination of Table IV shows that in all cases the measured energy for the lines $J_P=11$ is greater than the calculated value, while the reverse is true for $J_P=12$. The average observed minus the calculated value of $J_P=11$ is 2.6 ± 0.8 cm^{-1}, while for $J_P=12$ the difference is -2.5 ±0.5 cm^{-1}. This is in good qualitative agreement with prediction. The $J_P=12$ lines are the stronger.

An additional factor to note is the large deviations shown for the lines assigned as $J_R=15$. These lines are also unusually strong, as are their neighbors $J_P=11$, 12. It appears probable that the assignment $J_R=15$ is incorrect. The lines should be assigned to transitions from the $J=10$, 11 levels of the p' state.

The average difference between these lines and the perturbed $J_P=11$ lines is 11.4 ± 0.8 cm^{-1}. The $J=10$ level of the p' state is 11.8 cm^{-1} lower than the corresponding level of b', and gives rise to a line 11.8 cm^{-1} lower than $J_P=11$. This agrees well with the predicted value 11.4 cm^{-1}. The average difference from the perturbed $J_P=12$ line is 11.6 ± 0.4 cm^{-1}. The $J=11$ level of the p' state is 15.7 cm^{-1} higher than the corresponding level in b', and gives rise to a line 15.7 cm^{-1} higher than $J_P=12$. Again this agrees well with the calculated value, 11.4 cm^{-1}. Because of the proximity of these two lines, originating in the p' state, they are not resolved, but appear as a single line of high intensity.

Transitions from the p' state to high vibrational levels of the ground state would not ordinarily be possible because of the very small value of the overlap integral, but as a result of the mixing of first approximation eigenfunctions, the overlap integral for the perturbing and ground state may have an appreciable value. The large population of the p' state would then imply an appreciable intensity for these lines. Confirmation of the above interpretation is supplied by the works of Gaydon and Janin. The former, in analyzing the transitions from the p' state to the $a\,^1\Pi_g$ state, remarks that the rotational structure cannot be analyzed beyond $J'=10$ because of the strong perturbations at this point. Janin's data for the p' state (which he called c) also show perturbations for these levels. Tschulanowsky also shows perturbations for $J'=10$, 11, although he had no unusually strong lines, since the right-hand side of the potential curve from which his transitions take place is not overpopulated, as is the left, because of the short life of these levels. He observes no transitions from the p' state, since, again, such transitions would involve much larger changes in internuclear distances than are observed here.

We have seen that there are two groups of strong lines in the bands arising from transitions $v=1$ of b' to the ground state. The centers of these groups are about 40 cm^{-1} and 120 cm^{-1} from the band heads. The violet edges of these groups are about 35 cm^{-1} and 110 cm^{-1} from the heads, or at

$$\nu=104{,}386\ cm^{-1}, \quad \nu=104{,}311\ cm^{-1}.$$

These values are in good agreement with Birge and Hopfield's values for the two heads of their c system.

8. Conclusions

Birge and Hopfield's c state is in reality the $v=1$ level of the b' state. Since Worley's c state would produce a different set of perturbations than are observed here, we believe that this state is identical with Gaydon's p' state.

9. Acknowledgments

The author wishes to express his appreciation to Dr. R. E. Meyerott for suggesting the problems, and for the many stimulating discussions with him during this work. He also wishes to thank Dr. W. W. Watson for making his plates of N_2^+ available, and for helpful discussions concerning this phase of the work.

The Role of the Cathode Surface in Sparking Phenomena*

HAROLD JACOBS AND A. P. LAROCQUE
Sylvania Electric Products, Inc., Chemistry Laboratory, Kew Gardens, New York

(Received March 22, 1948)

Experimental data related to the minimum sparking potentials of barium, magnesium, and aluminum cathodes in helium, neon, argon, krypton, and xenon are summarized. The cathode material is found to play a major role in the sparking potential. Several applications are included.

1. INTRODUCTION

UNTIL 1922, the role of cathode phenomena in gas discharge devices was not appreciated. Largely because of the influence of the Townsend research group, it was thought that the initiation of electrons through the gas discharge was brought about by ionization of the gas by positive ions. Physicists of that period thought that the same sparking characteristics could be obtained independently of materials used on the electrodes. At this time, however, Holst and Oosterhuis[1] studied sparking voltages in inert gases by use of different electrode materials. They observed that at low pressures near the minimum sparking potentials, the sparking voltages "for the same gas varied by a factor of two or more depending on the electrode material, the potential being found lower, the lower the work function of the surface."

These findings were very important historically since they pointed towards the fact that at reduced pressures the cathode played a major role. It was this thinking which led to a revision of opinion concerning the liberation of the electrons prior to and just at the time of sparking. It pointed towards the later views that the mechanism of sparking was partly concerned with the liberation of electrons from the cathode surface by positive ion bombardment.

To this day, however, the mechanism of the spark is much disputed. In the period following 1923 there was much experimentation. Most of this was done under experimental conditions where the investigators were not aware of the importance of minute impurities in the gas, such as mercury, oxygen, water, etc. Consequently, there was much disagreement in the experimental data available and the theory suffered accordingly.

Bowls[2] and Hale[3] in 1938 and 1939 carried out careful investigations and showed the importance of mercury vapor in the vacuum systems. They showed that faint traces of mercury vapor, such as obtained from gauges, could mask the effect of the cathode. Unfortunately, Bowls chose nitrogen, a gas which could react with the electrodes. Had he chosen an inert gas highly purified and with the electrodes freed of any contaminants, including gases, his results would probably have been more reliable.

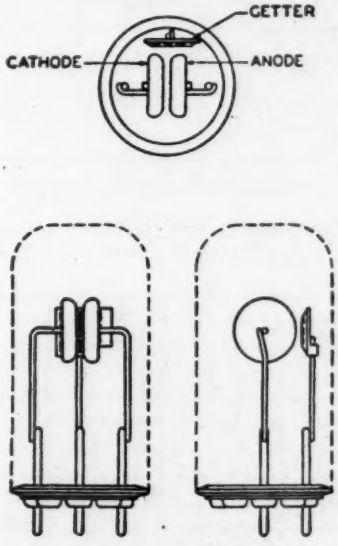

FIG. 1. Experimental tube.

* This work was undertaken in association with the Applied Physics Laboratory of the Johns Hopkins University under Section T Series Contract NOrd 7872, sponsored by the Bureau of Ordnance United States Navy.

[1] L. B. Loeb, *Fundamental Processes of Electrical Discharges in Gases* (John Wiley and Sons, Inc., New York, 1939), p. 381; Holst and Oosterhuis, Phil. Mag. **46**, 1117 (1923).

[2] W. E. Bowls, Phys. Rev. **53**, 293 (1938).

[3] D. H. Hale, Phys. Rev. **55**, 815 (1939).

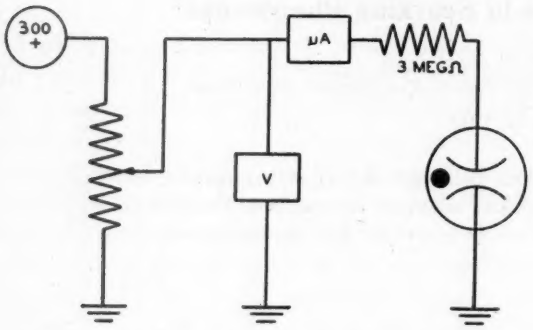

FIG. 2. Circuit for measuring sparking potential.

Because of the lack of care in regard to mercury, most of the data until this time were only approximate at best and usually quite erroneous in regard to minimum sparking potentials of inert gas combinations with various metallic electrodes. It was, therefore, found necessary to determine the minimum sparking potential when the information was needed by direct experiment in our own laboratories.

2. EXPERIMENTAL NOTES

Experimental diodes were made up as in Fig. 1. These diodes consisted of two electrodes made of "Grade A" nickel and a getter-container holding the material to be studied. The electrodes were cut so as to form surfaces creating uniform fields. With these electrodes it was possible to make quantitative measurements of the field between the cathode and the anode.

The tubes to be studied were sealed on the vacuum system together with a getter tube containing only a standard barium-aluminum getter. The latter was flashed just prior to testing to collect impurities such as oxygen, nitrogen, and hydrogen in the gas which was later to be admitted. During pumping out, the tubes and manifold were heated in an oven at 400°C for twenty minutes to drive off contaminations from the glass parts. Following bake-out, the electrodes were heated to roughly 900°C brightness for two or three minutes. The containers in each tube were then degassed as completely as possible prior to the evaporation onto the electrodes of the metal to be tested. The gas was then admitted into the vacuum system from a standard Airco Bottle (99.9+ percent pure). It should be noted that in the case of the helium, neon, and argon, liquid air was used at all times between the mercury manometer and the remainder of the vacuum system. This includes the time during the oven bake-out of the tubes. For krypton and xenon dry ice and methanol baths were used.

The sparking potentials were measured as a function of pressure times distance. The spark was observed by a sudden rise in current. (See Fig. 2.) However, before measurements were made, the tubes were tested for stability. That is, each tube was allowed to pass 3 microamperes of current. If the current and voltage were

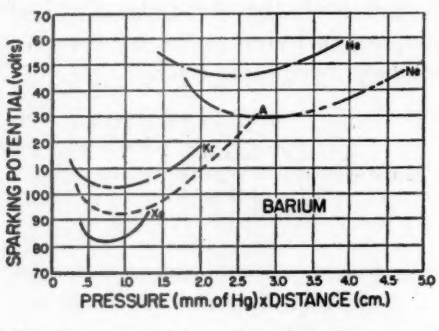

FIG. 3. Sparking potential as a function of pressure times distance for barium.

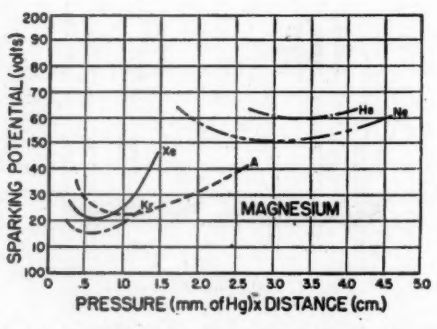

FIG. 4. Sparking potential as a function of pressure times distance for magnesium.

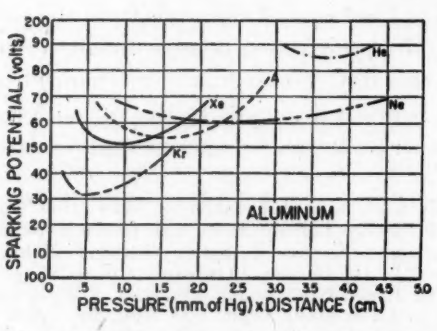

FIG. 5. Sparking potential as a function of pressure times distance for aluminum.

constant, as a function of time, a stable cathode surface was assumed to exist. A scope was used to insure that no oscillations were taking place during these measurements.

3. DATA

The sparking potentials of barium, magnesium and aluminum in the five inert gases are illustrated in Figs. 3, 4, and 5, respectively. It is noted that both sparking potentials and pressure times distance (min.) are functions of the gas and the cathode surface. Each curve represents an average of from three to eight tubes. That is, for a given surface and a given gas representing one of the lines in Figs. 3, 4, or 5, three to eight different tubes were utilized to get the data. Altogether 90 tubes were used during these experiments. Although the distance was varied as much as 100 percent, i.e., 1 millimeter to 2 millimeters, the average deviations in sparking potential were very slight, in some cases less than one percent. In general, as the gas increased in atomic weight there was a tendency for the minimum sparking potentials to be lower, although this does not hold in all cases. Also, the sparking potential seems directly related to the work function as in Fig. 6.

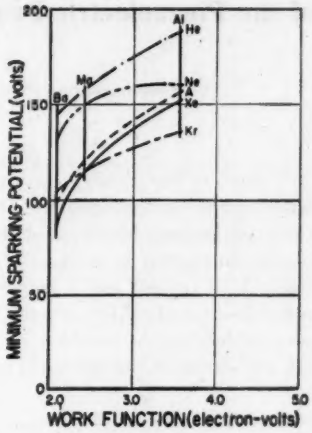

FIG. 6. Minimum sparking potential as a function of the surface work function.

4. CONCLUSIONS AND APPLICATIONS

We can conclude from these experiments that the cathode material plays a major role in the sparking potential of a cold-cathode gas discharge for a given gas at reduced pressures, i.e., in the vicinity of the minimum sparking potentials. In general, a lower work function has been found to indicate a lower minimum sparking potential for the materials studied thus far.

Acknowledgment is made to Mr. G. C. Rich of the Kew Gardens Laboratory, Sylvania Electric Products, Inc., for his active help during the course of this work.

Effect of the Piezoelectric Properties of a Crystal on Diffuse X-Ray Reflections

DAVID C. MILLER*
Department of Physics, Washington University, St. Louis, Missouri
(Received April 2, 1948)

A study of the diffuse x-ray reflections from piezoelectrically oscillating quartz and ammonium dihydrogen phosphate (ADP) crystals showed no increase in intensity during oscillation. Quantitative measurements of the intensity increase of the Laue and Bragg reflections during oscillation showed an increase of about 160 percent for the quartz, 7.7 percent for a 0.015 inch thick ADP crystal and 4 percent for a rochelle salt crystal. The intensity increase of Laue reflections for the ADP crystal was shown to be dependent upon its orientation. Since there was no decrease in intensity of the diffuse reflections, it eliminates the possibility that they are the source of the increased energy in the Laue and Bragg reflections.

I. INTRODUCTION

WHEN a quartz crystal, which is being used to diffract a beam of x-rays, is caused to oscillate piezoelectrically, in most cases the intensity of the diffraction pattern increases.[1–5] This raises the question as to the origin of the increased energy made available for diffraction.

G. E. M. Jauncey and W. A. Bruce undertook a careful study of the effect the oscillation would have on the intensity of the diffuse or background scattering, hoping to find a decrease sufficient to explain the intensity increase of the Bragg and Laue spots. However, no detectable change was found in the diffuse scattering intensity. Next, it was suggested that the main beam was the source of the additional energy, but no reproducible experiment showed any change in main beam intensity or shape during oscillation of the crystal.

Thus, when the existence of diffuse reflections was pointed out by J. Laval[6] and A. P. R. Wadlund,[7] it seemed worth while to see if these maxima would decrease in intensity when the crystal was being oscillated, thus at least partially explaining the problem of how energy is conserved in this experiment.

II. APPARATUS

A specially built, copper target x-ray tube, used with an x-ray spectrometer having a Geiger tube as a detector, was the heart of the apparatus. A scale of 128 counting circuit made it possible to cover a wide range of intensities. The spectrometer was built so that it could be easily converted from Geiger tube detection to photographic recording.

Three types of crystals, quartz, rochelle salt, and ADP ($NH_4H_2PO_4$) were used in the course of the investigation.

The x-ray tube, a cross-sectional view of which is shown in Fig. 1, is novel insofar as both the filament-target distance and the filament-focusing cup distance are easily adjustable, even while the tube is in operation. Since the maximum possible intensity is necessary in a study of diffuse maxima, this flexibility in the x-ray tube insured the maximum possible x-ray yield. The tube was continuously pumped and, although the new silicone DC 703 oil was used in the diffusion pumps, together with a dry ice-acetone trap, it was still found necessary to clean the water-cooled demountable target after every twenty-four hours of operation.

A second feature of the tube was the turnbuckle arrangement on the filament shown in Fig. 2, which enabled the filaments to be kept under a tension without a spot-welding job. This made the task of changing filaments quite simple.

The Geiger tube, operated with 1350 volts on the center wire, was one purchased from the North American Phillips Company, Inc. It was specially constructed for use as an x-ray detector and proved very satisfactory.

* Now at Montana State University, Missoula, Montana.
[1] C. S. Barrett and C. E. Howe, Phys. Rev. **39**, 889 (1932).
[2] J. M. Cork, Phys. Rev. **42**, 749 (1932).
[3] G. W. Fox and J. M. Cork, Phys. Rev. **38**, 1420 (1931).
[4] F. Klauer, Physik. Zeits. **36**, 208 (1935).
[5] M. Y. Colby and S. Harris, Phys. Rev. **46**, 445 (1934).
[6] J. Laval, Bull. Soc. Fr. Min. **62**, 137 (1939).
[7] A. P. R. Wadlund, Phys. Rev. **53**, 843 (1938).

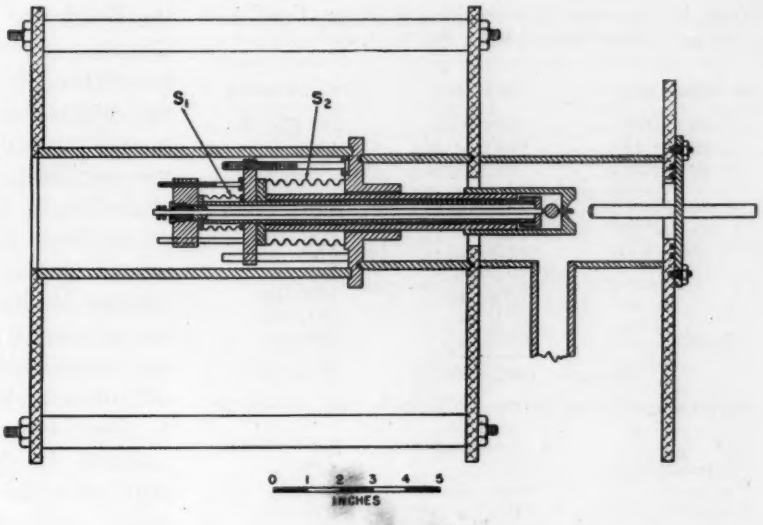

FIG. 1. Cross-sectional view of x-ray tube using sylphons S_1 and S_2 to permit the adjustment of the filament-focusing cup and the filament-target distance, respectively. This could be done even when the tube was in operation by using an insulated screw driver.

III. PROCEDURE

The quartz crystal was a 6.03-megacycle Y-cut crystal with a thickness of 0.0131 inch and a diameter of 1 inch. The crystal was mounted in the grid circuit of a conventional Pierce type oscillator.

Two 45° Z-cut ADP crystals were used. One was $\frac{1}{4}$ inch by 1 inch by $1\frac{1}{2}$ inches and oscillated at 40 Kc. The other was 0.672 inch by 0.969 inch by 0.015 inch and oscillated at 72 Kc. Both crystals were plated with aluminum foil on the 1 inch by $1\frac{1}{2}$-inches and the 0.672-inch by 0.969-inch faces, respectively. The rochelle salt crystal used was a 45° Y-cut crystal, 1 inch by $1\frac{1}{4}$ inches by $\frac{1}{4}$ inch, which had a resonant frequency of 40 Kc.

The crystals were placed in holders and a transmission rotation photograph of the diffraction pattern taken. This allowed the finding of the Bragg lines and the adjustment of the crystal so that the equatorial plane of the diffraction pattern coincided with the plane of motion of the Geiger tube.

Having once found the Bragg lines with the Geiger tube, the crystal was displaced about one degree from the Bragg position. The diffuse maximum remained where the Bragg line had been and measurements of its intensity while the crystal was oscillating and not oscillating gave the required data. A photograph of a diffuse maxima and accompanying Laue spot, taken while an ADP crystal was oscillating, is shown in Fig. 3. The fact that no doublet structure appears is probably due to the use of a thin unpolished crystal and relatively wide slits ($\frac{1}{32}$ inch).

It should be noted that in this paper the use of the term Bragg line means a line caused by the characteristic copper x-ray spectrum, whereas the use of the term Laue spot indicates a spot caused by the unfiltered background radiation. This method of distinguishing between the effects of characteristic and background radiation when both are present is convenient and has been used previously.[8]

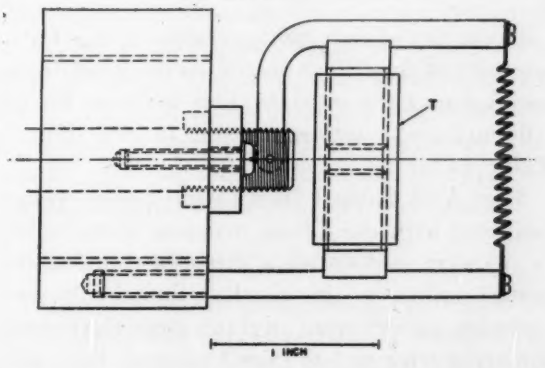

FIG. 2. View of turnbuckle arrangement used to keep filament from sagging and eliminating need to spot-weld the ends of the filament. One screw in turnbuckle T is made of an insulating material to prevent shorting of the filament.

[8] G. E. M. Jauncey and O. J. Baltzer, Phys. Rev. **59**, 699 (1941).

TABLE I. Variations in intensities of Bragg, Laue, and diffuse spots using a quartz crystal.

A. Diffuse spots	Oscillating	Non-oscillating
1. $\Delta\Theta=+26'$	$284\pm9c/m$	$292\pm9c/m$
2. $\Delta\Theta=+32'$	$108\pm3c/m$	$112\pm3c/m$
3. $\Delta\Theta=+51'$	$56\pm2c/m$	$56\pm2c/m$
B. Laue spots	**Oscillating**	**Non-oscillating**
1. $\Theta=76°\ 25'$	$1710c/m$	$805c/m$
	$1677c/m$	$777c/m$
	$1707c/m$	$798c/m$
	$1720c/m$	$789c/m$
	$1694c/m$	$761c/m$
	$1668c/m$	$766c/m$
Average	$1696\pm50c/m$	$783\pm30c/m$
Ratio of oscillating to non-oscillating = 1696/783 = 2.16		
	Oscillating	**Non-oscillating**
2. $\Theta=76°\ 06'$	$1927c/m$	$929c/m$
	$1980c/m$	$899c/m$
	$1973c/m$	$979c/m$
	$2039c/m$	$902c/m$
	$1938c/m$	$893c/m$
	$1952c/m$	$928c/m$
	$1968\pm60c/m$	$922\pm30c/m$
Ratio of oscillating to non-oscillating = 1968/922 = 2.13		
C. Bragg line	**Oscillating**	**Non-oscillating**
$\Theta=75°\ 34'$	$518c/s$	$194c/s$
	$515c/s$	$194c/s$
	$512c/s$	$196c/s$
	$515c/s$	$196c/s$
	$533c/s$	$198c/s$
	$520c/s$	$198c/s$
	$512c/s$	$194c/s$
	$520c/s$	$198c/s$
Average	$518\pm15c/s$	$196\pm6c/s$
Ratio of oscillating to non-oscillating = 518/196 = 2.54		

IV. EXPERIMENTAL RESULTS

It was found that no detectable change in the intensity of the diffuse maximum occurred during oscillation of the crystals. This is shown for the 6.03-megacycle quartz crystal in the data in Table I.

Part A of Table I shows some typical results obtained with the diffuse maxima. Three values of $\Delta\Theta$ were used to see if the crystal orientation would influence the results. Sufficiently long counting periods were used to reduce the random counting error to less than 1 percent, but variations in filament current, high voltage supply, and the target surface make an over-all 3 percent error possible in the data.

Part B shows the increase of intensity in the Laue spot upon oscillation and Part C shows the effect on the Bragg line. It will be noted that the Bragg line intensity increased by a factor of 2.5 when the crystal was oscillating. This illustrated the effect which has often been obtained for quartz but for which there is not much quantitative data.[9,10] Since the quartz crystal was oscillating in its thickness mode, there were antinodes of displacement at the surfaces and an antinode of pressure in the interior of the crystal. Since the increase in intensity occurs because of the decreased extinction accompanying a pressure antinode, it can be seen that only by using the Laue transmission method of obtaining a diffraction pattern could one hope to observe an intensity change.

Table II shows the data obtained for the 0.015-inch thick ADP crystal. Work with the larger ADP crystal gave no results since the reflecting faces of the crystal were at antinodes of displacement, and the x-ray tube did not have enough power to give a transmission photograph.

Part A of Table II shows the effect of the

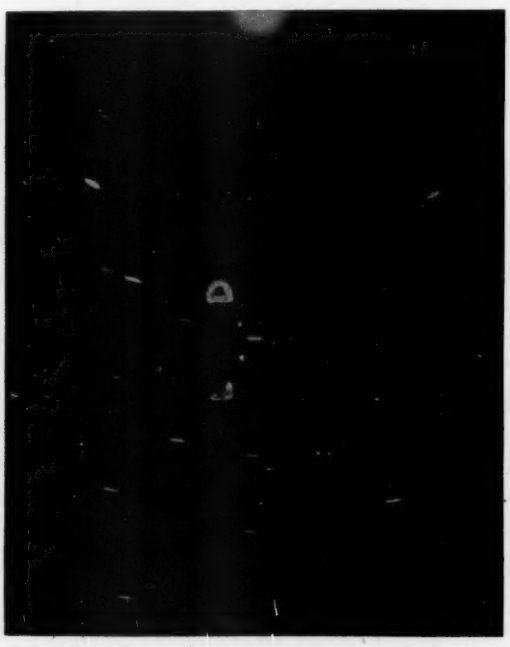

FIG. 3. Photograph of a Laue (*L*) and accompanying diffuse spot (*D*) for an ammonium dihydrogen phosphate (ADP) crystal. Exposure time: 14 hours at 20 milliamperes and 25,000 volts. Copper target with no filters.

[9] G. E. M. Jauncey and W. A. Bruce, Phys. Rev. **54**, 163 (1938).
[10] G. E. M. Jauncey and J. H. Deming, Phys. Rev. **48**, 462 (1935).

oscillation on the Bragg line. It will be noted that the 7.7 percent increase in intensity is much less than that obtained with quartz but still is much greater than the experimental error. The difference in effect as compared with quartz seems to be bound up with the fact that quartz is a relatively "perfect" crystal with a high characteristic temperature. On the other hand, an ADP crystal is an imperfect crystal with a low characteristic temperature. Since the change in intensity is bound up with the x-ray extinction in the crystals, it would appear reasonable that a less perfect crystal would have a lower extinction to begin with and so could not be expected to show up an effect depending upon a decrease in extinction as readily as the more perfect quartz crystal.

Part B of Table II shows some measurements made on a diffuse spot using the ADP crystal. The difference in intensity is well within the experimental error, showing that the diffuse spots do not contribute to the energy increase in the diffraction pattern.

The results taken with rochelle salt crystals are shown in Table III. Only the Bragg reflection method was used, and if the modes of vibration were as pure as in ADP crystals, the reflecting faces should have been antinodes of displacement, and no change in intensity could be expected. But, as the table shows, a 4 percent increase in the intensity of a Bragg line was observed during oscillation and this was definitely greater than the experimental error. Lycopodium powder studies show that the vibration of rochelle salt includes modes other than those being primarily excited, and such secondary modes might well result in a stress at the reflecting face of the rochelle salt crystal. This would result in the pressure antinode at the surface necessary to produce this intensity change. The small magnitude of the effect is explained in the same way as in the case of the ADP crystal, rochelle salt also being a relatively imperfect crystal. No work was attempted on the diffuse spots using rochelle salt because of the weakness of the effect.

TABLE II. Variations in the intensity of a Bragg line and diffuse spot for ammonium dihydrogen phosphate (ADP) crystal.

A. Bragg line	Oscillating	Non-oscillating
5th order	$4344c/s$	$4187c/s$
	$4418c/s$	$4007c/s$
	$4392c/s$	$4023c/s$
	$4373c/s$	$4056c/s$
Average	$4382\pm60c/s$	$4068\pm60c/s$

Percentage increase of oscillating over non-oscillating—7.7%

B. Diffuse spot	Oscillating	Non-oscillating
$\Delta\Theta=+55'$	$1384c/m$	$1417c/m$
	$1357c/m$	$1377c/m$
	$1383c/m$	$1376c/m$
	$1386c/m$	$1379c/m$
	$1393c/m$	$1416c/m$
	$1372c/m$	$1381c/m$
Average	$1377\pm40c/m$	$1391\pm40c/m$

TABLE III. Variations in intensity of a Bragg line using a rochelle salt crystal.

Bragg line	Oscillating	Non-oscillating
	$294\pm9c/s$	$274\pm9c/s$
	$299\pm9c/s$	$280\pm9c/s$
	$292\pm9c/s$	$274\pm9c/s$

V. CONCLUSION

Quantitative data were obtained concerning change in intensity of Bragg, Laue, and diffuse maxima for two different crystals—quartz and ammonium dihydrogen phosphate (ADP), when these crystals were oscillated piezoelectrically. Proof that the diffuse maxima showed no change in intensity during oscillation eliminates them as a source of the increased intensity of the Bragg and Laue spots. It would then seem that a decrease in intensity of the main beam must supply the required additional energy. An attempt is being made to detect this decrease.

ACKNOWLEDGMENT

The author wishes to express his gratitude for the generous and extensive help of the late Dr. G. E. M. Jauncey in the course of this study. He would also like to thank Dr. Franz Kurie and Dr. Henry Primakoff for their kind assistance and suggestions.

Positive and Negative Point-to-Plane Corona in Air

W. N. ENGLISH*
Department of Physics, University of California, Berkeley, California
(Received March 8, 1948)

The present work has involved a careful comparison of positive and negative corona and observations at reduced pressures in the range 756- to 210-mm Hg. Oscillographic observation of corona pulses with a time resolution of the order of 10^{-7} second, visual and photographic observation of the corona, and current-voltage measurements have thrown new light on fundamental corona processes. Some of the significant results obtained were as follows: For a polished platinum point of 0.38-mm diameter of curvature, the duration of positive pre-onset streamers and negative Trichel pulses near onset was about 0.4 microsecond; for positive breakdown streamers, 0.8 microsecond. A comparison of positive and negative current-voltage characteristics showed that the intermittent onsets were approximately equal but showed a small pressure-dependent difference. Both curves showed linear Ohm's law regions, and the negative current was always the larger; these effects are due to space charge. The negative corona revealed the fluctuations and dependence on surface conditions noted by previous workers.

INTRODUCTION

THE point-to-plane corona studies carried out during the last ten years at the University of California at Berkeley and elsewhere, have resulted in a rather complete understanding of the fundamental character of the positive and negative corona mechanisms. However, despite the pioneer work of Kip,[1] Loeb and Kip,[2] and Fitzsimmons[3] on positive point corona in air, of Trichel[4] and Loeb, Kip, Hudson, and Bennett[5] on negative point corona in air, and of Weissler[6] on corona in pure gases, no careful comparison of positive and negative point-to-plane corona in air had been made. The present work was designed to obtain current-voltage characteristics for a negative point to compare with the comprehensive positive point characteristics obtained by Kip. It was also important to obtain data on onset voltages for the intermittent and steady corona of both polarities, under constant conditions at various pressures, so as to arrive at an interpretation of the apparent equality of the intermittent onset voltages V_0^+ and V_0^- in air, as contrasted with the large difference reported by Weissler in pure hydrogen and pure nitrogen. Finally, the availability of a TS 28/UPN Navy synchroscope, with time resolving power much greater than that used by Trichel, Kip, *et al.*, opened up the possibility of obtaining new information on the shape and duration of corona current pulses.

* Acknowledgment is made to the Research Corporation of New York and to the Office of Naval Research, Contract No. N7ONR295, T.O. 11, for their support.

[1] A. F. Kip, Phys. Rev. **55**, 549 (1939); **54**, 139 (1938).
[2] L. B. Loeb and A. F. Kip, J. App. Phys. **10**, 142 (1939).
[3] K. E. Fitzsimmons, Phys. Rev. **61**, 175 (1942).
[4] G. W. Trichel, Phys. Rev. **54**, 1078 (1938).
[5] L. B. Loeb, A. F. Kip, G. G. Hudson, and W. H. Bennett, Phys. Rev. **60**, 714 (1941).
[6] G. L. Weissler, Phys. Rev. **63**, 96 (1943).

CORONA MECHANISMS

A comprehensive and up-to-date analysis of positive and negative corona mechanisms will shortly be published by Loeb.[7] Only a very brief statement of the main features of the point corona in air will be given here.

With increasing potential the *positive* point corona is characterized by: (1) an intermittent (Geiger counter) regime starting at a threshold V_0 where the current pulses are due to the building up of positive ion space charge formations by electron avalanches, either laterally, with a blue glow adhering closely to the point (burst pulses) or in faint luminous filaments out into the gap (pre-onset streamers). In this regime the current depends on the number of external triggering electrons introduced into the gap and on space charge limitation of the individual discharges. (2) A steady burst corona regime starting at a potential V_0, with a blue glow adhering closely to the point, where streamer formation is prevented by space charge weaken-

[7] L. B. Loeb, J. App. Phys. (to be published).

ing of the field. The current is then independent of external ionization. (3) Breakdown streamers, similar to pre-onset streamers but of much greater length and brilliance, which occur when the potential increase is sufficient to overcome the effect of space charge, and which result in a spark when a streamer crosses the whole gap and is successful in setting off secondary processes at the cathode.

With increasing potential on a *negative* point in air, corona onset is indicated by the appearance of the current pulses studied by Trichel[4] which may be regular or random at onset and which become regular with a repetition frequency corresponding to the transit time for negative ions across the gap (a few milliseconds) at a few hundred volts above onset. This frequency increases with increasing potential until it is unresolved on the oscilloscope, but no steady negative corona has been observed in air. The Trichel pulses occur only in negative ion forming gases. As the potential is raised further, spark breakdown eventually occurs at a voltage considerably higher than for positive point. Breakdown will result either through a positive streamer proceeding, by virtue of space charge gradients, from the anode or by the retrograde streamer mechanism discussed by Loeb and Meek[8] at the cathode. The characteristic glow discharge-like visual appearance of the negative corona is very striking, and is discussed in detail by Loeb.[7] The structure of the luminosity—with cathode glow, Crooke's dark space, negative glow, Faraday dark space, and positive column clearly discernable—is most readily observed at pressures from 5 to 12-cm Hg.

Apparatus and Technique

The circuit arrangements used are shown in Fig. 1. The stabilized high voltage supply and measuring potentiometer were those used by Kip.[1] The voltage could be set to plus or minus 50 volts, and read to plus or minus 25 volts over the range used. The corona gap was contained in a 26-cm diameter bell jar, lined with grounded screening and waxed to a glass base plate so that the corona could be operated at reduced pressure.

[8] L. B. Loeb and J. M. Meek, J. App. Phys. **11**, 438 (1940).

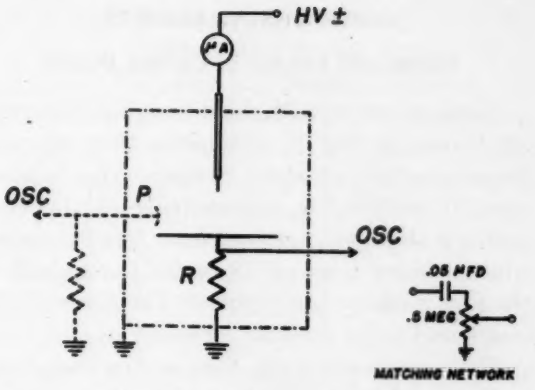

FIG. 1. Arrangement of apparatus for metal point corona. Resistance R was 1000 ohms for synchroscope, 0.5 megohm for Dumont 241. Matching network was usually used with Dumont 241. Probe P was not used for measurements.

Currents were read on a 0–3 "Sensitive Research Instrument" microammeter, on which 0.01 microampere could be detected.

Several oscilloscopes were used, so as to get an indication of the effect of amplifier pass band on the pulses. Characteristics were as follows:

Dumont 175-A—5 cycles to 100 kilocycles.
Dumont 171—15 cycles to about 100 kilocycles (used by Kip[1]).
Dumont 241—20 cycles to 2 megacycles.
Navy TS-28/UPN Synchroscope—1000 cycles to 5 megacycles.
Amplifier AM-73/UPAl (for use with synchroscope) 100 cycles to 6 megacycles.

Fifty grams of thorianite ore containing thorium oxide were placed 14 cm from the point, outside the bell jar, to provide triggering electrons. The brass plane was 12½ cm in diameter; gap distance was 6 cm for pulse shape work, 4.3 cm for I–V curves and onset studies. Except where noted, a polished platinum point prepared by Hudson[5] was used. For this point wire diameter was 0.5 mm, diameter of curvature of the tip, as determined from a photo-micrograph 0.38 mm. Room air was used throughout. The results do not differ materially from those obtained by Hudson in carefully dried air, or Weissler[6] in pure oxygen-nitrogen mixtures. Temperature and humidity were not controlled, but were measured from time to time, and variations found to produce a negligible effect on the results. Pressure was atmospheric, except where otherwise indicated.

EXPERIMENTAL RESULTS

Shape and Length of Corona Pulses

Pulses observed with the different oscilloscopes are shown in Fig. 2. It appears that an upper frequency limit of about 5 megacycles is necessary for reasonable reproduction of the short positive streamer and negative Trichel pulses, while a lower limit of 15 cycles is required for the long positive burst pulses. The Dumont 241 was found to be a useful compromise.

The synchroscope was used on fast sweep (one inch per microsecond) to examine and compare the pulses from positive pre-onset streamers, negative Trichel pulses, and positive breakdown streamers. Twenty or more of each were observed. Pulses were essentially uniform, and are drawn in Fig. 3. Low gain was used to prevent overloading and distortion in the amplifier. Increased gain altered the shape of the pulse considerably since the initial peak was amplified more than the "plateau," owing to the frequency characteristics of the amplifier. The Trichel pulses maintained their shape, but changed in amplitude with increasing voltage. They appeared to rise more slowly than the positive pre-onset streamers, whose rise was never visible.

Experiments of various types, including those of Kip,[1] Gorrill,[9] Hey and Zayentz,[10] and Raether,[11] have shown that the development of the streamer is on a time scale of the order of 10^{-8} second. The time resolution of the synchroscope was incapable of showing the change in charge distribution created in 1/100 of a microsecond. A steep spike was recorded whose shape was determined by the characteristics of the amplifier. The rise of burst pulses, because of instrumental characteristics, could not be reproduced by the synchroscope and the records with slower oscilloscopes are similarly obscured. It is not inconceivable that the burst pulse with its lateral spread over the point surface is on a slower time scale than the streamer, but definite information is lacking.

The rise of the negative Trichel pulses, the first phenomenon observed in negative corona, is much slower because it depends on the building out of an elaborate space charge distribution by the movement of positive ions. It is, therefore, possible that the shape of the negative Trichel pulses is resolved on the synchroscope.

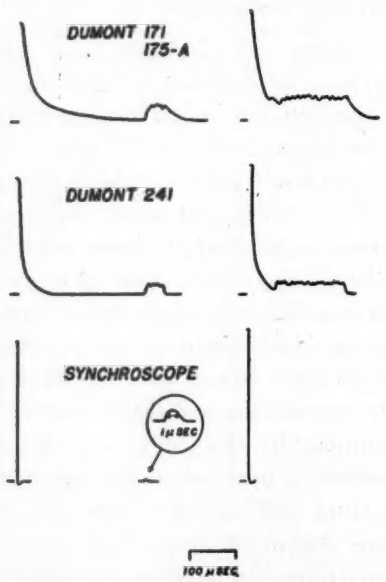

FIG. 2. Effect of amplifier characteristics. A streamer pulse, a burst pulse, and a streamer triggering a burst, as seen on different oscilloscopes. Positive point.

Current-Voltage Characteristics

Kip[1] made a thorough study of the onset of corona for positive metal points in air, beginning well down in the pre-onset region and carrying through nearly to breakdown potential. No systematic study of the pre-onset and onset regime for negative points in air had been made, giving current-voltage characteristics, etc., although Weissler[6] had made some measurements of this sort in very pure gases. The work with water point coronas made such an investigation imperative. It was necessary to make careful comparison of onset voltages at atmospheric pressure and below for positive and negative coronas, to compare current amplitudes for such coronas under comparable conditions, to ascertain the presence or absence of the linear Ohm's law region in negative corona observed by Kip for positive, and finally to note if there was a clearly defined onset voltage for steady negative corona similar to that observed by Kip for the positive.

[9] W. S. Gorrill, Dissertation, University of California (1939).
[10] V. Hey and S. Zayentz, J. Phys. U.S.S.R. **9**, 413 (1945).
[11] H. Raether, Zeits. f. Physik **107**, 91 (1937); **112**, 464 (1939).

It is to be noted in all corona studies that onset is dependent on the appearance of triggering electrons to start the discharge. In the pre-onset region for positive corona, and in the early onset region for negative corona where the current interrupts as a result of space charge action, a continuous source of triggering electrons is required for observation of the discharge. The situation in point-to-plane corona with a very limited high field volume about the point is particularly aggravated. For positive points where the electron avalanches move inward, except for the finest points,[12] ions can be provided by gamma-radiation from a radioactive source near the chamber. Such a source can have a considerable effect on the corona phenomena. If it is strong enough it may alter the initial part of the current-voltage characteristic as noted by Kip,[1] and through the cumulative action of the avalanches may give a spurious low value of the intermittent onset V_0^+. In this experiment a source just strong enough to give a 2- or 3-fold increase in burst pulses and pre-onset streamers was used, and onset voltages were checked with the source removed. For a negative point the sensitive volume for avalanche formation is too small for a radioactive source to be effective, since the triggering electrons must be produced practically on the point surface. Hudson[5] showed that the only way that Trichel pulses could be obtained reproducibly was to dust the point with fine Al_2O_3 or MgO, bringing into play what may be called the Paetow effect, discovered in connection with Geiger counters. The exact mechanism of this effect is not clear. It is assumed by some that the electron avalanches charge up the highly insulating oxide specks by electron bombardment to potentials causing field emission from negative points. For positive points such a mechanism is not satisfactory, and it may be that high energy photon emission of a delayed character is engendered in the specks by electron bombardment. At any rate, Hudson found such specks to be essential for negative point corona, and the same thing was found in these experiments. Mere dusting of the point did not steady the corona for long enough to enable a current-voltage characteristic to be obtained since the dust is quickly removed from the point by electrostatic effects. After trying various other techniques, including a radioactive source a few mm from the point, it was found that satisfactory results could be obtained with a negative point by dipping the point in 10 drops of acetone, to which had been added a drop of "Duco" cement (nitrocellulose), and then in MgO. The thin film so formed was not continuous and appeared to have negligible effect on the corona, but the MgO would then stay on the point for several runs, giving a fairly steady current. Without MgO the current above onset fluctuated continually, often dropping to zero as the discharge went out for a fraction of a second. A curve could sometimes be obtained by reading maximum current values, which agreed with the steadier results obtained with MgO.

Even with the dusted negative point, current variations were considerable. Sometimes a smooth curve would be obtained for several successive readings, then while the voltage remained constant the current would jump to a higher or lower value, only to return to the first value some seconds later. These current jumps were accompanied by a sudden change in frequency and amplitude of the Trichel pulses on the oscilloscope. At the same time the corona glow could sometimes be seen to shift its position on the point, or at least to flicker. A sudden current increase was always accompanied by an increase in frequency and decrease in amplitude of the pulses. Often the corona would favor just two such "modes" in a given voltage range, which could be identified by pulse amplitude. Sometimes the corona would stay in one "mode" over a considerable time and voltage range, enabling part or all of the current-voltage characteristic to be obtained. This is illustrated in Figs. 4 and 5.

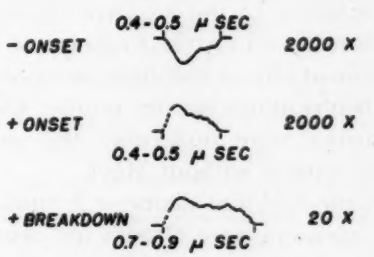

FIG. 3. Pulse shapes as seen on synchroscope. (One inch per microsecond.)

[12] W. N. English, Phys. Rev. **71**, 638 (1947).

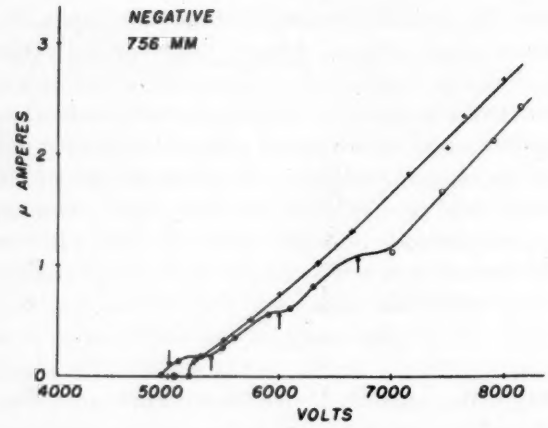

FIG. 4. Two runs, the first stepped due to "mode" changes (indicated by arrows), the second corresponding to a single "mode."

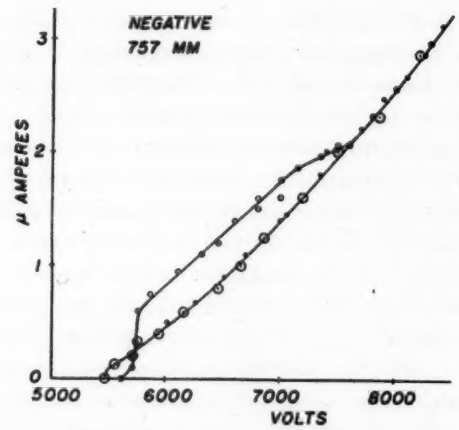

FIG. 5. Three successive runs. Small white circles voltage increasing, small black and large white circles voltage decreasing and increasing again. A gradual "mode" change takes place just above 6800 volts in the first run.

The transition between modes was not always abrupt. In the first run in Fig. 5 above 6800 volts two "modes" were present simultaneously as evidenced by pulses of amplitude 0.8 ± 0.05 inch and 1.0 ± 0.05 inch on the oscilloscope. The transition progressed gradually until at 7600 volts the second "mode" had completely replaced the first, and only one pulse amplitude appeared. On the second and third runs only one "mode" occurred.

"Double-moding" was observed on both increasing and decreasing voltage runs, but was more common on the former. As the voltage was changed, the amplitude of the Trichel pulses did not remain constant for a given "mode," but almost always decreased slowly with increasing voltage (and current). At the same time the pulse frequency increased as noted by Trichel.[4] But before this trend had gone very far towards a *steady* negative corona current a "mode" jump would occur, giving reduced frequency and increased amplitude, and the process would start again.

The stability of the negative corona did not appear to depend on the freshness of the MgO dusting until after a half-hour or more of operation, when readings became erratic. The current irregularities were noticeably less at reduced pressure, with or without MgO.

With the 0.38-mm diameter *positive* point, of course, currents were steady and reproducible. Curves were taken with and without MgO. There was no appreciable difference, as was to be expected. Positive and negative point characteristics, taken under as nearly identical conditions as possible, are given in Fig. 6.

For positive point Kip[1] has shown that the discharge at lower potentials consists of field intensified avalanches giving currents of the order of 10^{-9} ampere. At a potential which will be designated V_g are observed the pre-onset phenomena characteristic of the Geiger regime. The current abruptly increases to values of the order of 2×10^{-8} ampere, and random pulses of varying magnitudes are observed. As the voltage is increased to V_0 some 500 volts above V_g with positive point, the current suddenly jumps to a higher value of about 2×10^{-7} ampere and one reaches the onset of steady positive corona. Above this point the corona phenomena show current increase linear with potential for some 2000 volts, after which the current increases more rapidly. In the Ohm's law region the current increases by lateral spread of the discharge over the point.

Observations by Kip and others indicated that for the negative corona there was a region of field intensified currents at lower voltages. If a large point with fine dust particles and hairs was used, Kip and also Wijsman[13] found very faint discharges with glows and very low intermittent currents below onset. Similar phenomena were observed here where a distinctive type of

[13] R. A. Wijsman, unpublished results, University of California (1947).

negative pulse was always associated with the MgO dust (Fig. 7). Myriads of these tiny pulses would appear less than a hundred volts below onset, and continue with little change on up in voltage until they were lost in the plentiful Trichel pulses. These are ascribed to corona not from the point but from the small MgO dust specks. They appear to have nothing to do with the beginning of the proper negative corona. However, at a certain voltage hereafter designated V_0 in analogy to the positive corona, the current jumps by three orders of magnitude and large pulses appear.

Onset of the Intermittent Regime (V_0)

Casual observation in the laboratory had indicated that the starting potentials, V_0, for positive and negative corona at atmospheric pressure were about the same. No careful investigation had been made except that Weissler[6] had commented on this equality in contrast to his observations in H_2 and N_2. It was desirable to make a study of this effect.

Nature of the Onsets

A word must be said first about the nature of the positive and negative onsets, as observed in this experiment, and the accuracy with which they could be determined. Onset with positive point was consistent and could easily be determined to the accuracy of setting the voltage—plus or minus 50 volts. Over the pressure range studied, positive onset consisted of the appearance of burst pulses of about 50- to 300-microsecond duration, or occasionally longer (Fig. 2). These increased in amplitude by a factor of about 2 over the first fifty volts or so increase, when streamers triggering burst pulses set in. As indicated, negative onset began more or less abruptly with current pulses of the order of magnitude many thousand times the field intensified avalanches and discharges from fine dust specks. The exact voltage at which such onset occurred was not easy to ascertain. In the first place the onset appeared in two distinct forms. In general it would be indicated by an occasional isolated current burst registered on the oscilloscope whose average contribution to a microammeter current would be negligible. There were, however, cases with perhaps one or two such isolated bursts when onset took the form of regular pulses which registered a measurable microammeter current. With the first type of onset the single random pulses increased in frequency of appearance with increasing voltage until they were more or less regular at a few hundred volts above onset. These were the sort of pulses which Trichel believed occurred but which he was never able to obtain reproducibly with his conditions. These pulses had an amplitude two to four times that observed for the regular pulses at onset, as shown in Fig. 7. The larger currents for the regular pulse onset occur merely because the discharge is more continuous.

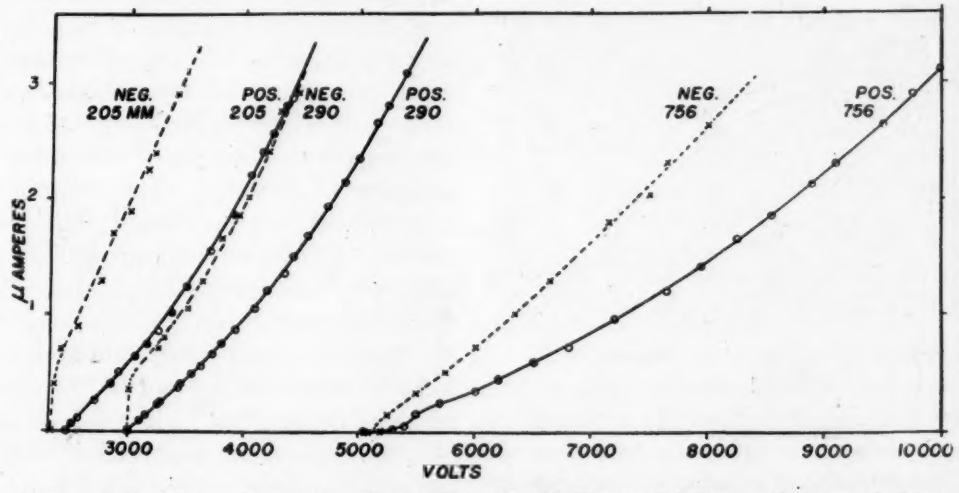

FIG. 6. Positive and negative characteristics for MgO coated 0.38-mm diameter platinum point. Gap length 4.3 cm.

TABLE I. Voltage for onset of intermittent corona (V_0) for 0.38-mm diameter. Pt. point, 4.3-cm gap. Number of separate determinations in brackets ( ).

Pressure	"Clean" point		Point with MgO	
	V_0^+	V_0^-	V_0^+	V_0^-
756-mm Hg	5050±50 (1)	4900±100 (6)	5050±50 (4)	4900±100 (16)
290-mm Hg	2850±75 (2)	3150±150 (3)	3000±50 (2)	3100±100 (5)
205-mm Hg	2450±50 (1)	2400±100 (3)	2450±50 (2)	2400±100 (6)

The regular pulse onset was usually from 50 to 250 volts higher than the random, the difference being at least partly due to the difficulty of determining a sudden onset accurately. Offset for the regular pulses was a little below onset.

It is believed that the difference between these two types of onset is not very fundamental. With adequate triggering electrons and a properly conditioned cathode spot, onset would favor the regular type. The larger amplitude for the random pulses is doubtless due to the fact that they form in an essentially clear gap, while the regular pulses, being closer together, encounter some of the negative space charge from a preceding pulse. The somewhat indefinite onset V_0 is usually higher than the potential at which the phenomenon ceases on decreasing the voltage from the operating region. With increasing potential the establishment of triggering agencies, and conditioning of the point do not occur for some time. Reducing the potential with the discharge operating gives a more reproducible threshold, but the phenomena may be somewhat different.

The limits of ±100 volts, as applied here to a negative onset, indicate the accuracy with which onset can be determined under the best conditions obtainable, and onsets will often be observed which are outside this limit. Positive and negative onsets were carefully measured at the beginning and end of each current-voltage run, and in addition determinations of onsets were made with the point alternately positive and negative, keeping other conditions as nearly unchanged as possible. Fifty-one separate observations of onset were made, over a period of several weeks, covering the pressures ⅓-atmosphere, ½-atmosphere, and 1 atmosphere. The individual values obtained have not been averaged, but each has been tabulated with specifications on the history of the point and the regularity and reproducibility of the oscilloscope pulses at onset. From this, estimates of the best values have been made, which are given in Table I.

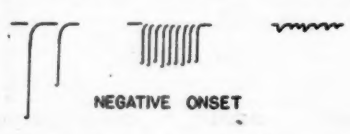

FIG. 7. Pulses observed at negative onset: random Trichel pulses, regular Trichel pulses, tiny pulses associated with MgO dust.

As regards Table I, it is noted that the difference in onset for positive and negative corona in air at atmospheric pressure with clean points and with MgO lies within the limits of individual experimental errors. However, the consistency with which negative onset lies below positive may have significance. On the other hand at 290-mm pressure there is a decided difference favoring lower onset for the positive corona. At 205-mm onsets are again almost identical and well within the probable error.

This variation is better shown by onset voltage *versus* pressure curves which were obtained for the MgO coated point by measuring onset as the pressure increased slowly from 210-mm Hg. Figure 8(A), (B), (C), shows three runs taken in this way, starting with fresh MgO on the point. The small over-all decrease in voltage from (A) to (B) and the higher onset voltage in all three runs was due to the nitrocellulose film, which was made slightly thicker than usual in an attempt to get longer reliable runs. Points at the beginning and end of each curve were checked several times. The bowing of the two negative curves relative to the positive indicates rather clearly the trend of differences suggested in Table I. It might be expected that the positive and negative onsets being dependent on the parameter X/p over a given distance from the point, would vary in a strictly linear way with pressure. The curve for positive onset is in fact linear over most of the range studies, though it shows definite curvature at either end. However, the theory for these corona thresholds has just recently been worked out by Loeb,[7] and his relations indicate that variations with pressure in electron emission by positive ion bombardment for negative point, and in photon emission and absorption in the gas for positive point play such

a role that the curves need be neither linear nor parallel.

DISCUSSION OF RESULTS

Shape and Length of Corona Pulses

As indicated earlier, care must be used in interpreting the pulses shown in Fig. 3. These corona pulses (positive streamer and negative Trichel pulses) must be due to (1) separation of charge due to motion of electrons, (2) subsequent movement of positive and/or negative ions. The shape of the oscilloscope pulse will also depend on the time constant of the pick-up electrode system (here the plane) and on the frequency response of the oscilloscope amplifier. The effect of gain, which is due to frequency characteristics, has been noted.

From the characteristics of the synchroscope one cannot expect it to do more than indicate the presence of the rapid field distortion created by the motion of electrons in the streamer advance lasting 2 to 3×10^{-8} second. Following this, however, the positive ion cloud will move into the gap, and such a motion, particularly in it's early stages in the high field region will produce a distortion which tails off as it advances into the gap. It is not unreasonable to ascribe the declining irregular portion of the pulses to such an action. The 0.4-microsecond time observed for the positive pre-onset streamer and negative Trichel pulses could conceivably be due to pick-up time constant, which could easily be of this order, although it cannot be calculated precisely. However, the time constant involved must be not greater than 0.4 microsecond, since pulses of this duration are observed. Hence, the duration and, after the initial spike, the shape of the 0.8-microsecond positive breakdown streamers should be nearly correct. Furthermore, the similarity in form of the positive pre-onset streamer pulses to the breakdown streamer pulses, and the fact that the two phenomenon have apparently much the same mechanism suggest that all but the spike of the pre-onset streamer pulses may well be correctly represented.

The mechanism indicated by Loeb[7] for the negative Trichel pulse is a complicated process, involving the building up of space charge formations, and could easily require a time of the order of 10^{-7} second, as compared to the 10^{-8}-second time scale of the positive streamer process. Thus the rise time of 0.2 microsecond observed on the synchroscope for Trichel pulses near onset, and the over-all shape of the pulse may be correct. Furthermore, these results indicate that the duration of the pulses cannot be more than the 0.4 to 0.5 microsecond observed. This observation is of vital importance in the development of negative corona theory. It at once rules out earlier interpretations of the motion of the negative ion space charge across the gap, as the agency controlling the length of the pulses, although it must still be responsible for determining the interval between pulses as indicated by Bennett.[5]

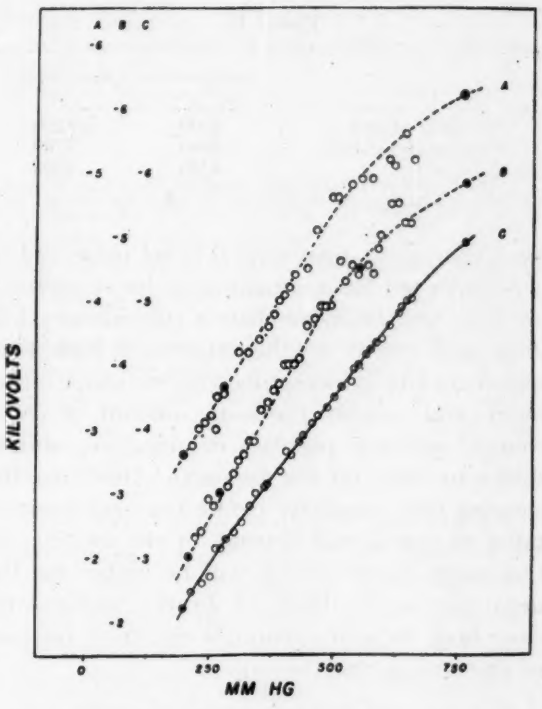

FIG. 8. Onset voltage V_0 *vs.* pressure for 0.38-mm diameter platinum point. Curves *A* and *B* negative point, curve *C* positive point. Black circle points were determined at stationary pressure and have considerably less probable error. (There is a different ordinate scale for each curve.)

These results mean that the time required for accumulation of enough space charge to produce a distortion of the field in the gap which can choke off the discharge is relatively short, and about equal for positive and negative points just above onset. This, and the approximately equiv-

TABLE II.

Point	Negative onset V_g^-	Positive onset V_g^+
FeS (first point)	8400	9250
FeS (second point)	8000	8700
CuO	4350	5300

alent charges in a negative Trichel pulse and in a positive pre-onset streamer or burst pulse in air may well be more than a coincidence. The form and extent of the important high field region are largely determined by the shape of the point, and roughly the same amount of space charge, whether positive or negative, should suffice to choke off the discharge. After that the clearing time necessary before the next burst or pulse of corona will depend on the mobility of the space charge, which will be higher for the negative case (in about a 3:2 ratio), particularly since here the space charge is electronic for part of its travel across the gap.

Current-Voltage Characteristics

The instability of the negative corona current can be readily understood from its dependence on triggering electrons and on the secondary electron emission characteristics of the point, which will change markedly on bombardment by positive ions. The change in "mode" is doubtless due to change from one active area to another. Note that current-voltage curves for different "modes" have practically the same slope.

The positive current-voltage characteristic is seen to lie always below the negative. This is doubtless due to the difference in mobility of the positive and negative space charges just mentioned. An Ohm's law region due to space charge limitation of the current is evident in both positive and negative curves a little above onset, and indicates that here limitation of the current takes place entirely in the low field region of the gap, without appreciably affecting the space charge producing mechanism at the point. Just below the Ohm's law region of the positive curve for 756-mm pressure a slight "hump" will be noted. This occurs in the intermittent streamer and burst pulse corona region and is probably due to the presence of the radioactive source, an effect which has been discussed by Kip.[1]

Onset of Intermittent Regime

The contrast between the starting potentials of the positive and negative point corona in nitrogen and hydrogen, where negative onset is much lower, and the effect in air and in H_2 or N_2 with O_2 added, where they are about the same, was noted by Weissler.[6] This equality is of added interest because Kip[5] found no appreciable effect on the onsets due to point material, with any of the common metals or carbon. An interpretation initially suggested by Loeb[14] was that in negative ion-forming gases, owing to the confined point volume, it would be necessary to create a field sufficient to knock electrons out of negative ions, out to a distance from the point surface such that adequate avalanches could build up. Loeb[14] has shown that values of X/p of the order of 90 are necessary to deionize O_2^- ions. However, the recent theory of the onset thresholds developed by Loeb[7] now indicates that this explanation is unlikely, and that the equality of V_g^+ and V_g^- in air is probably a coincidence resulting from an increase in the work function of the negative point caused by oxygen. Evidence for this point of view is contained in preliminary results obtained by the writer with points of CuO and FeS, and given in Table II.

Note added in proof: Experiments on the effect of point material and geometry on intermittent onset have now indicated that the lowering of V_g^- here was due to the roughness of the points used. Detailed results will be reported later.

These results show negative onset, V_g^-, well below the positive onset. This is difficult to reconcile with the $X/p \geq 90$ criterion, which would require a negative onset the same or higher than the positive. Further work with non-metallic and semimetallic points is in progress.

ACKNOWLEDGMENT

The writer is much indebted to Professor L. B. Loeb for encouragement and guidance during the experiment and for advice on the interpretation of the results.

[14] L. B. Loeb, Phys. Rev. **71**, 712 (1947); **48**, 684 (1935).

Corona from a Water Drop*

W. N. ENGLISH**
Department of Physics, University of California, Berkeley, California
(Received March 8, 1948)

Studies with a water drop point in a point-to-plane gap have yielded important results. Such a point has a very low secondary electron emission coefficient, and for the first time a large difference in positive and negative intermittent onset potentials in air, due to this, has been observed. The luminosity obtained with a negative drop point and the complex oscillograph pulses on both polarities have been accounted for by considering positive corona from charged droplets leaving the water point and assuming that true negative corona from a water surface is impossible. The space charge weakening of the field about a positive point, long assumed to explain the disappearance of the pre-onset streamers, is here confirmed by the reappearance of a stable drop point well above the initial potential required for disruption of the water surface.

A REVIEW of the beautiful experiments of W. A. Macky[1] on the disruption and sparking of water drops in an electric field had indicated certain peculiar effects which did not appear to be consistent with the generally accepted theory of the corona mechanism. Macky observed that water drops falling in a uniform field in excess of some 8000 volts per cm (depending slightly on the size of drop) became distorted. The induced positive end was drawn out into a fine point which emitted a spray and characteristic streamer-like corona processes. The induced negative end of the drop showed some pointing, but was mostly clearly defined and had a faint glow superficially resembling the negative point corona.

In view of the fact that the water surface should be a notoriously poor secondary emitter under positive ion bombardment, since it is a polar substance with no free electrons, it was felt that further study with stationary positive and negative water points, where the various techniques used with metal points could be applied, might throw important light on fundamental corona processes. Many years ago J. Zeleny[2] made a careful study of the effects obtained with positive and negative drop points, especially the former. He used liquids of different surface tension and a number of gases. This work was done before cathode-ray oscilloscopes and other modern instruments were available so that at that time the mechanism of the corona was little understood. Thus these excellent observations could not answer the questions at hand.

APPARATUS AND TECHNIQUE

In these experiments, as in all corona onset studies, the field strength at the electrode surface and outward is the important parameter. This field depends critically on the radius of curvature of the drop. The problem of using such a variable point was not easily solved. Difficulty was encountered in obtaining uniformity and stability of the drop without field at atmospheric pressure and below, and application of the field produced immediate distortion of the drop ending in its eventual rupture at the point where surface tension was overcome. In consequence, the available range of drop sizes was small, and the constant change of drop shape with potential made it impossible to determine more than an approximate average value of drop curvature and field.

Figure 1 shows the disposition of capillary tube and reservoir to give a liquid "point." The remainder of the apparatus has been described in a previous paper.[3] For reduced pressures both bell jar and reservoir were pumped. In arrangement b of Fig. 1 the capillary was tried with and without a coating of paraffin wax. At low

* The analysis of the data from this experiment was done under Contract No. N7ONR295, T.O. 11 with the Office of Naval Research.
** Eastman Kodak Fellow.
[1] W. A. Macky, Proc. Roy. Soc. **133**, 565 (1931).
[2] J. Zeleny, Proc. Camb. Phil. Soc. **71**, 18 (1914) and Phys. Rev. **16**, 102 (1920).
[3] W. N. English, Phys. Rev. **73**, 170 (1948).

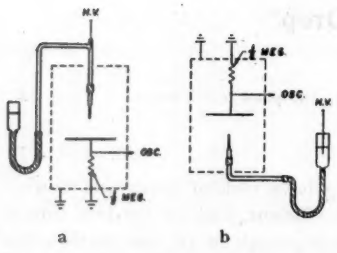

FIG. 1. Arrangement of apparatus for water drop corona studies.

pressures particularly Fig. 1b gave a less stable drop than Fig. 1a. The latter arrangement is essentially that used by Zeleny. Results obtained were the same with both. Resistance of the water column in Fig. 1a was three megohms for tap water, 30 megohms for distilled water. Adjustment of the reservoir height to give satisfactory results over the whole voltage range was critical. Generally, the hydrostatic pressure was varied until a nearly hemispherical drop was obtained just below corona onset. The reservoir level would then be about a centimeter above the capillary tip.

Although boiled distilled water was used, bubbles would often block the capillary at pressures below 300-mm Hg. At lower pressures also, the fields for corona onset were lower, so that the drop was not pulled out beyond the capillary, and negative corona sometimes took place from the glass corner. Adjustment of the reservoir under such conditions usually caused the drop to become unstable and fall off. These effects set the lower limit of observation at about 200-mm Hg pressure.

The following methods of observation were used:

(i) Corona gap: visual with 70X telemicroscope

- (a) Dark
- (b) Steady illumination at 135 degrees

(ii) Corona gap: photographic with Leica at f2, using Kodak Super XX film

- (a) Dark
  - (i) Time exposure
  - (ii) Moving film record obtained by winding film slowly by hand
- (b) Illumination at 90° from Edgerton flash lamp (50 μf at 1800 volts) with condensing lens. Flash time was about 300 microseconds (Fig. 2)

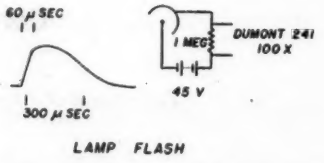

FIG. 2. Flash time for Edgerton lamp.

(iii) Dumont 241 oscilloscope

- (a) Visual
- (b) Photographic

(iv) Current-voltage characteristics

EXPERIMENTAL RESULTS

The drop on the end of the capillary will be referred to as the "main drop" or as the "point," the water spray emitted in discharge as "droplets."

It should be noted that the lack of exact control of drop curvature results in variation of the values of the potential for onset and other transitions. The values given are a typical run. A difference of several hundred volts might be observed under slightly different conditions. The important item in these studies was the *relative* values of the potential for the occurrence of the various phenomena. With care not to alter external conditions, these could be obtained to an accuracy not far short of that reached with a metal point.

One effect noted was that described by Zeleny[2] where the spray onset voltage increases steadily at first, then reaches a constant value several hundred volts above the initial onset. This he ascribed to the removal of surface impurities which lower the surface tension. Hydrostatic pressure had a large effect on the spray onset. Lowering the reservoir $\frac{1}{2}$ cm changed it from 6900 volts to 7500 volts in one instance. Vibration too played a significant part, and there was also apparently a variation in the way in which the main drop "sat" on the end of the capillary which sometimes caused a difference from one run to the next. Contamination of the water by electrolysis may also have entered. All these factors resulted in a variation of as much as 200 to 300 volts from one run to another, although if the point were not unduly disturbed a consistency of plus or minus 50 volts could often be obtained during a run of several hours.

Results with a Large Point

A capillary of 0.13-cm outer diameter, giving a point of about the same diameter of curvature, was used in the arrangement of Fig. 1b, with a 3.2-cm gap and atmospheric pressure.

Positive Point

When the potential was raised to 6800 volts, groups of positive pulses were observed on the oscilloscope. These were all of about 1000-microseconds duration and took one of three forms: increasing amplitude with almost no "streamer pulses" superposed; constant amplitude with a few "streamer pulses;" and decreasing amplitude with many "streamer pulses" (Fig. 3a). At the same time, under illumination, very fine spray droplets could be seen shooting from the tip of the main drop, causing an almost imperceptible wetting of the plane. In the dark, corona streamers were visible extending a few millimeters from the point. They were evidently associated with the spray, for the luminosity was "coarser" and more intermittent than for a metal point and was confined to the region out from the point where the spray appeared.

An increase in voltage above the onset gave an increase in spray, luminosity, and pulses up to 7100 volts. The spray pulses had been changing shape gradually since onset, the amplitude of the main pulse becoming less while that of the superposed streamer pulses increased, until at this voltage individual streamer pulses occurred separately. At 7500 volts the transition was complete, nothing but streamer pulses were to be seen on the oscilloscope, and the usual bright streamer "fan" was visible from the darkened point, with a steady burst pulse corona glow on the tip of the main drop. With illumination the main drop was seen to be rounded and stable, the ejection of water having ceased. This stable regime was noted by Zeleny,[2] but could not at that time be interpreted in terms of corona processes.

As the voltage was raised further, the point remained stable. The streamer pulses decreased in amplitude as the steady corona glow on the point increased until at 9000 volts only an occasional small streamer pulse occurred. The glow on the main drop could now be seen even with illumination, and it spread and got brighter as the voltage was further increased, as for a metal point.

The next transition occurred abruptly at 10,500 volts. The main drop was suddenly and violently disrupted. Large chunks of water were torn from its surface and drawn to the plane as drops, forming a puddle several centimeters across in a few minutes. Viewed in the dark, a bright ragged luminosity followed the broken water surface and at times shot out into the gap. On the oscilloscope large changes in potential were observed, while streamer pulses appeared intermittently. Further increase in voltage merely resulted in more and more water being drawn out of the capillary. Observations were made up to 16,000 volts.

The three voltage regions described above will be referred to as the "spray," "stable," and "drop" regimes.

Figures 3 and 4 show the oscilloscope pulses. The sequence of events for a positive drop with increasing voltage is summarized in Fig. 5. Figure 6 shows dark photographs of the gap and Fig. 7 flash photographs of the gap. A current voltage

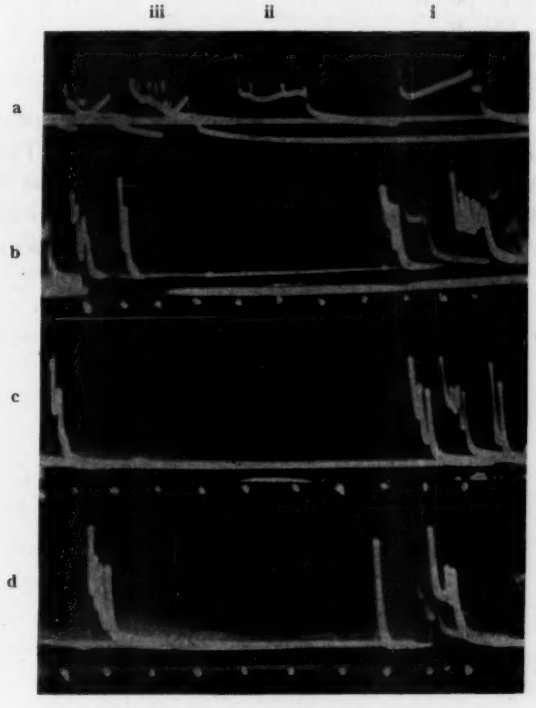

FIG. 3. Positive point spray pulses. 6800 volts. Timing interval in b, c, d is 0.001 second.

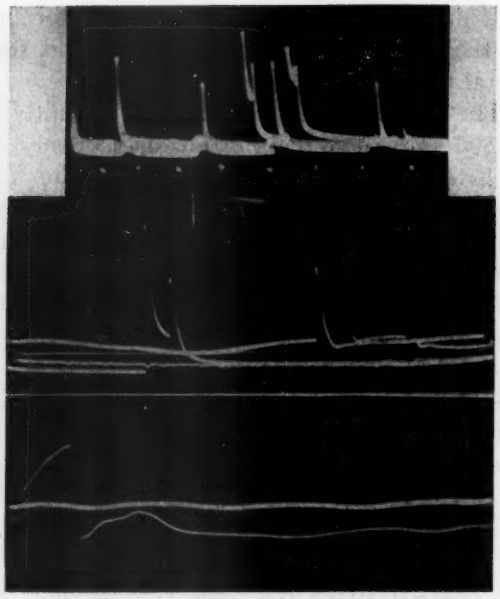

FIG. 4. (Top) Spray pulses and streamer pulses. Timing interval: 0.001 second. 6900 volts. (Center) Spray pulse, streamer pulses, and steady burst corona. Timing interval: 0.0002 second. 8000 volts. (Bottom) Electrostatic pulse due to large droplet leaving point, in "drop regime." Amplification very much less than in "spray" oscillograms. 16000 volts.

curve plotted from three different runs is given in Fig. 8.

Negative Point

Under the same conditions as above, spray onset for negative point was 6700 volts. Two types of pulses occurred on the oscilloscope as shown in Fig. 9, both of about 1000-microseconds duration, the many-peaked kind being

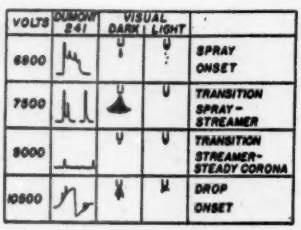

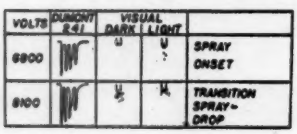

FIG. 5. (Top) Sequence for positive drop point. (Bottom) Sequence for negative drop point.

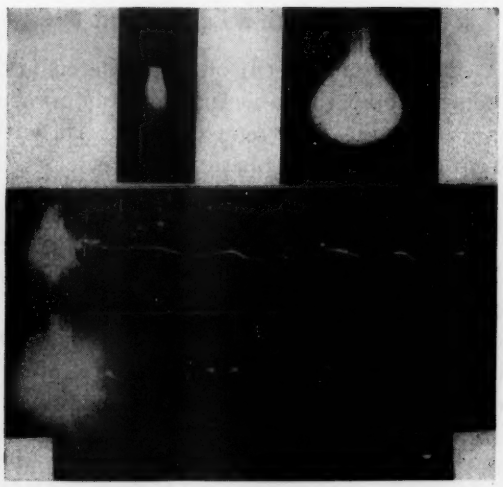

FIG. 6. (Reading from top to bottom) Dark photograph of spraying positive point. 3 min., 7300 volts. Dark photograph of stable positive point with streamers. 5 min., 8400 volts. Dark photographs of positive point in "drop regime," with moving film record obtained by winding film. 1 min. and 4 min., 13900 volts. Moving film record of 1-mm diameter positive platinum point showing steady corona. 8750 volts.

more frequent. Visually, with steady illumination, fine droplets of spray could be seen shooting into the gap, as for positive point. However, in the dark, no luminosity could be seen although it could be photographed in a ten-second exposure. An increase in voltage produced more frequent pulses of both kinds and more spray. At about 7100 volts a ragged fluctuating glow became visible in the dark. It differed markedly from that observed with positive water point in that it occurred intermittently all over the main drop, instead of being concentrated outward from its tip. Also it extended a much shorter distance into the gap and did *not* show the very characteristic structure of the negative corona from a metal point.

Further increase in voltage caused the spray emission and glow to spread still more over the point, while the pulses increased in numbers and amplitude. At 8000 volts spray emission and ragged glow covered the whole end of the capillary. About this voltage the "spraying" gave way to larger drops, which quickly wet the plane, as in the positive "drop" regime. Visually, the transition was fairly marked, and at times the discharge would fluctuate between "spray" and "drops." No noticeable change in current or

oscilloscope pulses accompanied the shift, but this is not surprising as the current fluctuated considerably over the whole range and the oscilloscope screen at this voltage was pretty well filled with pulses. Observations were carried up to 9200 volts, the increased voltage causing increased ejection of water.

A summary of the effects described above is given in Fig. 5. Oscillograms for several voltages appear in Fig. 9. Dark photographs of the corona appear in Fig. 10 and flash photographs in Fig. 11. A current-voltage curve plotted from two runs on successive days is given in Fig. 12, with the positive curve for comparison. The current fluctuations were at least twice as great with negative point.

Results with Small Point

A capillary of outer diameter 0.041 cm was used, giving a point of about that diameter of curvature. Observations were at atmospheric pressure with 3.2-cm gap.

Positive Point

No streamers occurred at any voltage. Spray onset (after initial increase) was at 4000 volts. "Spray" consisted of single, almost invisible droplets which snapped off the main drop at a frequency depending on the voltage. Somewhat above onset the pulses could be synchronized almost perfectly on the oscilloscope; Fig. 13 gives a *tracing* of the pattern. No luminosity could be seen up to 4450 volts, after which a steady corona glow appeared on the tip of the main drop and the pulses ceased. The drop was stable up to 9000 volts where it was drawn out to twice the capillary diameter. Above this voltage large droplets would "snap off" the tip of the main drop at a deliberate rate, increasing with voltage. Pulses produced here were similar to those for the large point in the drop regime.

Figure 13 also shows, for comparison, pulses obtained when small drops are forced from the large positive point by raising the reservoir, at a voltage below spray or corona onset. The ratio of positive to negative pulses is 10 to 1 or greater. These negative pulses are probably due to a drop shattering process and may be disregarded.

With a small point the fields producing disruption of the drop will be obtained at lower potentials, since the curvature of the drop is greater. Further, the high field region will be smaller. In addition, the drop point appeared unusually stable, ripples and other irregularities

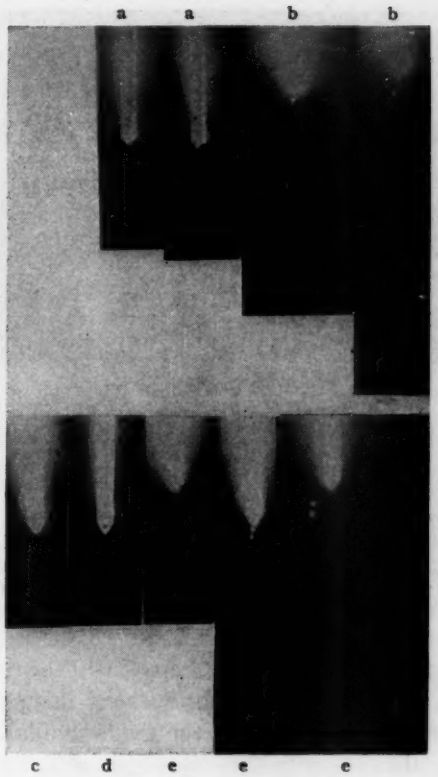

FIG. 7. Flash photographs of positive drop point. a. Distortion of spraying point. 6700 volts. b. Spray droplets from spraying point. 6800, 7600 volts. c. Stable drop: streamers. 8600 volts. d. Stable drop: steady corona. 9300 volts. e. Droplets ejected in "drop regime." 12500 volts. (Formation of droplets may be seen.)

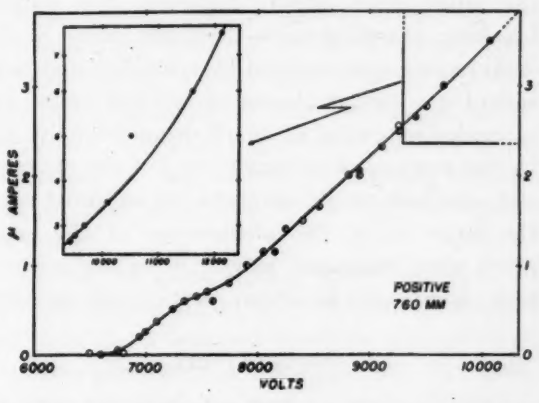

FIG. 8. Current-voltage characteristic for large positive water point. Three separate runs.

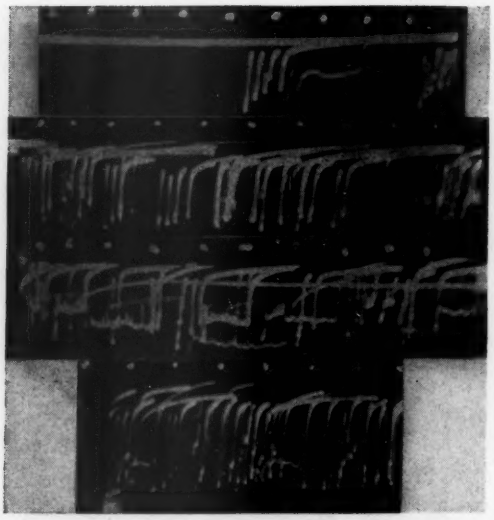

FIG. 9. (Reading from top to bottom.) Negative point spray pulses at 7350, 8100, 8100, 9000 volts. Note two types of pulse. Timing interval: 0.001 second.

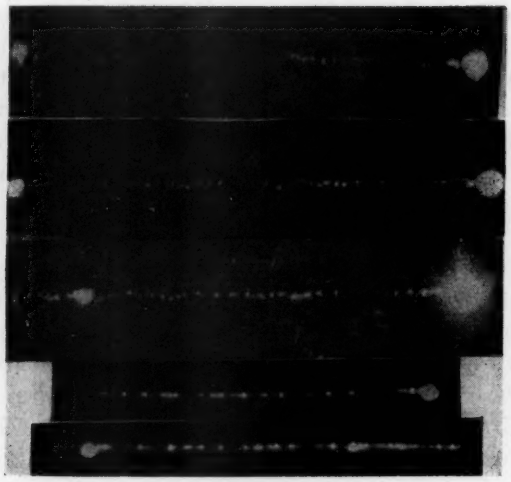

FIG. 10. (Reading from top to bottom.) Time exposure and moving film record of negative drop corona. 8100, 9100, 9100 volts. Time exposure and moving film record of corona on 1-mm diameter negative platinum point. 8750, 11900 volts.

being altogether absent. Apparently the droplets from such a point do not succeed in producing streamer breakdown in the fields available and the pulses observed are those due to the passage of charged droplets across the gap. This is confirmed by the similarity to the pulses obtained by forcing drops from the large point by raising the reservoir, at a voltage below corona onset. At 4450 volts the normal steady burst pulse corona appeared on the tip of the main drop, the space charge accumulation stabilized the point surface and, as for the larger positive point, a stable region was observed which here extended up to 9000 volts. Above this the fields are again able to disrupt the drop point. With the small drop point, however, the violent breaking observed with the large point in the drop regime was replaced by remarkable elongation of the point to almost twice its diameter and a regular snapping of small drops from its tip. In the absence of streamers and of the charging and discharging of droplets encountered with the large point, the phenomena at the small point were influenced primarily by surface tension conditions which were particularly uniform.

Negative Point

Here onset was at 4000 volts, and the behavior of the point the same as for positive. Pulses were very similar to those for positive point (Fig. 13) and became regular shortly above onset. Their frequency was not quite constant, giving a slight jitter on the synchronized trace. A faint glow, which flickered violently, was first visible at 4500 volts. It was close to the point at this and higher voltages, but ragged and intermittent.

Current-Voltage Characteristics

Current-voltage curves are given in Fig. 14 for positive and negative point. No rapid current fluctuations were evident on either polarity,

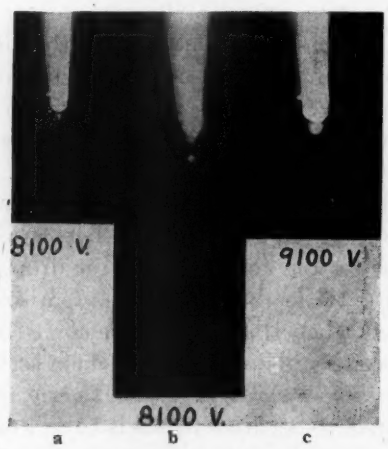

FIG. 11. a and c. Flash photographs of negative point showing corona luminosity in relation to point. Time exposure: about 10 seconds. Note the dark space. b. Spray droplets from a negative point.

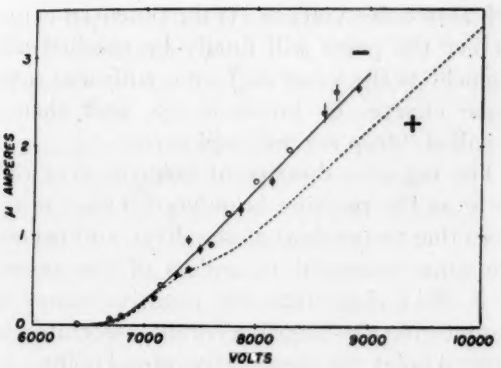

FIG. 12. Current-voltage characteristic for large negative drop point from two separate runs with positive characteristic for comparison. Vertical lines through points show *observed* variation in the current.

but there was considerable variation between readings taken some minutes apart.

There is no significant difference between these curves and those observed with the large point. In the absence of streamers and the strong drop charging and discharging mechanisms just above onset, the negative currents always lie above the positive for a given voltage because of the greater mobility of the negative space charge. The less conspicuous Ohm's law region may be ascribed to the normally narrow Ohm's law range for a smaller point, and also to the fact that space charges are less effective since a considerable part of the current is carried by charged droplets.

Intermittent Regime Onsets at Reduced Pressure

Comparison of Positive and Negative Onsets

The arrangement of Fig. 1a was used, with a capillary of 0.13-cm o.d. and a 4.2-cm gap.

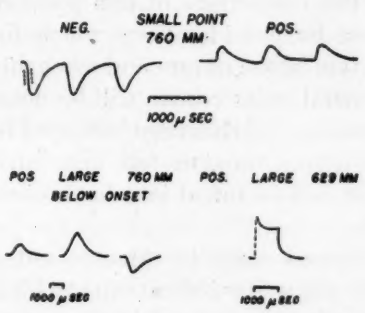

FIG. 13. (Left) Pulses from small negative drop point. Electrostatic pulses from large positive drop point below corona onset. (Right) Pulses from small positive drop point. Pulses from large positive drop point at slightly below atmospheric pressure.

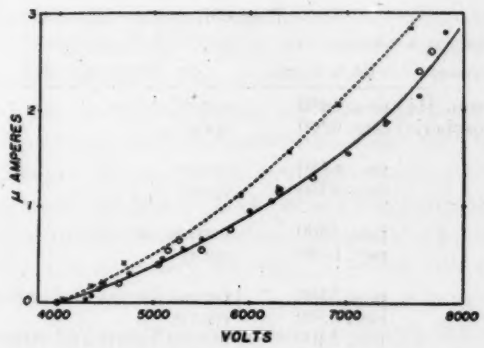

FIG. 14. Current-voltage characteristics for small drop point at atmospheric pressure. Dotted curve, negative; full curve, positive.

From the first observations it was now fairly clear that the negative water point corona mechanism must differ from that for a metal point. The crucial test lay in experiments at reduced pressure. The extent of this reduction was limited by difficulties already mentioned in obtaining a protruding stable drop. After some unsuccessful attempts measurements on onset potential were obtained at pressures of 756, 629, 505, 385, 310, and 206-mm Hg, other conditions being essentially constant. Positive and negative onsets were measured alternately, an interval of three minutes required to change polarity intervening. At 385 mm four consecutive determinations, alternately positive and negative, were made so as to detect any effect due to changed point conditions. In each determination the final steady value of spray onset was recorded after the initial rise due to surface impurities. Results are given in Table I. These results furnish a confirmation of the more elegant "onset *versus* pressure" curves to follow, from which the possibility of spurious results caused by change in drop characteristics has been practically eliminated. Since both sets of observations lead to the same conclusions, the discussion of the intermittent onset potential against pressure characteristics applies equally to Table I.

Curves of intermittent onset voltage, V_0, against pressure were obtained, first for a positive and then for a negative point, by increasing the pressure slowly from 236-mm Hg, and determining onset at frequent intervals. These are given in Fig. 15. The observations for negative

TABLE I.

Pressure	Onset voltage	Nature of onset
756-mm Hg atmospheric	pos. 6450	spray
	neg. 6250	spray
629	pos. 6450	spray
	neg. 6350	spray
505	pos. 5800	corona bursts
	neg. 6100	spray
385	pos. 5400	corona bursts and streamers
	neg. 6500	spray
	pos. 5400	corona bursts and streamers
	neg. 6700	spray
310	pos. 4700	corona bursts
	neg. 6400	spray
206	pos. 3400	corona bursts
	neg. over 6000	spray

point could not be taken below 420 mm without changing the reservoir level, owing to corona from the glass corner of the capillary. The amplitude of the corona burst pulses at onset, for a positive point, increased by a factor of about four as the pressure increased from 206 mm and 505 mm. The amplitude of the streamer pulses above onset also increased. The pulses observed at spray onset were very similar to those previously described for the large point at atmospheric pressure, except for positive spray onset at 629 mm. Here no streamers appeared on the pulses (Fig. 13). It will be noted at once that at the higher pressures the disruption of the water surface by the electrostatic forces occurs at a potential *below* the normal corona onset V_0. The breakup of the surface then initiates corona, which complicates interpretation. On reduction of pressure it is seen that below 629-mm Hg positive corona onset can occur without disruption of the water point.

Below this pressure the positive drop exhibits the normal corona onset phenomena observed with a metal point, beginning at a voltage which varies linearly with pressure. On examining Fig. 15 one might at first suppose that even though a positive corona at reduced pressure started at, say, 4000 volts, the drop would become unstable when the potential increased to the dotted line at 7250 volts. This does not occur, however, because the space charge from the corona has so reduced the field that the drop remains stable well above this voltage. As the potential is raised further the point will finally be reached where the field at the water surface is sufficient despite space charge, to break it up, and then the so-called "drop regime" will occur.

The negative drop point behaves very differently as the pressure is reduced. Onset is in all cases due to breakup of the drop, and occurs at the same potential regardless of the pressure. It is clear then, that the negative water drop cannot give the negative corona associated with a metal point, for the negative metal point corona onset shows a linear dependence on pressure very similar to that for a positive metal point (or a positive water point below 629 mm). This suggests strongly, as already indicated, that a water point with very low secondary electron emission cannot give normal negative corona.

DISCUSSION

It now remains to explain the peculiar luminosity, noted by Macky and in the present experiments, at a negative drop point. L. B. Loeb suggested the mechanism which appears to give the correct interpretation. It is that the light emission from the negative drop point is due to positive corona from the induced positively charged tips of receding droplets in the high electrostatic field near the point. In fact, when this suggestion was made it at once drew attention to the probability that, with both positive and negative drop points, the droplets would give the type of corona discharge observed by Macky in the high field region near the point. This materially aided in the interpretation of the oscilloscope pulses and other effects observed. The correctness of this point of view is borne out by considerations which follow. An appreciation of the nature and mechanism of the normal metal point corona will be necessary for the discussion. This has been indicated briefly in a previous paper,[3] and a full and authoritative treatment will be found in a forthcoming article by Loeb.[4]

Calculations made by Macky and Zeleny as well as by the writer indicate that with increasing field intensity the point becomes unstable with regard to conflict between the electrostatic and

[4] L. B. Loeb, J. App. Phys. (to be published).

surface tension forces at about the potential observed for onset.

The onset of discharge at atmospheric pressure must then be ascribed to a disruption of the water surface resulting in the fine spray observed. This potential is the same for positive and negative points and is not directly connected with any corona threshold for a point of this size. However, once the point begins to break up the intense electrostatic field, in conformity with Macky's observations, will result in electrical discharge from the spray droplets.

Let us regard the system of the large positive water drop point being drawn out by the field and emitting a succession of minute, positively charged droplets. The potential is sufficient to give streamers from the electrostatically deformed and breaking point. The droplet finds itself in a field in excess of 8000 volts per centimeter in the neighborhood of the positive point. In consequence, the droplet will be strongly polarized as shown by Macky, its own positive end will be drawn out to a point, and may give streamers if the field is sufficiently high.

We can envisage droplets leaving the corona point and experiencing one of several histories, depending on droplet size and field conditions. As the droplet leaves a positive streamer from the point gives it a high positive charge. In receding from the point with a velocity slow compared to the positive ions, it will from these receive an increase in positive charge. Macky has remarked on the ease with which a falling drop could receive a large charge in passing through the corona from a previous drop which had collected on one of the electrodes. If the charge which it receives and the field in which it finds itself are not adequate to discharge the drop, i.e., to give secondary streamers from its lower positive tip, a pulse will be observed as in Fig. 3a(i) in which the spike is produced by the primary streamer charging the droplet and the subsequent rise is caused by collection of positive ions. The exponential tail is instrumental. In cases where the drop is of such a size and shape and in such a field as to give a few secondary streamers from its lower positive end, one will observe the kind of pulse shown in Fig. 3a(ii). Where the droplet finds itself in a high field and is large enough and has enough charge to produce a powerful streamer tip at its lower positive end, it may materially discharge—giving pulses of the type shown in Fig. 3a(iii).

As the potential on the point is increased (at 7500 volts in our representative case) we reach the stable regime which appears when positive streamers and burst pulse corona are generating a substantial positive space charge. With metal points this region is characterized by the suppression of streamers by space charge and the appearance of the burst pulse corona as the sole manifestation at the point. In fact, it was this disappearance of pre-onset streamers which called forth an assumption of the building out of a positive space charge which lowered the field about the point to a value where streamers could no longer form. It is to be expected that the appearance of such a space charge would reduce the field at the surface of the drop below the value for disruption. The reappearance of the stable surface thus beautifully substantiates this hypothesis of space charge distortion. It may be noted that Zeleny, without knowledge of the space charge formations, correctly ascribed the reappearance of the stable drop to an increased *IR* drop in the gap.

With the disappearance of streamers the ordinary burst pulse corona with characteristic surface glow occurs, increasing in area over the

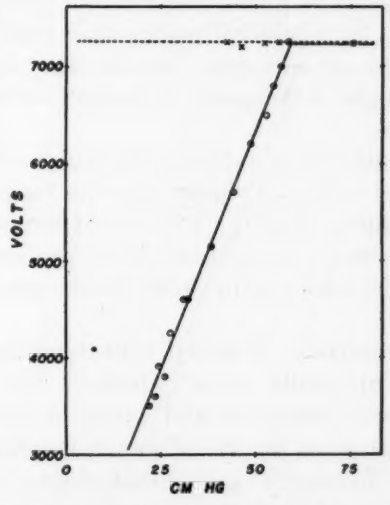

FIG. 15. Onset potential, V_0, *vs.* pressure curves. Full line: positive drop point; dotted line: negative drop point. ⊙ positive corona onset, point stable. + positive corona onset, point disrupted. × negative corona onset, point disrupted.

point surface. In this region, as with a metal point, space charge limitation of the current leads to a linear increase of I with V, the Ohm's law regime of Kip.[5] The symmetry and smoothness of a water point lead to an exceptional development of this region (Fig. 8).

On further increasing the potential (at 10,500 volts in our example) the field distortion from space charge is sufficiently compensated by the increased potential, and the water surface is again disrupted with intermittent streamers and strong burst pulse corona. This regime is characterized by a transition from the linear Ohm's law relationship to an up-curving I–V plot and by considerable fluctuation in the current (as would be expected from the violent disruption of the point).

With the large *negative* drop point the pulses observed were of two types (Fig. 9). The first closely resembled the Trichel pulses from a metal point, but the second implied a steady negative corona for about a thousand microseconds, something which has never been observed with a metal point. This second type of pulse is nicely explained by assuming that it represents positive burst pulse corona from the positive end of a droplet, while the many-peaked type of pulse would correspond to a series of streamers from the same positive droplet tip to the negative point, under slightly different field conditions. The pulses are different from those produced by a positive point under comparable conditions of spraying, because the negative point droplet is incapable of discharging from its lower end.

The pulses from a small water point where no streamers occur are almost identical for positive and negative polarity. This would be expected if the primary mechanism were the result of droplet formation with rather feeble burst pulse corona.

The luminosity observed with the large negative point would occur wherever the water surface was disrupted, and would be separated from the point by the distance necessary for droplet formation and development of the streamer or glow. Such a mechanism, dependent almost entirely on the surface tension forces governing drop break-up, would produce a dark space and luminosity very different from the typical glow-discharge-like negative metal point corona, and whose shape and extent was not materially affected by pressure change. A dark space can be seen on photographs of the negative drop point discharge at atmospheric pressure, but it was not observed to increase with decreasing pressure, an effect which is very marked with a metal point, either visually or photographically. (This evidence is not conclusive, as the writer had not at that time seen the effect with a metal point, and it was not specifically looked for with the water point; but careful visual observations were made at all pressures used and it should certainly have been noticed if present.) Further, there is no sign of the very characteristic "shaving brush" shaped positive column, and Faraday dark space of the negative metal point corona.

A moving film photograph of the negative drop point shows that the luminosity is intermittent, while for a positive point under the same conditions of spraying it is continuous. A comparison with photographs of a positive and negative platinum point of comparable radius suggests that this effect is not merely due to the normal fluctuations of a negative point corona. Figures 6 and 10 show typical observations.

The positive and negative current-voltage characteristics (Fig. 12) coincide in the initial stages where the mechanisms are similar. The positive current falls below the negative at the voltage where streamer pulses are starting to predominate over spray pulses, as is the case with the normal corona for metal points.

In metal point corona in most gases, especially at reduced pressures where positive streamer formation is less efficient while the production of secondary electrons by positive ion bombardment is effective, we observe a threshold for negative corona materially lower than for positive. In air, probably owing to the effect of O_2 on the work function of the point electrode, the two onsets are almost the same. For a water point in air, negative onset is at least 3000 volts *higher* than positive onset. This indicates that the secondary electron emission coefficient from a water point must be exceedingly low, and suggests that any corona from such a surface

[5] A. F. Kip, Phys. Rev. **54**, 139 (1938).

must be carefully scrutinized before being attributed to a normal negative corona process.

Corona from Non-Metallic Points

The peculiar characteristics of the negative water point have suggested a review of the effects obtained with materials of different secondary emitting properties, so as to establish a connection between secondary emission and the character of the negative corona obtained. Previous perfunctory work by Kip and others in this laboratory had shown no noticeable difference for any of the common metals or carbon in air, but a more careful study is needed. The need for such study was further indicated by a rather surprising effect which occurred with negative drop points and which hampered work at low pressures where the effect can occur at fields insufficient to pull the drop out beyond the end of the glass capillary. The phenomenon consisted of a bright brush-like corona, rather coarse and streaked, which was apparently a negative corona occurring at high fields from the glass corner of the capillary and which produced on the oscilloscope myriads of Trichel-like pulses of moderate amplitude which looked like "grass" on the screen. Some work has already been done on non-metallic points, using CuO and FeS, which has given a negative corona threshold from 700 to 900 volts below the positive. This is in conformity with the recent considerations of Loeb[4] as to the mechanisms of the two coronas. This subject is undergoing further investigation.

ACKNOWLEDGMENT

The writer wishes to express his appreciation to Professor L. B. Loeb, for suggesting the problem and particularly for his assistance in the interpretation of results.

Characteristic Values of Spheroidal Wave Functions*

W. F. EBERLEIN
The Institute for Advanced Study, Princeton, New Jersey
(Received February 16, 1948)

An asymptotic expansion for the characteristic values of the (prolate) spheroidal wave equation is obtained. The expansion contains the Ince-Goldstein expression for the characteristic values of the Mathieu equation as a special case ($m=-\frac{1}{2}$).

I. INTRODUCTION

THE differential equation

$$(1-x^2)y''-2(m+1)xy'+(b-c^2x^2)y=0 \quad (1)$$

arises on separation of the scalar wave equation in spheroidal coordinates. The solutions of physical interest are those for which $y(x)$ remains finite at $x=\pm 1$. Since the existing continued fraction techniques[1] for calculating the characteristic values b become unwieldy when $c\gg 1$, the expansion of b in inverse powers of c that we obtain may be of interest. We give only a brief sketch of the derivation; a critical discussion of the procedure and the character of the resulting series must await a later paper.

II. DERIVATION OF THE SERIES

Under the changes of variable $z=c^{\frac{1}{2}}x (c>0)$, $\mu=b/c$, $u(z)=y(x)$, Eq. (1) transforms into

$$[1-(z^2/c)]u''(z)-2(m+1)(z/c)u'(z)+(\mu-z^2)u(z)=0, \quad (2)$$

and the boundary condition is now that $u(z)$ remain finite at $z=\pm(c)^{\frac{1}{2}}$. If we let $c\to\infty$ the formal limit of (2) is

$$u''(z)+(\mu-z^2)u(z)=0, \quad (3)$$

plus the boundary condition that $u(z)$ remain finite at $z=\pm\infty$.

The characteristic functions of (3) are the well-known Hermite wave functions

$$\psi_l(z)=\exp(-z^2/2)H_l(z)=(-1)^l\exp(z^2/2)\left(\frac{d}{dz}\right)^l\exp(-z^2), \quad (4)$$

and the corresponding characteristic values are

$$\mu_l=2l+1 \quad (l=0, 1, 2, \cdots). \quad (5)$$

These heuristic considerations suggest the existence of expansions of the form

$$b=(2l+1)c+\sum_0^\infty \beta_i c^{-i}, \quad (c>0) \quad (6)$$

$$u(z)=\sum_0^\infty a_i\psi_i(z). \quad (7)$$

If we substitute the last expression in (2) and make use of the identities

$$z\psi_i=\tfrac{1}{2}(\psi_{i+1}+2j\psi_{i-1}), \quad \psi_i'=j\psi_{i-1}-\tfrac{1}{2}\psi_{i+1}, \quad (8)$$

we obtain a 5-term recursion relation for the coefficients a_i:

$$-a_{j-4}/16+\frac{m}{2}a_{j-2}+[b-(2j+1)c+m+\tfrac{1}{4}\{j(j-2)+(j+1)(j+3)\}]a_j-2m(j+1)(j+2)a_{j+2}-(j+1)(j+2)(j+3)(j+4)a_{j+4}=0. \quad (9)$$

Now set

$$a_j=1, \quad j=l; \quad a_j=\sum_1^\infty \alpha_i{}^j c^{-i}, \quad j\neq l. \quad (10)$$

We insert the expressions (6) and (10) in (9), combine terms, and equate to zero the coefficients of the various powers of c. The resulting infinite system of equations in the α's and β's can then be solved successively. We note here only that it is convenient to introduce the parameter $n=2l+1$, and that one finds $\alpha_q{}^{l\pm p}=0$ if $p-4q>0$. After some rather tedious calculations one finally obtains

$$b_l\sim nc-m-\frac{n^2+5}{8}-n\frac{n^2+11-32m^2}{2^6}c^{-1}-(1/2^{10})[5(n^4+26n^2+21)-3\cdot 2^7m^2(n^2+1)]c^{-2}-(n/2^{14})[33n^4+1594n^2+5621+2^7m^2(16m^2-37n^2-167)]c^{-3} \quad (c>0)$$
$$+\cdots \quad (n=2l+1) \quad (l=0, 1, 2, \cdots). \quad (11)$$

* Prepared under the sponsorship of the Office of Naval Research.

[1] L. J. Chu and J. A. Stratton, J. Math. and Phys. **20**, 259 (1941).

The special case $m=-\frac{1}{2}$ affords an interesting check. When $m=-\frac{1}{2}$ the substitution $x=\cos t$ reduces (1) to the Mathieu equation, and the series (11) reduces to the expansion obtained independently by Ince and Goldstein[2] by radically different methods. In this case the series approximates the characteristic values corresponding to ce_t and se_{t+1} simultaneously.

III. ADDENDUM

Professor A. N. Lowan of the Computation Laboratory of the National Bureau of Standards has communicated to the author a copy of a note by J. Meixner[3] (of Aachen, Germany) which has just reached this country. The note contains the series (11) but no indication of the method of derivation. Since this paper is unlikely to be generally available for some time, we reproduce here the two additional coefficients in (6) computed by Meixner and his collaborators:

$$\beta_4=-2^{-16}(63n^6+4940n^4+43327n^2+22470)+2^{-9}m^2(115n^4+1310n^2+735)-\tfrac{3}{8}m^4(n^2+1),$$

$$\beta_5=-2^{-20}n(527n^6+61529n^4+1043961n^2+2241599)+2^{-15}m^2n(5739n^4+127550n^2+298951)-2^{-9}m^4n(355n^2+1505)+(1/16)m^6n.$$

[2] E. Jahnke and F. Emde, *Tables of Functions* (Dover Publications, New York, 1943), p. 285.

[3] J. Meixner, Zeits. angewandte Math. Mech. **25/27** Heft 5/6 (Aug./Sept. 1947).

PHYSICAL REVIEW VOLUME 74, NUMBER 2 JULY 15, 1948

Stability of the Laminar Parabolic Flow of a Viscous Fluid between Parallel Fixed Walls

C. L. PEKERIS
The Institute for Advanced Study, Princeton, New Jersey and The Weizmann Institute, Rehovoth, Palestine*

(Received March 19, 1948)

Asymptotic expressions are derived for the characteristic values C of two-dimensional disturbances of the parabolic flow in the limit of small wave numbers α and large values of αR, where R denotes Reynolds number. For the first mode we get

$$C_1=1.617e^{i\pi/6}(\alpha R)^{-\frac{1}{3}}+\alpha^2[.395-.883e^{i\pi/6}(\alpha R)^{-\frac{1}{3}}+(i/\alpha R)]+0(\alpha^4).$$

An excellent check on the constants in C_1 was obtained by a detailed numerical integration of the differential equation at $\alpha R=5430$. The above result shows stability of the first mode at large αR and small α^2. The possible perturbations of the parabolic flow fall into two classes, one in which at $\alpha^2=0$, $C_r\to 0$, as $\alpha R\to\infty$, and another in which $C_r\to 1$ as $\alpha R\to\infty$. At large αR the characteristic values of the modes in the latter class for finite α^2 approach their values at $\alpha^2=0$, and are stable. All the modes of the first class are stable at large αR as far as α^2-terms in C are concerned. In the even modes of this class the phase velocity becomes negative (propagation upstream) for $\alpha^7R>M$, where M for the second mode has a value of 10700. The possible bearing of this result on stability experiments is discussed.

I. INTRODUCTION

THIS investigation is concerned with the problem of the stability of the laminar parabolic viscous flow between parallel fixed walls to infinitesimal two-dimensional disturbances. With the walls situated at $y=\pm h$ and U_0 denoting the maximum velocity at the center of the channel, we adopt a system of non-dimensional coordinates in which h, U_0, and (h/U_0) are the units of length, velocity, and time, respectively. The laminar flow U is then represented by

$$U=1-y^2. \tag{1}$$

Upon this flow we superimpose a two-dimensional disturbance

$$u=\partial\psi/\partial y,\quad v=-\partial\psi/\partial x,\qquad \psi=f(y)\exp i\alpha(Ct-x) \tag{2}$$

* This work was made possible by the general support of the Office of Naval Research, under Contract N6ori-139, Task I, on which project the writer served as a consultant.

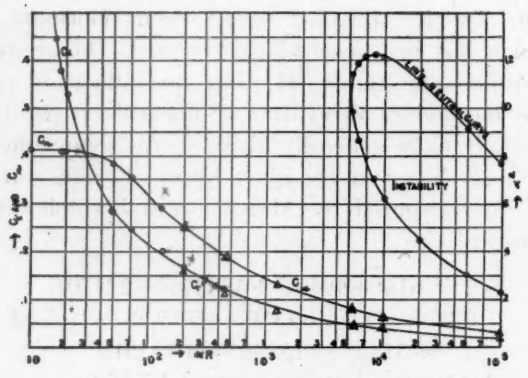

FIG. 1. The real part C_r and the imaginary part C_i of C in the case $\alpha^2=0$. Dots represent exact values, Δ-values computed from Eq. (30).

representing a wave of wave number α propagating with the complex velocity C in the x direction. Upon neglecting second-order terms in ψ, we find from the hydrodynamic equations that $f(y)$ must satisfy the differential equation

$$f^{iv}-2\alpha^2(\partial^2 f/\partial t^2)+\alpha^4 f+i\alpha R \times[2f+(1-y^2-C)((\partial^2 f/\partial t^2)-\alpha^2 f)]=0 \quad (3)$$

subject to the boundary conditions

$$f(1)=\dot{f}(1)=f(-1)=\dot{f}(-1)=0. \quad (4)$$

If the characteristic values C of the system (3) and (4) have all positive imaginary parts C_i, then the parabolic flow is considered to be stable to infinitesimal disturbances; if, on the other hand, there exists a mode for which C_i is negative the flow is unstable.

The system (3) and (4) determines C as a function of the two parameters α^2 and αR, R denoting the Reynolds number. Recently Schubauer and Skramstad[1] have demonstrated experimentally that in the case of the boundary layer flow there exists a region in the $(\alpha^2,\alpha R)$ plane where C_i is negative for the first mode, in confirmation of a theoretical prediction made by Tollmien[2] and Schlichting.[3] Subsequent to these experiments Lin[4] published a similar theoretical "neutral curve" for the parabolic flow, as shown in Fig. 1, from which it would follow that instability ensues for $R>5200$. Since Lin follows closely Tollmien's analysis, this result presumably refers also to the first mode. The stability of the parabolic flow has recently been studied also by Meksyn[5] who finds a critical Reynolds number of 6700 at $\alpha=1$.

The arguments employed by these authors, though chiefly analytical, involve a considerable amount of subsidiary numerical computations which the reader would have to check for himself. Since a previous attempt by the writer[6] to attack the stability problem of the parabolic flow *ab initio* numerically gave indications of stability, it was felt that further work was needed, preferably before the problem is solved experimentally.

In an effort to throw more light on this age-long problem, the writer attempted to derive explicit expressions for C valid asymptotically for large R, and to check these, where possible, by exact numerical computations based on the power-series solutions of (3). The result for the first mode is

$$C=C_0+\alpha^2 C_2+\cdots, \quad (5)$$

$$C_0=(1.401+0.809i)/(\alpha R)^{\frac{1}{3}}, \quad (6)$$

$$C_2=0.395-0.546C_0+(i/\alpha R). \quad (7)$$

Figure 1 shows that (6) gives accurate values for $\alpha R>500$, while Table I shows that already at $\alpha R=5430$, (7) is a good approximation to C_2. For small α^2 and large αR the imaginary part of C is therefore given by $0.809(1-0.546\alpha^2)/(\alpha R)^{\frac{1}{3}}$. Now it is seen from Fig. 1 that for $\alpha R=10^5$, α^2 on the lower branch of the "neutral curve" is 0.21, while at $\alpha R=10^6$, $\alpha^2=0.1$. For such small values of α^2, (5) would be expected to be adequate. Our results therefore give considerable damping at a point for which, according to Lin, the damping should vanish.

A closer inspection suggests that the disagreement is not likely to be due to the contribution from higher order terms in α^2 which were neglected in (5), but to an implicit wrong value for the imaginary part of C_2. Lin, namely, finds[7] that for large R the lower branch of his "neutral curve" is represented asymptotically by $\alpha^{\frac{3}{2}}R^{\frac{1}{2}}$

[1] G. B. Schubauer and H. K. Skramstad, J. Ae. Sci. **14**, 69 (1947).
[2] W. Tollmien, N.A.C.A. Tech. Memo. No. 609 (1931); N.A.C.A. Tech. Memo. No. 792 (1936).
[3] H. Schlichting, Göttinger Nachrichten **13**, 181 (1933); **1**, 47 (1935).
[4] C. C. Lin, Quart. App. Math, **3**, 288 (1946).
[5] D. Meksyn, Proc. Roy. Soc. **A186**, 391 (1946).
[6] C. L. Pekeris, J. Ae. Sci. **5**, 237 (1938).
[7] See reference 4, p. 287.

$=5.96$. This could be brought about by the imaginary part of the $\alpha^2 C_2$ term canceling the imaginary part of C_0, provided the former had the value of $-0.136\alpha^2$. Indeed, Lin arrives at the conclusion that above the lower branch of his "neutral curve" C_i is negative and is of the same order as C_r, which is $0(\alpha R^0)$. Equation (7) shows, however, that the imaginary part of C_2 is $0(\alpha R^{-4})$, so that for small α^2 we always have stability.

II. METHOD OF SOLUTION

Our derivation of C_2 is based on a method which avoids a troublesome complication that besets the work of Lin and Meksyn. In developing the solution of (3) for small α^2 in the form

$$f=f_0+\alpha^2 f_2+\cdots \tag{8}$$

with the associated expansion (5) for C, one finds from (3) that

$$f_0^{iv}+i\alpha R[2f_0+(1-y^2-C_0)(\partial^2 f_0/\partial t^2)]=0, \tag{9}$$

$$f_2^{iv}+i\alpha R[2f_2+(1-y^2-C_0)(\partial^2 f_2/\partial t^2)] = 2(\partial^2 f_0/\partial t^2)+i\alpha R[(1-y^2-C_0)f_0 + C_2(\partial^2 f_0/\partial t^2)]. \tag{10}$$

f_0 and f_2 must satisfy the boundary conditions (4). On solving (9) and then [illegible] boundary conditions one determines C_0 [illegible] be determined either similarly [illegible] f_2 from (10) and then imposing the [illegible] conditions on it, or by adopting the following standard procedure, which avoids the explicit solution for f_2. First we note that for the even solutions, with which we shall solely be concerned in the sequel, (9) integrates into

$$(\partial^3 f_0/\partial t^3)+i\alpha R[2yf_0+(1-y^2-C_0)f_0]=0; \qquad (\partial^3 f_0/\partial t^3)(1)=0. \tag{11}$$

Proceeding similarly with (10) we obtain

$$(\partial^3 f_2/\partial t^3)(1)=i\alpha R\int_0^1 f_0(y)(1-y^2-C_0)dy. \tag{12}$$

Now multiply (9) by $-(\partial^2 f_2/\partial t^2)$, (10) by $(\partial^2 f_0/\partial t^2)$, add, and integrate from 0 to 1, obtaining

$$(\partial^3 f_2/\partial t^3)(1)(\partial^3 f_0/\partial t^3)(1) - \int_0^1 \{(\partial^2 f_0/\partial t^2)+i\alpha R \times[(1-y^2-C_0)f_0+C_2(\partial^2 f_0/\partial t^2)]\}dy. \tag{13}$$

By multiplying (9) by f_0 and integrating from 0 to 1 we get

$$\int_0^1 \{(\partial^2 f_0/\partial t^2)^2+i\alpha R \times[2f_0^2+(1-y^2-C_0)(\partial^2 f_0/\partial t^2)f_0]\}dy=0. \tag{14}$$

From (13) and (14) it follows, by the use of [illegible], that

$$C_2=(i/\alpha R)+\left[2\int_0^1 f_0^2 dy+(\partial^2 f_0/\partial t^2)(1) \times\int_0^1 (1-y^2-C_0)f_0 dy\right] / \int_0^1 [illegible](\partial^2 f_0/\partial t^2)^2 dy. \tag{15}$$

We may also [illegible]

$$\int_0^1 (\partial^2 f_0/\partial t^2)^2 dy = i\alpha R\int_0^1 f_0[2yf_0+(1-y^2-C_0)f_0]dy, \tag{16}$$

a result which can be derived by partial integration and the use of (11).

The advantage of basing the computation of C_2 on (15) is that while the solution of (9) for f_0 can be readily obtained, the solution of (10) for f_2 is more difficult. One *exact* (inviscid) even solution of (9) is

$$f_0^{(1)}=1-y^2-C_0. \tag{17}$$

The second (viscous) even solution of (9) depends on R, and, as will be shown later, is significant only near the walls. The difficulty arises when one attempts to derive the inviscid solution for f_2 corresponding to $f_0^{(1)}$ in (17), because the viscous term f_2^{iv} has to be included along with the inviscid terms inside the brackets in (10) when continuing the solution through the Stokes point $1-y^2-C_0=0$.

III. ASYMPTOTIC EXPRESSIONS FOR f_0 AND C_0 IN THE FIRST CLASS OF PERTURBATIONS

In the following section we shall develop an asymptotic expression for C_2 in (15) valid for large values of the parameter αR. For this purpose we shall first obtain the asymptotic forms which f_0 and C_0 in (9) assume for large Reynolds numbers. These turn out to be of two classes,

one in which for $\alpha^2=0$, $C_r\to 0$ as $\alpha R\to\infty$, and another in which $C_r\to 1$. We shall first treat the former class because when the first mode is continued from $\alpha R=0$ it is found to terminate into this class at large αR. Let

$$\epsilon=e^{i\pi/6}(2\alpha R)^{\frac{1}{3}}, \quad y=1-(\gamma_1/\epsilon)+(z/\epsilon), \tag{18}$$

$$f=(1-y^2-C_0)+B\varphi(z);$$

$$\varphi(z)=\varphi_0(z)+(1/\epsilon)\varphi_1(z)+\cdots, \tag{19}$$

$$C_0\to(2\gamma_1/\epsilon)+(2\gamma_2/\epsilon^2)+\cdots;$$

$$z_0=\gamma_1-\epsilon; \quad z_1=\gamma_1, \tag{20}$$

where z_0 and z_1 are the values of z at $y=0$ and $y=1$, respectively. Since the second independent even solution [illegible] starts with the term y^2, and $\varphi(z)$ is even in y, we must have

$$\varphi(z_0)=\dot{\varphi}(z_0)=0. \tag{21}$$

Substituting (18) to [illegible] and equating each power of ϵ to zero [illegible]

$$(d^4\varphi_0/dz^4)+z(d^2\varphi_0/dz^2)=0;$$

$$\therefore \quad (d^3\varphi_0/dz^3)+z(d\varphi_0/dz)-\varphi_0=0, \tag{22}$$

$$(d^4\varphi_1/dz^4)+z(d^2\varphi_1/dz^2)$$
$$=\varphi_0-[\gamma_2+(\tfrac{1}{2})(z-\gamma_1)^2](d^2\varphi_0/dz_0^2). \tag{23}$$

With

$$(d^2\varphi_0/dz^2)\equiv F(z), \quad (\partial^2F/\partial t^2)(z)+zF(z)=0, \tag{24}$$

the boundary conditions (11) and (21) require that

$$\dot{F}(z_0)=\dot{F}(z_1)=0. \tag{25}$$

The solutions of (24) behave asymptotically as

$$(9/\pi^2z)^{\frac{1}{4}}\exp\{\pm i[(5/12)-(2/3)z^{\frac{3}{2}}]\}.$$

Since $z_0^{\frac{1}{2}}\simeq(\alpha R)^{\frac{1}{3}}(-1-i)$ one finds upon expressing $F(z)$ as a linear combination of two independent solutions and imposing the boundary conditions (25) that within terms of the order of $\exp[-(4/3)(\alpha R)^{\frac{3}{2}}]$ the appropriate solution of (24) is

$$F(z)=(z)^{\frac{1}{2}}H_{\frac{1}{3}}^{(2)}[(\tfrac{2}{3})z^{\frac{3}{2}}], \tag{26}$$

$$\dot{F}(z_1)=z_1H_{-\frac{1}{3}}^{(2)}[(\tfrac{2}{3})z_1^{\frac{3}{2}}]=0. \tag{27}$$

The roots of (27) are

$$z_1^{(m)}=\gamma_1^{(m)}=e^{i2\pi/3}\tau_m; \quad \tau_m=(3v_m/2)^{\frac{2}{3}};$$
$$[J_{\frac{1}{3}}(v_m)-J_{-\frac{1}{3}}(v_m)]=0. \tag{28}$$

The τ_m coincide with the roots x_m of $\dot{A}i(-x)$, which are tabulated in the B.A. Tables:[8]

[8] *B. A. Tables* (Cambridge University Press, Teddington, England, 1946), Vol. B.

$\tau_1=1.01879297$, $\tau_2=3.24819758$. It will be shown below that

$$\gamma_2^{(m)}=[(27-8\tau_m^3)/30\tau_m]\exp(-i2\pi/3) \tag{29}$$

so that, from (20), the characteristic value C_0 is expressed asymptotically by

$$C_0\to 2\tau_me^{i\pi/6}/(2\alpha R)^{\frac{1}{3}}$$
$$+(27-8\tau_m^3)e^{i\pi/3}/[15\tau_m(2\alpha R)^{\frac{2}{3}}]+\cdots. \tag{30}$$

We shall now determine B, and along with C_0, in (19). With $F(z)$ defined in (26) the solution of (22) is

$$\varphi_0(z)=\dot{F}(z)+z\int_{z_0}^{z}F(x)dx,$$

$$\dot{\varphi}_0(z)=\int_{z_0}^{z}F(x)dx. \tag{31}$$

It is shown in the Appendix that

$$\int_{z_0}^{z_1}F(x)dx=z_1F(z_1)N^{(m)}, \quad N^{(1)}=1.4825708, \tag{32}$$

so that

$$\varphi_0(z_1)=z_1^2F(z_1)N, \quad \dot{\varphi}_0(z_1)=z_1F(z_1)N. \tag{33}$$

The solution of (23) which makes $\varphi_1(z_0)=0$ is

$$\varphi_1(z)=[(z^2/3)-(2\gamma_1/3)]\varphi_0$$
$$+[\gamma_2+\gamma_1^2-(\gamma_1/3)+z^2/10)\dot{\varphi}_0+(9/10)\ddot{\varphi}_0. \tag{34}$$

Upon imposing the condition $\varphi_1(z_1)=0$ on (34), we get

$$[(9/10z_1)]-(4z_1^2/15). \tag{35}$$

With the aid of (33), (31), and (35) we now obtain on using (19)

$$f(1)=-C_0+B\varphi(z_1)=0, \tag{36}$$

$$\dot{f}(1)=-2+B\epsilon\dot{\varphi}(z_1)=0, \tag{37}$$

$$C_0=\frac{2\varphi(z_1)}{\epsilon\dot{\varphi}(z_1)}=\frac{2z_1}{\epsilon}$$
$$\times\left[1+\frac{z_1}{\epsilon}\left(-\frac{4}{15}+\frac{9}{10z_1^3}\right)+\cdots\right], \tag{38}$$

$$B=\frac{2}{\epsilon\dot{\varphi}(z_1)}=\frac{2}{\epsilon z_1F(z_1)N}$$
$$\times\left[1-\frac{z_1}{\epsilon}\left(\frac{4}{3}+\frac{\quad}{10z_1^3}\right)+\cdots\right] \tag{39}$$

which are asymptotic expansions in inverse powers of $(\alpha R)^{\frac{1}{3}}$.

IV. ASYMPTOTIC EXPRESSIONS FOR C_2 IN THE FIRST CLASS OF PERTURBATIONS

a. The First Mode

Turning now to the terms appearing in expression (15) for C_2, we have first

$$(\partial^2 f/\partial t^2)(1) = -2+\frac{2\epsilon\ddot{\varphi}(z_1)}{\dot{\varphi}(z_1)} = \frac{2\epsilon}{z_1 N}\left[1+\frac{z_1}{\epsilon}\left(-\frac{43}{30}-\frac{9}{10Nz_1^3}\right)+\cdots\right]. \quad (40)$$

Next we note that in evaluating $\int_0^1 f^2(y)dy$, the term

$$2B\int_0^1 (1-y^2-C_0)\varphi(z)dy \simeq -(4B/\epsilon^2)\times\int_{z_0}^{z_1} z\varphi_0(z)dz = 0(1/\epsilon^3), \quad (41)$$

so that we have, to within terms of the order of ϵ^{-3},

$$\int_0^1 (1-y^2-C_0)f(y)dy \simeq \int_0^1 f^2(y)dy = (8/15)-(4/3)C_0+C_0^2. \quad (42)$$

Further, on making use of the identities

$$\int(\ddot{\varphi}_0)^2dz = (\partial^3\varphi_0/\partial t^3)^2+z(\ddot{\varphi}_0)^2; \quad 3\int z(\ddot{\varphi}_0)^2dz = z(\partial^3\varphi_0/\partial t^3)^2-\ddot{\varphi}_0(\partial^3\varphi_0/\partial t^3)+z^2(\ddot{\varphi}_0)^2, \quad (43)$$

we get

$$\int_{z_0}^{z_1}(\ddot{\varphi}_0)^2dz = z_1F^2(z_1); \quad \int_{z_0}^{z_1} z(\ddot{\varphi}_0)^2dz = (1/3)z_1^2F^2(z_1), \quad (44)$$

$$\int_{z_0}^{z_1}(\ddot{\varphi})^2dz = z_1F^2(z_1)\times\left[1+\frac{z_1}{\epsilon}\left(N^2+\tfrac{1}{5}+\frac{9}{10z_1^3}\right)+\cdots\right], \quad (45)$$

$$\int_0^1(\partial^2 f/\partial t^2)^2dy = \frac{4\epsilon}{z_1N^2}\times\left[1+\frac{z_1}{\epsilon}\left(-\frac{37}{15}-\frac{9}{5Nz_1^3}+\frac{9}{10z_1^3}\right)+\cdots\right]. \quad (46)$$

Using now (40), (42), and (46) in (15) we obtain the following asymptotic expression for C_2 valid for large αR

$$C_2 \to \frac{i}{\alpha R}+\frac{4N}{15}\left[1+\frac{z_1}{\epsilon}\left(N-\frac{119}{30}-\frac{9}{10z_1^3}+\frac{9}{10Nz_1^3}\right)+0(z_1^2/\epsilon^2)\right]. \quad (47)$$

The above formulae have been checked at $\alpha R = 5430$ for which, according to Lin's "neutral curve," the imaginary part of C should vanish at $\alpha^2 = 1$. For this purpose the second solution $\varphi(z)$ in (19) was written in the form

$$\varphi(y) = \exp[-(\tfrac{1}{2})(i\alpha R)^{\frac{1}{3}}y^2]\times\sum_{n=2}^{\infty}B_ny^n, \quad (48)$$

and the coefficients B_n were computed from the recursion formula resulting from (9). The adoption of the exponential factor in (48) was resorted to because the straight series solution of (9) of the form $\sum b_n y^n$ is very small at $y=1$, so that in the sums $\sum b_n$ and $\sum nb_n$ all of the first ten significant figures canceled out. Using a value of C_0 of $(0.08092+0.04815i)$ as given by (30), it was found that the term $[(2/C_0)+(i\alpha R)^{\frac{1}{3}}]$ agreed with $[\sum nB_n/\sum B_n]$ to within 2 parts in 10^4, showing the accuracy of the adopted value of C_0. A better check was obtained at $\alpha R = 10000$ when the right value for C_0, as given by (30), was used; complete disagreement resulted, however, when the above value of C_0 for 5430 was erroneously used for $\alpha R = 10000$. At 5430 the value of $(\partial^2 f/\partial t^2)(1)$ was then computed by adding -2 to the second derivative of (48). Also the $\int_0^1(\partial^2 f_0/\partial t^2)^2dy$ was evaluated numerically by first computing $f_0(y)$ and $\dot{f}_0(y)$ at intervals of 0.025 in y, and then using (16). Relation (42) was found to be satisfied with high accuracy. A comparison of the numerical values thus obtained with those given by the asymptotic expressions (40), (46), and (47) is shown in Table I,

TABLE I. Numerical check on Eqs. (40), (46) and (47) for $\alpha R=5430$, plus some less refined numerical results for $\alpha R=10000$.

αR	$(\partial^2 f/\partial t^2)(1)$ Num	(40)	$\int_0^1(\partial^2 f/\partial t^2)^2 dy$ Num	(46)	C_2 Num	(47)
5430	22.66–14.68i	22.69–14.66i	29.03–19.79i	29.23–19.78i	0.3515–0.0242i	0.3519–0.0249i
10000		28.42–17.97i	37.33–24.23i	36.99–24.24i	0.3572–0.0221i	0.3599–0.0204i

where are also found some less refined numerical calculations for $\alpha R=10000$. *The agreement between the numerical and analytical values at 5430 proves that expression (47) for C_2 can be relied on to an accuracy of about 1 part in 10^3 at $\alpha R=5430$ and beyond.*

To complete the discussion of the characteristic values of the first mode we give in Table II some numerical results. The exact values for C and C_0 were computed from the power series solutions of (3) and (9), respectively, while the exact values of C_2 were computed from (15) by numerical integration. It is seen that at $\alpha R=450$ the exact value for C at $\alpha^2=1$ is approximated by (C_0+C_2).

b. The Higher Modes

Some interesting features are revealed when we examine the asymptotic forms assumed by the characteristic values of the higher order modes belonging to the class discussed in this section. These are determined by Eqs. (28), (30), and (47), with N in the latter taking on the values $N^{(m)}$ determined from (32). If we neglect the second term in (30) and write these equations in the form

$$C=ae^{i\pi/6}(\alpha R)^{-\frac{1}{3}}+\alpha^2 \times[b+de^{i\pi/6}(\alpha R)^{-\frac{1}{3}}+(i/\alpha R)]+\cdots, \quad (48')$$

TABLE II. Exact and asymptotic characteristic values for the first mode. $C=C_0+\alpha^2C_2+\cdots$.

	αR	C_0	C_2	C_0+C_2	C for $\alpha^2=1$
Exact	10	0.413 +1.004i			0.520+0.940i
	20	0.410 +0.528i			0.520+0.483i
	50	0.387 +0.286i			
	72	0.360 +0.241i			
	128	0.290 +0.198i			
	200	0.249 +0.165i	0.266−0.061i	0.515+0.104i	0.433+0.112i
	450	0.191 +0.124i	0.251−0.040i	0.442+0.080i	0.384+0.083i
Asymptotic	5430	0.0809+0.0481i	0.352−0.024i	0.433+0.023i	
	10^4	0.0658+0.0390i	0.357−0.022i	0.426+0.019i	
	10^5	0.0304+0.0177i	0.379−0.0095i	0.409+0.0082i	

we obtain the values of the constants given in Table III for the successive modes of this class: The fact that for the even modes, b is negative means that for large αR and small α^2 the phase velocity of the mode C_r becomes negative when $\alpha^2(\alpha R)^{\frac{1}{3}}>[0.866a/(-b)]$. The lowest value of α^7R_c is 10700 for the second mode. For $R>R_c$ we have the possibility of a disturbance originating at the *mouth* of a tube and being propagated *upstream*. Though these modes are damped, the amplitude of the disturbance emanating from the mouth is likely to have been large in the experiments of both Reynolds and Ekman. Whereas Reynolds, and especially Ekman, took great precautions to smooth the entry to their tube, no such care was given to the conditions at the exit. In this discussion it is implied that in the case of the flow through a tube, disturbances which are not axially symmetric are related to the two-dimensional disturbances of class one of the two-dimensional parabolic flow.

V. THE SECOND CLASS OF PERTURBATIONS

As mentioned before, the possible perturbations of the parabolic flow fall into two classes. In the first, $C_r\to 0$ at $\alpha^2=0$ and in the limit of $\alpha R\to\infty$. We shall now discuss the second class of perturbations which is characterized by $C_r\to 1$ as $\alpha R\to\infty$. We have seen in Eq. (48) and Table III that for large αR there is a denumerable set of modes belonging to the first class. It will be shown below that for large αR there is also a denumerable set of modes belonging to the second class. On the other hand, at small values of αR the possible perturbations of the (slow) parabolic flow are of a single set of modes only. In a previous paper[9] formulae were given for the characteristic values C_n of the nth mode valid for small αR. We quote here the results for the

[9] C. L. Pekeris, Proc. Camb. Phil. Soc. **32**, 62 (1936).

first three modes in the case $\alpha^2=1$:

$$C_1=(9.314/R)i +0.5198+0.000842Ri+\cdots, \quad (49)$$

$$C_2=(38.948/R)i +0.6514+0.000359Ri+\cdots, \quad (50)$$

$$C_3=(88.300/R)i +0.6615-0.0001092Ri+\cdots. \quad (51)$$

In the sequel we shall understand by the *first mode* the first possible mode at small αR, and, similarly, for the higher order modes. It will be seen from Fig. 1 and Table II that for large αR the first mode coincides with the first mode of class one. *We shall now show that the second and third modes terminate at large αR into the first and second modes, respectively, of class two.* The question of where the modes above the first in class one originate from, as well as the class to which the modes above the third belong to is left open.

Our discussion of the characteristic values for the second class will be limited principally to the case $\alpha^2=0$. It has been found by the use of a procedure similar to the one followed on another occasion[10] that for the first mode of this class $C_2=-(5i/3\alpha R)$, so that at large αR, C approaches its limit for $\alpha^2=0$. It is shown below that this result is also verified numerically for the second mode of this class. Putting $z=y^2$ we obtain from (11)

$$4z(d^3f_0/dz^3)+6(d^2f_0/dz^2) +i\alpha R[f_0+(1-z-C_0)(df_0/dz)]=0. \quad (52)$$

Let

$$x=(i\alpha R)^{\frac{1}{2}}z=(i\alpha R)^{\frac{1}{2}}y^2, \qquad a=[5-(1-C_0)(i\alpha R)^{\frac{1}{2}}]/4, \quad (53)$$

then upon differentiating (52) we get

$$x(d^4f_0/dx^4)+(5/2)(d^2f_0/dx^2) +[(5/4)-a-(x/4)](d^2f_0/dx^2)=0, \quad (54)$$

$$d^2f_0/dx^2=e^{-x/2}F(a,5/2,x), \quad (55)$$

where F denotes the confluent hypergeometric function. From the boundary condition $d^3f_0/dy^3=0$ at $y=1$ we obtain from (55), after some transformations,

$$b(a,x)=F(a,3/2,x) +F(a-1,3/2,x)=0; \quad x=(i\alpha R)^{\frac{1}{2}}, \quad (56)$$

a relation determining a, and with it C_0, as a function of αR.

Now for large αR it follows from

$$F(\alpha,\gamma,x)\rightarrow\frac{\Gamma(\gamma)}{\Gamma(\alpha)}e^{x}x^{\alpha-\gamma} \times\left[1+\frac{(1-\alpha)(\gamma-\alpha)}{x}+\cdots\right]+\cdots \quad (57)$$

that

$$b(a,x)\rightarrow\frac{\Gamma(3/2)}{\Gamma(a)}e^{x}x^{a-1.5} \times\left[1+\frac{(1-a)(0.5-a)}{x}+\cdots\right], \quad (58)$$

$$\therefore\ \frac{1}{\Gamma(a)}=0; \quad a=1-m, \quad m=1,2,\cdots, \quad (59)$$

$$C^{(m)}=1-(1+4m)/(i\alpha R)^{\frac{1}{2}}. \quad (60)$$

Equation (59) is a polynomial condition on the F's, as otherwise they become exponentially large. Using (60) and the result quoted above for C_2 in the case $a=0$, we get for the first mode of this class

$$C^{(1)}=1-5(i\alpha R)^{\frac{1}{2}}-(5i\alpha^2/3\alpha R), \quad (61)$$

and for the second mode of this class

$$C^{(2)}=1-9/(i\alpha R)^{\frac{1}{2}}. \quad (62)$$

Tables IV and V show that the second and third mode merge with the first and second modes of the second class. The exact values were computed from the power-series for $b(a,x)$ in (56). The second class of modes is of a similar nature to the axially symmetrical perturbations of the

TABLE III. Values of the parameters in the asymptotic expression (48) for the characteristic values of the modes belonging to the first class of perturbations.

Mode	a	b	d	N
1	1.617	0.3954	−0.883	1.48257
2	5.156	−0.2026	2.501	−0.75983
3	7.651	0.1432	−1.875	0.53696
4	9.784	−0.1220	2.647	−0.45747
5	11.703	0.1050	−2.193	0.3938

[10] C. L. Pekeris, Proc. Nat. Acad. Sci. (in press).

TABLE IV. Characteristic values C for the second mode at $\alpha^2=1$.

αR	C from (50)	C from (61)	C exact
10	$0.651+3.898i$		
20	$0.651+1.955i$		
50	$0.651+0.797i$		$0.659+0.771i$
100	$0.651+0.425i$	$0.646+0.337i$	$0.694+0.382i$
200	$0.651+0.267i$	$0.750+0.241i$	$0.752+0.232i$
450		$0.833+0.163i$	$0.834+0.162i$

TABLE V. Characteristic values C for the third mode at $\alpha^2=1$.

αR	C from (51)	C from (62)	C exact
10	$0.661+8.829i$		
20	$0.661+4.413i$		
50	$0.661+1.761i$		
100	$0.661+0.872i$	$0.364+0.636i$	$0.661+0.873i$
200	$0.661+0.420i$	$0.540+0.450i$	$0.654+0.432i$
450		$0.700+0.300i$	$0.709+0.284i$

laminar flow through a pipe of circular cross section,[9] where asymptotically C approaches the form (60).

SUMMARY

The stability of the parabolic flow is determined by the sign of the imaginary part of a characteristic value C which is a function of the parameters α^2, and αR, where α denotes the wave number of the disturbance, and R the Reynolds number of the laminar flow. C and the stream function f are developed into

$$C=C_0+\alpha^2C_2+\cdots;\quad f=f_0+\alpha^2f_2+\cdots, \quad (63)$$

and C_2 is determined from a knowledge of f_0 only, as given in Eq. (15), thus obviating the logarithmic complications arising in f_2. An asymptotic expression for C_0 is derived in Eq. (30). Exact values of C_0 were computed for the first mode by using the power-series solutions of (9) and are shown in Table II and Fig. 1. The latter shows that the asymptotic expression for C_0 given in Eq. (30) is a good representation for $\alpha R>500$. On the basis of (15) an explicit expression is derived for C_2 in (47) valid for large αR. Table I shows that at $\alpha R=5430$, Eq. (47) is in good agreement with results of a detailed numerical computation. As an additional check, a rough calculation of C_2 was made at $\alpha R=10000$ and, as shown in Table I, the agreement with (47) is to within the expected accuracy. At $\alpha R=450$, $C_0+C_2=(0.442+0.080i)$, whereas the exact value of C for $\alpha^2=1$ is $(0.384+0.083i)$, indicating a fair approximation to C at this value of αR by $(C_0+\alpha^2C_2)$ up to α^2 of about unity.

Some results on the asymptotic behavior of C for the first and some higher modes are set out in Eq. (48) and Table III. As far as the C_2 term in the expansion (63) for C goes, C_i is positive for all modes, indicating stability. Lin's result, that for large αR and small $\alpha^2(<0.2)$ the lower branch of his "neutral curve" (see Fig. 1) is given by $\alpha^7R=212$, would require the imaginary part of C_2 to be -0.136 instead of the actual term $[(1/2)d(\alpha R)^{-\frac{1}{2}}+(1/\alpha R)]$ in (48). Hence the lower portion of his "neutral curve" is not neutral, and, in view of the agreement cited above at $\alpha R=450$ it is probable that there is no region of instability for the parabolic flow.

Table III shows that in the evenly labeled modes the phase velocity C_r, as given by $[(\sqrt{3}/2)a(\alpha R)^{-\frac{1}{2}}+\alpha^2b]$, vanishes when $\alpha^7R_c=M$, M having the value 10700 for mode 2. When $R>R_c$, disturbances originating at the exit of the pipe are propagated *upstream* via these modes. It would be interesting to follow up this point experimentally.

Whereas in the class of modes discussed above $C\to0$ as $\alpha R\to\infty$ at $\alpha^2=0$, there exists for the parabolic flow another class of modes which is characterized by $C\to1$ as $\alpha R\to\infty$. In these modes the values of C for finite α^2 approach their values at $\alpha^2=0$. In the latter limit an asymptotic expression for C is derived in Eq. (60). Tables IV and V show that the second and third modes belong to the second class, and that their characteristic values can be computed by using Eqs. (50) and (51) for small αR, and then taking over with the asymptotic expressions (61) and (62) for large αR. For the second class of perturbations C_i of the "mth" mode approaches the positive value of $(1+4m)/(2\alpha R)^{\frac{1}{2}}$ at large αR.

It would be interesting to compute, with the aid of an electronic computer, the exact values of C at $\alpha^2=1$ for the last three values of αR given in Table II, in order to check the values predicted from (C_0+C_2). It would also be of interest to explore numerically, to smaller αR, the origin of the higher modes shown in Table

III. Some modification of the direct power-series solution of (3) will be required at large αR because in the sums for $f(1)$ and $\dot{f}(1)$ most of the first ten decimals will cancel out.

The author is indebted to Misses E. Herman and F. Jones for the computations made in this investigation.

APPENDIX

In order to calculate N in

$$\int_{z_0}^{z_1} F(x)dx = z_1 F(z_1) N;$$

$$F(x) = (x)^{\frac{1}{3}} H_{\frac{1}{3}}^{(2)}(\tfrac{2}{3}x^{\frac{3}{2}}), \quad (63)$$

where

$$z_1 = e^{i2\pi/3}\tau; \quad [J_{\frac{1}{3}}(\tfrac{2}{3}\tau^{\frac{3}{2}}) - J_{-\frac{1}{3}}(\tfrac{2}{3}\tau^{\frac{3}{2}})] = 0,$$

$$z_0 \simeq e^{-i\pi/2}(2\alpha R)^{\frac{1}{3}}, \quad (64)$$

we write

$$\int_{z_0}^{z_1} F(x)dx = \int_0^{z_1} F(x)dx - \int_0^{z_0} F(x)dx. \quad (65)$$

By partial integration and the use of (24) and (25) we obtain

$$\int_0^{z_1} F(x)dx = z_1 F(z_1) Q(z_1^3);$$

$$Q(x) \equiv \sum_{n=0}^{\infty} (-)^n (3x)^n n!/(3n+1)!. \quad (66)$$

Also, with

$$u = (2/3)e^{i\pi/2}x^{\frac{3}{2}}, \quad u_0 = (2/3)(2\alpha Re)^{\frac{1}{2}} e^{-i\pi/4}, \quad (67)$$

we have

$$\int_0^{z_0} (x)^{\frac{1}{3}} H_{\frac{1}{3}}^{(2)}(\tfrac{2}{3}x^{\frac{3}{2}})dx = e^{-i\pi/2}$$

$$\times \int_0^{u_0} H_{\frac{1}{3}}^{(2)}(e^{-i\pi/2}u)du \simeq e^{-i\pi/2}$$

$$\times \int_0^{\infty} H_{\frac{1}{3}}^{(2)}(e^{-i\pi/2}u)du = (2/\pi)e^{i\pi/6}$$

$$\times \int_0^{\infty} K_{\frac{1}{3}}(u)du = (2/\sqrt{3})e^{i\pi/6}. \quad (68)$$

Now

$$z_1 F(z_1) = -\frac{2}{\sqrt{3}} e^{i\pi/6}\tau^{\frac{1}{2}}[J_{-\frac{1}{3}}(\tfrac{2}{3}\tau^{\frac{3}{2}}) + J_{\frac{1}{3}}(\tfrac{2}{3}\tau^{\frac{3}{2}})]$$

$$= -2\sqrt{3}\tau e^{i\pi/6} Ai(-\tau). \quad (69)$$

Substituting (66), (68), and (69) into (65), we get

$$N^{(m)} = Q(\tau_m^3) + 1/[3\tau_m Ai(-\tau_m)]. \quad (70)$$

The values of N in Table III were computed from (70) by using the values of τ_m and $Ai(-\tau_m)$ given in the B. A. Tables and computing $Q(\tau_m^3)$ from (66).

The Mass-Energy Relation*

W. F. G. SWANN
Bartol Research Foundation of the Franklin Institute, Swarthmore, Pennsylvania

(Received April 5, 1948)

Relativity serves only to predict the relation for those portions of the mass and energy which are dependent upon the velocity. Electromagnetic theory comes near to providing for the rest mass in terms of ordinary electrostatic energy, but with the well-known discrepancy amounting to a factor of four-thirds. For uncharged particles electromagnetic theory does nothing. A hypothesis is developed according to which the whole of the rest mass arises from internal motions of the particles in a form consistent with the required behavior of the particles in respect to the apparent forces which they exert. The line of thought is analogous to that of the whole philosophy which sought to see all potential energy as a manifestation of kinetic energy. It has, moreover, the advantage of unifying the concepts of rest energy and kinetic energy in a form which gives the mass-energy relation a more clear-cut meaning. The development is carried out along classical lines following the general idea that in seeking ultimately to develop consistent quantum theory in relation to these matters it is good to start by seeking consistent classical representation.

I. INTRODUCTION

IN what follows there are many points which will bear such fuller elucidation as would cause this paper to be unduly long for publication here. For this reason a fuller account of the matters dealt with will be published elsewhere in the immediate future.[1] Even in the present paper, mathematical derivations which would interrupt the general course of the exposition will be relegated to an appendix.

The treatment is frankly classical, deviating from early classical only to the extent of seeking a formulation in terms of conservation laws of relativistic energy and momentum with light quanta treated, when they occur, as characterized, in a sense later to be formulated more precisely, by limiting cases in which the velocities are always the light velocity c.

The Sense in which the Term Mass Is Used

The quantities which really become involved in what follows are, for material particles, the ratios of the rest masses of the particular particles under discussion to the rest mass of some standard particle, and it will be simplest to consider these mass ratios as determined by impact experiments, preferably for low velocities, interpreted in terms of the conservation laws of energy and momentum later to be derived.

II. DISCUSSION OF THE PRESENT SITUATION OF THE PROBLEM

The relativistic expressions

$$M=\frac{M_0}{(1-\mathbf{u}^2/c^2)^{\frac{1}{2}}} \tag{1}$$

for the mass, in terms of the rest mass M_0, and

$$T=c^2\left[\frac{M_0}{(1-\mathbf{u}^2/c^2)^{\frac{1}{2}}}-M_0\right] \tag{2}$$

for the kinetic energy, contain in themselves the relation

$$T=(M-M_0)c^2 \tag{3}$$

and so establish the mass kinetic energy relation for that part of the mass which arises from motion. However, they provide no suggestion as to the relationship of the rest mass M_0 to anything having to do with the "rest energy" of the particle, which rest energy has, of course, normal meaning only in the sense of the potential energy of its forces.

In the case of an electrical particle producing a Coulomb field together with short-range forces to hold it together—which short-range forces can be conceived to result in but little potential

* Presented at the New York Meeting of the American Physical Society, January 29–31, 1948. The investigation was carried out as an adjunct to a program in nuclear physics research sponsored by the Office of Naval Research under Contract N6ori-144.

[1] In the Journal of the Franklin Institute.

energy—the potential energy arising from the Coulomb field has a close relation to the electromagnetic mass as calculated from the assumption that the particle in a system of axes in which it has zero velocity is a sphere, and in an external field moves with such an acceleration that the electrodynamic force on it is zero. However, the mass m_0 as calculated from this assumption is related to the potential energy W of the Coulomb forces by the relation

$$m_0c^2=4W/3, \tag{4}$$

so that there is a discrepancy with the mass-energy relation through the factor 4/3. This discrepancy is not to be eliminated by modifying the charge distribution on the particle. In fact, when one examines the mathematical reason for the existence of any kind of relation between the mass and potential energy along these lines, he sees that the existence of a discrepancy is basic to the geometry of the situation; indeed, such relationship as exists is little more than a matter of the theory of dimensions.

However, even if electrodynamics had succeeded in providing for the mass-energy relation for a charged particle, there would remain the need of accounting for the relationship for a neutral particle such as a neutron.

As one examines the way in which the relativistic approach provides for the relationship as regards the kinetic part of the mass, he cannot avoid the desire to make it operate in a similar manner for the "rest" mass. Such a desire invites an approach in which even rest mass results, as regards its essentials, from motion relative to a properly chosen center in the particle, and in which what we measure as potential energy of a particle is really the concealed kinetic energy of the particle. An approach along these lines forms the main thesis of this paper.

III. THE NEW APPROACH

We shall first consider the case where light quanta are absent or where their role may be neglected. Later we shall make the necessary extension to incorporate them.

We consider each material nuclear particle to be composed of a large number of parts which, for want of a better word, we shall call "specks." The subscripts (is) shall denote the sth speck of the ith nuclear particle. The rest mass of the speck shall be μ_{is} and shall never change. Its momentum P_{is} and its kinetic energy T_{is} shall be defined in terms of its velocity $\mathbf{u}_{is}$ by

$$P_{is}=\frac{\mu_{is}\mathbf{u}_{is}}{(1-\mathbf{u}_{is}^2/c^2)^{\frac{1}{2}}}, \tag{5}$$

$$T_{is}=\mu_{is}c^2\left[\frac{1}{(1-\mathbf{u}_{is}^2/c^2)^{\frac{1}{2}}}-1\right]. \tag{6}$$

So far the terms rest mass, momentum, and kinetic energy are simply names chosen so as to stimulate anticipation of the properties to be deduced.

We shall suppose that the specks are in motion in the nuclear particle and are constrained by forces—possibly rigid—to remain as part of the nuclear particle.

We shall suppose that the laws which control the interactions of the nuclear particles are such that

$$\sum_i \sum_s T_{is}=\text{const.}$$

This does not mean that the particles will not exhibit a behavior which permits discussion of their motions in terms of forces between them—forces which are in part related to a potential energy function for the system. However, it is the essence of our assumption that this potential energy is ultimately of the nature of kinetic energy of the specks, although this aspect may not be apparent in the interaction of the particles as a whole.

A situation in which one can view a system as involving wholly kinetic energy, or as one involving potential and kinetic energies, is not unfamiliar in classical dynamics and electrodynamics. In fact, a goal in which all potential energy is ultimately to be regarded as kinetic was one of the ideals of the physicists of the last century. An example is to be found in two current-carrying wire circuits interacting. The system can be discussed through Lagrange's equations entirely in terms of a kinetic energy

$$T_m+\tfrac{1}{2}L_{11}\dot{i}_1^2+L_{12}\dot{i}_1\dot{i}_2+L_{22}\dot{i}_2^2,$$

where T_m is the mechanical kinetic energy and the remainder is the electrical kinetic energy. Lagrange's equations, applied to this kinetic energy expression, yield the equations of motions

of the circuits without the incorporation of any potential energy term. On the other hand, the situation can equally well be treated by regarding the currents as replaced by their equivalent magnetic shells, in which case the interaction is represented by forces related to the potential energy of the shells.

The task of exhibiting the present problem in the foregoing light is more complex, and space will not permit its discussion here. It will have to suffice to admit that there is sense to a situation founded upon the postulate that

$$\sum_i \sum_s T_{is} = \text{const.}$$

We shall denote by S' a system of coordinates which moves with a nuclear particle as a whole, and by S a fixed system. We shall define the masses m_{is}' and m_{is} of the sth speck of the ith nuclear particles in these two systems as

$$m_{is} \equiv \mu_{is} k_{is}; \quad m_{is}' \equiv \mu_{is} k_{is}', \tag{7}$$

where

$$k = (1 - \mathbf{u}_{is}^2/c^2)^{-\frac{1}{2}}. \tag{8}$$

We shall choose as the representative point of the ith nuclear particle a point such that with it as a center of coordinates in S'

$$\sum_s' m_{is}' u_{xis}' = \sum_s' m_{is}' u_{yis}' = \sum_s' m_{is}' u_{zis} = 0. \tag{9}$$

In other words, the point is a kind of center of gravity of the particle. It is then easy to show[2] from the relativistic properties of the quantities concerned that

$$\sum_s m_{is} u_{xis} = \beta_i \omega_i \sum m_{is}', \tag{10}$$

$$\sum m_{is} = \beta_i \sum m_{is}', \tag{11}$$

where ω_i is the velocity of the ith particle in S and $\beta_i = 1/(1-\omega_i^2/c^2)^{\frac{1}{2}}$, the velocity being supposed to be along the axis of x for the moment.

Now we shall call $\sum m_{is}'$ the rest mass of the ith particle, and write it as

$$M_{0i} = \sum m_{is}', \tag{12}$$

and we shall call $\sum m_{is}$ the actual mass of the particle and write it as

$$M_i = \sum m_{is}, \tag{13}$$

so that

$$M_i = \beta_i M_{0i}. \tag{14}$$

[2] See Appendix, problem 1.

The sum of the momenta of all the specks for any resultant direction of motion symbolized by ω_i is

$$\sum_i \sum_s \mu_{is} k_{is} \mathbf{u}_{is} = \sum_i m_{is} \mathbf{u}_{is} = \sum_i \beta_i \omega_i \sum m_{is}' = \sum_i M_{0i} \beta_i \omega_i, \tag{15}$$

and the sum of the kinetic energies of all the specks is given by

$$\frac{T}{c^2} = \sum_i \frac{T_i}{c^2} = \sum_i \sum_s \mu_{is}(k_{is} - 1) = \sum_i m_{is} - \sum_i \sum_s \mu_{is} = \sum_i M_{0i}\beta_i - \sum_i \sum_s \mu_{is}. \tag{16}$$

Now if we assume conservation of momentum of all the specks and conservation of energy for all the specks (regarding these terms simply as names for the quantities to which they refer) we shall have

$$\sum_i M_{0i} \beta_i \omega_i = \text{const.} = 0, \tag{17}$$

$$\sum_i M_{0i} \beta_i = \text{const.} \tag{18}$$

since

$$\sum_i \sum_s \mu_{is} = \text{const.}$$

A comment is here necessary. Apart from minor imperfections which are discussed in the Appendix, problem 2, our definitions insure that, for a single nuclear particle, the four quantities $M_{0i}\beta_i\omega_i$, $jM_{0i}\beta_i c$ constitute a 4-vector (j being $(-1)^{\frac{1}{2}}$), with M_{0i} as an invariant, although not, of course, a constant. If we proceed to take the sum of all the momenta $M_{0i}\beta_i\omega_i$ and of all the quantities $M_{0i}\beta_i$ for the various particles and demand that both be constant in one system of axes, the result would only be true in another system of axes if the quantities for each particle were evaluated at their respective local times, so that in any other sense conservation of these sums would be meaningless. However, if we concern ourselves with two states in both of which the particles have attained constant (though not, in general, equal) velocities, this ambiguity vanishes. Even then the constancy of $\sum_i M_{0i}\beta_i$ in one system of axes does not provide for the constancy of the corresponding quantity in another system unless $\sum_i M_{0i}\beta_i\omega_i$ is also constant in the first frame.[3] With these fine points disposed of, however, we may say that, in any system of axes, on comparing initial

[3] This matter is elucidated in the Appendix, problem 3.

and final states in which all the nuclear particles have constant velocities, we shall have

$$\sum_i M_{0i}\beta_i\omega_i = \text{const.}, \tag{19}$$

$$c^2\sum M_{0i}\beta_i = \text{const.}, \tag{20}$$

where we have added a factor c^2 for convenience in subsequent statements.

The first of these two expressions enables rest mass ratios to be determined in the sense defined earlier. The second, while implying constancy of kinetic energy of all the specks, does not imply —and, in fact, denies—constancy of what is *measured* as the sum of the kinetic energies of the nuclear particles; for the quantity τ, which we call the kinetic energy of the particles, is given by

$$\tau = \sum_i M_{0i}c^2(\beta_i - 1). \tag{21}$$

Hence, since the change of $\sum_i M_{0i}c^2\beta_i = 0$, *the change of τ between the two states is equal to minus the change in $\sum_i M_{0i}c^2$.*

This result represents the mass-energy relation in its most meaningful form. Thus, suppose that in state 1 several nuclear particles are combined to form a nucleus which is at rest and has a rest mass

$$M_{0n} = \sum_i \sum_s m_{is}'.$$

The kinetic energy of the system as measured is zero. Suppose now that the nucleus breaks up into a number of nuclear particles of rest masses M_{0i}. Then the change in $\sum_i M_{0i}c^2$ is $-c^2(\sum_i \bar{M}_{0i} - M_{0n})$ where the bar indicates the rest mass in the final state, and since there is no kinetic energy initially, we have for the kinetic energy of the nuclear particles as measured

$$\sum_i \tau_i = (M_{0n} - \sum_i \bar{M}_{0i})c^2. \tag{22}$$

In other words, the sum of the kinetic energies of the nuclear particles, as measured, is equal to c^2 times the diminution of the sum of the rest masses of the particles from the state where they were combined in a single nucleus to the state where they were free—the rest masses having meaning (as regards ratio) in the sense defined by impact experiment measurements involving the conservation of momentum law.

It is to be observed that the success of this procedure has depended upon the kinetic nature which we have given to the rest mass, which characteristic enables the relativity relations to perform for rest mass the same service as that performed for kinetic mass in the usual treatment.

Incidentally, in view of the constancy of $\sum_i M_{0i}c^2\beta_i$, the relation

$$\tau = \sum_i M_{0i}c^2(\beta_i - 1)$$

yields

$$\tau + \sum_i M_{0i}c^2 = \text{const.}, \tag{23}$$

and so identifies $\sum_i M_{0i}c^2$ as the quantity which would be called the potential energy of the particles in a scheme which regarded the nuclear particles as single entities with forces between them. The variation of this potential energy throughout the changes of ordinary kinetic energy of the particles is simply the symbol of the variation of the internal kinetic energies of the particles.[4]

The Incorporation of Light Quanta

The very spirit of the modern quantum theory is to the effect that light quanta are not to be considered as entities inherent in the nucleus, to be subsequently ejected like material nuclear particles, and, indeed, this principle extends to other entities such as mesotrons, etc. Nevertheless, in order to maintain a consistent story along the lines of what has been written above, it is necessary to suppress this picture in favor of one in harmony with the behavior of the other particles—protons and neutrons—which we have discussed, leaving for another realm of treatment the transition from the classical picture so envisaged to the more formal picture of the quantum theory.

There is more than one way in which, following the above principle, we may attain the end in view. It must be our purpose to formalize a picture with a maximum richness of content, the minimum of artificiality, and with the capability of being incorporated with as little change as possible in the plan of procedure already developed. With this end in view we incorporate the concept of "specks" for a light quantum as for a material nuclear particle. The specialization lies in the assumption that the quantities μ_{is} must be regarded in the limit as zero in such a fashion

[4] Naturally, one is tempted to seek in the internal motions of the particles a basis for magnetic moments.

that the quantity m_{is}' of Eq. (7) is, in the limit, zero. Nevertheless, we shall suppose that the magnitude of this quantity really never attains this limit but is equal to a magnitude ϵ which may be chosen as small as we please. The light particle now behaves just as the other particles which we have discussed, except that when incorporated as part of a nucleus it contributes nothing (or rather, an infinitesimal amount, depending upon ϵ) to the momentum and energy of the nucleus. However, expressions similar to (5) and (6) have significance for the sth speck of the light particle, although P_{is} and T_{is} continue to be zero until u_{is} approaches the velocity of light. In fact, an equation similar to (12) holds for the light particle with M_{0i} of a magnitude approaching zero to an extent defined by ϵ, so that M_i as given by (13), only becomes finite as β_i approaches infinity. In the same sense, there is meaning to Eqs. (14) and (15), with the understanding now that light particles are to be included among the particles considered.

Now for any assigned ϵ—approaching zero as the limit—there is a value of the velocity ω_i of the particle for which $M_{0i}\beta_i\omega_i$ and $M_{0i}\beta_i$ have any finite and, of course, related values we wish to assign. However, all such values of the velocity lie in the limit (as ϵ approaches zero) infinitely near to the velocity of light. Nevertheless, within this infinitesimal range of velocities bordering upon the velocity of light are contained all possible finite values of the energy of the light particle corresponding to different values of ν in the expression $h\nu$ symbolic of quantum theory and, indeed, all values ranging from zero to infinity, with the corresponding momenta of these particles related to the energy through the multiplicative factor $1/c$.

In terms of the foregoing picture, all that has been developed for the material nuclear particles carries over to include the light particles. The only peculiarity of the light particles lies in the fact that they never contribute anything to the energy or the momentum unless they travel with a velocity infinitely near to the velocity c. In principle, they are not restricted to have only this velocity, but unless they do have it they play no part in observable phenomena. If, as an academic question, we proceed to inquire whether they can ever leave a nucleus with a velocity less than that of c, that question must seek its answer in the forces concerned in binding the nuclear particles together, and it has been our plan to formulate our problem in such a manner as to avoid discussion of this particular matter.

APPENDIX

Problem 1. Verification of Eqs. (10) and (11)

In view of the 4-vector characteristics of the quantities concerned,

$$k_{is}u_{xis}=\beta_i(k_{is}'u_{xis}'+\omega_i k_{is}'), \tag{A1}$$

$$k_{is}u_{yis}=k_{is}'u_{yis}', \tag{A2}$$

$$k_{is}u_{zis}=k_{is}'u_{zis}', \tag{A3}$$

$$k_{is}=\beta_i(k_{is}'-k_{is}'u_{xis}'\omega_i/c^2). \tag{A4}$$

Since $\mu_{is}k_{is}$ and $\mu_{is}k_{is}'$ represent the masses m_{is} and m_{is}' of the speck in the two systems (A1) to (A4) yield

$$m_{is}u_{xis}=\beta_i m_{is}'\omega_i+\beta_i m_{is}'u_{xis}', \tag{A5}$$

$$m_{is}u_{yis}=m_{is}'u_{yis}', \tag{A6}$$

$$m_{is}u_{zis}=m_{is}'u_{zis}', \tag{A7}$$

$$m_{is}=\beta_i m_{is}'-\beta_i\omega_i m_{is}'u_{xis}'/c^2. \tag{A8}$$

Let us now sum both sides of (A5) and (A8), using (9). Then (A5) yields

$$\sum_s m_{is}u_{xis}=\beta_i\omega_i\sum m_{is}', \tag{A9}$$

and (A8) yields

$$\sum_s m_{is}=\beta_i\sum m_{is}', \tag{A10}$$

both expressions referring to constant t'. The approximation involved in the assumption that these expressions hold at constant t is discussed in problem 2 of this Appendix.

Problem 2. Concerning Matters Pertaining to Local Times

As pointed out in problem 1 above, the summations in the equations in the undashed system S are to be evaluated at constant t' (in S') and consequently at local times τ in S given by

$$\tau=\beta_i(\tau'+\omega_i\epsilon'/c^2),$$

where τ' is the time, constant throughout S', and applicable in that system, while ϵ' is the coordinate distance of the speck in question,

measured in S', parallel to the direction of ω_i. Now regardless of the smallness of the uncertainty involved in the time τ by the term $\beta_i\omega_i\epsilon'/c^2$, there is sense to regarding the summations on the left-hand sides of (A9) and (A10) as evaluated at constant t', without violating any fundamental concept natural to the theory of relativity. The system S' is a very specialized system for the particle. Indeed, in electrodynamics one has no compunctions about thinking of a system of axes moving with an electron and of evaluating such a fundamental quantity as the electromagnetic rest mass in terms of a law characterized by that system, in spite of the fact that this quantity afterwards makes its appearance as the rest mass in a system of axes in which the electron is in motion. Thus, while we might make a good apology for neglecting the quantity $\beta_i\omega_i\epsilon'/c^2$ altogether on the basis of smallness, symmetry, etc., it is ultimately not necessary to do so, provided that we formulate our conservation laws for energy and momentum from (15) and (16) of the text with the above understanding. A more serious matter in the utilization of (15) and (16) to this end comes from the different local times to be associated with the different nuclear particles, each taken as a whole. This matter becomes disposed of by the artifice, adopted in the text, of recognizing that, in practice, we are only concerned with comparing the sum of the momenta or energies of the system in two conditions in which all the particles have attained constant—though not, of course, equal—velocities.

Problem 3. The Invariance of Conservation of Energy and Momentum

Suppose that in one system symbolized by S'' we have conservation of momentum and energy in the form

$$\sum_i M_{0i}\beta_i''\omega_{xi}'' = A_x, \tag{A11}$$

$$\sum_i M_{0i}\beta_i''\omega_{yi}'' = A_y, \tag{A12}$$

$$\sum_i M_{0i}\beta_i''\omega_{zi}'' = A_z, \tag{A13}$$

$$\sum_i c^2 M_{0i}\beta_i'' = B, \tag{A14}$$

where A_x, A_y, A_z, and B are constants.

Now since $\beta_i\omega_i$, $\beta_i jc$ is a 4-vector, if we transfer to another system of axes S in which S'' moves with velocity v, and if $\gamma=(1-v^2/c^2)^{-\frac{1}{2}}$

$$M_{0i}\beta_i\omega_{xi} = \gamma[M_{0i}\beta_i''\omega_{xi}'' + vM_{0i}\beta_i''], \tag{A15}$$

$$M_{0i}\beta_i\omega_{yi} = M_{0i}\beta_i''\omega_{yi}'', \tag{A16}$$

$$M_{0i}\beta_i\omega_{zi} = M_{0i}\beta_i''\omega_{zi}'', \tag{A17}$$

$$cM_{0i}\beta_i = \gamma[cM_{0i}\beta_i'' + (v/c)M_{0i}\beta_i''\omega_{xi}'']. \tag{A18}$$

Now, if we sum the left- and right-hand sides of (A15) to (A18) at constant t'' and utilize (A11) to (A14), we have

$$\sum_i M_{0i}\beta_i\omega_{xi} = \gamma[A_x + vB/c^2],$$
$$\sum_i M_{0i}\beta_i\omega_{yi} = A_y,$$
$$\sum_i M_{0i}\beta_i\omega_{zi} = A_z,$$
$$\sum_i c^2 M_{0i}\beta_i = \gamma[B + vA_x].$$

Hence, at constant t''

$$\sum_i M_{0i}\beta_i\omega_i = \text{const.}$$
$$\sum_i c^2 M_{0i}\beta_i = \text{const.}$$

A Note on Perturbation Theory*

EUGENE FEENBERG
Washington University, St. Louis, Missouri
(Received April 13, 1948)

The perturbation theory for a stationary state is developed in the form of an implicit equation for the eigenvalue and an explicit equation (involving the eigenvalue) for the amplitudes. With the aid of a formal algebraic identity the equation for the eigenvalue is transformed into a semi-explicit form by a procedure having a wider range of validity than the more obvious iteration or power series processes.

THE physical system under discussion possesses quantum states in the space defined by the complete orthonormal set of functions $\psi_1, \psi_2, \cdots\psi_n\cdots$. These functions need not be eigenfunctions of any set of commuting operators; in particular, it is possible to dispense with the conventional separation of the Hamiltonian operator into an unperturbed part H_0, of which the ψ's are eigenfunctions, and a perturbation operator H_1 which couples the unperturbed states.

The eigenfunction of H

$$\psi=\sum a_n\psi_n \tag{1}$$

with the eigenvalue E, is determined by the system of linear homogeneous equations:

$$(E-H_{mm})a_m=\sum_{m\neq n} H_{mn}a_n. \tag{2}$$

An essential preliminary step in the solution of Eq. (2) is the reduction to diagonal form of one or more subspaces in which the diagonal matrix elements of H all have the same value. After the reduction the condition $H_{nm}=0$ for $n\neq m$ holds within each reduced subspace. Following this step Eq. (2) can be solved (at least formally) by a process of successive approximation.

If ψ_k is a good approximation to an eigenfunction of H a suitable starting point is $a_m=\delta_{km}$, $E=H_{kk}$. Successive orders of approximation are derived by inserting the values of a_m from the preceding order into the right-hand member of Eq. (2). The formal solution has the form[1]

$$a_k=1,$$
$$a_m=[H_{mk}/(m)]+\sum_{n\neq k}[(H_{mn}H_{nk})/(m)(n)]+\cdots,$$
$$E=H_{kk}+\sum_{m\neq k}[H_{km}H_{mk}/(m)] \tag{3}$$
$$+\sum_{mn\neq k}[(H_{km}H_{mn}H_{nk})/(m)(n)]+\cdots,$$

in which $(m)=E-H_{mm}$ and only non-diagonal matrix elements occur in the numerators of the sums. Wigner[2] has shown that the energy formula in an odd order $2\nu+1$ is precisely the expectation value of H with respect to the normalized wave function of the ν'th order.

An obvious iteration process starting from $E^{(1)}=H_{kk}$ and employing the expansion

$$[1/(E^{(\mu)}-H_{mm})]=[1/(H_{kk}-H_{mm})]$$
$$\times\sum_{\nu=0}^{\infty}[(H_{kk}-E^{(\mu)})/(H_{kk}-H_{mm})]^{\nu} \tag{4}$$

transforms Eq. (3) into an explicit formula for E in which all energy denominators have been reduced to differences of diagonal matrix elements. This last form is equivalent to the Schroedinger perturbation formula[3] derived as a rule by assuming that all eigenfunctions and eigenvalues can be expressed as power series in an expansion parameter (i.e., the fine structure constant in the electromagnetic self-energy problem). In many applications the convergence condition for the infinite series of Eq. (4) fails and the explicit formula for E then embodies an

* This research was supported in part by U. S. Navy Contract N6ORI117.

[1] L. Brillouin, J. de phys. et rad., III, 373 (1932).

[2] E. P. Wigner, Math. u. Naturwiss. Anzeig. d. Ungar. Akad. Wiss. 1 III, 475 (1935).

[3] E. C. Kemble, *The Fundamental Principles of Quantum Theory* (McGraw-Hill Book Company, Inc., New York, 1937).

infinitely reiterated series of logical contradictions. One important characteristic of the iteration process is that it removes an infinite series of higher order terms (generated by the expansion of the denominators) from each summation in Eq. (3).

The present note is concerned with the transformation of Eq. (3) into a semi-explicit form by a procedure having a wider range of validity than the iteration process.

The discussion of Eq. (3) is facilitated by the introduction of the set of auxiliary functions.

$$\mathcal{E}_{km\cdots pq}\equiv H_{qq}+\sum_{r\neq km\cdots pq}\frac{H_{qr}H_{rq}}{(r)}+\sum_{rs\neq km\cdots pq}\frac{H_{qr}H_{rs}H_{sq}}{(r)(s)}+\cdots. \quad (5)$$

It is clear that $\mathcal{E}_{km\cdots q}$ can be identified with an eigenvalue only when $k=m=\cdots=q$; then $E=\mathcal{E}_{kk\cdots k}(E)\equiv\mathcal{E}_k(E)$.

The formal algebraic identity

$$\sum_{\nu=0}^{\infty}[(\mathcal{E}_{km\cdots pq}-H_{qq})/(E-H_{qq})]^{\nu}=1+\sum_{r\neq km\cdots p}[(H_{qr}H_{rq}/((q)(r))]+\sum_{rs\neq km\cdots p}[(H_{qr}H_{rs}H_{sq})/((q)(r)(s))]+\cdots. \quad (6)$$

$(q\neq km\cdots p)$ can be verified by expanding the right-hand sums as products of sums like those which appear in Eq. (5). Identical products of sums then occur on both sides of Eq. (6) multiplied by identical binomial coefficients. An essential factor in the identity is the absence of terms in Eq. (5) for which the variable indices take on the value q. If

$$|\mathcal{E}_{km\cdots pq}-H_{qq}|<|E-H_{qq}|, \quad (7)$$

Eq. (6) reduces to

$$1/(E-\mathcal{E}_{km\cdots pq})=[1/(q)][1+\sum_{r\neq km\cdots p}[(H_{qr}H_{rq})/((q)(r))]+\sum_{rs\neq km\cdots p}[(H_{qr}H_{rs}H_{sq})/((q)(r)(s))]+\cdots], \quad (q\neq km\cdots p). \quad (8)$$

If the convergence condition (7) fails, then it is suggested that the left-hand member of Eq. (8) is equivalent to the series on the right in the sense of an analytical continuation. In the application of Eq. (8) the left-hand member replaces the infinite (and possibly divergent) series on the right whereas the reverse procedure is followed in the application of Eq. (4).

The general term in the formal series for a_m is expanded in the algebraic identity

$$\sum_{np\cdots rs\neq k}\frac{H_{mn}\cdots H_{sk}}{(m)\cdots(s)}\equiv\sum_{np\cdots rs\neq km}\frac{H_{mn}\cdots H_{sk}}{(m)\cdots(s)}+\sum_{np\cdots rs\neq k}\frac{H_{mn}\cdots H_{rm}}{(m)\cdots(r)}\frac{H_{mk}}{(m)}+\cdots+\sum_{n\neq k}\frac{H_{mn}H_{nm}}{(m)(n)}\sum_{p\cdots rs\neq km}\frac{H_{mp}\cdots H_{sk}}{(m)\cdots(s)}. \quad (9)$$

With the aid of Eqs. (8) and (9) the formal series for a_m is transformed into

$$a_m=\frac{H_{mk}}{E-\mathcal{E}_{km}}+\sum_{n\neq km}\frac{H_{mn}}{E-\mathcal{E}_{km}}\left[\frac{H_{nk}}{(n)}+\sum_{p\neq km}\frac{H_{np}H_{pk}}{(n)(p)}+\sum_{pq\neq km}\frac{H_{np}H_{pq}H_{qk}}{(n)(p)(q)}+\cdots\right]. \quad (10)$$

Again employing Eq. (8) and an obvious generalization of Eq. (9), the factor in square brackets in Eq. (10) can also be transformed and the process continued indefinitely to yield the result

$$a_m=\frac{H_{mk}}{E-\mathcal{E}_{km}}+\sum_{n\neq km}\frac{H_{mn}H_{nk}}{(E-\mathcal{E}_{km})(E-\mathcal{E}_{kmn})}+\sum_{\substack{n\neq km\\ p\neq kmn}}\frac{H_{mn}H_{np}H_{pk}}{(E-\mathcal{E}_{km})(E-\mathcal{E}_{kmn})(E-\mathcal{E}_{kmnp})}+\cdots. \quad (11)$$

Equation (2) now yields

$$E=H_{kk}+\sum_{m\neq k}H_{km}a_m=H_{kk}+\sum_{m}{}^{*}\frac{H_{km}H_{mk}}{E-\mathcal{E}_{km}}+\sum_{mn}{}^{*}\frac{H_{km}H_{mn}H_{nk}}{(E-\mathcal{E}_{km})(E-\mathcal{E}_{kmn})}+\cdots. \quad (12)$$

The star on the summation symbol signifies that there are no duplications among the variable indices $mnpq\cdots$ and furthermore that $mnpq\cdots \neq k$:

$$\sum_{mnp\cdots}^{*} \equiv \sum_{mnp\cdots} (m\neq k,\ n\neq km,\ p\neq kmn,\ \cdots). \quad (13)$$

Since $E=\mathcal{E}_{k\cdots k}(E)\equiv\mathcal{E}_k(E)$ the energy denominators in Eqs. (11) and (12) can be replaced by

$$\mathcal{E}_k(E)-\mathcal{E}_{km\cdots pq}(E)=H_{kk}-H_{qq}$$
$$+\left[\sum_{r\neq k}\frac{H_{kr}H_{rk}}{(r)}-\sum_{r\neq km\cdots pq}\frac{H_{qr}H_{rq}}{(r)}\right]+\cdots, \quad (14)$$

which may be convergent even when $\mathcal{E}_k$ and $\mathcal{E}_{km\cdots pq}$ are separately divergent. There is also the possibility that the usual substitution of $H_{kk}-H_{qq}$ for $E-H_{qq}$ in the second- and third-order terms of Eq. (3) may be justified in particular cases even when $|E-H_{qq}|\gg|H_{kk}-H_{qq}|$.

A straightforward generalization of the procedure yielding Eqs. (11) and (12) transforms $\mathcal{E}_{km\cdots pq}$ into a form similar to Eq. (12). The result is

$$\mathcal{E}_{km\cdots pq}=H_{qq}+\sum_{r\neq km\cdots pq}\frac{H_{qr}H_{rq}}{E-\mathcal{E}_{km\cdots pqr}}$$
$$+\sum_{\substack{r\neq km\cdots pq\\ s\neq km\cdots pqr}}\frac{H_{qr}H_{rs}H_{sq}}{(E-\mathcal{E}_{km\cdots pqr})(E-\mathcal{E}_{km\cdots pqrs})}$$
$$+\cdots. \quad (15)$$

For computing the required energy denominators Eq. (15) may be replaced, with advantage, by

$$\mathcal{E}^{*}_{km\cdots pq}=H_{qq}+\sum_{r\neq km\cdots pq}\frac{H_{qr}H_{rq}}{\mathcal{E}_k-\mathcal{E}^{*}_{km\cdots pqr}}$$
$$+\sum_{\substack{r\neq km\cdots pq\\ s\neq km\cdots pqr}}\frac{H_{qr}H_{rs}H_{sq}}{(\mathcal{E}_k-\mathcal{E}^{*}_{km\cdots pqr})(\mathcal{E}_k-\mathcal{E}^{*}_{km\cdots pqrs})}$$
$$+\cdots. \quad (16)$$

Now $\mathcal{E}^{*}_{km\cdots pq}=\mathcal{E}_{km\cdots pq}$ when $E=\mathcal{E}_k(E)$ so that the physical solution of Eq. (12) is also a solution of the modified equation obtained by substituting $\mathcal{E}_k-\mathcal{E}^{*}_{km\cdots pq}$ for $E-\mathcal{E}_{km\cdots pq}$ in Eq. (12).

For the special case of a finite matrix (of order N) the right-hand members of Eqs. (11), (12), and (15) are finite rational functions of the energy and the matrix elements. In this case the analytical continuation mentioned in the sentence following Eq. (8) has a precise meaning. First suppose that all non-diagonal matrix elements are multiplied by a convergence factor λ. For a sufficiently small upper bound on the absolute value of λ, Eq. (3) is unobjectionable and can be solved rigorously by the iteration process; furthermore, all the infinite sums involved in Eqs. (6) and (8) are convergent. Adding the fact that Eq. (12) is an algebraic equation of degree N in E, the conclusion follows that it is simply a convenient way of writing the characteristic equation

$$||E\delta_{mn}-H_{mn}||=0. \quad (17)$$

Since Eqs. (12) and (17) are both algebraic equations of degree N in E, the irrelevant restriction on λ may be dropped. The special cases $N=2$ and 3 provide instructive, though trivial, illustrations of the above remarks.

The Quantization of Space and Time

H. T. FLINT
Bedford College, University of London, London, England
(Received February 3, 1948)

THERE have been indications during the past twenty years that existing physical theories break down when applied to the microscopic phenomena of physics. The limits within which the difficulties arise have been investigated and the conclusion drawn that in the physical world no meaning can be attached to a subdivision of the geometrical continuum beyond a certain limit.[1]

This naturally suggests the development of a geometry based on indivisible units of length.

The concept of the existence of a minimum length and time has been described by means of a five-dimensional continuum[2] in which the coordinates $(x_1 \cdots x_4)$ are regarded as the space-time coordinates of the theory of relativity, and x_5 is an additional coordinate appearing very simply in all cases examined hitherto. Thus this variable occurs only in the factor $\exp(2\pi i x_5/l_0)$, where l_0 is a fundamental length and has been recognized as the Compton wave-length (h/m_0c).

Thus the coordinate x_5 is associated with the rest mass m_0 of the particle located by these five coordinates.

When describing the path of any particle it is meaningless to attribute to x_5 any value less than l_0. This can be shown to be equivalent to the statement that in describing the motion of a particle, it is meaningless to associate with it elements of proper time less than h/m_0c^2. The appearance of x_5 in the exponential factor makes it analogous to the time, t, in many problems in physics, especially in electricity, where the time occurs in the factor $\exp(2\pi i\nu t)$. The limitation of x_5 to the value l_0 places it in the position of the azimuthal angle in the old quantum theory. In that case no meaning was attached to the position of an electron in its orbit described by values of θ.

It is thus assumed that when x_5 occurs in any equation of significance in physics it can be given the value l_0. A recent suggestion by H. S. Snyder[3] for the description of space-time quantization is that certain operators should be introduced to form the basis of a physical theory of which this quantization is to be regarded as a characteristic feature. For this purpose five variables (η_μ) are introduced which may be regarded as the coordinates appropriate to a de Sitter continuum.

Let it be supposed, however, that these coordinates are chosen as they would be in the usual method of describing physical phenomena; that is to say, let them be chosen as in the original work of Kaluza with the limitations now suggested with regard to η_5. It is now supposed in accordance with Snyder's suggestion that these coordinates do not provide a suitable framework within which interactions in the microscopic domain of physics can be described.

Guided by the analogy provided by the quantum theory the following operators are introduced:

$$M_{\mu\nu} = -i\hbar[\eta_\mu(\partial/\partial\eta_\nu) - \eta_\nu(\partial/\partial\eta_\mu)] \qquad (\mu,\nu = 1, 2, 3, 4, 5). \quad (1)$$

These operators satisfy the relations

$$M_{\lambda\mu}M_{\nu\lambda} - M_{\nu\lambda}M_{\lambda\mu} = i\hbar M_{\nu\mu}, \quad (\lambda \text{ not summed}). \quad (2)$$

If the cases $\mu = m$, $\nu = 5$ be considered,

$$M_{m5} = -i\hbar[\eta_m(\partial/\partial\eta_5) - \eta_5(\partial/\partial\eta_m)]. \quad (3)$$

In the case of a five-dimensional quantity such as $M_{\mu\nu}$ the components M_{m5} can be related to a four vector. Thus it is natural to represent the coordinate operators, as Snyder does, by means of these components with an appropriate dimensional factor.

Thus, the coordinate operator x_m is written in

[1] H. T. Flint, Proc. Roy. Soc. **A117**, 630 (1927); A. E. Ruark, Proc. Nat. Acad. Sci. Wash. **14**, 322 (1927); H. T. Flint and O. W. Richardson, Proc. Roy. Soc. **A117**, 637 (1927); L. Landau and R. Peierts, Zeits. f. Physik **69**, 56 (1931); E. Schroedinger, S. B. Preuss. Akad. Wiss. **12**, 238 (1932); A. March, Zeits. f. Physik **104**, 93, 161 (1936); **105**, 620 (1936); **106**, 49 (1936); **106**, 291 (1937).

[2] T. Kaluza, S. B. Akad. Wiss. Berlin 966 (1921); H. T. Flint, Phil. Mag. **7**, 29, 33 (1940).

[3] H. S. Snyder, Phys. Rev. **71**, 1, 38 (1947).

the form

$$x_m = a[\eta_m(\partial/\partial\eta_5) - \eta_5(\partial/\partial\eta_m)], \quad (4)$$

where a has the dimension of length.

It appears a natural assumption that this factor a should be simply related to the fundamental length l_0 already introduced. Bearing in mind that $\partial/\partial\eta_5 = 2\pi i/l_0$, according to the assumption that η_5 appears only in the exponential factor, it is suggested that $a = l_0/2\pi i$. Thus,

$$x_m = (l_0/2\pi i)[\eta_m(\partial/\partial\eta_5) - \eta_5(\partial/\partial\eta_m)] \quad (5)$$

and

$$M_{m5} = m_0 c x_m. \quad (6)$$

Let the case of a free particle be considered and let its wave function be ψ.

The observed value of the coordinate x_m is $\bar{x}_m = \psi^+ x_m \psi$. Thus,

$$\bar{x}_m = (l_0/2\pi i)[\psi^+\eta_m(\partial\psi/\partial\eta_5) - \psi^+\eta_5(\partial\psi/\partial\eta_m)];$$

and since

$$\partial\psi/\partial\eta_5 = 2\pi i\psi/l_0,$$
$$\bar{x}_m = \psi^+\eta_m\psi - (l_0/2\pi i)\psi^+\eta_5(\partial\psi/\partial\eta_m)$$
$$= \bar{\eta}_m - (l_0/2\pi i)\psi^+\eta_5(\partial\psi/\partial\eta_m). \quad (7)$$

The quantity $\bar{\eta}_m$ is the average value of the coordinate η_m, but, according to the formula (7), the observed value of the coordinate operator x_m differs from it by the second term on the right-hand side. According to the assumption that the value to be attached to η_5 is l_0, and since $\partial\psi/\partial\eta_m = (2\pi i/h)p_m\psi$, where p_m is the momentum conjugate to η_m, this term becomes $l_0^2\psi^+ p_m\psi/h$.

If the particle is moving with velocity v in the direction of η_m, this term has the value $h\beta/m_0c(1-\beta^2)^{\frac{1}{2}}$, where $\beta = v/c$. This may be interpreted as meaning that in any attempt to measure the coordinate of the particle there is an error of magnitude $h\beta/m_0c(1-\beta^2)^{\frac{1}{2}}$. It is thus impossible to locate the particle with greater accuracy than this.

By applying the formula (7) to the case $m = 4$ it follows, according to the same assumption, that it is impossible to locate the particle in time with a greater accuracy than $h/m_0c^2(1-\beta^2)^{\frac{1}{2}}$. Both these results can be combined in the statement that there is no physical significance in associating any interval of proper time less than h/m_0c^2 with a particle of rest mass m_0.

PHYSICAL REVIEW VOLUME 74, NUMBER 2 JULY 15, 1948

The Threshold for Spark Development by Streamer Mechanism in Uniform Fields

LEONARD B. LOEB
Department of Physics, University of California, Berkeley, California

(Received March 22, 1948)

THE streamer mechanism of the ordinary spark required a quantitative criterion for streamer advance for its promulgation. A semi-empirical condition for streamer advance was simultaneously and quite independently proposed by J. M. Meek[1] and by H. Raether.[2] The writer as well as Meek[3] and Raether[2] accepted the proposed condition that a streamer could advance when the positive space charge tip field created by the avalanche was approximately equal to the imposed field only as a temporary makeshift in order to launch the theory, since the more correct solution including photoelectric ionization appeared to lie well in the future. In a recent article the writer[4] indicated that the correct solution must retain a formal analogy to the well-known Townsend criterion for the spark at lower pressure, i.e., that the condition would have to have the form $Kfe^{\alpha\delta} = 1$. Recent analysis of the pre-onset positive burst pulse corona threshold has now shown the way to a proper procedure for calculating the threshold for streamer advance.[5] While the present lack of

[1] J. M. Meek, Phys. Rev. **57**, 722 (1940); L. B. Loeb and J. M. Meek, J. App. Phys. **11**, 438, 459 (1940).
[2] H. Raether, Zeits. f. Physik **117**, 375, 524 (1941); Archiv. f. Elektrotech. **34**, 49 (1940).
[3] L. B. Loeb and J. M. Meek, *Mechanism of the Electric Spark* (Stanford University Press, Stanford University, California, 1941), pp. 40 and 42.
[4] L. B. Loeb, Rev. Mod. Phys. **20**, 151 (1948).
[5] L. B. Loeb, Phys. Rev. **73**, 798 (1948).

fundamental data precludes a detailed study and test at the present time, it was felt important to indicate the line of reasoning in the hope that it will guide further work on the problem. It must also be indicated that while the problem may perhaps better be solved by some other approach, the present approach is the only one now obvious. In this, as in all threshold problems, one must work with equations involving average values of quantities subject to considerable fluctuations.

Consider a uniform electrical field of strength X. As shown elsewhere[6] an electron proceeding a distance δ from the cathode to close to the anode will produce an avalanche of $e^{\alpha\delta}$ electrons and positive ions lying within an average distance ρ of the avalanche axis. The value of ρ depends on the coefficient of electron diffusion D and is

$$\rho=(4Dt)^{\frac{1}{2}}, \tag{1}$$

with

$$t=(\delta/\bar{v}) \tag{2}$$

representing the time of avalanche advance at an average drift velocity $\bar{v}$. In a distance dx of advance, when the avalanche has progressed as far as δ, the number of new ions formed is

$$n=\alpha e^{\alpha\delta}dx, \tag{3}$$

where α is Townsend's first coefficient in the field X. The density of positive ions left behind by the electrons created in dx at δ is then given by

$$N=n/\pi\rho^2dx=\alpha e^{\alpha}/\pi\rho^2. \tag{4}$$

If ρ is not too large compared to $1/\alpha$, one can approximate the space charge field X^1 produced by the density of positive ions N, at any distance x from the center of the charge of radius ρ at the end of the run δ by assuming the ions distributed uniformly in a sphere of radius ρ and volume $(4/3)\pi\rho^3$. Then

$$X^1=q\epsilon/x, \tag{5}$$

with

$$q=(4/3)\pi\rho^3N \tag{6}$$

and ϵ the electron. Inserting N from (4) into (6),

$$q=(4/3)\rho\alpha e^{\alpha\delta} \tag{7}$$

and

$$X^1=(4/3)\epsilon\rho\alpha e^{\alpha\delta}/x^2=E/x^2. \tag{8}$$

[6] See reference 3, pp. 34–37; L. B. Loeb and J. M. Meek, J. App. Phys. 11, 440 (1940).

The streamer theory ascribes spark breakdown of the gas to the advance of the positive space charge initiated by the avalanche, from the anode backward towards the cathode, producing a conducting filament of plasma that bridges the gap. The advance takes place as a result of new avalanches initiated by photoelectrons created *in the gas* from the cathode side and which move towards the positive space charge in the combined fields $X+X^1$. Accompanying the creation of q positive ions within the sphere of radius ρ, the electron impacts also produced fq high energy photons[4, 5] of absorption coefficient μ, which on absorbtion ionize the gas surrounding the sphere. Now if one of these photons is absorbed far enough from the surface of the sphere of radius ρ on the cathode side so as to produce an electron and a new avalanche in the vector field

$$X_1=X+X^1=X+\frac{E}{x^2}, \tag{9}$$

which extends the space charge, the streamer will advance. Thus the threshold for streamer advance is fixed[4] as

$$Kqf=(4/3)K\rho\alpha Kfe^{\alpha\delta}=1. \tag{10}$$

Here the coefficient K is a complicated expression determining the chance of absorption and photoionization which may be regarded as follows. Assume a critical distance x_1 from the center of the space charge such that a photoelectron produced beyond x_1 towards the cathode in the field X_1 is capable of yielding the needed ionization. Then K will be given by[5]

$$K=\frac{\underline{a}}{4\pi}\exp(-\mu x_1). \tag{11}$$

The quantity $\underline{a}$ defines a solid angle within which the photon beam must lie in order that the streamer be extended effectively towards the cathode. Rigorously, an evaluation of such a solid angle would require a complicated averaging process involving the radius of x_1 and the variation of the field X_1 off the axis of the avalanche and relative to the direction of X. Roughly, since it simplifies calculation to set X_1 as the algebraic sum of X and X^1, one could evaluate $\underline{a}$ as the solid angle subtended at the

center of the space charge by the intersection of a cylinder of radius ρ in the direction of streamer advance and a sphere of radius x_1 drawn about the center of the space charge. With $\underline{a}$ designated, it requires only the evaluation of x_1 to complete the solution. With this approach the Meek-Raether[1,2] condition for streamer advance is replaced by defining x_1 in such a way that the *new*, photoelectrically initiated avalanche, in moving from x_1 to ρ, must *create the same number* q of ions as *did the initiating avalanche.* This is indicated by equating q in Eq. (7) to the ionization produced by the new avalanche in going from x_1 to ρ in the field X_1, where Townsend's coefficient is now represented by α^1, yielding the relation

$$\rho^1\bar{\alpha}^1 \exp\left(\int_{x_1}^{\rho}\alpha^1 dx\right)=\rho\alpha e^{\alpha\delta}. \qquad (12)$$

The quantity $\bar{\alpha}^1$ is the value of α^1 in the field X_1 at a distance ρ. The quantity ρ^1 is the value of ρ for the new avalanche, which by Eq. (1) is $\rho^1=[4D(x_1/\bar{v})]^{\frac{1}{2}}$, such that with $\bar{v}$ sensibly constant

$$\rho/\rho^1=(\delta/x_1)^{\frac{1}{2}}. \qquad (13)$$

Equation (12) then becomes

$$\int_{x_1}^{\rho}\alpha^1 dx=\alpha\delta+\log_e(\alpha/\bar{\alpha}^1)(\delta/x_1)^{\frac{1}{2}}. \qquad (14)$$

Now in the region at which sparking takes place in a given gas at a field X and pressure p, experimental data yield the relation between α, p, and X as

$$\alpha/p=F(X/p). \qquad (15)^7$$

In the limited region of X/p, involved in any solution, the observed curves can be fitted by empirical analytical functions which give satisfactorily $\alpha=pF(X/p)$ for use in the solution of Eq. (14).[7] For example, in the case of air near atmospheric pressure, $F(X/p)$ is a quadratic which for simplicity of illustration in this case can be set as

$$\alpha=(A/p)(X^2). \qquad (16)$$

Then replacing X of (16) by its value X_1 in this analysis, given by $X_1=X+E/x^2$ as in Eqs. (8) and (9), and placing this in turn into Eq. (14), one has

$$(A/p)\int_{x_1}^{\rho}[X+(E/x^2)]dx = \alpha\delta+\log_e(\alpha/\bar{\alpha}^1)(x_1/\rho)^{\frac{1}{2}}. \qquad (17)$$

Solution of this equation yields x_1.

To utilize this theory for the evaluation of a sparking threshold the procedure is as follows (assuming that δ and p are given, with $\alpha=pF(X/p)$, D, $\bar{v}$, f, and μ known): From relations (1) and (2) evaluate ρ. Choose a likely value of X for the spark. Evaluate α from (15) or (16) and solve for X^1 and E by means of (8). Calculate $e^{\alpha\delta}$. With these data solve (17) graphically, for x_1 using the value of α at X and of $\bar{\alpha}^1$ as derived from (8) and (15) with $x=\rho$. With x_1 evaluated, determine $\underline{a}$ as indicated and proceed to evaluate K from (11) using μ. With the values of f, K, and $e^{\alpha\delta}$ solve Eq. (10). If $(4/3)\rho\alpha Kfe^{\alpha\delta}$ as computed is greater than unity repeat with a lower value of X. Solution for the sparking field strength and sparking potential is then accomplished by trial and error as with Townsend's or Meek's equations,[1] with obviously a much more elaborate procedure. It is, however, a procedure that is in principle correct and now includes the effects of pressure on the absorption coefficient μ as well as on ionization density. The inclusion of this further pressure variation will increase the deviations from Paschen's law and should bring theory more into line with observations than does the Meek equation.[8] This derivation applies primarily to the calculation of breakdown in a uniform gap, presupposing that the streamer progresses primarily through the ionization by one effective avalanche primarily in the field direction. For the case of the pre-onset streamers in a highly divergent field, it is probable that streamer advance can be determined initially by the simultaneous influx of several electron avalanches. The condition for streamer onset on this basis, using the same procedure, has been developed by R. A. Wijsman, and leads to an equation which has the same general form as Eq. (10) with, however, a different set of constants.

[7] L. B. Loeb, *Fundamental Processes of Electrical Discharge in Gases* (John Wiley and Sons, Inc., New York, 1939), pp. 344 and 347.

[8] C. G. Miller and L. B. Loeb, Phys. Rev. **73**, 84 (1948).

Evidence for Heavy Nuclei in the Primary Cosmic Radiation

PHYLLIS FREIER, E. J. LOFGREN, E. P. NEY, AND F. OPPENHEIMER
University of Minnesota, Minneapolis, Minnesota
AND
H. L. BRADT AND B. PETERS
University of Rochester, Rochester, New York

(Received June 8, 1948)

RECENT high altitude flights in free balloons have given evidence for the existence of nuclei of atomic number up to about 40 and kinetic energies of about ½ Bev per nucleon as a component of cosmic radiation above 90,000 feet.

Tracks of such particles were observed both in a cloud chamber and in Ilford nuclear emulsions.

The cloud chamber and associated equipment was enclosed in a sphere of aluminum 30 inches in diameter and 0.040-inch thick, which was kept at atmospheric pressure and within a temperature range between 58 and 98 degrees F throughout the flight. The balloon reached an altitude of 94,000 feet (14 g/cm² below the top of the atmosphere), spent three hours above 90,000 feet, and four hours above 65,000 feet.

Stacks of photographic plates in groups of twelve were placed above and below the chamber, the emulsion lying in the vertical plane. Tracks which entered the photographic plates below the chamber within 30° from the vertical had to pass through all or part of the four ¼-inch lead plates placed in the chamber.

In the photographic plates we observed tracks many times denser and heavier than those which are obtained from fragments produced in nuclear explosions. A further feature which clearly distinguishes these tracks from those produced by ordinary nuclear fragments is the very large number of slow electrons (δ-rays) issuing from the dense and completely solid filament of silver grains which constitutes the core of the tracks. Figures 1, 2 and 3 show examples of such tracks. For comparison, Fig. 4 shows tracks of a π-meson, three protons, and a Li^8 nucleus disintegrating into two slow α-particles. All tracks are reproduced at the same magnification.

Most of these tracks pass through the entire stack of plates and can be followed from one emulsion to the next after penetrating the 1.4-mm thick glass backing of the plates. Not all of the penetrating tracks are equally heavy; some are only slightly heavier than those of slow α-particles, but their ranges are about 1000 times larger.

In cases where the angle is favorable, the track may be pursued through all twelve plates, and tracks have been observed whose range is certainly greater than 7.5 cm of glass or 20 g/cm². If one combines this information with the observation that these tracks are everywhere much heavier than α-particles near the end of their range and that, therefore, at no point of the track is the energy loss smaller than 0.6 Mev/(mg/cm²), one obtains for such a track a minimum charge $Z=16$ and a minimum kinetic energy $E=13$ Bev. Actually, since for many of these tracks the central core of developed silver grains is more than three times as wide as the corresponding core for slow α-particles, the minmum energy loss is probably in the neighborhood of nine times 0.6 Mev/(mg/cm²) or 5.4 Mev/(mg/cm²).

As an example, we now consider a track which enters plate No. 3 at an angle of 37° with the vertical and stops in the glass between plates No. 10 and 11. This particle has a range of 1.5

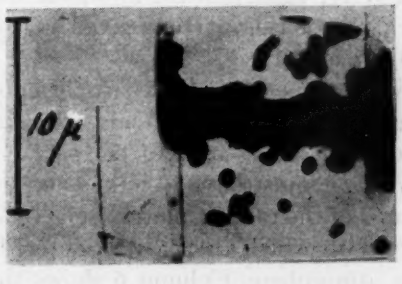

FIG. 1. A very heavy track produced by a particle (estimated $Z=40$) with a range of 1.5–1.9 cm of glass. Four δ-rays can be distinguished in the 10-micron path length shown in the photograph.

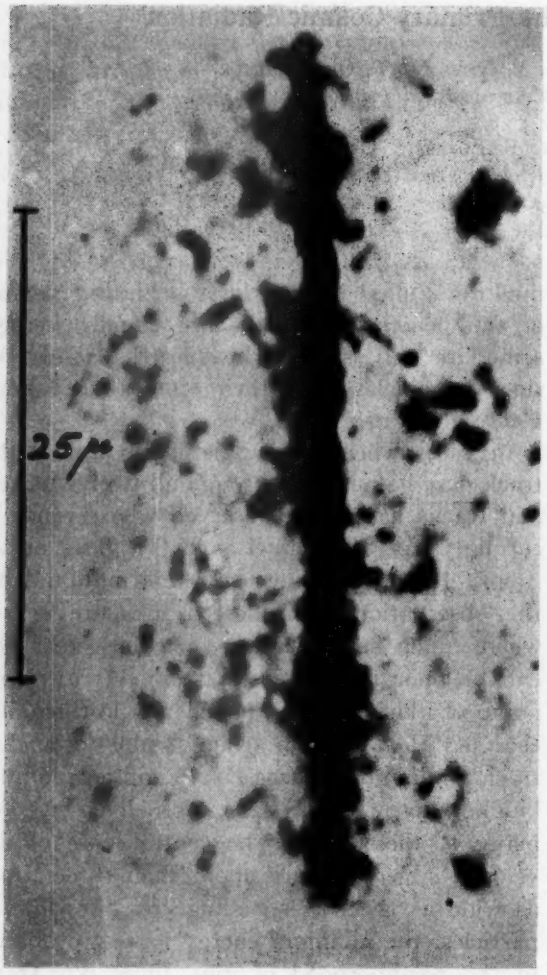

FIG. 2. Another heavy track showing a large number of δ-rays.

cm to 1.9 cm in glass. Assuming an energy loss, at the point where the track enters the stack of plates, of 4 Mev/(mg/cm²) and 6 Mev/(mg/cm²), respectively, we obtain the limits for the energy and charge of this particle given in columns 2 and 3 of Table I.

If we assume that this particle entered the atmosphere from the outside, it must have passed through $14/\cos 37°$ g/cm² = 17.5 g/cm² of air, where it must have lost the energy given in column 4 of the table. Column 5 gives the kinetic energy with which the particle entered the top of the atmosphere. Column 6 shows the cut-off energy for such particles due to the sun's magnetic field. (If one assumes that the sun's field is responsible for the knee of the latitude curve at $\lambda = 48°$, and that the cut-off kinetic energy for protons is 2.3 Bev.)

Comparison of columns 5 and 6 shows that the initial energy assigned is indeed sufficiently high to permit the particle to penetrate the sun's magnetic field.

Another example is provided by the track shown in Fig. 5 which is a stereophotograph of a penetrating heavily ionizing particle taken at 94,000 feet in the twelve-inch cloud chamber filled with argon at 110-cm pressure. The chamber was temperature compensated by a scheme modified from that of Leighton.[1] At the time the

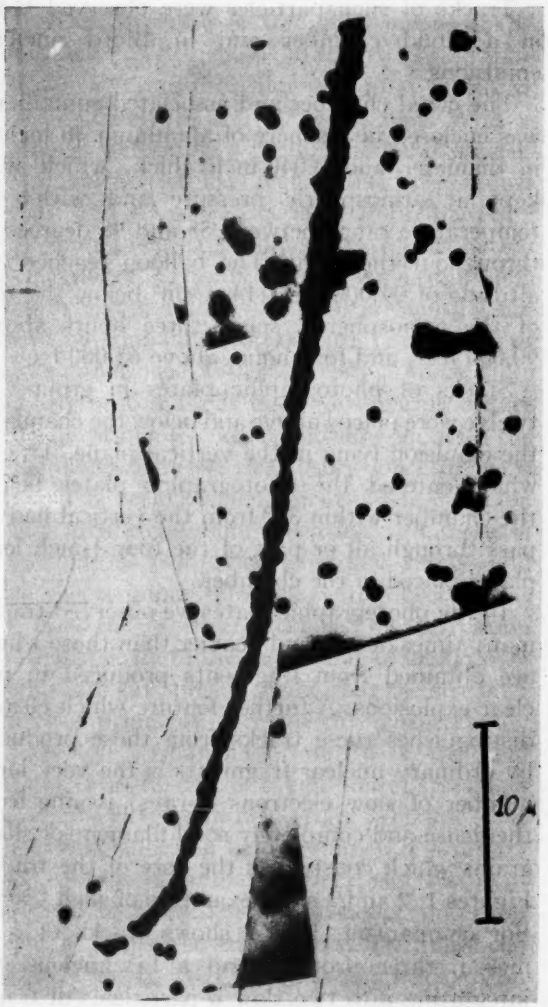

FIG. 3. A medium heavy track ($Z \sim 10-15$) ending in the emulsion. The particle has a low velocity; δ-rays are almost entirely absent. Thinning of track towards the end of the range suggests gradual filling of electronic shells.

[1] R. B. Leighton, Rev. Sci. Inst. 19, 274 (1948).

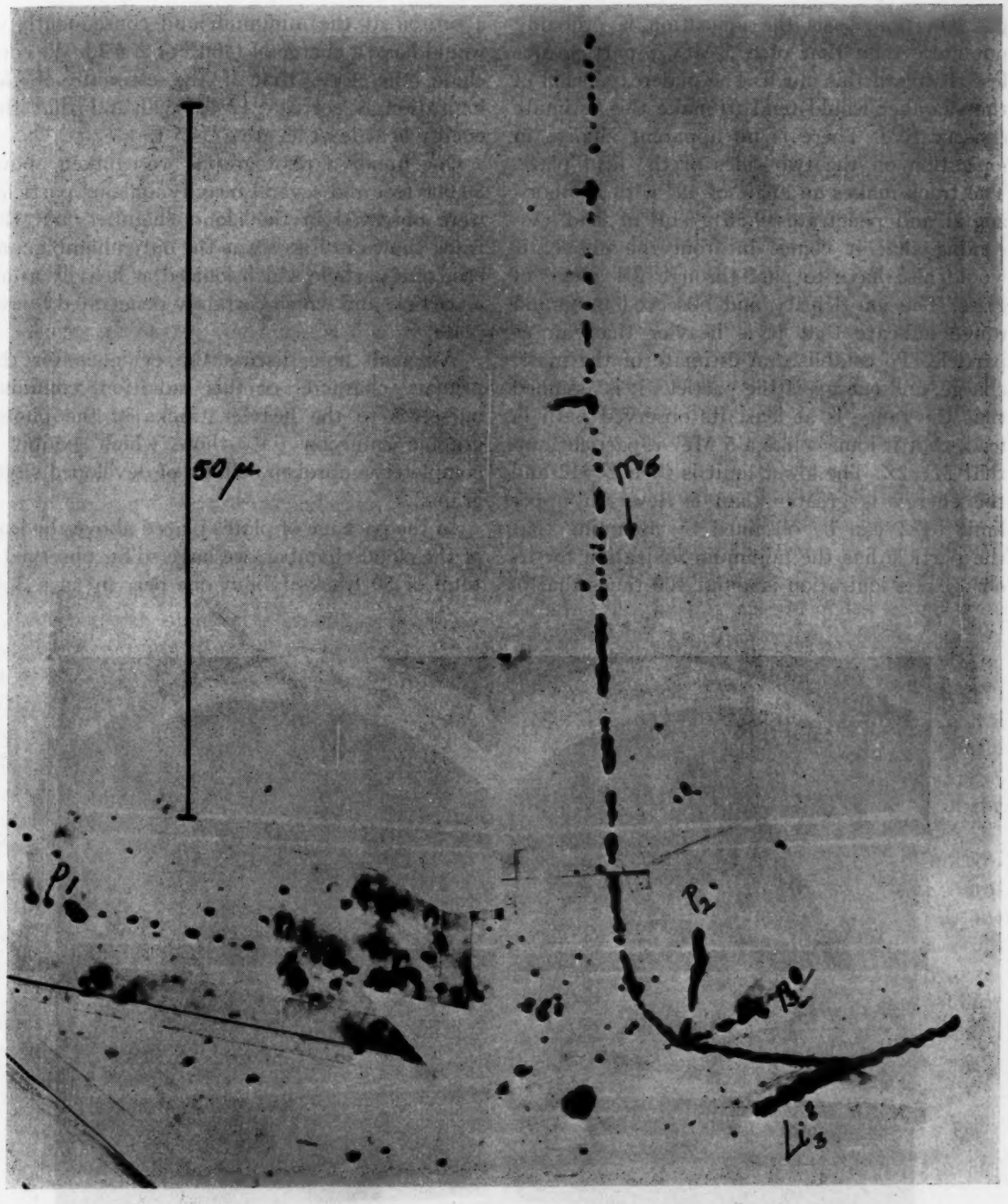

FIG. 4. Nuclear disintegrations produced by a slow meson showing tracks of fast protons, slow proton, slow π-meson, Li^8 nucleus disintegrating into two slow α-particles.

photograph was taken the temperature was rising and compensation had not been completely established, hence the chamber was under-expanded. The ionization was estimated by a comparison with alpha-tracks taken in the same chamber, at the same pressure, with the same

gas. On that basis the ionization is probably not more than that of a 5-Mev α-particle nor less than half this much. The underexpansion of the chamber would tend to make this estimate conservative. There is no apparent change in ionization on the two sides of the lead plate. The track makes an angle of 49° with the horizontal and penetrates 9.56 g/cm² of lead. Assuming that it comes in from the above, it would also have to pass through 2.4 g/cm² of glass. The ion density and observed minimum range indicate that it is heavier than an α-particle. To establish an estimate of the mass, charge, and energy of the particle, it is assumed that the range is at least its observed path in lead, that it ionizes like a 5 Mev α-particle, and that $M=2Z$. The lower limit is then $Z=12$ and the energy is greater than 5 Bev. An upper limit to Z can be obtained by assuming that the particle has the minimum ionization for its charge. Its ionization is about 400 times that of a proton at the minimum and consequently it would have a charge of $(400)^{\frac{1}{2}}$ or $Z=20$. We conclude, therefore, that if the estimate of the ionization is correct, $12<Z<20$ and that the energy is at least as great as 5 Bev.

One hundred photographs were taken above 80,000 feet and several heavily ionizing particles were observed in the cloud chamber, but the track shown in Fig. 5 was the only unambiguous case of a particle which ionized as heavily as an α-particle and which certainly penetrated a lead plate.

We shall now discuss the evidence for the primary character of this radiation, confining ourselves to the heavier tracks in the photographic emulsion (i.e., those which exhibit a completely unbroken column of developed silver grains).

In the package of plates placed above the lead of the cloud chamber, we have so far observed a total of 50 tracks (about one per cm² in a 3–4-

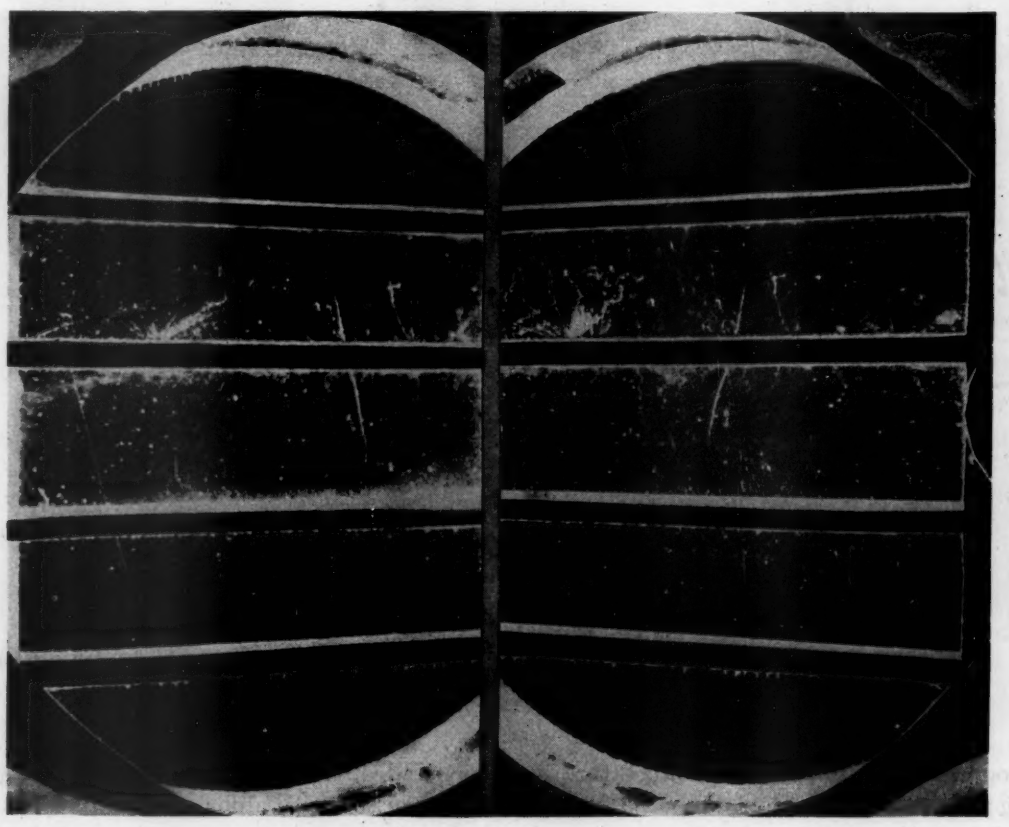

FIG. 5. Cloud-chamber stereophotograph of heavily ionizing penetrating particle taken at 94,000 feet.

TABLE I.

1 Energy loss in Mev/(mg/cm²) when entering stack of plates	2 Kin. energy in Bev	3 Atomic number Z	4 Energy loss in 17.5 g of air	5 Kin. energy at top of atmos.	6 Energy necessary for penetrating solar magnetic field
4	$22<E<26$	$39<Z<41$	61 Bev	85 Bev	69 Bev
6	$35<E<41$	$49<Z<52$	88 Bev	126 Bev	88 Bev

TABLE II.

1 Angle of incidence θ	2 Percentage of tracks	3 Average flux per cm² per second and steradian
$0<\theta<30°$	30%	1.4×10^{-4}
$30°<\theta<60°$	60%	0.51×10^{-4}
$60°<\theta<90°$	10%	0.04×10^{-4}

hour exposure). The angular distribution with respect to the zenith is given in column 2 of Table II. Taking into account the variation of the effective area of the plates with angle of incidence, we obtain the average flux per cm² per second and per unit solid angle. The values for the three angular intervals indicated are given in column 3 of Table II.

(a) The rapid decrease of flux with zenith angle is not compatible with the assumption that these particles are secondaries produced for instance by protons of $\sim10^{11}$ ev, because the angular distribution of protons of this energy must be almost isotropic at this altitude.

(b) Since the intensity is greatly reduced by increasing the thickness of air traversed from 14 g/cm² at $\theta=0°$ to 28 g/cm² at $\theta=60°$, the majority of these particles must have at 94,000 feet a remaining range of less than 14 g/cm². This is confirmed by comparing the number of tracks observed in plates below and above the 1 inch of lead in the cloud chamber. The number of tracks below the lead is smaller than the corresponding number above the lead by about a factor of 6. All but one of the 13 particles observed below the lead enter from outside the cone subtended by the lead plates.

The lead difference also confirms the previous conclusion that the particles are not secondaries produced in the lead plates.

(c) Further confirmation that these particles are much more rapidly absorbed than primary protons was obtained from an earlier flight of one-hour duration at an altitude between 57,000 and 69,000 feet (50 g/cm² of air). In this flight the plane of the emulsion was horizontal. No very heavy tracks were observed. However, in 30 square centimeters of emulsion three tracks were observed which penetrated at least one glass plate and which ionize only slightly more than α-particles.

The sun's magnetic cut-off is high enough such that all particles of $Z<40$ which enter the top of the atmosphere from the zenith will penetrate to 94,000 feet. Therefore, we may assume that the flux on top of the atmosphere is of the same order of magnitude as the flux incident normally at 94,000 feet (1.4×10^{-4} particles per cm² per second and unit solid angle). This corresponds to about one heavy particle for 1000 primary protons, an intensity ratio which is not inconsistent with the assumed relative abundance of heavier atoms ($Z>15$) of the Russel mixture.

We wish to extend our thanks to the Office of Naval Research for its support, to the Aeronautical Research group of General Mills for their cooperation, to the pilots from the Wold Chamberlain Air Base who have assisted in recovering the apparatus, to Mr. Tom Putnam for help in preparing the photographs, and to Dr. R. E. Marshak, Dr. J. T. Tate, and Dr. J. Weinberg for helpful discussions.

Letters to the Editor

PUBLICATION of brief reports of important discoveries in physics may be secured by addressing them to this department. The closing date for this department is five weeks prior to the date of issue. No proof will be sent to the authors. The Board of Editors does not hold itself responsible for the opinions expressed by the correspondents. Communications should not exceed 600 words in length.

A Convergent Expression for the Magnetic Moment of the Neutron

D. RIVIER AND E. C. G. STUECKLBERG
University of Geneva, Geneva, Switzerland
June 2, 1948

CALCULATION of the magnetic moment of the neutron has always yielded a divergent result.[1] We have avoided this difficulty by the use of an invariant perturbation method based upon the S matrix theory.[2] The magnetic moment remains finite but no definite numerical value comes out of the calculations. Our method is quite general and can be applied to all diverging expressions arising from field quantization.

The diverging terms are due to the Dirac δ function appearing in

$$D_\kappa^{\,a}(r,t)=(\epsilon/2|t|)D_\kappa^{\,0}(r,t)$$
$$=(1/4\pi)[\delta(T^2)-\tfrac{1}{2}\theta(T^2)(\kappa/T)J_1(\kappa T)]$$

with

$$T^2=t^2=r^2 \quad \text{and} \quad \theta(T^2)=0 \quad \text{for} \quad T^2\gtrless 0,$$

where $D_\kappa^{\,0}(r,t)$ is the antisymmetric invariant function appearing in the commutation relations of a field of quanta of restmass κ. If we define $\delta(T^2)$ by the following limiting process:

$$\delta(T^2)=\lim_{\kappa_i\to\infty}-\tfrac{1}{2}\theta(T^2)\sum_1^N c_i(\kappa_i/T)J_1(\kappa_i T),$$

with

$$\sum_1^N c_i=-1 \qquad \lim_{\kappa_i\to\infty}\sum_1^N (c_i/\kappa_i^2)=0,$$

a calculation then shows that it is always possible to find a set of $c_i=c_i(\kappa_1^2,\cdots\kappa_N^2)$, identical for each individual diverging term, such that each such term gives a finite contribution to the magnetic moment. Our calculations could be described as the generation of the S matrix by the usual Hamiltonian and its correction[3] by (2). Thus corrected our S matrix might not satisfy causality anymore. That it still does can be seen in the following way. All the terms of the S matrix contain space-time integrations upon invariant $D_\kappa(r,t)$ functions. In our calculations these appear only in the form

$$D_\kappa^{\,c}=D_\kappa^{\,a}+(i/2)D_\kappa^{\,1}$$

where $D_\kappa^{\,1}$ is the symmetric invariant D function involving a T^{-2} singularity. This is exactly the condition that expresses causality[4] or this complex function contains only incoming waves in the past and outgoing waves in the future. This condition reduces to that introduced by Wentzel[5] in his non-relativistic wave optics of the S matrix.

[1] J. M. Jauch, Phys. Rev. 63, 334 (1943), does obtain a finite value but it seems to us that he has discussed only one of many terms.
[2] E. C. G. Stueckelberg, Helv. Phys. Acta 17, 3 (1944); *ibid.* 18, 3 (1945).
[3] In this interpretation (2) could be considered as an "invariant substraction."
[4] E. C. G. Stueckelberg, Helv. Phys. Acta 19, 242 (1946); Phys. Soc. Cambridge Conference Report 199 (1947).
[5] Wentzel, Helv. Phys. Acta 21, 49 (1948).

Comments on the Theories Interpreting the Magnetism of Celestial Bodies

M. FORRÓ
Institute for Experimental Physics, University of Budapest, Budapest, Hungary
May 4, 1948

THE recent works of Babcock[1] and Blackett[2] have directed a new general interest toward the proportionality between magnetic and angular momenta of celestial bodies; accordingly several attempts[3] have been made to explain this phenomenon with the help of a general field theory. All these theories have in common is that they set out from one or two postulates stating explicitly or implicitly a connection between a moving charge (magnetic field) and an impulse-like quantity and arrive finally at the experimental connection of Wilson:[4] $e\sim M(G)^{\frac{1}{2}}$ i.e., to its formulation given by Blackett: $P=\beta(G^{\frac{1}{2}}/c)U$. These considerations involve, perforce, that not only to every mass an electric charge should be associated, but conversely that every moving (rotating) charge must be endowed with a momentum, i.e., with a mass: $M=e/(G)^{\frac{1}{2}}$. This second inference is, however, obviously not true as it may be proved by a simple laboratory experiment: taking a metallic globe of 10 cm diameter and loading it electrically to 1500 volt potential, will you observe when moving it an inert mass corresponding to 100 kg?

It is not sufficient to deduce an empirical expression merely formally in a Lorentz invariant form. From Wilson's observations it follows only that we arrive in the case of earth and sun to a right order of magnitude for their magnetic momenta, if we assume that celestial bodies have electric charges equal to their mass multiplied by the square root of the gravitational constant, but it does not make any statement regarding the inverse relationship. The difficulty in interpreting Wilson's relation arises actually not so much in finding a field theory which can account for the proportionality between mass and charge, but in explaining the fact that this relationship is not reversible.

A field theory can be constructed for any material if two requirements are fulfilled: 1) the prevailing of a re-

pulsive or attractive force similar to Newton's general law of gravitation and 2) the validity of Newton's first axiom. In the case of the general theory of relativity these attributes were for real masses furnished by experimental observations; moreover, it was found that the ratio of inert mass to gravitating mass has the same value for every substance. Conversely, if direct experimental results furnish only one of these requirements (for instance in the case of electric charges only Coulomb's law) and we have to deduce the second attribute of necessity, the inertia of charge, by means of a postulate, we have albeit satisfied the mathematical requirements of a field theory, but we have beforehand no guarantee that such a theory has any bearing on physical reality. I believe that this may be the reason why the theories developed hitherto for interpreting the proportionality between angular and magnetic momenta of celestial bodies have failed to explain the cause of the irreversibility of Wilson's empirical formula. The only theory which has so far been able to deduce Wilson's formula and account for its irreversibility is Barnóthy's theory.[5] However, this theory, similarly to all the others, encounters difficulties in explaining the large static potentials arising together with the correct values of the magnetic momenta.

[1] Babcock, Astr. Soc. Pac. **59**, 112 (1947).
[2] Blackett, Nature **159**, 658 (1947).
[3] Giao, Port. Physica **2**, 1 (1946) and **5**, 145 (1946); Mariani, Phys. Rev. **73**, 78 (1948); Szamosi, Nature (in press).
[4] Wilson, Proc. Roy. Soc. **A104**, 451 (1923).
[5] Barnóthy, Papers of Terrest. Magn. No. 2. Budapest. (See also report of Cowling, Nature **160**, Dec. 13, 1947.)

The *S*-Level Shift in Ionized Helium

G. R. Fowles
Department of Physics, University of California, Berkeley, California
June 1, 1948

THE previously reported measurement[1] of the doublet separation of the ionized helium line at 1640A has been improved by obtaining the line in the third order of the grating. With the three-meter vacuum spectrograph this gives a dispersion of one A/mm. The source was a liquid-air cooled Schüler-type discharge tube. The aluminum hollow cathode was one cm in diameter and ten cm long. Mild excitation was used in order to obtain sharp lines, and this necessitated an exposure time of about one hour.

As a result of the *S*-level shift,[2] the short wave-length component of the main doublet is split into two, and the center of gravity of the resulting pair is shifted toward the red, producing a smaller main doublet separation than that predicted by Dirac theory. Furthermore the weak center component due to the transition $2^2S_{\frac{1}{2}}-3^2P_{\frac{1}{2}}$ is shifted to the red by an amount just equal to the shift of the $2S$ level. A determination of this change in the position of the center component, with respect to the position calculated by Dirac theory, permits a direct evaluation of the shift. These facts are shown in Fig. 1.

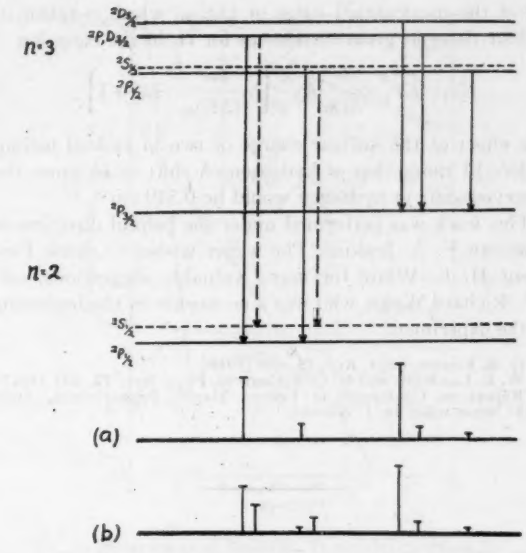

FIG. 1. Diagram showing fine structure of the line HeII λ1640 with (a) Dirac theory, and (b) modification due to the *S* level shift.

Figure 2 shows a microphotometer trace of one of the recent spectrograms. The center component is resolved from the two principal peaks, and its position with respect to these peaks has been measured. The separation of the maxima of the two main components is $5.16_2\pm0.01_8$ cm^{-1}. The center component is found to lie $3.18_1\pm0.04_0$ cm^{-1} from the longer wave-length main peak. The Dirac theory predicts 5.314 cm^{-1} and 3.586 cm^{-1}, respectively, for these two values as the separations of the centers of gravity of the three unresolved pairs. The observed values correspond to a shift of $0.44_8\pm0.05_0$ cm^{-1} in the $2S$ level. In this calculation the effect of the very weak component

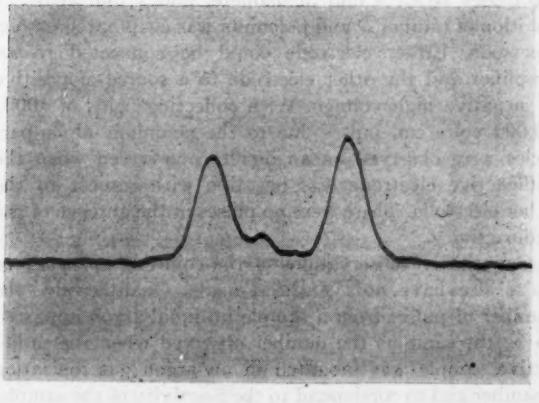

FIG. 2.

$2^2P_{\frac{1}{2}}-3^2S_{\frac{1}{2}}$ upon the position of the observed center peak is taken into account.

The measured value agrees favorably with the theoretical value of 0.442 cm^{-1} obtained from the recent calculations given by Schwinger and Bethe.[3] This involves the

use of the recalculated value of $(\Delta E)_{Av}$, which is taken to be four times as great for He^+ as for H, in the equation

$$Es_{\frac{1}{2}} - Ep_{\frac{1}{2}} = \frac{8e^2}{3\pi\hbar c} Ry \frac{Z^4}{n^3}\left[\ln\frac{mc^2}{(\Delta E)_{Av}} - \ln 2 + \tfrac{1}{2}\right].$$

The effect of the nuclear charge of two in ionized helium a shift 13 times that of hydrogen. A shift of 16 times the observed shift in hydrogen would be 0.540 cm^{-1}.

This work was performed under the helpful direction of Professor F. A. Jenkins. The writer wishes to thank Professor H. E. White for many valuable suggestions, and Mr. Richard Weiss, who was a co-worker in the beginning of the experiment.

[1] G. R. Fowles, Phys. Rev. 73, 639 (1948).
[2] W. E. Lamb, Jr. and R. C. Retherford, Phys. Rev. 72, 241 (1947).
[3] Report on Conference at Pocono Manor, Pennsylvania, April, 1948: Notes taken by J. Wheeler.

Conductivity Pulses in Liquid Argon

NORMAN DAVIDSON AND A. E. LARSH, JR.
Gates and Crellin Laboratories of Chemistry, California Institute of Technology, Pasadena, California
June 7, 1948

THE recent interest in the topic of crystal counters has prompted us to attempt a similar experiment with insulating liquids instead of crystals, in order to investigate whether, in such liquids, ionizing radiations excite electrons into conduction levels in which the electrons can move rapidly in an applied field. The purpose of this preliminary communication is to report that we have observed conductivity pulses due to polonium alpha-particles in liquid argon. No such effect was obtained in liquid nitrogen or in *n*-heptane at room temperature.

The counter tube contained two plane parallel platinum electrodes about 5 mm in diameter and 1 mm apart. A solution of radium *D* and polonium was evaporated on one electrode. Either electrode could be connected to an amplifier and the other electrode to a source of positive or negative high voltage. With collecting fields of 1000–10,000 volts/cm, pulses due to the polonium alpha-particles were observed on an oscilloscope screen when the radioactive electrode was negative with respect to the other electrode. There were no pulses in the absence of the radioactivity.

Quantitative observations of the counting efficiency or pulse size have not yet been made. Qualitatively, the number of pulses from a sample in liquid argon appeared to be the same as the number observed when the radioactive sample was mounted in an argon gas ionization chamber and to correspond to the β-activity of the sample. The pulses were not of uniform size. The pulse size increased as the collecting voltage was raised to 5000 volts/cm, but not markedly thereafter. Even at fields of 10,000 volts/cm, they were only about half the size of the pulses in a gas counter of comparable capacity. The collection time of the pulses was no greater than 12 μsec, the rise time of the amplifier used, implying that the electron mobility is not less than 4 cm/sec/volt. With 1000 volts across plane electrodes about 1 cm apart, pulses were not observed in liquid argon.

When the liquid argon was cooled and solidified, presumably in a polycrystalline condition, conductivity pulses were still observed.

When the radioactive electrode was positive, about one-tenth as many pulses of a size about a fourth the maximum pulse size were observed. We suspect that these do not correspond to the migration of positive holes, but were due to *RaE* β-particles that spent a major fraction of their range in the liquid argon.

Pulses were not observed in liquid nitrogen even when deoxidized by a recommended technique.[1] About 5 mole percent nitrogen dissolved in liquid argon did not affect the number or the size of the pulses. A concentration of oxygen of 0.7 percent in argon completely quenched the pulses; at an oxygen concentration of 0.2 percent, the number and the size of the pulses each decreased by about 50 percent. Passage of the tank argon through a deoxidizer did not improve its counting characteristics.

The *n*-heptane was Phillips "pure" grade[2] that was treated with sulfuric zcid and molten sodium to remove any electron trapping impurities.

It is pertinent to recall that Ogg has reported experiments supporting the idea of conduction levels for electrons in liquid ammonia.[3]

More extensive and precise studies of the behavior of electrons in liquid media are planned. From a practical point of view, it would be desirable to search for liquids that will count at room temperature.

An advantage of a liquid counter over a crystal counter would be the absence of space charge accumulation.

This work has been supported by the Office of Naval Research. Mr. Alvin Tollestrup and Mr. J. M. Miller have given us helpful advice about electronic equipment.

[1] Pollack, Pringsheim, Terwoord, J. Chem. Phys. 12, 295 (1944); Meyer and Ronge, Zeits. f. Angew. Chem. 52, 63 (1939).
[2] Kindly supplied by the Phillips Petroleum Co. to Professor H. J. Lucas.
[3] Ogg, J. Am. Chem. Soc. 68, 155 (1946).

Characterization of Tc Activities Produced by Deuteron Bombardment of Separated Mo Isotopes*

E. E. MOTTA
Oak Ridge National Laboratory, Oak Ridge, Tennessee
AND
G. E. BOYD
Department of Terrestrial Magnetism, Carnegie Institution, Washington, D. C.
May 26, 1948

IN a previous letter [Phys. Rev. 73, 1470 (1948)] a preliminary report was given on a number of short-lived element 43 (Tc) activities produced by the irradiation of the separated Mo isotopes with *ca.* 16 Mev deuterons. At this time, it is possible to communicate further informa-

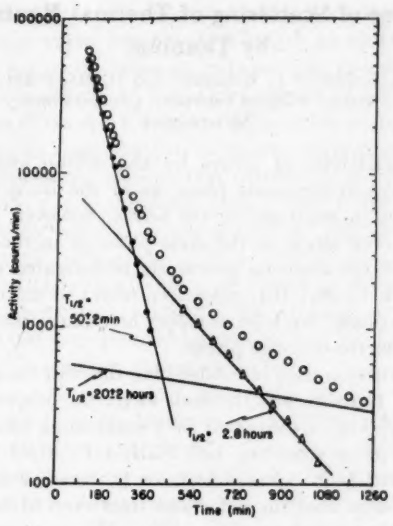

FIG. 1. Decay curve of the 50-minute Tc activity produced by the deuteron bombardment of Mo enriched in Mo^{94}.

tion on several longer-lived Tc isotopes which were also found.

50-minute Tc.—Deuteron bombardments on Mo^{94} of about one hour's duration led to the formation of a Tc activity in good yield, which decayed with a half-life of 50±2 minutes (Fig. 1) and emitted positrons of 2.5±0.3-Mev energy (Fig. 2). A gamma-ray of 0.9±0.1-Mev

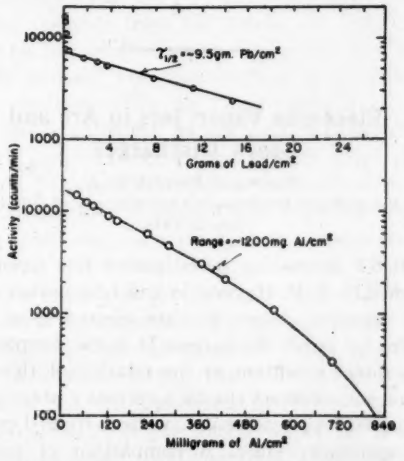

FIG. 2. Aluminum absorption curve for the positrons and a lead absorption curve for the γ-rays from the 50-minute Tc.

energy was found to be associated with this period also (Fig. 2). These characteristics appear to be in good agreement with previous observations on a 53-minute activity produced in natural molybdenum by proton bombardment.[1,2] On the basis of the yield of the activity from the molybdenum enhanced in Mo^{94}, the assignment of the 50-minute Tc period to mass 94 is considered probable.

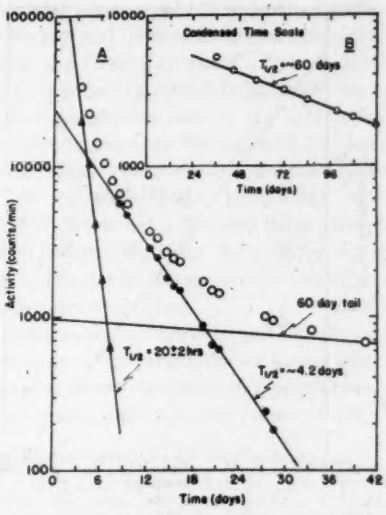

FIG. 3. Decay curve of the 20-hr. Tc activity produced by deuteron bombardment of Mo enriched in Mo^{95}.

20-hour Tc.—One-hour deuteron bombardments on Mo^{95} were observed to give rise to a Tc activity of 20±2-hour half-life (Fig. 3) which decayed with the emission of 16.5±1.5-kev x-rays. ($\tau_{\frac{1}{2}}$ = 110±15 mg Al/cm²) and a gamma-ray of 0.8±0.1-Mev energy (Fig. 4). Yield considerations have lead to the assignment of this period to mass 95. Quite recently the formation of what appears to have been the same radioactive species of Tc by decay from Ru^{95} has been reported.[3]

2.8-day Tc.—Deuteron irradiations on Mo^{98} varying between forty minutes and one hour were found to yield another Tc activity of 2.8±0.1-day half-life in good abundance (Fig. 5). Beta-rays of 1.3±0.2-Mev maximum

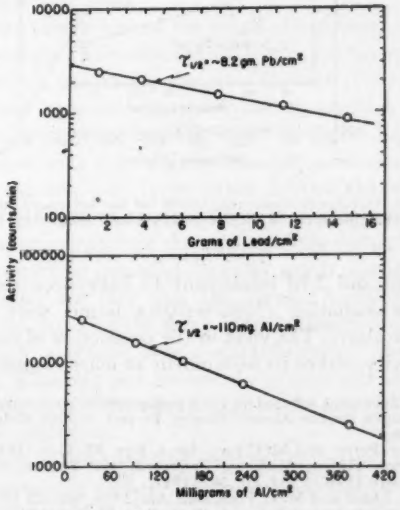

FIG. 4. Aluminum absorption curve for the x-rays and a lead absorption curve for the γ-rays from the 20-hr. Tc.

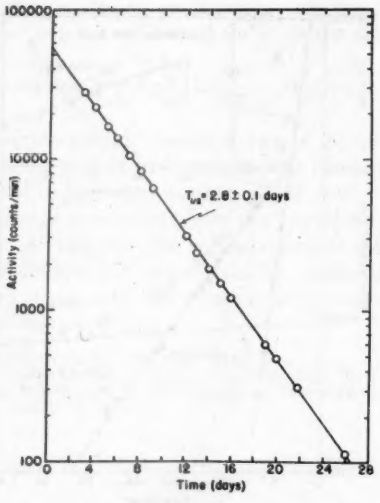

FIG. 5. Decay curve of the 2.8-day Tc activity produced by deuteron bombardment of Mo enriched in Mo^{98}.

energy and gamma-rays of 0.9±0.1-Mev were found to be associated with this period (Fig. 6). Previously half-lives

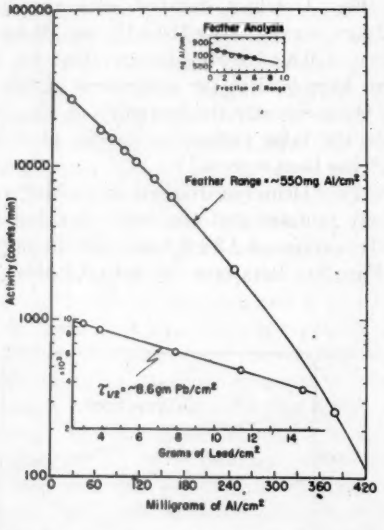

FIG. 6. Aluminum absorption curve for the beta-rays and a lead absorption curve for the γ-rays from the 2.8-day Tc.

of *ca.* 2d and 2.7d in element 43 have been reported,[4–6] but the radiation characteristics found were different from the above. The yield in the production of our 2.8-day Tc activity makes its assignment to mass 98 probable.

* This document is based on work performed under Contract Number W-7405eng26 for the Atomic Energy Project at Oak Ridge National Laboratory.

[1] Ewing, Perry, and McCreary, Phys. Rev. **55**, 1136 (1939).
[2] Gugelot, Huber, Medicus, Preiswerk, and Steffen, Helv. Phys. Acta **19**, 418 (1946); *ibid.* **20**, 240 (1947).
[3] D. T. Eggen and M. L. Pool, Bull. Am. Phys. Soc. **23** [3], 56 (1948).
[4] G. T. Seaborg and E. Segrè, Phys. Rev. **55**, 808 (1939).
[5] Glendenin, Plutonium Project Record **9B** (12.9).
[6] P. Abelson, Phys. Rev. **56**, 753 (1939).

Phase of Scattering of Thermal Neutrons by Titanium

S. S. SIDHU,* L. WINSBERG AND D. MENEGHETTI
Argonne National Laboratory, Chicago, Illinois
May 28, 1948

SCATTERING of x-rays by the orbital electrons is always in the same phase as of the incident wave. Scattering of neutrons by the nuclei, however, has been shown[1] to be either in the same phase or in the opposite phase. Of the elements previously investigated three elements, H, Li and Mn, have been found to scatter in the opposite phase. We wish to report here that titanium, too, scatters in the opposite phase.

The criterion used in establishing the neutron scattering phase of titanium was the same as for the other elements. Each element is contained in a compound which has a NaCl type of structure, i.e., NaH, LiF, MnO and TiC. Except for NaH, x-ray diffraction patterns of these compounds show that the reflections from even Miller indices atomic planes such as (200), (220), (222), etc., give strong intensities, and those from odd Miller indices planes such as (111), (113), (133), etc., give weak intensities. In the neutron diffraction patterns of these compounds the intensities are reversed.

Our results were determined from a neutron diffraction pattern of TiC obtained with the rotating shutter mechanism.[2] They were confirmed with the neutron crystal spectrometer by Dr. C. G. Shull of the Oak Ridge National Laboratory to whom we are greatly indebted.

* On leave from the University of Pittsburgh.
[1] E. Fermi and L. Marshall, Phys. Rev. **71**, 666 (1947).
[2] T. Brill and H. V. Lichtenberger, Phys. Rev. **72**, 585 (1947).

Electrode Vapor Jets in Arc and Spark Discharges

WOLFGANG FINKELNBURG
Engineer Research and Development Laboratories, Fort Belvoir, Virginia
June 3, 1948

A MOST interesting investigation was recently published by J. R. Haynes[1] in which he proves that high velocity mercury vapor jets are ejected from mercury electrodes by spark discharges. It is the purpose of this note to direct attention to the relation of this work to some investigations on the high current carbon arc,[2] with which similar jet phenomena have been studied extensively in the stationary state. A comparison of our results with those of Haynes seems to support his reasonable assumption "that the mechanism of vapor jet production is the same in arc and spark discharge," and leads to an understanding of the mechanism of vapor jet production.

The sparks studied by Haynes had current intensities of a few hundred amperes, anodic current densities (computed from his photographs) of the order of 20,000 amperes/cm² and a duration of 0.25 to 5 micro-seconds. Our high current carbon arc, on the other hand, burned continuously with currents between 50 and 1000 amperes

and an anodic current density of 100 to 500 amperes/cm², the positive vapor jets having a length up to more than 10 cm. One more difference between the two discharges should be mentioned: While the current density at the electrodes of the spark seems to adjust itself automatically to a more or less constant value, the current density of most forms of the high current carbon arc is determined by the current and the anode surface, which in these cases is completely covered by the discharge. Only the hissing high current carbon arc with a homogeneous positive carbon (without core) shows an anodic contraction, the current density in the anodic spot reaching a value of about 50,000 amperes/cm² independent of the anode surface and the absolute current intensity.[3]

In order to demonstrate, after these general remarks, how far the similarity between the jet phenomena of high current carbon arc and mercury spark goes, the following comparison of our results with Haynes' summary of experimental facts (see reference 1, p. 901) is given:

1. A jet of vapor consisting of the vaporized material of the positive carbon and its core is ejected from the positive arc crater and at very high currents some vaporized material is ejected also from the negative tip, in agreement with Haynes' findings for the mercury spark.

2. The anodic jets are ejected normal to the electrode surface, i.e., in the prolongation of the positive carbon, again in agreement with Haynes' results.

3. Spectrograms show that the jets are composed of the dissociated and partly ionized compounds of the positive carbon, in agreement with Haynes' findings.

4. The velocity of the jet decreases exponentially with increasing distance from the anode. Its initial velocity depends on the anodic current density and is of the order of 5×10^3 cm/sec. The first result is in agreement with Haynes' findings while his larger velocity of 1.5×10^5 cm/sec can be explained by the larger current density of the spark, *viz.*, two orders of magnitude larger than that for the arc. Finally, a dependence of the initial jet velocity on the current density could not be found by Haynes because he could vary only the current and not the current density.

5. The afterglow of the jet vapors (the "anode flame" of the arc) is several orders of magnitude larger than the average lifetime of excited atoms (10^{-8} sec), again in agreement with Haynes' results. The same applies for the explanation of this effect, published in 1939.

6. The potential of the anodic vapor jet is constant throughout its extent, being negative to the anode by the amount of the anode drop.

7. The anode drop of the fully developed high current carbon arc is 30 ± 5 volts and the cathode drop is approximately 10 volts, the sum being in agreement with Haynes' result for the spark. The anode drop increases with increased anodic current density.

This summary reveals the striking similarity of the vapor jet phenomena of high current carbon arc and mercury spark, at least as far as positive jets are concerned. For the large number of detailed results on the carbon vapor jets and their electric and magnetic behavior, as well as for the "negative flame" of the arcs, the reader is referred to our publications.[2] In spite of the agreement between the experimental results, the mechanisms of the jet production proposed by Haynes and the author differ considerably. While Haynes offers an essentially electric theory of the jet phenomenon, the author, in the years since 1939, has developed a thermal theory which, having been checked independently by Rohloff,[4] seems to be able to describe satisfactorily the mass of observations on high current carbon arc vapor jets.

On the same basis, we hope to publish shortly a theoretical treatment of the production of vapor jets by sparks and arcs which seems to account quantitatively for all experimental results known at the present time.

[1] J. R. Haynes, Phys. Rev. 73, 891 (1948).
[2] W. Finkelnburg and collaborators, Zeits. f. Physik 112, 305, 113, 562, 114, 734 (1939); 116, 214 (1940); 117, 344 (1941); 119, 206 (1942); 122, 714 (1944). Naturwiss. 33, 55 (1946); Zeits. f. Naturforsch. 1, 305 (1946); Zeits. f. Physik, 1948 (in press). Monograph, including unpublished data, *Der Hochstromkohlebogen*, Springer-Verlag, Heidelburg und Berlin, 1948. English presentation: *The High Current Carbon Arc*" FIAT Final Report 1052, 1947 (PB-81644, Office of Technical Services, Department of Commerce, Washington, D. C.).
[3] H. Schluge and W. Finkelnburg, Zeits. f. Physik 122, 714 (1944).
[4] E. Rohloff, Reichsberichte f. Physik 1, 47 (1944).

Saturation Effects in Microwave Spectroscopy

ROBERT KARPLUS*
Mallinckrodt Chemical Laboratory, Harvard University, Cambridge, Massachusetts
June 1, 1948

THE results of experimental investigations[1–3] of saturation effects in microwave spectroscopy[4] as well as conflicting theoretical discussions[5,6] have recently been published. Since the experiments were carried out under different conditions, a theory is needed to reduce the data to a comparable basis.

The two derivations of the shape of saturated, collision-broadened absorption lines[5,6] start from the same assumptions and use essentially the same method. The difference in the final equations can be traced to the fact that the value of $|V_{12}|^2$ used in reference 5 to obtain Eq. (13) is inconsistent with the "slightly relaxed" assumption (*b*) of the introduction. The prescription dictates that one averages the *absorptions* produced by the (independent) Zeeman components and not the squares of the matrix elements of the interaction potential. In other words, one must take into account the fact that the Zeeman components are not all saturated to the same extent. Hence, Eq. (35) of reference 6, averaged over a suitable energy distribution in space, is appropriate to describe phenomena that occur in a wave guide, where the transitions are induced by plane polarized radiation.

The data of Bleaney and Penrose[2] have been shown to substantiate this theory.[7] In an entirely similar way, it may be shown that the data of Carter and Smith[3] also agree (see Table I, second and fourth columns). Agreement

TABLE I. Saturation of the ammonia (3,3) line in a rectangular guide.

Incident power Milliwatts	Relative saturation Theoretical	Theoretical	Experimental (ref. 3)
2.7×10^{-4}	1.00	(1.00)	1.00
5.5×10^{-3}	0.89	(0.88)	0.82
5.5×10^{-1}	0.45	(0.43)	0.48
5.3	0.10	(0.08)	0.08

with the equation of Snyder and Richards[5] is obtained if one assumes that only 62 percent of the collisions effective in broadening the absorption line also restore thermal equilibrium (see Table I, third column).

The results of Pond and Cannon[1] are more difficult to interpret, because in their experiment the energy density varied strongly along the guide as well as on a cross section, due to the standing waves set up in the equipment. Still, from the magnitude of the effect one can estimate the relaxation time to be of the order of ten microseconds. This means that collision with the wall is the mechanism that re-establishes thermal equilibrium. Most of the width of the line is therefore due to a non-dissipative cause, the Doppler effect. The theory so far developed cannot be applied to interpret the experiment. One may notice, however, that over the 200-fold variation in incident power investigated by Pond and Cannon, the absorption coefficient varies inversely as the cube root of the power. Hence, this is the transition region from constant absorption coefficient (low power level) to constant total power absorbed (high power level). It is somewhat surprising that the transition is so gradual.

To summarize, then: the data on the saturation of absorption lines broadened only by intermolecular collisions are in agreement with a theory which treats Zeeman components as independent contributors to the absorption and assumes that all collisions restore thermal equilibrium.

* U. S. Rubber Company, Predoctoral Fellow.
[1] T. A. Pond and W. F. Cannon, Phys. Rev. **72**, 1121 (1947).
[2] B. Bleaney and R. P. Penrose, Proc. Phys. Soc. **60**, 83 (1948).
[3] R. L. Carter and W. V. Smith, Phys. Rev. **73**, 1053 (1948).
[4] C. H. Townes, Phys. Rev. **70**, 665 (1946).
[5] H. S. Snyder and P. I. Richards, Phys. Rev. **73**, 1178 (1948).
[6] R. Karplus and J. Schwinger, Phys. Rev. **73**, 1020 (1948).
[7] R. Karplus, Phys. Rev. **73**, 1120 (1948).

On Infinite Field Reactions in Quantum Field Theory

SIN-ITIRO TOMONAGA
Physics Institute, Tokyo Bunrika Daigaku, Tokyo, Japan
June 1, 1948

IN interpreting the level-shift of the hydrogen atom in terms of the radiative reaction, Bethe[1] proposed a method of dealing with this problem without touching the inherent divergency of the current quantum field theory. By his theory it has become possible to treat the problem involving field reactions for the first time in close connection with the reliable experimental data. On the other hand, Lewis[2] and Epstein[3] analyzed the infinities occurring in the radiative correction to the scattering cross-section of an electron in an external field of force and found that also these infinities could be got over by means of a procedure similar to Bethe's. In a recent issue of the PHYSICAL REVIEW, Schwinger[4] pointed out that in these problems the method of canonical transformation was useful, by which the separation from the fields of the parts belonging to free photons and non-radiating electrons was performed, a method which can be regarded as a relativistic generalization of the procedure used by Bloch and Nordsieck[5] as well as by Pauli and Fierz[6] in the discussions about the self-field of an electron.

Almost the same line of attack was taken independently of these American authors also by our Tokyo group and some results are now in course of publication in our English journal, *Progress of Theoretical Physics*. Under the unfavorable conditions after wartime, however, it will be a long time before these papers will appear in print. So I should like to give here a brief summary of the state and views of our investigations.

We first treated the effect of field reactions in the collision problem on the *f*-field theory of Pais[7]—or the *C*-meson theory of Sakata,[8] which had been developed by Sakata independently of Pais—intending to examine whether this theory which had been put forward aiming at the elimination of the infinity occurring in the self-energy of charged particles, was also capable of cancelling out the infinity occurring in the scattering cross section of an electron. We found that this was really the case: the *f*-field was proved capable of compensating one part of the infinite reactions of the radiation field in this phenomenon. The other part of infinities, that is, of the positron theoretical origin, however, could not be eliminated by introducing this new field.[9]

Then the above mentioned work of Bethe appeared. We tried[10] to formulate Bethe's procedure in a mathematically more closed form by using a relativistic generalization of the canonical transformation of Pauli and Fierz. By this transformation an infinite term could be separated in the Hamiltonian density, and this term, we found, had the same form as the mass term in the Dirac equation, being bilinear in ψ^* and ψ. Because of its structure this infinite term can be amalgamated into the mass term of the Dirac equation and one can reinterpret the electron mass in such a way that the compound mass is just what we observe, corresponding to the idea of Bethe. This procedure violates neither the invariance of the theory nor the integrability condition of the generalized Schrödinger equation.[11] In order to investigate the effectiveness of this amalgamation of infinity into the electron mass, we applied the method to the problem lying close at our hand, i.e., the radiative correction to the scattering cross section of an electron.[12] We found this amalgamation was in fact effective in eliminating the non-positron theoretical infinity in this problem, a fact that was pointed out independently by Lewis. It was also shown that the infinity of the positron theoretical origin could be eliminated by reinterpreting the scattering external potential or by reinterpreting the electron charge.

The result of the canonical transformation shows on the other hand that there occurs an infinity of another type, a term containing electromagnetic potential bilinearly. Because of this structure this infinity is to be attributed to the vacuum polarization effect. In order to see the role to be played by this effect in collision phenomena we analyzed the infinities occurring in the e^2-correction to the Klein-Nishina formula.[13] In this problem, we found, besides the infinities of the types mentioned above, an infinity which is closely related to the above mentioned vacuum effect. Infinity of this kind can be, in fact, driven away from the cross section when we substract beforehand the infinite term of the vacuum type from the Hamiltonian. But for this subtraction we cannot find a reasoning so natural and plausible as that used in the case of mass-type and charge-type infinities, where the subtraction was considered as an amalgamation. This is because it would necessarily result in a drastic change of the Maxwell equation for the radiation.

A way out of this difficulty was suggested:[14] it might be possible to introduce some fields which would give rise to the vacuum effect with the opposite sign so that a compensation method similar to the *f*-field theory might be used here. In fact, one finds, applying the same method, that a Pauli-Weisskopf field has this property.[15] An alternative possibility is to consider, in the style of Dirac's theory of the classical electron, that the "original equation" for the radiation contained, in the same way as the "original mass" of the electron, in itself an infinity with the opposite sign so that, supplemented with the infinity appearing as the result of the interaction, the equation for the observable field becomes just of the Maxwellian form.

The calculation of the level-shift of a bound electron was also undertaken.[16] This work is not yet completed but it was confirmed that the result converges by virtue of our subtraction prescription. We found further, in agreement with Schwinger, that a part of the radiative correction to the energy can be interpreted as caused by an anomalous moment of the electron the existence of which had been expected by Breit.[17]

We hope that various postwar difficulties will soon be settled and that our results will appear in print in the near future.

[1] H. A. Bethe, Phys. Rev. **72**, 339 (1947).
[2] H. W. Lewis, Phys. Rev. **73**, 173 (1948).
[3] S. T. Epstein, Phys. Rev. **73**, 177 (1948).
[4] J. Schwinger, Phys. Rev. **73**, 415 (1948).
[5] F. Bloch and A. Nordsieck, Phys. Rev. **52**, 54 (1937).
[6] W. Pauli and M. Fierz, Nuovo Cimiento, **15**, No. 3, 1 (1938).
[7] A. Pais, Phys. Rev. **68**, 227 (1946).
[8] S. Sakata, Prog. Theor. Phys. **2**, 30 (1947).
[9] D. Ito, Z. Koba and S. Tomonaga, Prog. Theor. Phys. **2**, 216, 217 (L) (1947).
[10] T. Tati and S. Tomonaga, lecture at the symposium on the theory of elementary particles, Nov. 1947. Full account of this lecture will be published in Progress of Theoretical Physics.
[11] S. Tomonaga, Prog. Theor. Phys. **1**, 27 (1946); Z. Koba, T. Tati and S. Tomonaga, Prog. Theor. Phys. **2**, 101, 198 (1947).
[12] Z. Koba and S. Tomonaga, Prog. Theor. Phys. **2**, 218 (L) (1947).
[13] Z. Koba and G. Takeda, appearing in Prog. Theor. Phys.
[14] M. Taketani, private conversation.
[15] K. Baba, M. Sasaki and R. Suzuki, to be published in Prog. Theor. Phys. It was first pointed out by Sakata and Umesawa in the Nagoya University that the Pauli-Weisskopf field gives rise to a positive self-energy of a photon in contrast to a negative one due to the electron field and this would result in the compensation of the vacuum effect mentioned above.
[16] Y. Nambu, to be published in Prog. Theor. Phys.
[17] G. Breit, Phys. Rev. **72**, 984 (1947).

Note on the Above Letter: In transmitting to the Physical Review the accompaning review by Tomonaga of the remarkable work carried out in Japan in recent years, there is one technical note that may be helpful.

Tomonaga remarks in the fifth paragraph from the end that in addition to the infinite terms which may be recognized as contributions to mass and charge, there are other infinities which appear, particularly in the corrections to the Klein-Nishina formula. These have to do with the familiar problem of the light quantum self-energy. As long experience and the recent discussions of Schwinger and others have shown, the very greatest care must be taken in evaluating such self-energies lest, instead of the zero value which they should have, they give non-gauge covariant, non-covariant, in general infinite results. From manuscripts kindly sent by Tomonaga, I would conclude that the difficulties referred to in this note result from an insufficiently cautious treatment, and therefore inadequate identification, of light quantum self-energies.

J. R. Oppenheimer
Institute for Advanced Study
Princeton, New Jersey

The Absorption of Cosmic Radiation in Meteorites

Carl August Bauer
University of Michigan, Ann Arbor, Michigan
May 26, 1948

A PREVIOUS letter[1] showed that cosmic radiation has produced an appreciable amount of the helium found in metallic meteorites. Since the rate of helium production is directly proportional to the intensity of the cosmic radiation, the radial variation of this cosmic-ray helium within a spherical iron meteorite can be calculated from the radial variation in the intensity of primary cosmic radiation.

If N_0 and $N(r)$ are, respectively, the number of primary cosmic-ray particles passing through a unit sphere (cross

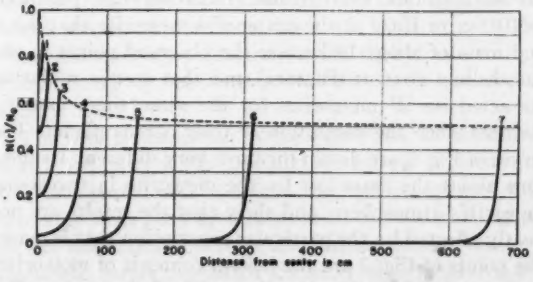

FIG. 1. The radial variation in the intensity of primary cosmic radiation (or in the relative helium content) in spherical iron meteorites of various masses. The numbers at the top of the curves are log mass in kg.

section = 1 cm²) per second in free space and at a point P at a distance r from the center of an iron sphere of radius R and density $\rho = 7.8$ g/cc, then the relative intensity of primary cosmic radiation at P is,

$$\frac{N(r)}{N_0} = \frac{1}{4\pi}\int e^{-d/D}d\omega = \frac{1}{4r}\int_{R-r}^{R+r} e^{-d/D}dd + \frac{R^2-r^2}{4r}\int_{R-r}^{R+r}(e^{-d/D}/d^2)dd.$$

D (19.2 cm for iron) is the distance in which a primary cosmic-ray particle will, on the average, produce one disruption, and d is the distance from P to a point on the surface of the iron sphere. Figure 1 shows the radial variation of $N(r)/N_0$ and thus also of the relative helium content of spherical iron meteorites of various masses. These results can be applied with considerable accuracy to metallic meteorites of any compact shape.

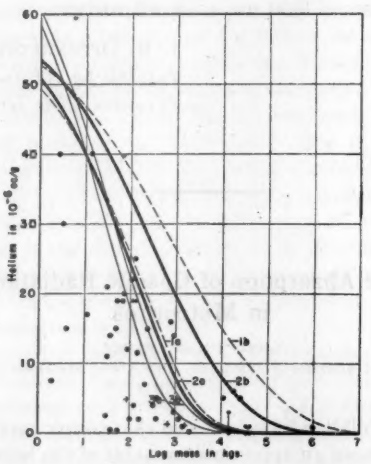

FIG. 2. The variation of the helium content with mass for metallic meteorites. The curves are drawn for the following assumptions for the ratio, m/M, of the final to the pre-atmospheric mass. $m/M = 0.729$, curve 1*a*—center of meteorite, 1*b*—edge of meteorite; $m/M = 0.512$, 2*a*—center, 2*b*—edge; $m/M = 0.125$, 3*a*—center, 3*b*—edge. The points represent the helium content and mass of the meteorites measured by Paneth.

The curves of Fig. 2 show the calculated helium contents at the centers and at the edges of meteorites as a function of their masses. These curves are calculated on the assumptions that cosmic radiation has produced 4×10^{-6} cc of He/g at the center of a meteorite that has a final mass of about 10 kg (see the observed points in the mass-helium content diagram) and that cosmic radiation has acted on all meteorites for the same time, namely, the time since the disruption of their parent planet. The curves of Fig. 2 are drawn for three very different assumptions about the mass lost by the meteorite in traversing the earth's atmosphere, and show that the results are not greatly affected by the particular assumption that is made. The points of Fig. 2 are the helium contents of meteorites measured by Paneth[2] plotted against their masses. Significantly, the curves parallel the upper boundary of the observed points and thus account for the most important feature of the mass-helium content diagram. In addition, it is apparent that if cosmic radiation has produced the helium in small meteorites, then this process is sufficient to produce, in the same time, all of the helium observed in any meteorite.

[1] C. A. Bauer, Phys. Rev. **72**, 354 (1947).
[2] F. A. Paneth, Nature **149**, 235 (1942).

On the Origin of the Neutrons Associated with the Extensive Cosmic-Ray Showers

VANNA TONGIORGI COCCONI
Laboratory of Nuclear Studies, Cornell University, Ithaca, New York
June 4, 1948

IN a previous work evidence has been obtained of the presence of neutrons in the extensive cosmic-ray showers.[1]

We are now reporting preliminary results of further experiments performed at sea level in order to study the mechanism of production of those neutrons.

The same apparatus and the same technique of delayed coincidences between Geiger-Müller counters and BF_3 proportional counters, as described in reference 1, have been used.

Coincidences $S=a+b+c$ selected extensive showers, a, b, and c consisting of unshielded Geiger-Müller counters of 2000-cm² surface, arranged in a horizontal plane, at the vertices of a triangle of 4-m sides.

Neutrons were recorded by two identical detectors, N_1 and N_2, each consisting of four BF_3 counters imbedded in a paraffin box of $45\times45\times50$ cm³ volume (counter surface 2.5×45 cm²).

Coincidences $S+N_1$ and $S+N_2$ indicated neutrons associated with extensive showers.

Incoherent neutrons N_1 and N_2 (i.e., neutrons not associated with extensive showers) were also simultaneously recorded, as well as coincidences N_1+N_2, not associated with extensive showers.

The experiments were performed by varying absorbers around absorber N_1. Detector N_2 was always kept far from any absorber, so that its constant rates provided a check of the regular running of the apparatus.

In Fig. 1, the arrangements of the absorbers around detector N_1 and the corresponding results are reported. Column 1 gives the rate $S+N_1$ of neutrons detected in N_1 associated with showers $S=a+b+c$. Column 2 gives the rate of incoherent neutrons in detector N_1, and column 3 the rate of coincidences N_1+N_2 between neutrons in detectors N_1 and N_2.

Tests with Cd shields around the BF_3 counters showed that the background caused by spurious phenomena was zero for both $S+N_1$ and N_1+N_2, while it was about 6 percent of the recorded rates for N_1.

Consider first the results for $S+N_1$, i.e., for neutrons associated with extensive showers:

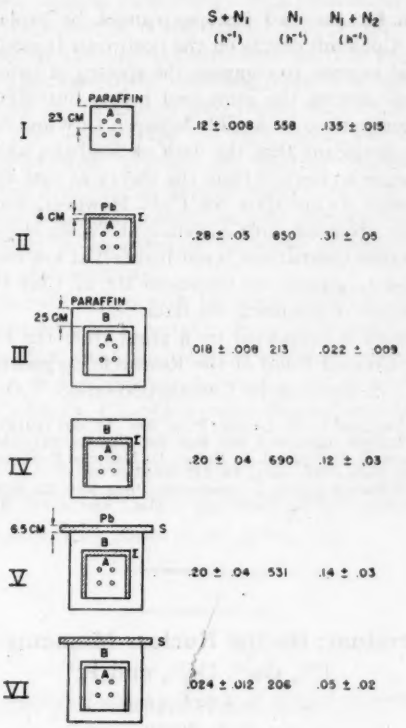

FIG. 1.

Arrangement I: Neutrons associated with extensive showers may be either locally generated in the paraffin A or generated in air, i.e., pre-existing in the showers before entering the detector.

Arrangement II: The large increase in the rate due to the lead Σ (4 cm) reveals production of many neutrons in lead. Two hypotheses may be put forward: (a) Neutrons are generated by the soft component of the extensive showers. (b) Neutrons are generated by the penetrating component of the extensive showers.

Arrangement III: The extra paraffin B (25 cm) prevents the neutrons coming from the air, with energies smaller than ~10 Mev, from reaching the detector. The strong decrease in the rate shows that most of the neutrons recorded with Arrangement I are generated in the atmosphere, and have energies lower than 10 Mev.

Arrangement IV: The production of neutrons in the lead is confirmed.

Arrangement V: The lead S (6.5 cm) does not vary appreciably the rate observed with Arrangement IV. This means that if the neutrons are produced by the soft component (hypothesis (a)), they must be produced mostly in S (a substantial fraction of the soft component arrives in the vertical direction and is absorbed by 6.5 cm Pb), and their energies must be very high in order to cross more than 40 cm of paraffin. If the neutrons, instead, are produced by the penetrating component (hypothesis (b)), they may be produced in Σ, with not necessarily high energies (<10 Mev).

Arrangement VI: The strong reduction due to the withdrawal of the lead Σ indicates that hypothesis (a) is inconsistent, so that neutrons must be principally produced in lead *by the particles* (mesons or nucleons) *of the penetrating component.*

It is interesting to note that the same behavior is shown by the rates of both the incoherent neutrons N_1 and the coincidences N_1+N_2. We also think that the incoherent neutrons produced in lead are mostly generated by a penetrating component, rather than by $\gamma-n$ reactions or any other processes originated by the soft component.

As for the fraction of neutrons produced in the air, no direct information may be drawn from our experiments, but it is reasonable to assume that most of these neutrons also, both associated and not associated with extensive showers, are genetically correlated to some penetrating component, with a small contribution, if any, from the soft component. Furthermore, the well-known strong altitude dependence of the total neutron component probably rules out light mesons as parent of the neutrons and supports the nucleonic component as the mean responsible for the production of neutrons in the cosmic radiation.

[1] Vanna Tongiorgi, Phys. Rev. **73**, 923 (1948).

Shape of the Positron Spectrum of Cu^{61}

C. SHARP COOK AND LAWRENCE M. LANGER
Indiana University, Bloomington, Indiana
June 3, 1948

IN order to investigate further the large deviation from the Fermi theory of beta-decay previously observed[1] in the positron spectrum of Cu^{64}, we have studied the momentum distribution of the positrons of Cu^{61} in the same high resolution 40-cm radius of curvature shaped field magnetic spectrometer.[2]

The measurements were made under the same ideal conditions that prevailed for the Cu^{64} study. The Cu^{61} source was prepared by bombarding a nickel target with 12-Mev deuterons. The active copper was electrochemically separated and uniformly deposited on 0.02-mg/cm² Zapon backing. The 0.4-cm wide source had a thickness of less than 0.1 mg/cm². The same thin window G-M counter, which transmits electrons down to 2.0 kev, was used. Measurements were limited to the region in which the transmission of the counter window is independent of energy.

The results are shown in the Fermi plot of the data in Fig. 1. All parts of the spectrum were found to decay with the same period of 3.33 hours. The high energy end of the spectrum is in good agreement with the straight line predicted theoretically for an allowed transition. Since the statistical errors are based on more than 25,000 counts per point, the extrapolated end point can be determined quite accurately as $W_0=3.36$ mc², which is equivalent to 1.205 ± 0.005 Mev. This is in good agreement with the

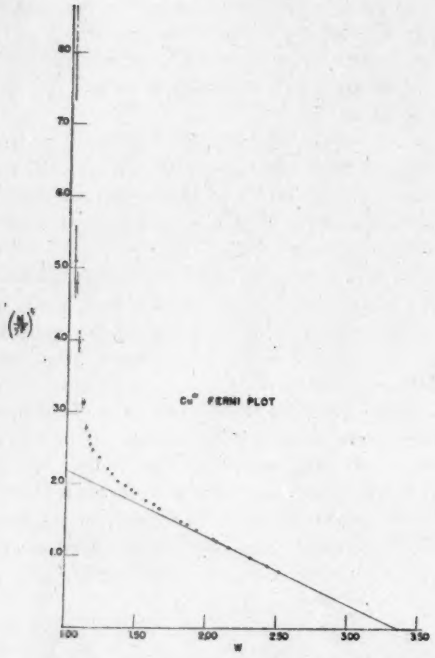

FIG. 1. Fermi plot of the momentum spectrum of Cu^{61} positrons. The extrapolated end point is at $W_0=3.36$ mc², corresponding to 1.205 Mev. The deviation from the theoretical straight line begins at $W=2.0$ mc².

value obtained by Bradt *et al.*,[3] and considerably higher than the value shown in the Segrè chart.[4]

As in the case of Cu^{64}, a large deviation from the Fermi theory is observed at low energies. In this case, the excess of positrons appears for all energies below $W=2.0$ mc².

In Fig. 2 we have plotted the ratio of the experimental number of positrons per unit momentum interval to that predicted by the theory as a function of the energy, W. The data for Cu^{64} are shown for comparison.

Since Cu^{61} and Cu^{64} have the same nuclear charge, Z, it would appear that the difference in the nature of the deviation for the two isotopes cannot be explained in terms of Coulomb effects on the positrons. It would be of additional interest to compare the spectra of two allowed transitions having the same end points but different Z. Such a comparison is possible between Cu^{61} and N^{13}. It is perhaps significant that the data of Siegbahn and Slätis[5] for N^{13} begin to deviate from the theory at just about the same energy as our data for Cu^{61}. However, since their data were obtained with a source of "some mg/cm²," a more detailed comparison is not justified at low energies.

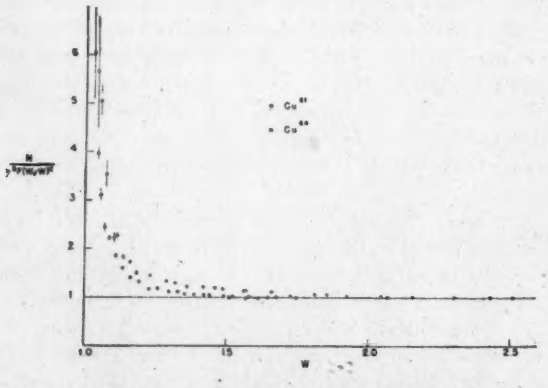

FIG. 2. The ratio of the observed number of positrons per unit momentum interval to that predicted by the Fermi theory for an allowed transition as a function of the total positron energy. The open circles are for Cu^{61}. The closed circles show the data for Cu^{64}.

We wish to express our thanks to Mr. H. Clay Price, Jr. for assistance in obtaining the data.

This work is supported by a grant from the Frederick Gardner Cottrell Fund of the Research Corporation, and by the U. S. Navy under Contract N6ori-48, T.O. I.

[1] C. S. Cook and L. M. Langer, Phys. Rev. **73**, 601 (1948).
[2] L. M. Langer and C. S. Cook, Rev. Sci. Inst. **19**, 257 (1948).
[3] H. Bradt, P. C. Gugelot, O. Huber, H. Medicus, P. Preiswerk, and P. Scherrer, Helv. Phys. Acta **18**, 252 (1945).
[4] L. N. Ridenour and W. J. Henderson, Phys. Rev. **52**, 889 (1937).
[5] K. Siegbahn and H. Slätis, Ark. f. Mat., Astr. o Fys. **32A**, No. 9 (1945).

Erratum: On the Nuclear Moments of I^{127}, Ga^{69}, Ga^{71}, and P^{31}

[Phys. Rev. **73**, 1112 (1948)]

R. V. POUND
Lyman Laboratory of Physics, Harvard University, Cambridge, Massachusetts

IN the above letter, line 13 of column two on page 1112 should read

$$\nu(Ga^{71})/\nu(Na^{23})=1.1529\pm0.0004$$

instead of

$$\nu(Ga^{71})/\nu(Ga^{69})=1.1529\pm0.0004.$$

Errata and Addendum: On the Mechanism of Electron Emission at the Cathode Spot of an Arc

[Phys. Rev. **73**, 1214 (1948)]

JEROME ROTHSTEIN
Signal Corps Engineering Laboratories, Fort Monmouth, New Jersey

IN a recent Letter to the Editor under the above title, several errors appear, *viz.*: p for rho in the first two formulae, alpha for d in the first formula, $10^{-4}N$ for $10^{4}N$ in the third formula, Mc for sec in the next to the last paragraph. As normal velocity components are considered, a factor $\frac{1}{2}$ should appear before the integral in the second formula. The error in the third formula, the only one of consequence, invalidates the temperature calculation. It seems better to replace transit time considerations by the following picture of processes taking place at the cathode surface.

In a Hg arc, some 10^{21} ions hit unit area of the cathode spot per unit time. Having energies of about 10 e.v. many of them may penetrate to depths of one or more atomic

diameters, sharing their energy with cathode atoms. The heat of vaporization is less than 1 e.v. per particle. Accordingly, in the spot microvolume, particle energies are so high that conditions resemble those of a highly compressed gas in the supercritical region more than those of the solid or liquid state. To this region electrons flow metallically, from it they are emitted thermionically. More than a superficial parallel appears to exist between steady state arc spot conditions and transient conditions encountered in experiments on wires exploded by tremendous peak currents.

This picture agrees with the experiments of Plesse[1] on the important role of metallic vapor at the cathode spot. He found, for example, that the essential characteristics of Zn, Cd, or Hg arcs could be obtained with a Ni cathode supplied with Zn, Cd, or Hg vapor, respectively, by evaporation from an oven or from the cathode of an auxiliary discharge. The vapor source could be inside or external to the cathode. Nitrogen was the gas employed.

[1] H. Plesse, Ann. der Physik 22, 473 (1935).

Photoelastic Properties of Cubic Crystals

ELIAS BURSTEIN AND PAUL L. SMITH
Crystal Section, Naval Research Laboratory, Washington, D. C.
June 7, 1948

THE photoelastic effects in cubic crystals have been explained by Mueller[1] in terms of the anisotropy of the Lorentz-Lorenz and Coulomb forces produced by a distortion of the lattice. The contribution of the optical anisotropy of the ions was taken into account by means of phenomenological constants. This contribution was found to be negative for the few crystals for which data were available at the time, and Mueller assumed that it would also be negative for other crystals.

Additional photoelastic data have been obtained recently at this laboratory[2] which show that Mueller's conclusions concerning the optical anisotropy contribution must be modified. A summary of these and other recent data is given in Table I.

The purpose of this note is to present these results and to discuss further the significance of the optical anisotropy constant λ_0. Some qualitative relations between λ_0 and the temperature dependence of the refractive index will also be discussed.

In general, Mueller's predictions for crystals having NaCl structures are correct but his predictions of the sign of $(p_{11}-p_{12})$ for diamond and CsCl structures (thallium halides) are wrong. Assuming the correctness of the theory in evaluating the $L-L$ and Coulomb contributions, the error apparently lies in Mueller's assumption concerning the optical anisotropy contributions. For diamond which is monatomic and covalent this contribution (as measured by Mueller's optical anisotropy constants ($\lambda_{12}-\lambda_{11}$)) can be unambiguously calculated using the theory and the experimental values of $(p_{11}-p_{12})$. This calculation yields $\lambda_{11}=+0.7$; $\lambda_{12}=+2.0$; $\lambda_{44}=+1.8$. The optical anisotropy contribution is positive ($\lambda_{12}-\lambda_{11}=+1.3$) and larger than the $L-L$ contribution of -0.66. It is suggested that in the thallium halides the optical anisotropy contribution is also positive and large enough to more than compensate for the negative $L-L$ and Coulomb contributions. Such a positive contribution could result from the fact that in a CaCl structure the cation-anion bond is directed along [111], and a [100] strain alters the anion-anion distance more than the cation-anion distance. A similar effect would be expected for ZnS and diamond structures.[5]

TABLE I.

Crystal	$p_{11}-p_{12}$	p_{44}	p_{11}	$\rho dn/d\rho$ obs	λ_0
LiF	-0.108 (−)**	-0.064 (−)**	~0.02	~0.1	~0.7
NaCl	-0.043 (−)	-0.010 (−)	0.11	0.24	0.60
KCl	$+0.046$ (+)	— (−)	0.17	0.23	0.60
KBr	$+0.049$ (+)	-0.26 (−)	0.22	0.35	0.50
KI	$+0.041$ (+)	— (−)	0.21	0.43	0.50
MgO	-0.24 (−)	— (−)	~−0.13	~−0.4	~1.4
TlCl*	+~0.03 (−)	+~0.06 (+)	—	—	—
Diamond[3]	+0.45 (−)	+0.011 (+)	0.125	−2.62	1.5
K-Alum[4]	−0.08	−0.0056	0.27	0.53	0.06

$$\lambda_0=1-\frac{\rho(dn/d\rho)\text{obs}}{\rho(dn/d\rho)\text{calc}} \qquad \rho(dn/d\rho)\text{obs}=\frac{n^2}{6}(p_{11}+2p_{12})$$

$$\rho(dn/d\rho)\text{calc}=\frac{(n^2-1)(n^2+2)}{6n}$$

* Values for TlCl approximate.
** The signs of the photoelastic constants as predicted by Mueller are given in parenthesis.

Values for the change in refractive index with density ($\rho dn/d\rho$) and the optical anisotropy constant for hydrostatic pressure λ_0 (corresponding to the change in molar polarizability with volume) are also given in Table I. In all cases the observed values of $\rho dn/d\rho$ were smaller than the calculated values, and in MgO and diamond the measured $\rho dn/d\rho$ is actually negative; that is, a hydrostatic pressure is found to cause a decrease in refractive index. As a result, the λ_0 values for these crystals are greater than one, indicating that the change in ionic polarizability is greater than the effect of changing the number of ions per unit volume.

Since the change in ionic polarizability with strain results from a change in the overlap of the ions, it is suggested that its magnitude depends on the amount of overlap present in the unstressed crystal and that λ_0 may be used as a measure of the amount of homopolar bonding. This is borne out by correlation with other methods of estimating homopolar bonding.

Data on the change of index with temperature are also of interest. From existing data on dn/dT it appears that for those simple crystals which contain no radicals and have small λ_0 values, the change of index with temperature is determined mainly by the density contribution $(\partial n/\partial\rho)_T \times (d\rho/dT)$; the temperature contribution $(dn/dT)_\rho$ is small, and dn/dT is negative. For crystals with large λ_0 the temperature contribution is positive and about the same order of magnitude as the positive density contribution. From these considerations one would, therefore, predict MgO to have a positive dn/dT. For ZnS, which is known

to have a positive dn/dT and is considered to have large homopolar bonding, similar reasoning predicts that $dn/d\rho$ is positive; i.e., $\lambda_0 > 1$. In crystals containing radicals and in many glasses, positive dn/dT values are frequently obtained although their $dn/d\rho$ values are negative. In these materials there are effects within the radical which contribute mainly to dn/dT and only slightly to $dn/d\rho$. A more complete treatment of these subjects will be presented in a forthcoming paper.

[1] H. Mueller, Phys. Rev. **47**, 947 (1935).
[2] Burstein, Smith, and Henvis, Bull. Am. Phys. Soc. **23** (2), 33 (1948).
[3] G. N. Ramachandran, Proc. Ind. Acad. Sci. **A25**, 266 (1947).
[4] S. Bhagavantam and S. Suryanarayana, Proc. Ind. Acad. Sci. **A26**, 97 (1947).
[5] C. D. West and J. Makas, Chem. Phys. **16**, 427 (1948) reported $+(p_{11}-p_{12})$ for two mixed thallium halides in agreement with our results. Their data also gives a $+(p_{11}-p_{12})$ and $-p_{44}$, for AgCl in agreement with Mueller's prediction for NaCl structures with small ratio of negative to positive ion polarizibilities. We do not agree with West and Makas concerning the sign of the diamond constants and believe them to be correct as given by Ramachandran.[3]

The Transistor, A Semi-Conductor Triode

J. Bardeen and W. H. Brattain
Bell Telephone Laboratories, Murray Hill, New Jersey
June 25, 1948

A THREE-ELEMENT electronic device which utilizes a newly discovered principle involving a semiconductor as the basic element is described. It may be employed as an amplifier, oscillator, and for other purposes for which vacuum tubes are ordinarily used. The device consists of three electrodes placed on a block of germanium[1] as shown schematically in Fig. 1. Two, called the emitter and collector, are of the point-contact rectifier type and are placed in close proximity (separation ~.005 to .025 cm) on the upper surface. The third is a large area low resistance contact on the base.

The germanium is prepared in the same way as that used for high back-voltage rectifiers.[2] In this form it is an N-type or excess semi-conductor with a resistivity of the order of 10 ohm cm. In the original studies, the upper surface was subjected to an additional anodic oxidation in a glycol borate solution[3] after it had been ground and etched in the usual way. The oxide is washed off and plays no direct role. It has since been found that other surface treatments are equally effective. Both tungsten and phosphor bronze points have been used. The collector point may be electrically formed by passing large currents in the reverse direction.

Each point, when connected separately with the base electrode, has characteristics similar to those of the high

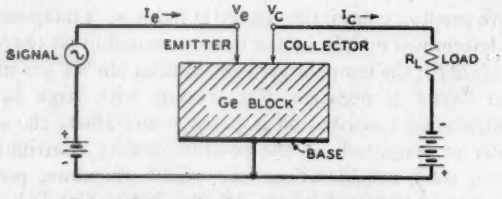

FIG. 1. Schematic of semi-conductor triode.

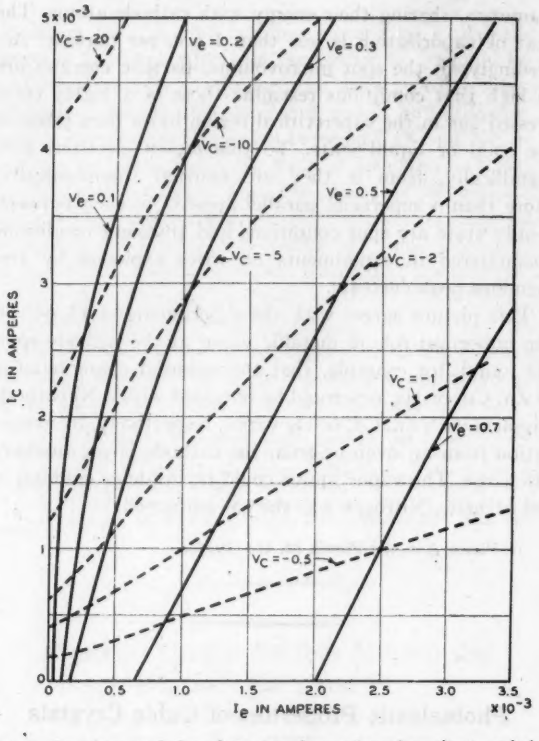

FIG. 2. d.c. characteristics of an experimental semi-conductor triode. The currents and voltages are as indicated in Fig. 1.

back-voltage rectifier. Of critical importance for the operation of the device is the nature of the current in the forward direction. We believe, for reasons discussed in detail in the accompanying letter,[4] that there is a thin layer next to the surface of P-type (defect) conductivity. As a result, the current in the forward direction with respect to the block is composed in large part of holes, i.e., of carriers of sign opposite to those normally in excess in the body of the block.

When the two point contacts are placed close together on the surface and d.c. bias potentials are applied, there is a mutual influence which makes it possible to use the device to amplify a.c. signals. A circuit by which this may be accomplished in shown in Fig. 1. There is a small forward (positive) bias on the emitter, which causes a current of a few milliamperes to flow into the surface. A reverse (negative) bias is applied to the collector, large enough to make the collector current of the same order or greater than the emitter current. The sign of the collector bias is such as to attract the holes which flow from the emitter so that a large part of the emitter current flows to and enters the collector. While the collector has a high impedance for flow of electrons into the semi-conductor, there is little impediment to the flow of holes into the point. If now the emitter current is varied by a signal voltage, there will be a corresponding variation in collector current. It has been found that the flow of holes from the emitter into the collector may alter the normal current flow from the base to the collector in such a way that the change in collector

current is larger than the change in emitter current. Furthermore, the collector, being operated in the reverse direction as a rectifier, has a high impedance (10^4 to 10^5 ohms) and may be matched to a high impedance load. A large ratio of output to input voltage, of the same order as the ratio of the reverse to the forward impedance of the point, is obtained. There is a corresponding power amplification of the input signal.

The d.c. characteristics of a typical experimental unit are shown in Fig. 2. There are four variables, two currents and two voltages, with a functional relation between them. If two are specified the other two are determined. In the plot of Fig. 2 the emitter and collector currents I_e and I_c are taken as the independent variables and the corresponding voltages, V_e and V_c, measured relative to the base electrode, as the dependent variables. The conventional directions for the currents are as shown in Fig. 1. In normal operation, I_e, I_c, and V_e are positive, and V_c is negative.

The emitter current, I_e, is simply related to V_e and I_c. To a close approximation:

$$I_e = f(V_e + R_F I_c), \tag{1}$$

where R_F is a constant independent of bias. The interpretation is that the collector current lowers the potential of the surface in the vicinity of the emitter by $R_F I_c$, and thus increases the effective bias voltage on the emitter by an equivalent amount. The term $R_F I_c$ represents a positive feedback, which under some operating conditions is sufficient to cause instability.

The current amplification factor α is defined as

$$\alpha = (\partial I_c / \partial I_e)_{V_c = \text{const.}}$$

This factor depends on the operating biases. For the unit shown in Fig. 2, α lies between one and two if $V_c < -2$.

Using the circuit of Fig. 1, power gains of over 20 db have been obtained. Units have been operated as amplifiers at frequencies up to 10 megacycles.

We wish to acknowledge our debt to W. Shockley for initiating and directing the research program that led to the discovery on which this development is based. We are also indebted to many other of our colleagues at these Laboratories for material assistance and valuable suggestions.

[1] While the effect has been found with both silicon and germanium, we describe only the use of the latter.
[2] The germanium was furnished by J. H. Scaff and H. C. Theuerer. For methods of preparation and information on the rectifier, see H. C. Torrey and C. A. Whitmer, *Crystal Rectifiers* (McGraw-Hill Book Company, Inc., New York, New York, 1948), Chap. 12.
[3] This surface treatment is due to R. B. Gibney, formerly of Bell Telephone Laboratories, now at Los Alamos Scientific Laboratory.
[4] W. H. Brattain and J. Bardeen, Phys. Rev., this issue.

Nature of the Forward Current in Germanium Point Contacts

W. H. Brattain and J. Bardeen
Bell Telephone Laboratories, Murray Hill, New Jersey
June 25, 1948

THE forward current in germanium high back-voltage rectifiers[1] is much larger than that estimated from the formula for the spreading resistance, R_s, in a medium of uniform resistivity, ρ. For a contact of diameter d,

$$R_s = \rho/2d.$$

Taking as typical values $\rho = 10$ ohm cm and $d = .0025$ cm, the formula gives $R_s = 2000$ ohms. Actually the forward current at one volt may be as large as 5 to 10 ma, and the differential resistance is not more than a few hundred ohms. Bray[2] has attempted to account for this discrepancy by assuming that the resistivity decreases with increasing field, and has made tests to observe such an effect.

In connection with the development of the semi-conductor triode discussed in the preceding letter,[3] the nature of the excess conductivity has been investigated by means of probe measurements of the potential in the vicinity of the point.[4] Measurements were made on the plane surface of a thick block. Various surface treatments, such as anodizing, oxidizing, and sand blasting were used in different tests, in addition to the etch customarily employed in the preparation of rectifiers.

The potential, $V(r)$, at a distance r from a point carrying a current, I, is measured relative to a large area low resistance contact at the base. In Fig. 1 we have plotted some typical data for a surface prepared by grinding and etching, and then oxidizing in air at 500°C for one hour. The ordinate is $2\pi r V(r)/I$ which for a body of uniform resistivity, ρ, should be a constant equal in magnitude to ρ. Actually it is found that the ratio is much less than ρ at small distances from the point, and increases with r, approaching the value ρ asymptotically at large distances. The departure from the constant value indicates an excess conductivity in the neighborhood of the point.

The manner in which the excess conductivity varies with current indicates that two components are involved. One is ohmic and is represented by the upper curve of Fig. 1 which applies for reverse (negative) currents and for small forward currents. This component is attributed to a thin conducting layer on the surface which is believed to be P-type (i.e., of opposite type to that of the block). A layer with a surface conductivity of .002 mhos is sufficient to account for the departure of the upper curve from a constant value. The second component of the excess conductivity increases with increasing forward current, and

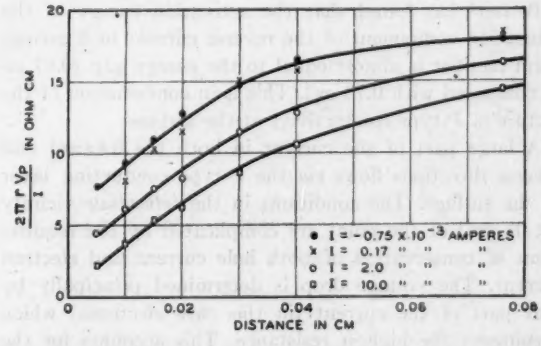

FIG. 1. Measurements of potential, V_p, at a distance r from a point contact through which a current I is flowing into a germanium surface.

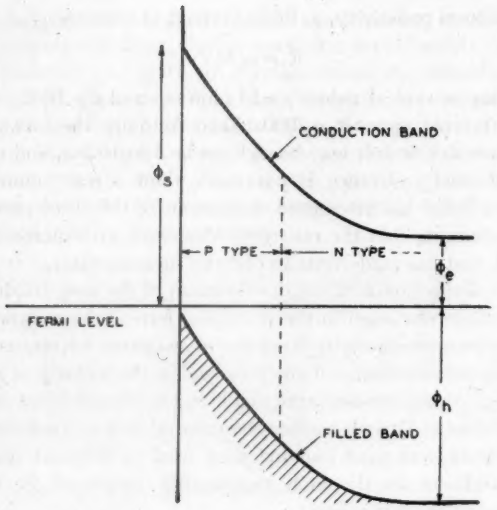

FIG. 2. Schematic energy level diagram of an N-type semi-conductor with a thin layer of P-type conductivity next to the surface.

is attributed to an increase in the concentration of carriers (holes and electrons) in the vicinity of the point with increasing forward bias. The relative as well as the absolute magnitudes of these two components vary with surface treatment. Two different crystal faces on the same block may have different characteristics.

The thin P-type conducting layer may result from an excess of acceptor impurities near the surface or from a space charge barrier layer which is sufficient to raise the filled band to a position close to the Fermi level. The latter situation is shown in the energy level diagram of Fig. 2. It is assumed that there is a uniform excess of donor impurities in the interior. The surface states are such as to require the Fermi level to cross the surface near the top of the filled band.[5] The conductivity in the layer right next to the surface is then P-type, and this layer is separated from the normal N-type region in the interior by the $P-N$ rectifying barrier. The energy gap in germanium is about 0.75 ev. Approximate values for the other energies shown on the diagram are: $\varphi_e=0.25$ ev, $\varphi_h=0.50$ ev, $\varphi_s=0.70$ ev. The thickness of the space charge layer is about 10^{-4} cm.

Benzer[6] has found that the activation energy of the saturation component of the reverse current in a germanium rectifier is almost equal to the energy gap (0.67 ev as compared with 0.75 ev). This is in confirmation of the picture of P-type conductivity at the surface.

A large part of the current in both the forward and reverse directions flows *via* the P-type conducting layer at the surface. The conditions in the *immediate* vicinity ($<.01$ cm) of the point are complicated by the requirement of conservation of both hole current and electron current. The voltage drop is determined principally by that part of the current (in this case electrons) which encounters the highest resistance. This accounts for the high resistances found for reverse biases and for small forward biases, in spite of the relatively high conductivity of the surface layer.

[1] H. C. Torrey and C. A. Whitmer, *Crystal Rectifiers* (McGraw-Hill Book Company, Inc., New York, New York, 1948), Chap. 12.
[2] R. Bray, Bull. Am. Phys. Soc. **23**, 21 (1948), Abstract 63 of Washington Meeting, April 29–30, 1948.
[3] J. Bardeen and W. H. Brattain, Phys. Rev., this issue.
[4] The micromanipulator used for this work was designed by W. L. Bond.
[5] J. Bardeen, Phys. Rev. **71**, 717 (1947).
[6] S. Benzer "Temperature dependence of high voltage germanium rectifier D-C characteristics," NDRC 14-579, Purdue University, October 31, 1945.

Modulation of Conductance of Thin Films of Semi-Conductors by Surface Charges

W. SHOCKLEY AND G. L. PEARSON
Bell Telephone Laboratories, Murray Hill, New Jersey
June 25, 1948

WHEN a charge is induced on the free surface of a semi-conductor, by making it one plate of a parallel plate condenser for example, some of the charge density δq goes into the surface states and some into the space charge in the barrier layer beneath the surface.[1] Figure 1 shows the energy level diagram for an N-type semiconductor under no external field (solid lines) and under the field due to negative voltage on the other plate (dotted). If the applied field produces a change in potential δV on the surface, then δq_s, the increased charge per cm² in the surface states, will be $qN_s\delta V$ where q is the electronic charge and N_s is the number of surface states per unit area per unit voltage. The charge in the interior can be estimated from the Schottky exhaustion layer theory which gives $\delta V=4\pi\rho b\delta b/\epsilon$ where ρ is the net charge density of the impurities, ϵ the dielectric constant, and b the thickness of the exhaustion layer. This gives a charge of $\delta q_b=\rho\delta b=\epsilon\delta V/4\pi b$ per unit area, which is produced by removing conduction electrons. Hence a fraction,

$$\beta=\delta q_b/(\delta q_b+\delta q_s)=(\epsilon/4\pi b)/[qN_s+(\epsilon/4\pi b)],$$

of the total charge induced per unit area on the semiconductor is accounted for by reduced conduction electrons in the interior.

If the semi-conductor consists of a thin layer of thickness L with exhaustion layers of thickness b on both sides, then the total charge per unit area of conduction electrons is

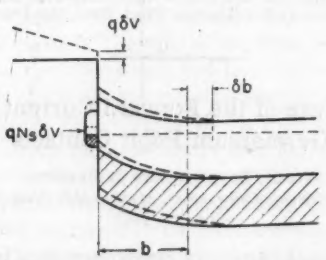

FIG. 1. Energy level diagram showing charge induced in surface states by external field.

$-\rho(L-2b)$ and the conductance parallel to the layer is $\sigma=\rho(L-2b)\mu$ where μ is the mobility. The applied field changes the charge by $\delta q_b=\beta\delta q$ and, therefore, changes the conductance of the layer by

$$\delta\sigma/\sigma=\pm\beta\delta q/\rho(L-2b)=\pm\beta\delta q\mu/\sigma,$$

where the minus sign holds for N-type material (i.e., when $\delta q_b>0$, there are less electrons and $\delta\sigma<0$) and plus for P-type.

The charge δq on the surface is induced by using the semi-conductor as one plate of a parallel plate condenser, and the change in conductance is simultaneously determined for current flow parallel to the plate. The experimental arrangement consists of a condenser with rectangular plates about 1×2 cm of gold and semi-conductor evaporated on opposite sides of a slab of fused quartz 0.003 inch thick. The current used to measure the change in conductance flows between two additional gold electrodes evaporated on the two ends of the semi-conductor. According to the above theory, the capacity of this unit is that of the quartz C_q in series with $C_s=qN_s$ and $C_b=\epsilon/4\pi b$ in parallel, and is thus chiefly determined by C_q. The value δq is determined directly from the measured capacity per unit area and the applied voltage. (Experiments to check the equivalent circuit for the unit, including relaxation effects, will be communicated later.)

Measurements on a number of films of P-type germanium, copper oxide, and N-type silicon show that $\delta\sigma/\sigma$ is correctly given in sign by the theory and is linear in $\delta\sigma$. Values as high as 0.11 have been obtained for Cu_2O with fields of 400,000 volts/cm. Values of β depend on the mobility, which was measured for two P-type germanium films and give results as follows:

$\delta\sigma/\sigma\,\delta q$ cm²/coulomb	σ mhos	μ cm²/volt-sec.	β	L cm	N_s/cm² volt
1.0×10^4	3.1×10^{-4}	33	0.10	2×10^{-3}	6×10^{13}
5.5×10^3	7.7×10^{-4}	49	0.09	5×10^{-3}	5×10^{13}

Using the exhaustion layer theory with $V=2\pi\rho b^2/\epsilon$, the unknown values for b and ρ can be eliminated from the equations giving (for b/L and β both $\ll1$)

$$N_s=1.31\times10^{13}(\epsilon\mu/LV\sigma)^{\frac{1}{2}}\sigma\delta q/\delta\sigma,$$

where the units are N_s/cm² volt, μ cm²/volt-sec., L cm, V volts, σ mhos, δq coulombs/cm², $\epsilon=19$ for Ge. The result is not sensitive to the value of V. Assuming a representative value of 0.5 volts, the value of N_s was computed. This value is comparable with that previously obtained for silicon by another method.[2]

We are indebted to many of our colleagues for discussions and advice and to R. B. Gibney, J. R. Haynes, and M. Sparks for preparation of the films.

[1] J. Bardeen, Phys. Rev. 71, 717 (1947).
[2] W. H. Brattain and W. Shockley, Phys. Rev. 72, 345 (1947).